Author:
Seager, Richard A

Title:
Investigating the role of SUMOylation of Mitochondrial Fission Factor in Mitochondrial Dynamics

Investigating the role of SUMOylation of Mitochondrial Fission Factor in Mitochondrial Dynamics

Richard A. Seager

A dissertation submitted to the University of Bristol in accordance with the requirements for award of the degree of Doctor of Philosophy in the School of Biochemistry, Faculty of Life Sciences

September 2019

Word Count 45,216

Abstract

The dynamic nature of mitochondrial fusion and fission allows rapid adaptability to changing metabolic demands and stress to restore homeostasis. The principal fission protein is the cytosolic GTPase dynamin related protein-1 (DRP1), which binds to the outer membrane receptors mitochondrial fission protein 1 (Fis1), mitochondrial dynamics proteins (MiD49/51) and mitochondrial fission factor (MFF). MFF is the predominant pro-fission receptor, whereas MiD proteins sequester inactive DRP1 and form a trimeric complex of DRP1-MiD-MFF.

The fusion and fission machinery are subject to multiple forms of post-translational modifications (PTM) to regulate mitochondrial function. AMPK phosphorylation of MFF at S155/S172 promotes fission under energetic stress, and parkin-mediated ubiquitination promotes mitophagy. The small ubiquitin-like modifier (SUMO) isoform SUMO-1 promotes DRP1 recruitment, whereas SUMO-2/3-DRP1 represses fission during oxygen/glucose deprivation (OGD).

I present a novel finding that MFF is SUMOylated at K151, which is enhanced by phosphorylation at S155. A SUMO-deficient MFF mutant (K151R) has reduced ubiquitination, which occurs at a separate site to K151, suggesting SUMOylation promotes ubiquitination. The K151R mutant has reduced binding to DRP1, but surprisingly, the MFF phospho-null and phospho-mimetic mutants also have reduced binding. SUMOylation of MFF reduces the association of MFF with MiD proteins, and I present a model whereby the degree of SUMOylation mediates the ratio of MiD in the DRP1-MiD-MFF complex. Intriguingly, expression of the K151R mutant in primary neurons enhances dendritic mitochondrial size and reduces density, with no effect on axonal mitochondria, suggesting differential compartment-specific regulation and/or roles of MFF SUMOylation. My data indicate that MFF SUMOylation is enhanced following OGD and is required for DRP1 binding following mitochondrial depolarisation. Taken together, these results demonstrate that there is substantial crosstalk between the PTMs of MFF, and MFF SUMOylation is required to regulate the fine-tuning of mitochondrial dynamics under basal conditions and is also involved in the stress response.

Author’s declaration

I declare that the work in this dissertation was carried out in accordance with the requirements of the University's *Regulations and Code of Practice for Research Degree Programmes* and that it has not been submitted for any other academic award. Except where indicated by specific reference in the text, the work is the candidate's own work. Work done in collaboration with, or with the assistance of, others, is indicated as such. Any views expressed in the dissertation are those of the author.

SIGNED: ..... DATE: .....

Acknowledgements

First and foremost, I would like to thank my supervisor Jeremy, for giving me the opportunity to undertake my PhD in your lab and for all the support and encouragement along the way. Also, thank you for the freedom you gave me to pursue my own ideas, no matter how superfluous they were!

My thanks go to Suko, Kev and Dan, for help, advice, liking good music and for all the neurons! I will miss the science (and philosophical) discussions. Particularly, my thanks go to Kev, for his assistance, dedication and teaching me almost everything during this PhD. I learnt so much from you, and this PhD would not have been possible were it not for your help. If ever I become as good a scientist as you, I know I would have made it.

To everyone else in the Henley/Hanley labs, past and present, thank you for making my PhD a fulfilling and enjoyable time. A special thanks goes to Dr Luis, for all the laughs, lunch breaks and craziness.

I would like to thank all those who have provided advice and assistance along the way; to Dr Stephen Cross for image analysis, your macros saved me a lot of time and headaches! Professor Jeremy Tavaré for the AMPK cells, Professors David Chan and Michael Schrader for supplying the MEF cells. My thanks also go to Mr. Paul Murphy for advice and reagents for the deubiquitination *in vitro* experiment, to Dr Nadia Rawlings for help with OGD experiments, and to Dr Laura Lee for trying to muddle through the complicated world of MFF ubiquitination together!

Thank you to the Wellcome Trust for funding me and for giving me the opportunity to carry out this programme of research, and to my course mates, Dani and Jenny, for going through this together and always being up for a pint!

To Sofia, thank you for your encouragement, support and making me believe I can do anything. Also, for reminding me to take it easy from time to time (and all the amazing food and coffee!). You have made this journey so enjoyable, through the highs and lows, and you always put a smile on my face.

And, of course, thank you to my family for your support. My deepest thanks go to my parents, I would not be where I am if it wasn't for your continued belief in me. I am truly grateful for your love and encouragement in all my endeavours.

Abbreviations

AD	Alzheimer's Disease
ADP	Adenosine Diphosphate
AMP	Adenosine Monophosphate
AMPK	AMP-activated protein kinase
ATP	Adenosine Triphosphate
BRAC	Breast Cancer Type 1 Susceptibility Protein
BSA	Bovine Serum Albumin
CCCP	carbonyl cyanide m-chlorophenylhydrazone
CENP-E	Centromere protein-E
DIV	Days *in vitro*
DRP1	Dynamin Related Protein 1
Dyn2	Dynamin-2
Elk-1	ETS domain transcription factor
ER	Endoplasmic Reticulum
ERMES	ER-Mitochondrial Encounter Structure
ETC	Electron Transport Chain
FBS	Foetal Bovine serum
Fis1	Mitochondrial Fission protein 1
GTP	Guanosine Triphosphate
HDAC	Histone Deacetylase
HEK	Human Embryonic Kidney
HIF-1α	Hypoxia-inducible factor 1-alpha
HSF	Heat Shock factor
IκBα	NF-kappa-B inhibitor alpha
IP	Immunoprecipitation
IMM	Inner Mitochondrial Membrane
MAPK	Mitogen Activated protein Kinase

MARCH5	Membrane Associated RING-finger 5
MAPL	Mitochondrial Anchored Protein Ligase
MR	Mitochondrial Reticulum
MFF	Mitochondrial Fission Factor
MEF	Mouse Embryonic Fibroblast
MEF2A	Myocyte-specific enhancer factor 2A
MiD	Mitochondrial Dynamics proteins
MOM	Mitochondrial Outer Membrane
NB	Nuclear Body
NEM	N-Ethylmaleimide
NF-κB	Nuclear Factor Kappa-light-chain-enhancer of activated B cells
OGD	Oxygen Glucose Deprivation
OXPHOS	Oxidative Phosphorylation
PD	Parkinson's Disease
PDL	Poly D-Lysine
PDSM	Phosphorylation Dependent SUMO consensus motif
PGC-1α	Peroxisome proliferator-activated receptor gamma coactivator 1-α
PINK1	PTEN Induced Kinase-1
PKA	Protein Kinase A
PKC	Protein Kinase C
PLL	Poly L-Lysine
PML	Promyelocytic Leukaemia Protein
PTM	Post Translational Modification
Ran-Gap	RAS-related Nuclear GTPase activating Protein
RCF	Relative Centrifugal Force
RING	Really Interesting New Gene
RNF4	RING Finger Protein 4
SAE	SUMO Activating Enzyme
SDM	Site Directed Mutagenesis

SDS	Sodium Dodecyl Sulphate
SDS-PAGE	Sodium Dodecyl Sulphate Polyacrylamide Gel Electrophoresis
SENP	Sentrin/SUMO-specific proteases
SIM	SUMO Interacting Motif
SIMH	Stress Induced Mitochondrial Hyperfusion
STAT	signal transducer and activator of transcription
STUbL	SUMO targeted Ubiquitin Ligase
SUMO	Small Ubiquitin like Modifier
TF	Transcription Factor
TCA	Tricarboxylic acid cycle
Ubl	Ubiquitin Ligase
ULK1	Unc-51-Like Kinase 1
USP	Ubiquitin Specific Protease
WT	Wildtype

List of Figures

Figure 1.1 The SUMO cycle 10

Figure 1.2 Phosphorylation-dependent SUMOylation 15

Figure 1.3 SUMOylation can initiate multiple downstream effects 21

Figure 1.4 The complex SUMO-ubiquitin “code” 23

Figure 1.5 Mitochondrial compartments 25

Figure 1.6 The fusion and fission balance determine mitochondrial morphology 29

Figure 1.7 The mitochondrial lifecycle 34

Figure 1.8 Mitochondrial fusion and fission are mediated by GTPases 36

Figure 1.9 AMPK sites MFF across species 49

Figure 1.10 Summary of mitochondrial fission 54

Figure 1.11 Regulation of mitochondrial size in neurons 70

Figure 2.1 Schematic of *in vitro* deSUMOylation and deubiquitination assay . 103

Figure 2.2 Comparison of MiNA and my adapted image processing workflow 109

Figure 2.3 Workflow of ImageJ macro to analyse mitochondrial morphology . 111

Figure 2.4 Image processing of neuronal mitochondria 115

Figure 3.1 MFF is a novel SUMO substrate 121

Figure 3.2 MFF is modified at K151 123

Figure 3.3 MFF is SUMOylated by endogenous SUMO at K151 125

Figure 3.4 The non-SUMOylatable MFF mutant K151R has reduced ubiquitination 127

Figure 3.5 MFF is not modified by SUMO-Ubiquitin hybrid chains 129

Figure 3.6 Models of SUMOylation and ubiquitination of MFF 130
Figure 3.7 Phosphorylation at S155 enhances MFF SUMOylation 132
Figure 3.8 Phosphorylation is upstream of MFF SUMOylation 134
Figure 3.9 MFF phosphorylation differentially regulates SUMOylation 137
Figure 3.10 Quantification of mono and higher molecular species of MFF phospho-mutants 138
Figure 3.11 Phosphorylation of the two MFF AMPK sites S155 and S172 enhances MFF SUMOylation 142
Figure 3.12 Model of AMPK phosphorylation enhancing MFF SUMOylation .. 146
Figure 3.13 Phosphorylation at S155 and S172 have differential effects on MFF SUMOylation 150
Figure 4.1 Non-SUMOylatable MFF displays reduced DRP1 binding 156
Figure 4.2 SUMO-MFF mediated model of DRP1 recruitment 157
Figure 4.3 MFF SUMO and phosphorylation mutants reduce DRP1 binding .. 158
Figure 4.4 MiD49 contains a SIM 160
Figure 4.5 MFF phosphorylation and SUMOylation reduces MiD49 binding ... 162
Figure 4.6 Conceptual representation of ratios of fission proteins within pre-fission complexes under differential MFF PTM's 164
Figure 4.7 Oxygen/Glucose deprivation increases global SUMO-2/3 conjugation, decreases SENP3 levels and increases SUMO-1 conjugation to MFF 166
Figure 4.8 DRP1 binding to MFF wildtype and K151R during rotenone treatment 168

Figure 4.9 Model of mitochondrial fission: Does MFF SUMOylation act as a molecular switch? 173
Figure 5.1 MFF is required for DRP1-mitochondrial recruitment..... 185
Figure 5.2 MFF is required to maintain mitochondrial morphology 187
Figure 5.3 CFP-MFF isoform 1 rescues MFF deficient MEFs..... 188
Figure 5.4 Differential mitochondrial size in axons and dendrites of primary hippocampal neurons..... 190
Figure 5.5 MFF SUMOylation is required to maintain dendritic mitochondrial size and distribution..... 193
Figure 6.1 Conceptual SUMO-regulation of mitochondrial fission..... 211
Figure 8.1 Bacterial MFF SUMOylation assay 254
Figure 8.2 MFF SUMOylation in AMPK-α null cells..... 255
Figure 8.3 MFF phosphorylation-induced mitochondrial changes in neurons . 256
Figure 8.4 MiD49 contains a SIM for SUMO-1..... 257
Figure 8.5 Putative SIM motifs in human DRP1 and MiD49 258

List of tables

Table 1 Oligonucleotide primers used for Site-Directed Mutagenesis..... 80

Table 2 List of antibodies for Western blotting and immunocytochemistry..... 86

Table 3 Components of PCR reactions..... 97

Table 4 PCR thermocycler settings..... 98

Table 5 Components of the RevertAid cDNA synthesis reaction 100

Table 6 Components of PCR Product and Vector digestion reaction..... 100

Contents

Chapter 1 General Introduction 1

1.1 Post translational modifications 2

1.1.1 SUMOylation 3

1.1.2 The SUMO-cycle 6

1.1.3 Poly-SUMO chains 12

1.1.4 Co-regulation of SUMO and phosphorylation 14

1.1.5 SUMO-ubiquitin hybrid chains 18

1.2 Mitochondria 24

1.2.1 Mitochondrial Dynamics 28

1.2.2 The mitochondrial lifecycle 30

1.3 The mitochondrial fusion and fission machinery 35

1.3.1 Mitofusins (Mfn1/2) 37

1.3.2 Optic Atrophy Protein 1 (OPA1) 39

1.3.3 Dynamic related protein 1 (DRP1) 40

1.3.4 Mitochondrial Fission protein 1 (Fis1) 43

1.3.5 Mitochondrial Fission Factor (MFF) 44

1.3.6 Mitochondrial Dynamics proteins (MiD49/51) 50

1.4 SUMO regulation of mitochondria 55

1.5 The mitochondrial stress response 57

1.5.1 Nutrient stress 57

1.5.2 Ischemic stress 59

1.5.3 Mitochondrial inhibitors 60

1.6 AMP-activated Protein Kinase (AMPK) 61

1.6.1 AMPK activation 61
1.6.2 AMPK function 63
1.6.3 AMPK and mitochondria 63
1.6.4 AMPK and OGD 64
1.7 Mitochondria in neurons 66
1.7.1 Mitochondria fusion in neurons 67
1.7.2 Mitochondrial fission in neurons 67
1.7.3 Mitochondria in axons versus dendrites 68
1.8 Mitochondrial dynamics and disease 71
1.8.1 Fusion 72
1.8.2 Fission 73
1.8.3 Neurodegeneration 74
Aims 76
Chapter 2 Materials and Methods 77
2.1 Materials 78
2.1.1 Bacterial reagents 78
2.1.2 Molecular Biology reagents 78
2.1.3 Electronic Equipment 81
2.1.4 Cell culture reagents 81
2.1.5 Protein biochemistry reagents 83
2.1.6 Recipes of commonly used solution 84
2.2 Methods 87
2.2.1 Cell culture of HEK293T and MEF cells 87
2.2.2 Passaging of cells 87
2.2.3 Plating cells 87

2.2.4 Haemocytometer counting cells 88
2.2.5 Total protein cell lysis 88
2.2.6 HEK293T Transfection 88
2.3 Primary Neuronal Culture 89
2.3.1 Preparation of glass coverslips 89
2.3.2 PDL coating and borate buffer 89
2.3.3 Rat embryonic brain dissociation 90
2.3.4 Neuronal transfection 91
2.4 Western blotting 92
2.4.1 SDS-PAGE 92
2.4.2 Transfer 92
2.4.3 Immunoblotting 93
2.4.4 Chemiluminescence detection 93
2.5 Immunoprecipitations 94
2.5.1 Cell lysis 94
2.5.2 Pull Downs 94
2.6 Molecular biology methods 96
2.6.1 Bacterial transformation 96
2.6.2 Bacterial amplification and DNA purification 96
2.6.3 Polymerase Chain Reaction (PCR) 97
2.6.4 PCR product and vector digestion purification 98
2.6.5 RNA extraction 99
2.6.6 cDNA synthesis 99
2.6.7 Restriction digestion for ligation 100
2.6.8 Ligation 101

2.6.9 Cloning 101

2.7 *In vitro* deSUMOylation and deubiquitination assay 102

2.8 Oxygen/Glucose deprivation (OGD) 104

2.9 Imaging 105

2.9.1 Immunocytochemistry 105

2.9.2 DRP1 colocalisation analysis 106

2.9.3 Developing an ImageJ macro to analyse mitochondrial morphology 107

2.9.4 Branch analysis 112

2.9.5 Circularity analysis 113

2.9.6 Analysing neuronal mitochondrial area 114

2.9.7 Analysing neuronal density 115

2.9.8 Statistical analysis 116

Chapter 3 Characterising MFF SUMOylation 117

3.1 Introduction 118

3.2 Aims 119

3.3 Results 120

3.3.1 MFF is a novel SUMO substrate 120

3.3.2 MFF is SUMOylated at lysine 151 122

3.3.3 MFF K151R has reduced ubiquitination 126

3.3.4 MFF is not modified by SUMO-Ubiquitin chains 128

3.3.5 Phosphorylation of MFF enhances SUMOylation 131

3.3.6 Phosphorylation is upstream of SUMOylation 133

3.3.7 Phosphorylation and dephosphorylation of MFF at S155 and S172 have differential effects on SUMOylation 135

3.3.8 Phosphorylation at the AMPK sites enhances SUMOylation..... 139

3.4 Discussion..... 143

Chapter 4 Investigating the function of MFF SUMOylation ... 151

4.1 Introduction..... 152

4.2 Aims..... 154

4.3 Results..... 155

4.3.1 MFF SUMOylation promotes DRP1 binding..... 155

4.3.2 MFF phosphorylation null and mimetic mutants have reduced DRP1 binding 157

4.3.3 MiD49 contains a SUMO interacting motif..... 159

4.3.4 MFF phosphorylation reduces MiD49 binding 161

4.3.5 Oxygen/Glucose deprivation enhances global SUMO-2/3 conjugation, decreases SENP3 levels, and enhances MFF SUMOylation 165

4.3.6 MFF SUMOylation promotes DRP1 binding under mitochondrial stress 167

4.4 Discussion..... 169

Chapter 5 Exploring the role of MFF SUMOylation in Mitochondrial Morphology 179

5.1 Introduction..... 180

5.2 Aims..... 183

5.3 Results..... 184

5.3.1 MFF recruits/stabilises DRP1 at mitochondria 184

5.3.2 MFF is required to maintain mitochondrial morphology..... 186

5.3.3 MFF SUMOylation is required to maintain mitochondrial size and distribution in dendrites..... 189

5.4 Discussion 194

Chapter 6 General Discussion 204

6.1 Summary of Research 205

6.1.1 Regulation of MFF SUMOylation 205

6.1.2 MFF SUMOylation as a stress response 207

6.1.3 MFF SUMOylation – fine tuning the fission rate? 209

6.1.4 MFF SUMOylation in neurons 212

6.1.5 Mitochondrial morphology analysis 214

6.1.6 MFF and disease 215

6.2 Outstanding Questions 217

6.3 Future Work 218

6.4 Conclusions 222

Chapter 7 References 223

Chapter 8 Appendix 254

Chapter 1 General Introduction

1.1 Post translational modifications

Post translational modifications (PTM) bestows a rapid and dynamic layer of complexity to the proteome, allowing an expansion beyond the genome, from perhaps a few ten-thousand genes to over a million possible “proteoforms”(Smith *et al*., 2013; Vu *et al*., 2018). Once a protein is made, if unmodified, it is relatively stable and its structure is only altered by stochastic fluctuations in conformation, but PTMs allow alterations to a protein’s stability, interactions, activity, localisation and function. Eukaryotic physiology can thus be integrated and interconnected into the complexity of cell signalling pathways, and allows information processing, dynamic and fine-tuned responses to changing environmental contexts (Prabakaran *et al*., 2012; Spoel, 2018; Vu *et al*., 2018). Almost every protein is post translationally modified, and as such, PTMs regulate almost every biological process studied. Indeed, one of the most abundant modifications, phosphorylation, is mediated by kinases which account for 1.5-2.5% of eukaryotic genes (Manning *et al*., 2002), and the tumour suppressor protein p53 contains at least 50 sites of modification (Meek and Anderson, 2009), highlighting how wide-spread PTMs are.

Over 200 PTMs have been identified (Duan and Walther, 2015) and come in many forms, involving the reversible, covalent attachment of chemical groups (e.g. phosphorylation, acetylation), small polypeptides (e.g. ubiquitination, ubiquitin-like proteins) and addition of complex molecules (e.g. glycosylation) to amino acid residues of the primary polypeptide sequence (Spoel, 2018). A single protein can be modified in multiple ways, on multiple sites and at different times,

exponentially increasing the layers of complexity and modulation. This allows individual PTMs to coordinate and regulate one another, in a PTM “crosstalk” manner (Huang *et al*., 2015). Such multiple modifications are defined by the type of modification, the position of the covalent attachment, the effect it has on protein function, and on other PTMs (Nussinov *et al*., 2012; Vu *et al*., 2018). In this way, the number of modifications a single protein can harbour is vastly greater than the single product of the gene. Additionally, just as PTMs alter protein function and interactions, different protein complexes can therefore be formed and regulated by PTMs.

1.1.1 SUMOylation

Small ubiquitin-like modifier (SUMO) is a member of the ubiquitin-like family of proteins, which is enzymatically conjugated to lysine residues on target proteins. It is a small protein of ~11kDa with a globular structure similar to that of ubiquitin, however, unlike ubiquitin, is not implicated in the degradation of target proteins (Mahajan *et al*., 1997; Matunis *et al*., 1996). There are four isoforms of SUMO, designated SUMO-1 to SUMO-4. SUMO-2 and SUMO-3 share ~97% homology with each other, only differing in three N-terminal amino acid residues and are often denoted as SUMO-2/3, since they cannot be differentiated by current antibodies. SUMO-1 shares ~50% sequence homology with SUMO-2/3 (Flotho and Melchior, 2013; Wilkinson and Henley, 2010). SUMO-4 has ~87% sequence similarity to SUMO-2 and is unique in that it cannot undergo maturation and conjugation (Owerbach *et al*., 2005). The functional significance of this is not yet clear, and although only low levels of mRNA have been detected in kidney, spleen

and lymph nodes (Bohren *et al*., 2004; Guo *et al*., 2004), mature SUMO-4 has only been observed under extreme stress (Wei *et al*., 2008), However, no endogenous SUMO-4 protein has been detected, and a definitive role of SUMO-4 is lacking, although it has been proposed that SUMO-4 may interact non-covalently with target proteins to alter function (Owerbach *et al*., 2005). One group report a SUMO variant, termed SUMO-5, which has ~88% identity with SUMO-1, although further evidence is required to determine a role of this potential 5th SUMO isoform (Liang *et al*., 2016).

To date, all eukaryotes examined express at least one SUMO isoform, with *Caenorhabditis elegans, Drosophila* and *Saccharomyces cerevisiae* expressing only one. Higher eukaryotes express several SUMO isoforms, with humans expressing all four. Functionally, SUMOylation has been shown to play roles in many aspects of physiology, examples including, but are not limited to:

- the DNA damage response (Galanty *et al*., 2009; Morris *et al*., 2009)
- transcription factor regulation (Rosonina *et al*., 2017)
- chromosome segregation and nuclear architecture (Nacerddine *et al*., 2005)
- endocytosis of receptors (Martin *et al*., 2007)
- cytoskeletal rearrangements required for cell migration (Castillo-Lluva *et al*., 2010)
- regulation of mitochondrial function and dynamics (Guo *et al*., 2013, 2017; Prudent *et al*., 2015)

Indeed, it seems that each year, large scale mass spectrometry studies identify an increasing number of SUMOylated proteins, from ~1,600 proteins in 2014 (Hendriks *et al*., 2014), to >3,600 in 2016 (Hendriks and Vertegaal, 2016), to over 6,700 in 2017 (Hendriks *et al*., 2017).

Evidence for the importance of SUMOylation comes from knockout mouse studies, where Ubc9$^{-/-}$ (the sole SUMO E2 conjugating enzyme, abolishing all SUMO conjugation) mice die early post-implantation, demonstrating a critical need of SUMOylation during embryonic development (Nacerddine *et al*., 2005). Similarly, SUMO-2$^{-/-}$ mice are viable a little longer than Ubc9$^{-/-}$, but failed to develop past E10.5 (Wang *et al*., 2014). However, SUMO-1$^{-/-}$ and SUMO-3$^{-/-}$ mice are viable and show no overt phenotype (Wang *et al*., 2014; Zhang *et al*., 2008a), suggesting a compensatory effect among the SUMO isoforms.

Important functional distinctions were made between the SUMO isoforms by Saitoh and Hinchey, who identified that SUMO-2/3 make up a greater amount of the total cellular SUMO proteins, and that the majority is in a “free”, non-conjugated SUMO pool, while non-conjugated SUMO-1 was almost undetectable. Moreover, they show that following various cytotoxic insults (heat stress, oxidative stress by using H_2O_2) induced a substantial and dynamic increase in the degree of SUMO-2/3 conjugation, with a concomitant decrease in free SUMO-2/3. Upon recovery, after the stress was removed, SUMO-2/3 conjugation was reduced and the free SUMO-2/3 restored. No such change was observed for SUMO-1, suggesting SUMO-2/3 may function specifically as a stress-responsive pool of SUMO (Saitoh and Hinchey, 2000). Mass spectrometry analysis of proteins that

were SUMOylated by SUMO-2/3 following heat shock revealed many to be involved in apoptosis, cell cycle control, protein degradation, protein and DNA quality control. Remarkably, maximal SUMO-2/3 conjugation was reached within 5 minutes of insult, indicating SUMOylation is a very rapid response and fairly direct (Golebiowski *et al*., 2009). SUMO-2/3 levels increase following oxygen glucose deprivation (OGD), an *in vitro* model of ischemia (Guo *et al*., 2013) and depletion of SUMO-2/3 using siRNA in primary neurons increases vulnerability to ischemic stress, reducing neuronal viability and ATP levels (Datwyler *et al*., 2011). This reveals that SUMO-2/3 conjugation is involved in the stress response to various genotoxic and proteotoxic insults, which occurs rapidly and reversibly, and is involved in recovery and integrity of cells, whereas SUMO-1 has a constitutive function.

1.1.2 The SUMO-cycle

Conjugation

SUMO conjugation resembles that of ubiquitin, since it involves an E1 activating enzyme, E2 conjugating enzyme (Ubc9), and an E3 enzyme, which catalyses the transfer to the target protein, although Ubc9 is often sufficient for conjugation in the absence of an E3. SUMO proteins are synthesised as SUMO precursors, which must undergo cleavage at their C-terminus to expose a di-glycine motif, allowing conjugation. This activation step is carried out by a family of proteases called sentrin/SUMO-specific proteases (SENP). Once matured, SUMO is activated by formation of a thioester bond with the E1 enzyme in an ATP-dependent manner. E1 is a heterodimer formed of two subunits SAE1 and SAE2

(SUMO-activating enzyme 1/2) (Johnson *et al*., 1997). SUMO is then transferred to Ubc9, which binds directly to the target protein and conjugates SUMO to the target protein via an isopeptide bond (Desterro *et al*., 1997; Johnson and Blobel, 1997). The E3 enzymes appear to act as a scaffold between SUMO-loaded Ubc9 and the target protein and accelerate the rate of SUMOylation of the target protein. See Figure 1.1 for details.

Consensus Sequence

Unlike ubiquitination, SUMOylation of target proteins occurs at a consensus sequence: ψ-K-x-D/E, where ψ is a large hydrophobic residue and x is any amino acid. The consensus sequence enhances the interaction between the substrate and Ubc9 (Bernier-Villamor *et al*., 2002) Indeed, *in vitro* SUMOylation assays often only require a substrate containing a consensus sequence, Ubc9 and E1. Although it should be noted that not all proteins with a SUMO consensus motif are SUMOylated, and SUMOylation can also occur at non-consensus sequences (Hendriks and Vertegaal, 2016).

Deconjugation

In addition to maturing SUMO precursor proteins, SENP enzymes also remove SUMO. Mammals have six SENP enzymes (SENP1-3 and SENP5-7), which vary in their specificity of deconjugation; SENP1 can deconjugate both SUMO-1 and SUMO-2/3, whereas SENP2 favours SUMO-2/3, but can also deconjugate SUMO-1. SENP1 and SENP2 also are the major enzymes responsible for maturation of pre-SUMO. SENP3 and SENP5 favour deconjugating SUMO-2/3, as does SENP6 and SENP7, the latter two also having roles in SUMO chain

deconjugation and editing (discussed later in section 1.1.3) (Hickey *et al*., 2012). Other enzymes have also been identified to have deSUMOylating action; the deSUMOylation isopeptidase 1 and 2 (DeSI-1/2) can deSUMOylate both SUMO-1 and SUMO-2/3 *in vitro* but have no pre-SUMO activating activity (Shin *et al*., 2012), and there is little evidence of their targets.

The overall SUMOylation status of a protein is therefore a result of the opposing actions of Ubc9 and SENPs, and due to the importance of SUMOylation, tight regulation of conjugation and deconjugation is required under certain conditions and different contexts. For example, under basal condition, SENP3 is degraded by the ubiquitin system, however, following mild oxidative stress, SENP3 levels are stabilised and it translocates to the nucleus where it deSUMOylates p300, a co-activator of HIF-1α, which promotes transcription of stress responsive genes. SUMOylated p300 is inactive, and so upon SENP3 levels increasing, the SUMO-mediated repression is relieved and HIF-1α promotes the transcription of stress responsive genes (Huang *et al*., 2009). On the other hand, following OGD, SENP3 is rapidly degraded, with a concomitant increase in global SUMO-2/3 levels. A major target of SENP3 is dynamin related protein 1 (DRP1), which is involved in mitochondrial fission. During OGD, DRP1 is SUMOylated by SUMO-2/3 and inactivated. Upon reperfusion, SENP3 levels are restored, DRP1 is deSUMOylated and translocates to the mitochondria to promote mitochondrial fission (Guo *et al*., 2013).

Oxidative stress can affect the SUMOylation machinery in multiple ways; at 15 minutes treatment of a low dose of H_2O_2, SUMO conjugation is increased,

however, following lethal doses for the same amount of time, SUMOylation is reduced. High concentrations of H_2O_2 can inhibit SUMOylation by forming a disulphide bond between the cysteine active sites of E1 and E2, thus inactivating the SUMO conjugation machinery, and H_2O_2 also oxidises SENP3, protecting it from proteasomal degradation. At lower doses, ROS can inactive SENPs by forming disulphide bonds between SENP dimers, rendering them inactive. Secondly, ROS can increase binding between the target protein and the E3 enzyme (Stankovic-Valentin *et al*., 2016). SUMO conjugation and deconjugation is reviewed in Flotho and Melchior, 2013; Hay, 2005; Wilkinson and Henley, 2010.

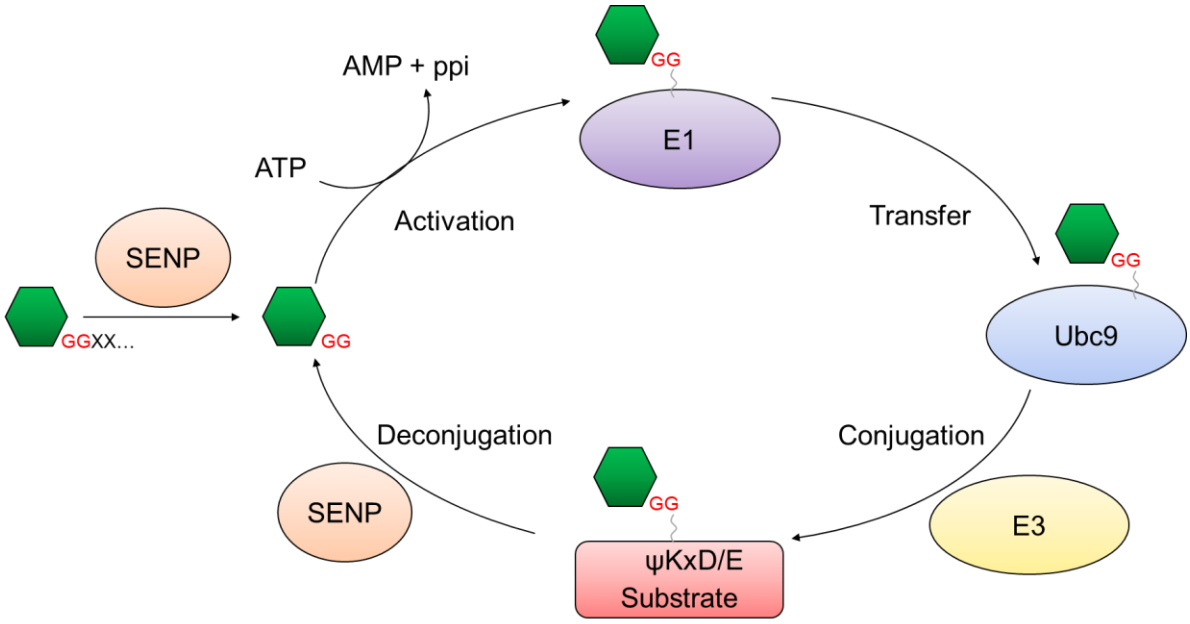

Figure 1.1 The SUMO cycle

Schematic of reversible SUMOylation of a target protein. SUMO precursor protein (green hexagon) is matured by SENP enzymes to expose the C-terminal di-glycine (GG) motif. SUMO is activated in an ATP-dependent manner and forms a thioester bond with the heterodimeric activating E1 enzyme. SUMO is transferred to the E2 Ubc9 enzyme, which then catalyses isopeptide bond formation with the target protein at the SUMO consensus motif ψ-K-x-D/E, possibly with a specific E3 enzyme. SUMO is enzymatically cleaved from its target protein via SENP enzymes to release SUMO, which is then available for further cycles.

The SUMO enigma

SUMOylation is a very dynamic, labile and readily reversible PTM, and as such, detecting endogenous SUMOylation can be a challenge, and to do so requires inhibition of the SENP enzymes and/or strong denaturing conditions. It is often the case that only a small proportion of the available protein substrate is SUMOylated at a given time, as observed for HIF-1α (Matic *et al*., 2008) and GluR6 (Martin *et al*., 2007). However, SUMO mutants have substantial impacts on protein function. So how can such a small pool of SUMOylated proteins exert their effects? This has become known as the “SUMO enigma”, proposed by R. Hay (Hay, 2005). Taking transcription factors (TF) as an example, SUMOylation often leads to their repression, and the SUMO-TR may associate within a repression complex. But upon deSUMOylation, the TF is still retained in the repressive state, and only upon disassembly of the complex will the SUMO-mediated repression be relieved. Therefore, in this example, SUMOylation is only required to initiate inhibition, not to maintain repression, and so SUMO-induced changes persist after deSUMOylation has occurred. This hypothesis offers an explanation to the small proportion of substrate modified, but over a period of time, many protein molecules will undergo SUMOylation and the consequences of this modification persist after its removal (Hay, 2005; Wilkinson and Henley, 2010).

1.1.3 Poly-SUMO chains

SUMO-2 and SUMO-3 contain internal SUMOylation consensus motifs at K11, and so themselves can be SUMOylated. Therefore, like ubiquitin, SUMO can form chains, as has been shown *in vitro* and *in vivo* (Matic *et al*., 2008; Tatham *et al*., 2001). SUMO-1 does not contain the typical SUMO consensus site and does not share SUMO-2/3's ability to undergo SUMO chain formation. However, SUMO-1 is incorporated into SUMO chains, and acts as a terminator of SUMO-2/3 chains, since addition of SUMO-1 abrogates elongation of SUMO-2 chains *in vitro*, preventing excessive SUMO chain formation (Matic *et al*., 2008). It was discovered that SUMO-1 contains an inverted SUMO consensus site (D/E-x-K-ψ), which can form atypical SUMO chains. However, this has only been detected by mass spectrometry and may only occur at low levels and low efficiency (Matic *et al*., 2010) and the physiological relevance of such chains are unknown.

Among the initial poly-SUMO substrates identified were HIF-1α, which contains two SUMO sites (K391, K477) and is poly-SUMOylated by SUMO-2 at K391, forming a chain of up to eight SUMO proteins (Matic *et al*., 2008). Histone deacetylase-4 (HDAC4) contains a single modifiable lysine at 559, which can be mono-SUMOylated by SUMO-1, and also modified by a chain of two SUMO-2 molecules (Matic *et al*., 2008; Tatham *et al*., 2001).

One of the first SUMO substrates identified was PML (promyelocytic leukaemia protein) (Boddy *et al*., 1996, 1997), a defining protein of PML nuclear-bodies (PML-NB), which are discrete nuclear multi-protein structures, with roles in DNA damage response, apoptosis and the cell cycle (Hsu and Kao, 2018).

SUMOylation of PML at K160 by SUMO-1 is essential for the recruitment of other PML-NB proteins and for the stability and formation of the structure (Eskiw *et al*., 2003; Zhong *et al*., 2000). SUMO-3 is also an essential component of PML-NB, and knockdown of SUMO-3 liberates PML from the PML-NB, a phenotype that could not be rescued by SUMO-1 overexpression, indicating that the SUMO isoforms have distinct functions in this context. In addition, expressing SUMO-2 and SUMO-3 K11R mutants (which cannot form poly-SUMO chains) reduced the number of PML-NB in the nucleus, suggesting that SUMO conjugation is required for PML-NB formation and stability (Fu *et al*., 2005). SENP6 favours the deconjugation of SUMO-2/3 chains, and reduction in SENP6 activity by depletion or expression of a catalytic mutant increases SUMO-2/3 conjugation. This leads to SUMO accumulation in the nucleus, and an increase in the size and number of PML-NB formed, with PML specifically identified to be a poly-SUMO substrate and a target of SENP6 (Hattersley *et al*., 2011).

SUMO-1 and SUMO-2/3 localises to different structures during the cell cycle, and global SUMO-1 conjugation is low throughout mitosis and increases as cells re-enter G1. SUMO-2/3 is reduced early in mitosis, but increases during cell division. This indicates that SUMO-1 and SUMO-2/3 are differentially regulated and conjugate to different subpopulations of proteins. Centromere protein-E (CENP-E) is a microtubule motor protein that localises to the kinetochore during mitosis and ensures correct chromosomal alignment. This localisation is dependent on CENP-E non-covalently interacting with SUMO-2/3 chains. Interestingly, CENP-E has no binding capacity for mono or poly-SUMO-1 chains, indicating that the

SUMO paralogs and chain length facilitate different interactions (Zhang *et al*., 2008b).

These reports demonstrate that SUMOylated proteins can undergo both mono and poly-SUMO events, and in some cases at the same residue. In general, SUMOylation functions to alter protein-protein interactions, by masking an interaction site, or competing with other PTM, such as ubiquitin (Desterro *et al*., 1998; Ulrich, 2008). However, it is hard to see how a poly-SUMO chain could achieve this function more efficiently than a mono-SUMO event. It seems that increasing the local concentration of SUMO by chain formation can act as a "hub" for recruitment of other factors, as highlighted with PML, and also recruits specific factors with the capacity to bind chains of certain SUMO isoform and length, as highlighted with CENP-E.

1.1.4 Co-regulation of SUMO and phosphorylation

The tetrapeptide of the SUMO consensus site (ψ-K-x-D/E) is all that is required for SUMOylation of a substrate *in vitro*. However, proteins with this site are not SUMOylated all the time, indicating additional layers of regulating SUMOylation. Hendricks *et al* identified that in over 6,000 SUMOylated proteins, 807 were co-modified by phosphorylation (Hendriks *et al*., 2017). SUMO and phosphorylation pairs occurred in close proximity to each other, usually in the +4 and +5 position, with respect to the lysine (ψ-K-x-E-x-(x)-S), (Hendriks *et al*., 2018; Hietakangas *et al*., 2006). The interaction between SUMOylation and phosphorylation has been extensively investigated in transcriptional regulators. HSF-1, HSFb, GATA-1 and MEF2A all contain a ψ-K-x-E-x-x-S motif, and phospho-mimetics enhance

SUMOylation, whereas phospho-null mutants have decreased SUMOylation, demonstrated *in vivo* and *in vitro*. The finding that SUMOylation is regulated *in vitro* with phospho-mimetics, the assay involving just the E1, E2, (and E3 in some cases), SUMO-1 and either wildtype, phospho-mimetic or phospho-null mutants, demonstrates that phosphorylation-mediated SUMOylation is due to enhanced SUMO conjugation, and not reduced deSUMOylation. Phosphorylation dependent SUMO motif (PDSM) is used to describe the amino acid sequence ψ-K-x-E-x-(x)-S, where phosphorylation promotes SUMOylation, and is a good predictor of positive regulation of SUMOylation (Hietakangas *et al*., 2003, 2006), see Figure 1.2 for schematic.

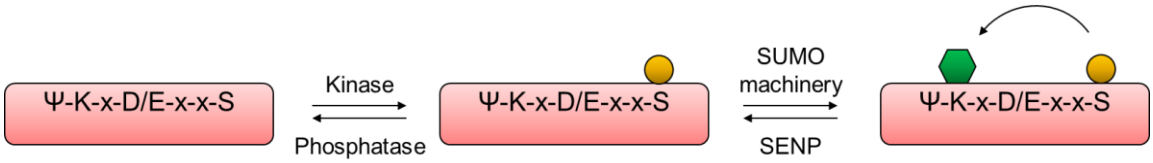

Figure 1.2 Phosphorylation-dependent SUMOylation

Schematic of phosphorylation dependent SUMOylation (PDSM). SUMO substrates containing a PDSM motif (ψ-K-x-E-x-(x)-S) can be phosphorylated at the +4 or +5 site, which enhances the recruitment of the SUMO machinery, promoting SUMOylation. The regulation of SUMOylation is therefore a balance between the phopshorylation pathway i.e. the relative activity of kinases and phosphatases, and the activation of the SUMO pathway i.e. E1, Ubc9 and E3, and the SENP deconjugating enzymes.

In most cases, SUMOylation reduced transcriptional activity (Collavin *et al*., 2004; Hietakangas *et al*., 2006), but the mechanisms appear to differ. For example,

MEF2C SUMOylation at K391, promoted by phosphorylation at S396, does not affect its DNA binding ability, and has been proposed to recruit, as yet unknown, transcriptional repressors (Kang *et al*., 2006). Conversely, HSF-1 SUMOylation at K298 increased by phosphorylation at S303, increases following heat stress and is required for formation of nuclear bodies, DNA binding ability and transcription of stress related genes. The non-SUMOylatable mutant K298R and phospho-null mutant S303A lacked all SUMO recruitment, transcriptional activity and nuclear body formation under stress (Hietakangas *et al*., 2003; Hong *et al*., 2001).

Non-PDSM regulation of SUMOylation by phosphorylation

Phosphorylation has also been shown to enhance SUMOylation from a distal site, and so does not conform to the PDSM motif. For example, signal transducer and activator of transcription 1 (STAT1) is phosphorylated at S727 and SUMOylated by SUMO-1 at K703. STAT1 is activated by phosphorylation, mediated by the stress response pathway p38 MAPK. Phosphorylation at S727 increases SUMOylation, whereas inhibition of this pathway leads to dephosphorylation, which abrogates SUMOylation. Therefore, SUMOylation of STAT1 appears to promote activity (Vanhatupa *et al*., 2008), although other reports suggest SUMOylation inhibits activation (Grönholm *et al*., 2012). The nuclear factor erythroid-derived 2 (NF-E2) is a heterodimer of the subunits p45 and p18, and phosphorylation by PKA enhances complex formation and activity. Both subunits can be SUMOylated and phosphorylated, and *in vitro* experiments showed that PKA phosphorylation of p18 increased SUMOylation in a dose-dependent

manner, and that PKA phosphorylation of p45 enhances SUMOylation only when forming a heterodimer with p18 (Su *et al*., 2012).

Although phosphorylation dependent SUMOylation has primarily been investigated in transcription factors, there is evidence that it can also occur outside the nucleus. The kainate receptor subunit GluR6 is phosphorylated by PKC at S868 and S846 in response to agonist activation, promoting SUMOylation at K886, which is required for receptor endocytosis, again demonstrating that distal phosphorylation events can regulate SUMOylation (Chamberlain *et al*., 2012; Konopacki *et al*., 2011; Martin *et al*., 2007).

Phosphorylation negative regulation of SUMOylation

Phosphorylation not only promotes SUMOylation but can also negatively regulate SUMOylation. The transcription factors c-Jun and p53 are SUMOylated by SUMO-1 at K229 and K386, respectively, which negatively regulates transcriptional activity. Unlike the PDSM, phosphorylation occurs at distal sites (S63/S73) in c-Jun, whereas p53 is hyperphosphorylated at multiple sites by many different pathways (Meek and Anderson, 2009), and inhibition of serine/threonine phosphatases prevented the formation of SUMO-1-p53 (Müller *et al*., 2000). The ETS domain transcription factor (Elk-1) is phosphorylated by the MAP kinase pathway, triggering its activation. Stimulation of the MAPK pathway increases Elk-1 phosphorylation, with a concurrent decrease in SUMOylation. Conversely, SUMO-1-Elk-1 represses activity, indicating that the phosphorylation event relieves repression by inhibiting the SUMOylation of Elk-1. It was further shown that the reduced SUMOylation is not a general reduction in

the SUMO pathway, since other SUMO targets remain unaffected, therefore this is specific regulation of Elk-1 (Yang *et al*., 2003).

The mechanism of such distal regulation is not clear. It is possible that the conformation of a protein may bring distal phosphorylation sites close to SUMOylation sites in such a way as to promote SUMOylation in a similar manner to the PDSM. Additionally, conformational changes may expose or hinder the access to SUMOylation sites. Alternatively, phosphorylation may promote or inhibit the binding of factors which increase the capacity for SUMOylation or may regulate the recruitment of the deconjugation machinery.

These reports demonstrate significant crosstalk between phosphorylation and SUMOylation, and that phosphorylation can either positively or negatively regulate SUMOylation. This increases our understanding of the complexity of PTMs, and that phosphorylation and dephosphorylation pathways, together with SUMOylation and deSUMOylation pathways regulate the overall “PTM signature” of a protein, thus determining the biological function.

1.1.5 SUMO-ubiquitin hybrid chains

There is ~26% overlap between SUMOylated and ubiquitinated lysine residues (Hendriks and Vertegaal, 2016), indicating that not only SUMOylation targets lysines of the SUMO consensus motif, but they can also be ubiquitinated, and likewise, lysines that are ubiquitinated can also be SUMOylated. Indeed, SUMO and ubiquitin can compete for the same lysine, having differential functions, as exemplified in the regulation of IκBα, the inhibitor of the transcription factor NF-κB. IκBα usually forms a complex with NF-κB in the cytosol, with IκBα being mono-

SUMOylated by SUMO-1 at K21. Upon an appropriate signal, IκBα becomes mono-ubiquitinated at K21, initiating its degradation, release of NF-κB and transcription activation (Desterro *et al*., 1998).

SUMO-targeted ubiquitin ligases

A further step in our understanding of the interplay between ubiquitin and SUMO came from yeast studies, which identified a class of ubiquitin ligases (Ubl) that promote ubiquitination and degradation of SUMOylated proteins. The yeast ubiquitin ligase (ULS) families ULS1 and ULS2 were identified to promote ubiquitination and degradation of SUMOylated proteins, since their deletion results in an accumulation of SUMO conjugates, genome instability, reduced cell growth and increased sensitivity to genotoxic stress (Prudden *et al*., 2007; Sun *et al*., 2007; Uzunova *et al*., 2007). ULS proteins, also called SUMO targeted ubiquitin ligases (STUbL), contain two structural characteristics; a RING finger domain, which mediates the interaction with a ubiquitin E2 enzyme, and a SUMO interacting motif (SIM), which non-covalently interacts with the SUMO protein (Sriramachandran and Dohmen, 2014). A SIM is a short hydrophobic motif (ψ-x-ψ-ψ or ψ-ψ-x-ψ) where ψ=V/I/L, which is often juxtaposed to a cluster of acidic residues, and is thought to form a β-sheet and interact within a groove between an α-helix and a β-sheet of SUMO (Kerscher, 2007). Many of the STUbLs have multiple SIMs, and therefore can interact with multiple SUMO molecules within a poly-SUMO chain. Indeed, SUMO-2/3 chains are preferentially targeted for ubiquitination, raising the possibility that SUMO chains are targets for proteolytic degradation via a STUbL mechanism (Uzunova *et al*., 2007).

The most studied and highly conserved eukaryotic STUbL is RNF4 (Sun *et al*., 2007). RNF4 functions as a homodimer and contains three SIM motifs, which favour the binding to poly-SUMO chains of at least three SUMO proteins (Tatham *et al*., 2008). The first substrate of RNF4 ubiquitination to be identified was poly-SUMOylated PML. As discussed earlier, SUMOylated PML is important for NB formation in response to stress. RNF4, ubiquitin and proteasomes are recruited to NB, where RNF4 binds to poly-SUMOylated PML and ubiquitinates the SUMO chain, initiating PML proteasomal degradation. Conversely, inactive RNF4 or non-SUMOylatable PML prevents PML SUMO-ubiquitin mediated degradation and results in abnormal PML-NB formation (Lallemand-Breitenbach *et al*., 2008; Tatham *et al*., 2008).

Additional roles for RNF4 have been implicated in the DNA damage response; following DNA double stand breaks, DNA damage factors are recruited. The RNF4 SIM motifs and ubiquitination function were shown to be important for clearance of the nuclear foci and recruitment of stress response factors (Yin *et al*., 2012). Interestingly, RAP80, a component of the BRAC1-A complex (breast cancer type 1 susceptibility protein) targets BRAC1-A to sites of DNA damage. RAP80 contains two ubiquitin interacting motifs (UIM) and a SIM, and is recruited to SUMO-ubiquitin hybrid chains formed by RNF4 (Guzzo *et al*., 2012). These findings suggest that both SUMOylation and ubiquitination function in concert to degrade proteins, but also act as a recruitment platform to form protein complexes. See Figure 1.3 for schematic of the role of SUMO-ubiquitin chains.

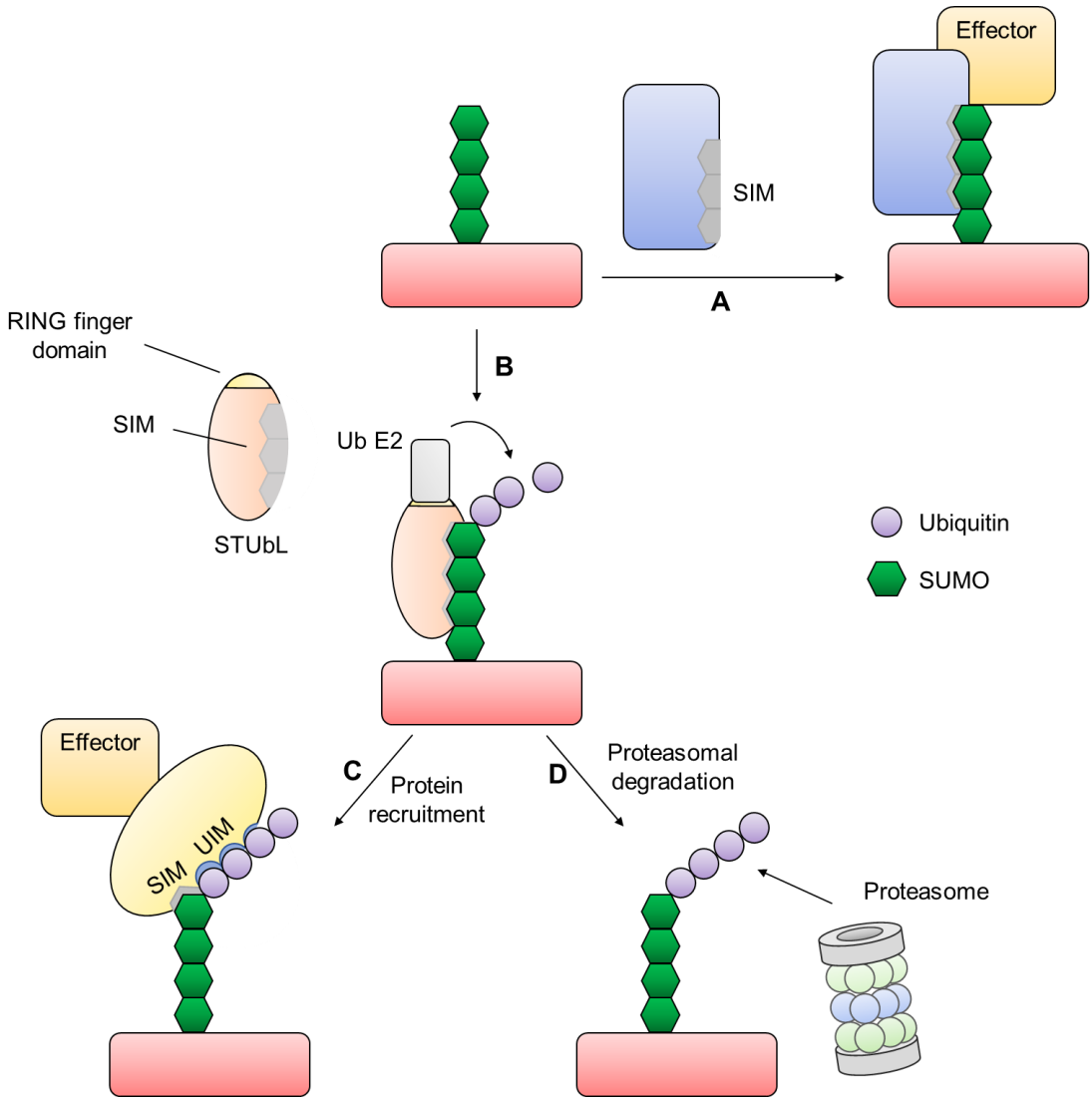

Figure 1.3 SUMOylation can initiate multiple downstream effects

Schematic of the varied outcomes of SUMOylation. **A** SUMOylation can act to recruit proteins containing a SUMO interacting motif (SIM) which will bind non-covalently and can recruit further effector proteins to carry out cellular functions. **B** SUMO chains can also be ubiquitinated by SUMO targetted ubiquitin ligases (STUbL) which contain SIM motifs to bind to the SUMO molecules, and a RING domain to recruit ubiquitin E2 ligases. The SUMO-ubiquitin chain can recruit proteins containing SIM and ubiquitin interacting motifs (UIM), which can then recruit further downstream effector proteins or be a signal for targetting to the proteasome for degradation (**D**).

A key feature of ubiquitin is that is has seven lysines, all of which can be ubiquitinated. By far the major linkage are K48-linked chains, often >50% of all ubiquitin chains, which are classically thought to be involved in degradation. However, non-degradative roles of ubiquitin have emerged. For example, K6 and K11-linkages are placed on depolarised mitochondria by the ubiquitin E3 ligase parkin, having roles in mitochondrial degradation by mitophagy (Durcan *et al*., 2014; Ordureau *et al*., 2014). K27-linkages serve as a platform for the recruitment of DNA damage response proteins, K33-linkages have been implicated in Golgi trafficking, whereas K63-linkages are involved in inflammatory responses, lysosomal targeting and NF-κB activation (Komander and Rape, 2012). An additional layer to SUMO-ubiquitin chains was the finding that the chains are not necessarily linear, but can form complex branches, as identified in mass spectrometry studies (Hendriks and Vertegaal, 2016; Lamoliatte *et al*., 2014). Moreover, K6, K11, K27, K48 and K63 of ubiquitin can also be SUMOylated, adding greater complexity and specificity to SUMO-ubiquitin chains, and increasing the possible intertwining of these modifications. See Figure 1.4 for schematic of SUMO-ubiquitin chains.

The differential ubiquitin linkages, and their distinct functions and cellular outcomes have been termed the “ubiquitin code”, taking nomenclature from the histone field, and have been extensively reviewed in Komander and Rape, 2012; Swatek and Komander, 2016; Yau and Rape, 2016.

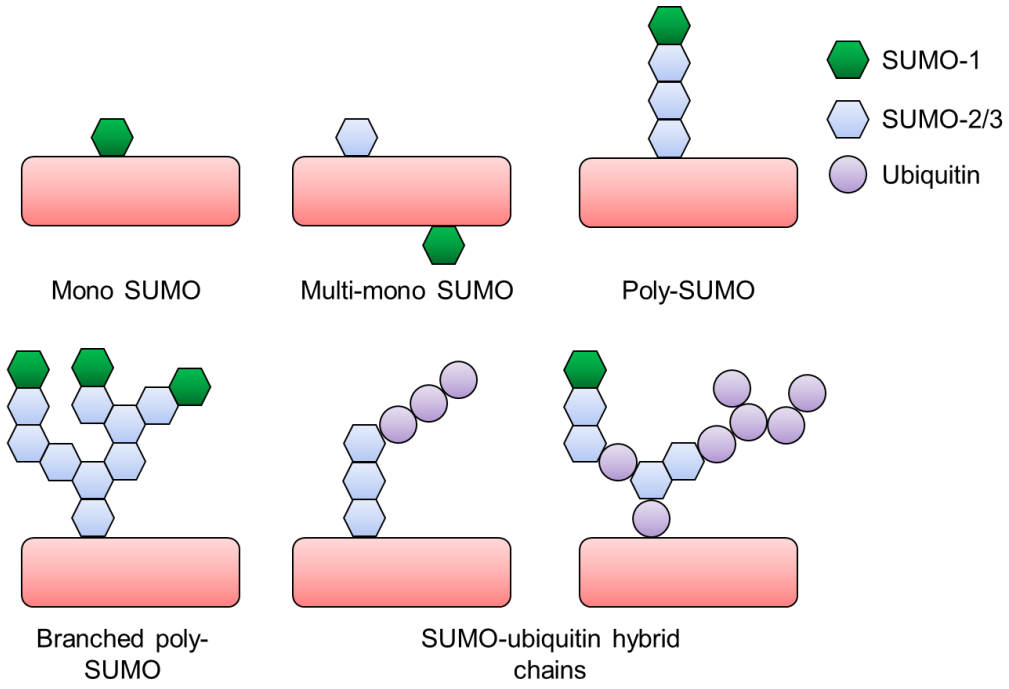

Figure 1.4 The complex SUMO-ubiquitin "code"

Conceptual representation of possible SUMO and SUMO-ubiquitin modifications. SUMOylation modifications can take place on one lysine of a target protein (mono-SUMO) or on multiple sites (multi-mono SUMO events). SUMO-2/3 can be SUMOylated, forming chains which are "capped" by SUMO-1. SUMO can be modified by ubiquitin, and ubiquitin can be modified by SUMO, forming many possible linear or branched hybrid chains.

1.2 Mitochondria

For four billion years life has existed on Earth, but up until 1.5-2 billion years ago, life remained single-celled and relatively simple (Lane, 2015). A eukaryotic progenitor cell engulfed a free-living α-proteobacterium, forming an endosymbiotic relationship (Gray *et al*., 1999). The engulfed bacterium was assimilated and became the ancestor of modern-day mitochondria. The union of the two genomes allowed an expansion of possible genes on which the cell can evolve, and the additional energy supplied by the proto-mitochondria supported new gene expression. It is thought that this event precipitated a turning point in evolution, whereby multi-cellular, complex life diverged from single-celled life due to the acquisition and assimilation of mitochondria (Lane and Martin, 2010).

Like their bacterial ancestors, modern mitochondria have retained the core machinery of generating the energy currency of the cell, in the form of adenosine triphosphate (ATP) via oxidative phosphorylation (OXPHOS). Mitochondria are also composed of a double membrane, creating two spatially and functionally distinct compartments; the matrix, enveloped by the inner membrane is the site of many biochemical processes, for example the tricarboxylic acid cycle (TCA) cycle, and the intermembrane space (IMS), forms the partition between the outer and inner membranes and is where the proton-motive force (PMF) is generated to produce ATP (illustrated in Figure 1.5). Although during evolution the proto-mitochondria lost much of its genome via gene transfer to the host, the mitochondrial DNA (mtDNA) still retains a small number of genes, contained in small, circular nucleoids, in multiple copy number. The mtDNA is ~16.6kb in

length and codes for 13 proteins, fundamental components of the OXPHOS machinery, 22 tRNAs and 2 mitochondrial rRNAs (Friedman and Nunnari, 2014).

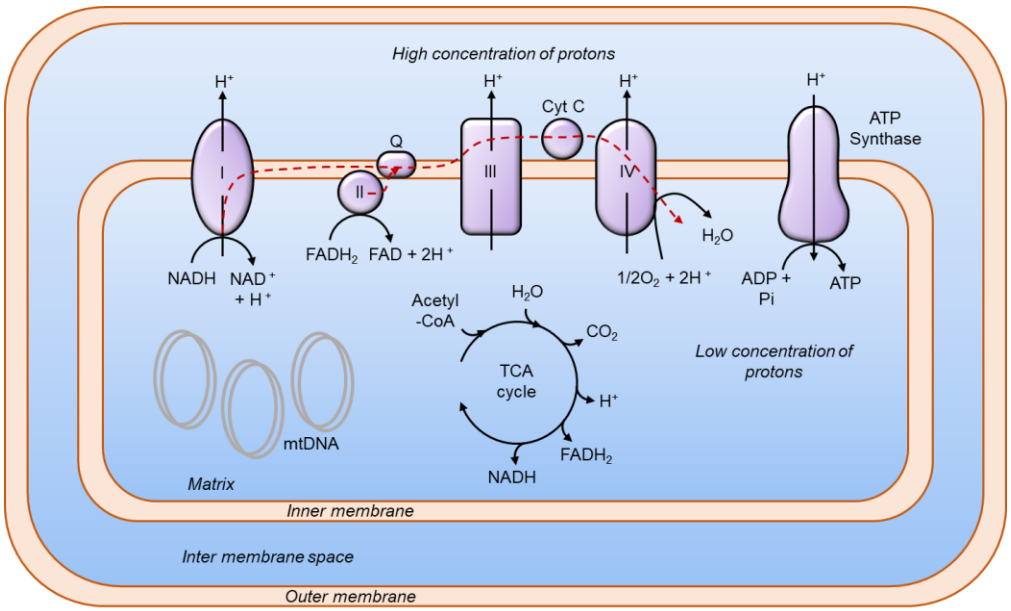

Figure 1.5 Mitochondrial compartments

Schematic of the outer and inner membranes of the mitochondria, and the processes that take place in each compartment. The inner membrane and inter membrane space (IMS) is the site of the electron transport chain. Electrons and protons are extracted from NADH and $FADH_2$, which are generated from the TCA cycle in the matrix, and protons are pumped across the inner membrane to the IMS, generating a differential concentration gradient of protons, known as a chemi-electric gradient, or proton-motive force (PMF). The electrons are transferred from one multi-subunit complex to the next, and passed to oxygen as the final electon acceptor at complex IV, in turn generating water. The high concentration of protons is used to power the molecular turbine ATP-Synthase, which uses the dissipation of the PMF to generate ATP from ADP and Pi. The matrix is the site of many biochemical processes, one of which is the TCA cycle, and it also houses multiple copies of mtDNA (Lodish *et al*., 2007).

It is a common misconception that mitochondria exist as static, isolated, “bean-shaped” structures floating in the cytosol. Indeed, this is often how they are depicted in textbooks, but with improved imaging technologies and live cell imaging, it is now appreciated that mitochondria can take on a plethora of different structures, which is both context and cell type specific. For instance, mitochondria in cardiomyocytes occupy over 30% of the cellular volume and are organised in a tight, compact manner and appear immobile (Piquereau *et al*., 2013), whereas in neuronal axons the mitochondria are actively transported to distal regions of the neurites and are sparse and punctate in nature (Cagalinec *et al*., 2013; Chang *et al*., 2006). Many other cell types, such as fibroblasts, exhibit mitochondria that are cellular-wide, tubular, mobile and interconnected (Liesa *et al*., 2009; Tilokani *et al*., 2018). In light of this dynamic nature, the mitochondria are not considered as isolated structure, but rather an interacting and inter-connected network, sometimes referred to as the mitochondrial reticulum (Glancy *et al*., 2015; Mattie *et al*., 2019). As a result, fixed cell imaging of mitochondria only provides a “snap-shot” of the mitochondrial network at a single moment in time, and the mitochondria appear as a heterogenous population, existing in multiple states and forms (Hewitt and Whitworth, 2017). Indeed, the word “*Mito-chondria*”, coined in the late 19th century, derives its origins from the Greek words “*mitos*”, meaning thread, and “*chondros”*, meaning grain, alluding to the mitochondrial networks many and varied morphologies, which were recognised over 100 years ago (Benda, cited in Liesa *et al*., 2009).

Beyond OXPHOS, mitochondria have gained a plethora of cellular functions, such as β-oxidation of fatty acids, lipid, steroid, nucleotide, amino acid, Fe-S clusters and heme synthesis, Ca^{2+} homeostasis, integrators of nutrient supply and metabolic demand, innate immunity and are executioners of programmed cell death (McBride *et al*., 2006; Nunnari and Suomalainen, 2012; Osellame *et al*., 2012). It is estimated that mitochondria are composed of over 1000 different proteins (Calvo *et al*., 2016), the vast majority are nuclear-encoded mitochondrial genes, and since mitochondria cannot be generated *de novo*, import machinery is responsible for the transport of proteins and lipids to the mitochondria (biogenesis), and likewise, removal and quality control mechanisms are in place to ensure a healthy population of mitochondria. Due to the integration with many cellular signalling pathways and the numerous functions of mitochondria, it is not surprising that any dysfunction in mitochondrial biology can lead to cellular stress, which can manifest as disease (Nunnari and Suomalainen, 2012).

1.2.1 Mitochondrial Dynamics

Mitochondrial dynamics is a term to define the varied behaviours mitochondria exhibit, namely fusion, fission (division) and transport, processes which take place along the cytoskeletal tracks of the cell, although this term can also describe broader behaviours such as mitophagy (selective mitochondrial degradation by autophagy), cristae remodelling, recycling, endoplasmic reticulum-mitochondrial contact sites and biogenesis (Dorn, 2018; Eisner *et al*., 2018; Pernas and Scorrano, 2016). The many behaviours of mitochondrial network morphology help to balance energy supply and demands, localise mitochondria to sites of high energy expenditure and remove damage. The shape of mitochondria is regulated by two opposing forces; fusion and fission. Fusion involves the union of two mitochondria, whereas fission is the division of a single mitochondrion into two daughter mitochondria. The relative rates of these processes therefore dictate the overall structure of the mitochondrial network.

Under basal conditions, the mitochondria constantly undergo cycles of fusion and fission, the rates of which equal each other, with no net change in morphology (Detmer and Chan, 2007; Twig *et al*., 2008a). However, the rates can be adjusted to favour one process or the other; increasing fusion, or decreasing fission, will lead to unopposed fusion and result in a more connected network. On the other hand, increasing fission, or inhibiting fusion, will result in a more fragmented mitochondrial network. Figure 1.6 shows examples of the extreme differences in mitochondrial morphology during unbalanced fusion and fission.

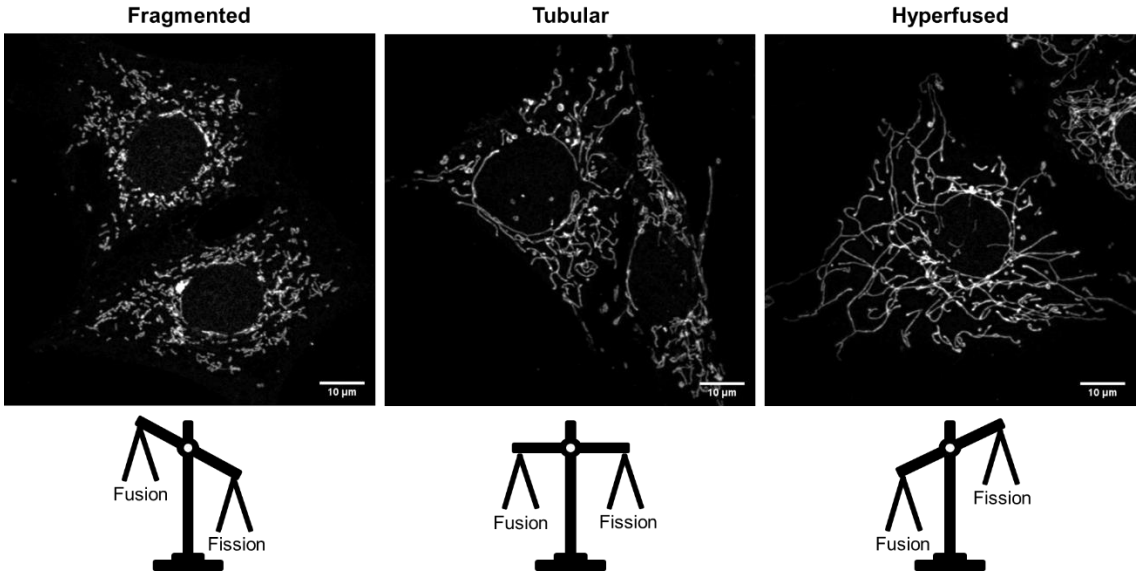

Figure 1.6 The fusion and fission balance determine mitochondrial morphology

Confocal images of MEF cells displaying differerent mitochondrial morphologies. Under basal conditions, the mitochondrial network exists as a mixture of short and long tubular structures, some isolated and some fused, to form multiple branched structures (centre panel). Increasing fission or decreasing fusion will lead to unopposed fission, reduced connectivity and more fragmented, shorter mitochondria (left panel). Increasing fusion or inhibiting fission will lead to unopposed fusion and result in increased connectivity and longer mitochondra (right panel). Scale bar 10µm.

But why do the mitochondria undergo continuous, energy demanding cycles of fusion and fission in the first place? And why would the mitochondrial network need to change structure?

1.2.2 The mitochondrial lifecycle

Outlined below are the reasons for continuous cycles of fusion and fission. The major reason is to maintain a biochemically and functionally homogenous population of mitochondria, and to segregate and remove damage.

Alterations in mitochondrial dynamics is very context specific, and the mediators of fusion and fission are highly regulated to coordinate mitochondrial morphology (discussed in section 1.3).

Fusion

Mitochondrial fusion is a fundamental mitochondrial process, conserved in all eukaryotic cells, from yeast to humans (Hales and Fuller, 1997) and is essential for life, since disruption of mitochondrial fusion is embryonically lethal (Chen *et al*., 2003). Fusion is also important to:

- mixing and complementation of mitochondrial components, such as protein, lipids and mtDNA, to compensate for any mitochondria that are operating at a sub-optimal level (Youle and Van Der Bliek, 2012)
- maintain mtDNA copy number and replication fidelity (Chen *et al*., 2003, 2005)
- increase ATP production during G2 phase of the cell cycle to support cell growth (Martínez-Diez *et al*., 2006)
- mitochondrial elongation (increased fusion) protects cells from apoptosis and maintains ATP levels during starvation stress (Gomes *et al*., 2011; Neuspiel *et al*., 2005; Olichon *et al*., 2003; Sugioka *et al*., 2004).

- increasing fusion during stress prevents mitophagy, maintains OXPHOS and preserves mitochondrial integrity, known as stress-induced mitochondrial hyperfusion (SIMH) (Wai and Langer, 2016)

A single mitochondrion can contain thousands of copies of mtDNA, but they are not all genetically identical (termed heteroplasmy) because of inherited or acquired mutations (Stewart and Chinnery, 2015). Low level (<1%) mutant mtDNA is common among healthy individuals (Elliott *et al*., 2008), which does not manifest as disease because fusion is sufficient to compensate and restore mitochondrial function (Nakada *et al*., 2001; Ono *et al*., 2001). If the level of pathogenic mtDNA mutations exceeds a threshold (>60-80%), then the efforts of fusion to compensate for the damage are overwhelmed and the mitochondria becomes biochemically compromised. Indeed, high mtDNA mutational loads accelerate ageing in mice (Ross *et al*., 2013; Trifunovic *et al*., 2004) and are also implicated in human neurodegenerative disease (Bender *et al*., 2006). The existence of mtDNA repair machinery within mitochondria is well established, and like the nuclear genome, mtDNA can undergo repair (e.g. base excision repair), and there is some evidence suggesting other mechanisms typical of nuclear DNA repair exist in mitochondria (i.e. homologous recombination), however, the mechanisms of such repair pathways require further investigation, reviewed in Zinovkina, 2018.

Pioneering work by Twig *et al.* used live cell imaging of fluorescently labelled mitochondria to show that fusion of mitochondria is not a random process but is selective. Tracking mitochondria between successive fusion-fission events

demonstrated that fusion occurs only between mitochondria with high membrane potentials, thus presumably with high functionality and integrity (Twig *et al*., 2008a). Using photoactivatable fluorophores, which can selectively activate 10-20% of the mitochondria in a cell, complete diffusion of the fluorophore occurs within ~45 minutes, and fusion events for a single mitochondrion occur once every 5-20 minutes, demonstrating this is a very active and rapid process (Karbowski *et al*., 2004; Twig *et al*., 2008a, 2008b).

Fission

On the other hand, fission is important to:

- ensure equal distribution of mitochondria to daughter cells during mitosis (Martínez-Diez *et al*., 2006; Taguchi *et al*., 2007)
- generate sufficiently small mitochondrial units for transport, particularly important in polarised cells such as neurons (Cagalinec *et al*., 2013; Lewis *et al*., 2018; Li *et al*., 2004; Verstreken *et al*., 2005)
- isolate mitochondria before mitophagy (selective mitochondrial autophagy) to fit mitochondrial fragments into the autophagosome (Kageyama *et al*., 2014; Tanaka *et al*., 2010)
- release cytochrome c during apoptosis (Gandre-Babbe and van der Bliek, 2008; Guo *et al*., 2013; Osellame *et al*., 2016; Prudent *et al*., 2015)
- maintain mtDNA levels and efficient mitochondrial respiration (Ishihara *et al*., 2009; Parone *et al*., 2008)

The study by Twig *et al.* also showed that fission generates asymmetric daughter mitochondria, with one mitochondrion becoming hyperpolarised, whereas the other loses membrane potential. Approximately 1 in 5 post-fission mitochondria remained depolarised and were fusion-deficient and underwent mitophagy. Mitochondria which regained membrane potential could then go on to further fusion events (Twig *et al*., 2008a). The mechanism for the asymmetric and differential membrane potentials is unclear, although similar asymmetric division occurs in bacteria (Kysela *et al*., 2013; Lindner *et al*., 2008). It is conceivable that a similar process occurs in mitochondria, where less functional components are sequestered within one daughter mitochondrion, which has reduced membrane potential and is targeted by the PINK1/parkin pathway (Suen *et al*., 2010), while the other has greater functionality and higher membrane potential, which is retained to fuse with the network.

These reports lead to a notion of selective fusion and mitophagy as a mechanism of quality control; fusion between mitochondria of only high membrane potential facilitates the mitigation of damage while retaining functional components, and therefore excluding dysfunctional and fusion-deficient mitochondria destined for degradation. The mitochondrial lifecycle is depicted in Figure 1.7.

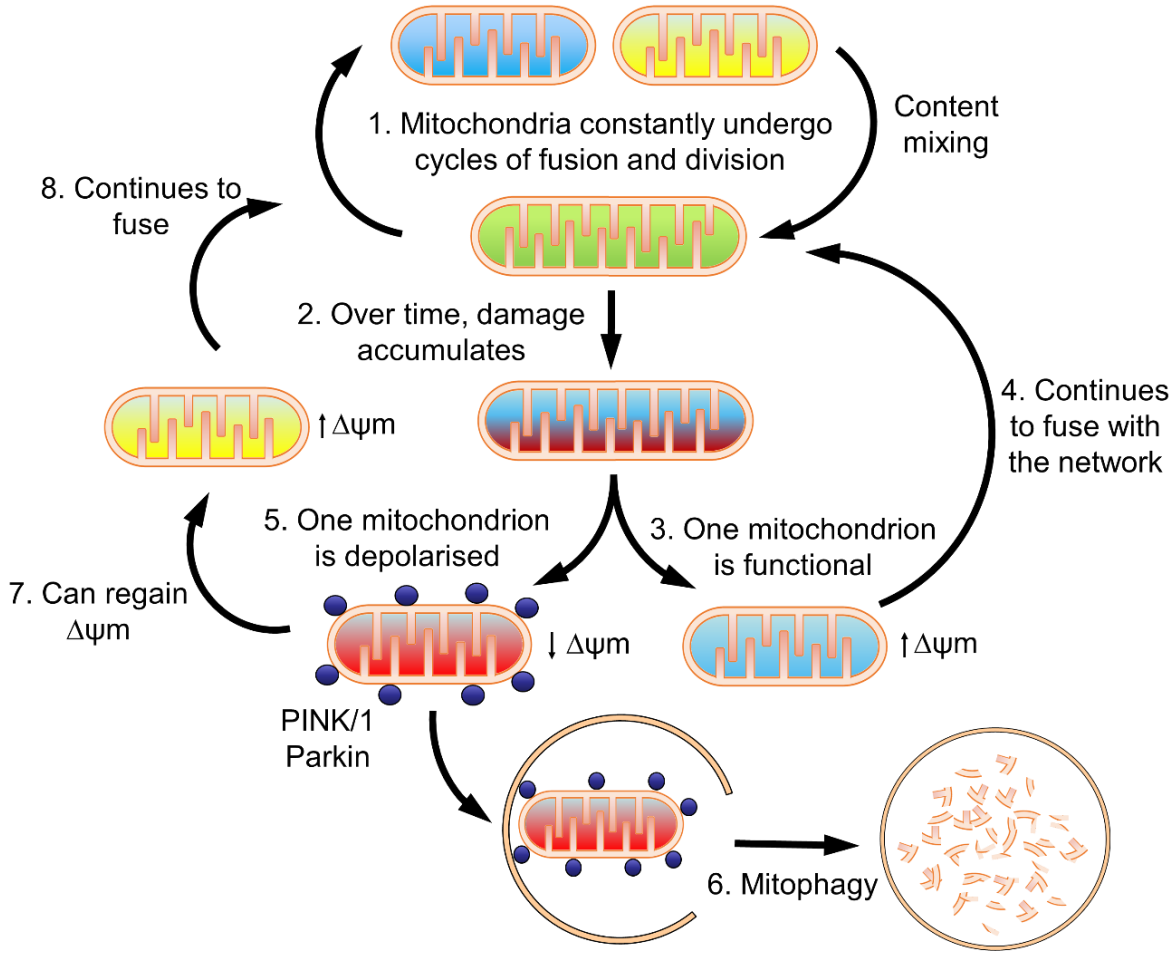

Figure 1.7 The mitochondrial lifecycle

Schematic showing the lifecycle of the mitochondria. 1) Constant cycles of fusion mix mitochondrial components to maintain a homogenous, biochemically and genetically unified population of mitochondria. 2) Over time damage accumulates from mtDNA mutations and protein or lipid oxidation, and asymmetric fission results in daughter mitochondria of increased (3) and decreased (5) membrane potentials (Δψm). 4) The mitochondria with higher membrane potential are fusion-competent, whereas if the other mitochondria can not regain sufficient Δψm, it will be targetted for mitophagy via the PINK1/parkin pathway (6). 7) If membrane potential is restored, the mitochondria can fuse back with the network (8), therefore only functional mitochondrial units persist, while damage is removed.

1.3 The mitochondrial fusion and fission machinery

Fusion and fission are mediated by large GTPases, which modify membrane curvature upon GTP hydrolysis. Mitofusins 1 and 2 (Mfn 1/2) are outer membrane proteins, which tether and fuse the mitochondrial outer membrane (MOM) of two mitochondria, and optic atrophy protein 1 (OPA1) is an inner membrane protein which fuses the inner membrane, and also has roles in regulating cristae morphology. The combined actions of Mfn proteins and OPA1 thus unifies all mitochondrial membranes and the IMS and matrix.

One GTPase is involved in fission, the cytosolic protein dynamin related protein 1 (DRP1), which binds to receptors on the MOM, of which there are four; mitochondrial fission protein 1 (Fis1), mitochondrial fission factor (MFF), mitochondrial dynamics protein 49 and 51 (MiD49 and MiD51). The recruitment of DRP1 forms a helix around the mitochondria, and upon GTP hydrolysis, inducing a conformational change, constricts the membrane, inducing fission. Fusion and fission are illustrated in Figure 1.8.

Discussed below are the mechanisms, function and regulation by PTMs of the fusion and fission machinery, which has been extensively reviewed in Hoppins *et al*., 2007; Labbé *et al*., 2014; Liesa *et al*., 2009; Tilokani *et al*., 2018.

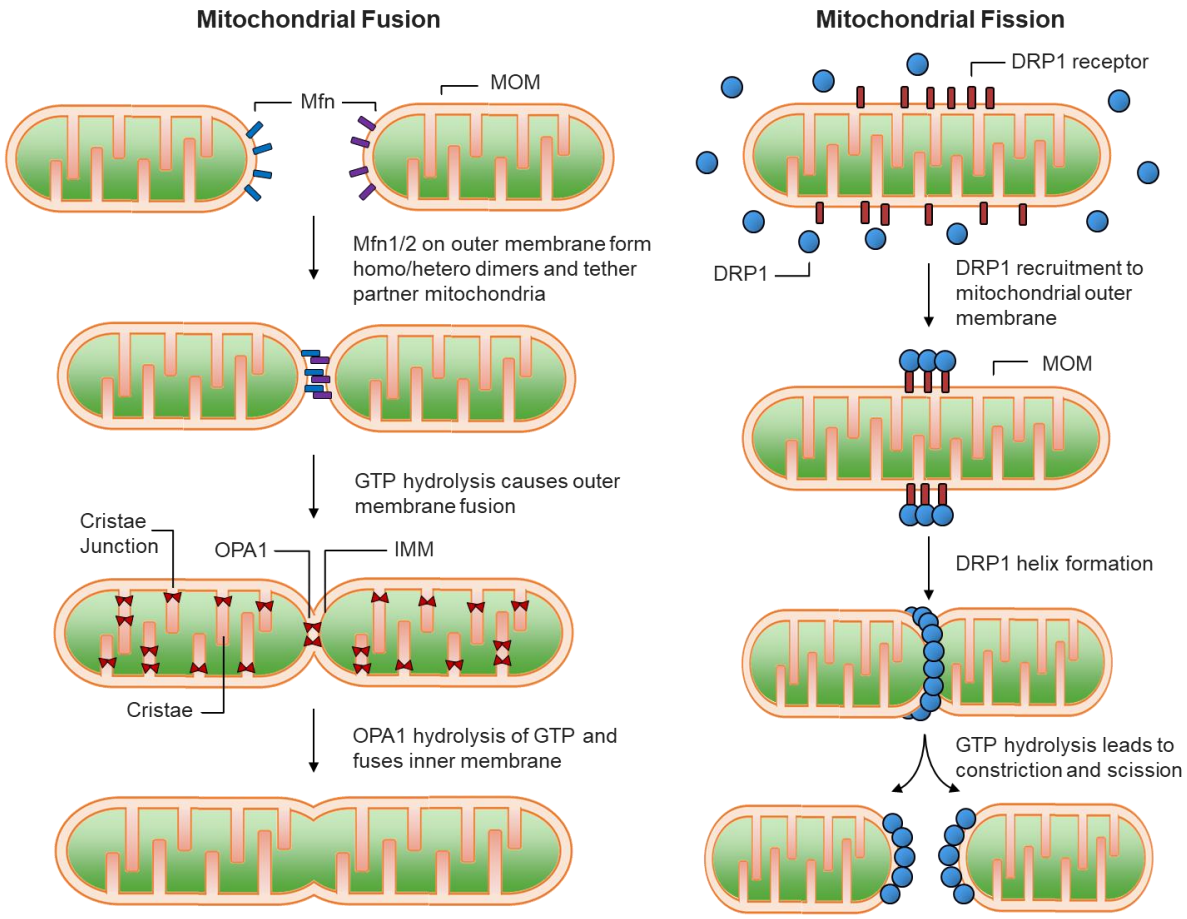

Figure 1.8 Mitochondrial fusion and fission are mediated by GTPases

Mitochondrial fusion involves the union of the outer mitochondrial membrane (MOM), and then subsequently fusion of the inner mitochondrial membrane (IMM). Mitofusins (Mfn1 and 2) form homo and hetero dimers which tether the two partner mitochondrion, and via GTP hydrolysis induce conformational changes in the Mfn complexes, fusing the MOM together. OPA1 regulates cristae structure and fusion of the IMM, thus unifying the matrix. Mitochondrial fission is mediated by the cytosolic GTPase dynamin-related protein 1 (DRP1) which is recruited to adapter proteins on the MOM (Fis1, MFF, MiD49/51). DRP1 oligomerises into a spiral around the mitochondria, and via GTP hydrolysis, induces sission of the membrane.

1.3.1 Mitofusins (Mfn1/2)

Mfn1 and 2 are highly conserved, double pass transmembrane GTPase proteins which localise to the MOM. They share ~63% sequence identity with each other and both contain a GTPase and two coiled-coil regions (Hales and Fuller, 1997; Liesa *et al*., 2009; Mertins *et al*., 2016; Santel and Fuller, 2000). They have a wide tissue expression pattern, with a high ratio of Mfn2/Mfn1 in heart and skeletal muscle tissue (Santel *et al*., 2003). They form homo and hetero-dimeric complexes on opposing membranes (in *trans*) via the coiled-coil regions (Koshiba *et al*., 2004). The GTPase activity of the Mfn proteins and the membrane potential are required for efficient fusion (Hales and Fuller, 1997; Legros *et al*., 2002). Mice ablated for Mfn1 and 2 do not survive mid-gestation, and MEF cells null for both proteins have a severe fusion deficit and the mitochondria fragment, although Mfn1 can rescue fusion in Mfn2-null cells, and *vice versa*, suggesting there is a level of redundancy between the two Mfn proteins (Chen *et al*., 2003). Moreover, double Mfn1/2-null MEF cells have reduced growth, wide-spread differences in membrane potential, with many mitochondria unable to sustain membrane potential, resulting in reduced respiration (Chen *et al*., 2005). However, the GTPase activity of Mfn1 is higher than that of Mfn2 and has a greater tethering capacity (Ishihara *et al*., 2009). On the other hand, Mfn2 acts as a tether between the mitochondria and the endoplasmic reticulum (de Brito and Scorrano, 2008), raising the possibility that specific functions of the Mfn proteins, and different ratios of Mfn1/2 proteins, could confer tissue specific fusion activities (Liesa *et al*., 2009; Santel *et al*., 2003). Mfn1 activity and stability are regulated by PTM under

different stress conditions, which fine tunes the balance of fusion to either promote fusion (SIMH), or initiate fission. Park *et al* show that using antimycin A (ETC complex III inhibitor) for short periods of time causes Mfn1 levels to accumulate and the mitochondria undergo SIMH. Under prolonged treatment, Mfn1 is ubiquitinated by the mitochondrial ubiquitin ligase membrane-associated RING-finger 5 (MARCH5). The interaction between MARCH5 and Mfn1 is dependent on Mfn1 acetylation, which increases upon mitochondrial stress, thus increasing Mfn1 ubiquitination by MARCH5. This mechanism regulates Mfn1 levels under stress and prevents prolonged fusion when mitochondrial fission needs to occur (Park *et al*., 2014). Following glucose starvation, Mfn1 is deacetylated by histone deacetylase 6 (HDAC6), which promotes fusion and decreases oxidative stress (Lee *et al*., 2014), presumably to prevent MARCH-dependent ubiquitination to favour fusion. Mfn1 is phosphorylated during OGD and H_2O_2 treatment by extracellular-signal regulated kinase (ERK), inhibiting Mfn1 function, promoting fission and apoptosis (Pyakurel *et al*., 2015). Both Mfn1 and 2 are ubiquitinated by the PINK1/parkin pathway following mitochondrial depolarisation, therefore inhibiting fusion and segregating mitochondria for mitophagy (Gegg *et al*., 2010). Jun N-terminal Kinase (JNK) phosphorylates Mfn2 in response to genotoxic stress, which recruits the E3 ubiquitin ligase Huew1 to promote Mfn2 degradation, leading to fission and apoptosis (Leboucher *et al*., 2012).

1.3.2 Optic Atrophy Protein 1 (OPA1)

OPA1 is a large protein localised to the IMM, with the bulk of the protein facing the IMS. It has a predicted size of over 100kDa, however, exists as multiple smaller fragments, an 86kDa form predominating (Olichon *et al*., 2002). *In vitro* experiments confirm OPA1 as a pro-fusion protein, since knockdown triggers mitochondrial fragmentation, Δψm loss, and apoptosis (Griparic *et al*., 2004; Olichon *et al*., 2003). Homozygous OPA1 mutant mice die *in utero*, but heterozygous mice are viable, but show progressive loss of optic nerve axons (Alavi *et al*., 2007). Cristae house the vast majority (>90%) of ATP-Synthase and complex III, over 80% of cytochrome c, and OPA1 is involved in regulating cristae shape and structure, and thus plays an important function in regulating apoptosis and OXPHOS (Cogliati *et al*., 2016). Indeed, loss of OPA1 results in disorganised cristae structures and susceptibility to apoptosis (Alavi *et al*., 2007; Olichon *et al*., 2003). OPA1 is proteolytically cleaved at two sites by the membrane bound metalloproteases OMA1 and YME1L, each one cleaving at a different site. The differential cleavage of OPA1 generates different isoforms of OPA1 (termed long and short OPA1 (L-OPA1 and S-OPA1) (MacVicar and Langer, 2016). OMA1 levels increase upon mitochondrial depolarisation, leading to increased OPA1 processing (increased S-OPA1) and mitochondrial fragmentation (Alavi *et al*., 2007), whereas YME1L activity is stimulated by efficient OXPHOS, and is thought to be involved in constitutive OPA1 processing (Griparic *et al*., 2007; Mishra *et al*., 2014). Although the mechanism has not yet been fully elucidated, it is thought that increasing OMA1 S-OPA1 products facilitates fission/prevents fusion,

whereas YME1L processing promotes fusion (MacVicar and Langer, 2016).

1.3.3 Dynamic related protein 1 (DRP1)

DRP1 is an evolutionarily conserved mechanochemical GTPase of ~80kDa, that is primarily a cytosolic protein, with ~3% on the mitochondrial outer membrane at any given time. DRP1 shuttles from the cytosol to sites of potential fission, where it oligomerises and initiates membrane fission (Smirnova *et al*., 2001). Lacking the plekstrin homology domain of other dynamins, DRP1 must bind to adaptor proteins on the MOM (Fis1, MiD49/51, MFF) to be recruited to the membrane. DRP1 exists in an equilibrium of dimers and tetramers in the cytosol (Macdonald *et al*., 2014; Michalska *et al*., 2018), and forms higher order oligomers on the MOM in a helix around the mitochondria, and via a GTP-hydrolysis dependent mechanism, causes a conformational change that induces membrane constriction (Francy *et al*., 2015; Mears *et al*., 2011). DRP1-null cells or expression of a DRP1 GTPase dead mutant exhibit extended and elongated mitochondrial networks (Smirnova *et al*., 2001; Wakabayashi *et al*., 2009), confirming DRP1's role as a positive regulator of mitochondrial fission. However, a concept is emerging that DRP1 shuttling is not an "all or nothing" mechanism but is in fact in equilibrium between cytosolic and membrane bound DRP1. Indeed, DRP1 continuously cycles from the cytosol to the MOM, as Wasiak *et al* elegantly show using live cell imaging and fluorescence recovery after photobleaching. There is ~80% recovery of DRP1 at the MOM with a half-life of ~50 seconds, meaning that the majority of DRP1 is dynamically shuttling, while some are stable at the MOM (Wasiak *et al*., 2007). Adding to this model, DRP1

complexes on the MOM can fuse to form larger complexes, and can laterally move along the mitochondrial membrane (Ji *et al*., 2015). Pro-fission signals thus promote stable association with the MOM and formation of fission-competent DRP1 complexes, although such a complex and the mechanism are poorly understood.

DRP1 is heavily modified by PTMs, integrating with many cell signalling pathways and the cell cycle. The best characterised PTM of DRP1 is phosphorylation at two sites, S616 and S637, with differential effects on mitochondrial morphology. Cyclin-dependent kinase 1 (CDK1) phosphorylates DRP1 at S616 during cell division to promote mitochondrial fission, to ensue distribution of mitochondria to the two daughter cells (Taguchi *et al*., 2007). In an *in vitro* model of heart failure and myocardial hypertrophy, excessive activation of Ca^{2+}/calmodulin-dependent kinase II (CaMKII) phosphorylates DRP1 at S616, induces translocation to the mitochondria, DRP1-mediated mitochondrial dysfunction and apoptosis (Xu *et al*., 2016a). DRP1 is also phosphorylated at S616 by the Ras-Erk2 pathway in cancer, and inhibition of DRP1 or a phospho-null S616A mutant prevent mitochondrial fragmentation and tumour growth (Kashatus *et al*., 2015). Phosphorylation at S637 by PKA inhibits DRP1 function, protecting cells against mitophagy during nutrient deprivation and cell stress (Chang and Blackstone, 2007; Cribbs and Strack, 2007; Gomes *et al*., 2011) whereas S637 is dephosphorylated by calcineurin during cell death (Cereghetti *et al*., 2008; Cribbs and Strack, 2007). Interestingly, phosphorylation of these two sites have little effect on GTPase activity, and it appears that the translocation events promoted by S616

phosphorylation and S637 dephosphorylation increases the localisation and stability at mitochondria, and therefore fission, and other factors are involved in promoting mitochondrial fission beyond the DRP1 phospho-state (Cereghetti *et al*., 2008).

Increased O-GlcNAcylation (addition of a sugar moiety) of DRP1 was found to be linked to decreased S637 phosphorylation levels and mitochondrial fragmentation (Gawlowski *et al*., 2012). DRP1 ubiquitination by MARCH5 has been shown to affect mitochondrial morphology, whereby MARCH5 overexpression induces fusion, whereas MARCH-deficient cells exhibit fragmentation (Karbowski *et al*., 2007; Nakamura *et al.*, 2006; Yonashiro *et al.*, 2006). A mechanism still remains to be delineated, however it is likely that MARCH5-mediated ubiquitination of DRP1 inhibits fission and therefore leads to unopposed fusion, such as has been shown for parkin mediated ubiquitination of DRP1, leading to its proteasomal degradation (Wang *et al*., 2011), although MARCH5-null cells exhibit normal DRP1 levels, so possibly the ubiquitination event leads to a non-degradative function (Xu *et al*., 2016b). DRP1 is also modified by S-Nitrosylation (addition of a NO moiety), with evidence linking this modification to neurodegenerative disease by promoting fission (Cho *et al*., 2009; Haun *et al*., 2013), and recently it was demonstrated that reduced S-Nitrosylated DRP1 results in reduced S616 phosphorylation, with a concomitant mitochondrial elongation phenotype in neurons (Lee and Kim, 2018).

SUMOylation of DRP1 with SUMO-1 increases its stability, and SUMO-1-DRP1 is recruited to the mitochondria during mitosis (Harder *et al*., 2004; Zunino *et al*.,

2009), and it was speculated that DRP1 deSUMOylation promotes fission (Zunino *et al*., 2009). Mitochondrial-anchored protein ligase (MAPL) mediated DRP1 SUMOylation of SUMO-1 enhances the DRP1 oligomeric state, has roles in mitochondrial-ER contact site formation, and is required for Ca^{2+} transfer from the ER to mitochondria, cristae remodelling and cytochrome c release under apoptotic conditions (Prudent *et al*., 2015). On the other hand, DRP1 SUMOylation by SUMO-2/3 partitions DRP1 in the cytosol during OGD, and SENP3 mediated deSUMOylation promotes DRP1 recruitment to the MOM upon reperfusion, initiating cell death (Guo *et al*., 2013).

1.3.4 Mitochondrial Fission protein 1 (Fis1)

Fis1 is a relatively small protein of 152 amino acids (~16.9kDa) and was the first DRP1 receptor identified (Mozdy *et al*., 2000). It localises to the MOM and its overexpression and knockdown induce mitochondrial fragmentation and fusion, respectively, which is impaired in DRP1 dominant negative expressing cells, indicating that Fis1 functions through DRP1 (James *et al*., 2003; Stojanovski *et al*., 2004). However, the role of Fis1 in DRP1-mediated fission has been questioned, since others report that Fis1 has little effect on DRP1 recruitment and mitochondrial morphology (Loson *et al.*, 2013; Otera *et al*., 2010), and that Fis1 is dispensable for fission (Koirala *et al*., 2013; Otera *et al*., 2016). Alternative roles for Fis1 have been proposed; a recent report shows that Fis1 binds to Mfn proteins and impairs the GTPase activity of the fusion machinery, suggesting that Fis1 acts as a negative regulator of fusion, rather than a positive regulator of fission (Yu *et al*., 2019). Evidence suggests a potential role in apoptosis, since

loss of Fis1 impairs apoptosis induction (Lee *et al*., 2004), and Fis1 was identified as a binding partner of the ER outer membrane protein Bap31, which forms a platform for procaspase 8 activation and Ca^{2+} transfer to the mitochondria to signal apoptosis (Iwasawa *et al*., 2011).

1.3.5 Mitochondrial Fission Factor (MFF)

MFF was first identified by Gandre-Babbe and Van der Bliek in 2008 during a siRNA screen to identify novel proteins affecting mitochondrial morphology (Gandre-Babbe and van der Bliek, 2008). There are multiple splice variants of MFF; three were identified in mouse, differentially expressed across multiple tissues (Ducommun *et al*., 2015). Nine were predicted for human MFF, based on cDNAs from the MFF gene, generated from either the presence or absence of exon 1, and various splice variants generating combinations of exons 5, 6 and 7. A region towards the C-terminus is predicted to form coiled-coils (Gandre-Babbe and van der Bliek, 2008), which could be used for potential dimer formation, although no structure for MFF has been determined. Human isoform 1 encodes a 342 amino acid protein of ~38.5kDa. MFF shows high expression in the brain, liver, heart, muscle and kidney, and lower levels in other tissues. Localising to both the mitochondria and the peroxisomes, siRNA knockdown of MFF results in elongated mitochondria and peroxisomes (Gandre-Babbe and van der Bliek, 2008). This mitochondrial phenotype has since been confirmed by others, where the majority of DRP1 on the mitochondria is redistributed to the cytosol (Loson *et al*., 2013; Otera *et al*., 2010). It was elegantly demonstrated that MFF functions via recruitment of DRP1 to the MOM to induce fission, since mitochondrial

fragmentation upon MFF overexpression is abrogated in DRP1-null cells (Otera *et al*., 2010). MFF localises to fission sites independently of DRP1, implying that MFF may “mark” sites of DRP1 recruitment (Friedman *et al*., 2011).

Investigations into the role of each DRP1 receptor individually determined that MFF plays a major role in promoting fission, since MFF-null cells exhibit the greatest fusion phenotype compared to Fis1-null cells (Loson *et al*., 2013; Otera *et al*., 2010). Furthermore, Osellame *et al* show that sequential loss of the DRP1 adaptor proteins has an additive effect on impairing DRP1 recruitment and increasing mitochondrial fusion (Osellame *et al*., 2016), demonstrating that the receptors work cooperatively, agreeing with previous findings (Loson *et al*., 2013), although MFF alone is sufficient to recruit DRP1 (Otera *et al*., 2010). Loss of MFF confers protection against various stress stimuli, such as CCCP-induced mitochondrial fragmentation and etoposide-induced cell death (Loson *et al*., 2013; Otera *et al*., 2016). These reports demonstrate that MFF is a major DRP1 receptor, having roles in DRP1 recruitment and mitochondrial morphology under basal conditions, and is also important in regulating mitochondrial fission and fragmentation under severe stress conditions.

A study by Lui and Chan interrogated the interaction between MFF and DRP1, and identified the first 50 amino acids of the N-terminal region of MFF is required for DRP1 binding, and that MFF favours binding to tetramers and higher order oligomers, whereas the MiD proteins are not selective in their DRP1 binding ability (Liu and Chan, 2015). Indeed, MFF fails to bind to DRP1 mutants incapable of higher order assembly, whereas GTPase mutants can still bind MiD proteins

(Palmer *et al*., 2011). Additionally, *in vitro* experiments show that MFF enhances the GTPase activity of DRP1, whereas MiD51 inhibits DRP1 GTPase activity (Osellame *et al*., 2016). Such differences in receptor specificity of the DRP1 oligomer state and on its function may be the reason for differential roles of the DRP1 receptors. Moreover, these findings highlight that MFF is involved in higher order assembly and DRP1 GTPase activation, thus MFF is a major receptor of pro-fission, and likely regulates the assembly of a fission competent complex on the MOM.

MFF ubiquitination

MFF is ubiquitinated by parkin at K251 (K302 in isoform 1) in response to CCCP induced mitochondrial depolarisation. MFF ubiquitination recruits the autophagy adaptor p62, which subsequently facilitates the clearance of damaged mitochondria. MFF-null cells fail to recruit parkin and p62 following CCCP treatment, however, expression of a ubiquitin mutant K251R restored recruitment of parkin but failed to recruit p62 (Gao *et al*., 2015). We have shown that the larger isoform of MFF (isoform 1) has at least three ubiquitination sites, and that parkin knockdown reduces MFF ubiquitination by ~50%, indicating at least one other ubiquitin ligase targets MFF (Lee *et al*., 2019). Parkin ubiquitination of MFF is not only involved in MFF ubiquitination during mitophagy, but also regulates the constitutive turnover of MFF via lysosomal degradation (Lee *et al*., 2019).

MFF phosphorylation by AMPK

MFF is also phosphorylated by AMP activated protein kinase (AMPK), a major regulator of cellular energy homeostasis (Kahn *et al*., 2005). MFF was first

identified as a target of AMPK in a mass spectrometry screen from primary mouse hepatocytes using an antibody against the consensus phospho-AMPK substrate motif. The authors identified two sites in mouse MFF isoform 4, S129 and S146 (corresponding to S155 and S172 in human isoform 1), which increased in phosphorylation upon activation of AMPK (Ducommun *et al*., 2015). MFF phosphorylation was also identified in a high-throughput mass spectrometry screen of phosphorylated proteins in breast cancer tissues (Mertins *et al*., 2016) and also a mass spectrometry screen of wildtype and AMPK-null HEK cells identified enriched MFF S172 phosphorylation (isoform 2 and 5) upon treatment with an AMPK activator (Chen *et al*., 2019). See Figure 1.9 for alignment of AMPK sites in MFF.

The significance of AMPK phosphorylating MFF was shown by Toyama *et al*., who observed mitochondrial fragmentation upon treatment with the ETC complex inhibitors rotenone or antimycin A, or when chemically activating AMPK with an AMPK activator (A769662) or AMP mimetic (AICAR). MFF phosphorylation at S155 and S172 increases upon rotenone and AICAR treatment in an AMPK-dependent manner. Significantly, using MEF cells deficient for endogenous MFF, Fis1 and MiD51, an MFF double phospho-mimetic, mimicking AMPK phosphorylation at S155 and S172 (2SD) is sufficient to induce mitochondrial fragmentation to the same degree as observed when using AMPK activation in wildtype cells. MFF 2SD therefore has gain of function activity in the absence of AMPK activation. Conversely, a double phospho-null (2SA) could still promote DRP1 recruitment, similar to wildtype MFF levels, however, 2SA failed to enhance

DRP1 recruitment when treated with AICAR or rotenone. The authors further confirm phosphorylation of MFF as a pro-fission PTM by using *in utero* electroporation of WT, 2SA and 2SD MFF and imaged mitochondrial area in mouse neuronal dendrites. Expression of wildtype and 2SD MFF fragmented the mitochondria, whereas 2SA had no effect (Toyama *et al.*, 2016). This report demonstrates that phosphorylation of MFF by AMPK promotes fission as a stress response and is necessary and sufficient to promote fission.

A AMPK consensus motifs of Human MFF isoforms

AMPK motif	-5	-4	-3	-2	-1	0	+1	+2	+3	+4
	Φ	x	B	x	x	S	x	x	x	Φ
Primary	L	R	R	V	x	S	x	x	N	L
Secondary	M	K	K	S	x	S	x	x	D	V
Additional	I	x	H	R	x	S	x	x	E	I
MFF S155										
All isoforms	L	K	R	E	R	S	M	S	E	N
MFF S172										
Isoform 1 (S172)	L	V	R	N	D	S	L	W	H	R
Isoform 2 (S146)	L	V	R	N	D	S	L	V	T	P
Isoform 3 (S146)	L	V	R	N	D	S	L	W	H	R
Isoform 4 (S146)	L	V	R	N	D	S	L	Y	G	I
Isoform 5 (S146)	L	V	R	N	D	S	L	P	V	L

B AMPK sites across species and isoforms

AMPK motif	-5	-4	-3	-2	-1	0	+1	+2	+3	+4
	Φ	x	B	x	x	S	x	x	x	Φ
MFF S155										
Human (Isoform 1, S155)	L	K	R	E	R	S	M	S	E	N
Mouse (Isoform1, S129)	L	K	R	E	R	S	M	S	E	N
Rat (Isoform1, S129)	L	K	R	E	R	S	M	S	E	N
MFF S172										
Human (Isoform 1, S172)	L	V	R	N	D	S	L	W	H	R
Mouse (Isoform 1, S146)	L	V	R	N	D	S	I	V	T	P
Mouse (Isoform 4, S146)	L	V	R	N	D	S	M	Y	G	I
Rat (Isoform 1, S146)	L	V	R	N	D	S	M	Y	G	I

Figure 1.9 AMPK sites MFF across species

MFF has two sites corresponding to the consensus AMPK motif Φ-x-B-x-x-S-x-x-x-Φ. Φ = Hydrophobic, B = Basic residue**. A** The optimal, secondary and additional elements of the AMPK phosphorylation motif are highighted. S155 of human MFF (found in all isoforms) shows a high degree of conformity to the consensus sequences. **B** The AMPK sites are conserved across species. The S155 site (corresponding to S129 in mouse and rat) are identical. The S172 (S146 in mouse and rat) also show a high

degree of conformity. Human isoform nomenclatrue based on Uniprot entries; Isoform 1: Q9GZY8-1. Isoform 2: Q9GZY8-2, and so on.

1.3.6 Mitochondrial Dynamics proteins (MiD49/51)

Mitochondrial dynamics proteins of 49 and 51kDa (MiD49 and MiD51) are integral MOM proteins which directly recruit DRP1, although there is conflicting evidence as to whether the MiD proteins are positive or negative regulators of fission (Palmer *et al*., 2011; Zhao *et al*., 2011). Both of these early studies noted that exogenous expression of MiD51 induces increased mitochondrial elongation, and increasing MiD expression enhances DRP1 recruitment to the mitochondria (Palmer *et al*., 2011). Palmer *et al* also show that siRNA double knockdown of MiD49 and MiD51 results in a fused mitochondrial phenotype, which contradicts findings by Zhao *et al*, which observed fragmented mitochondria upon MiD51 knockdown (Zhao *et al*., 2011). Confirmation of a positive role in fission came when MiD proteins were shown to recruit DRP1 and induce mitochondrial fission in yeast (Koirala *et al*., 2013). Subsequent studies show that knockdown of the individual MiD proteins causes mitochondrial elongation, and double knockdown has no additional effect, suggesting a level of redundancy, and double knockdown in Fis1/MFF-null cells further induces mitochondrial elongation (Loson *et al*., 2013). In agreement with this report, Osellame *et al* show that in MFF-null and Fis1-null cells, there is residual fission, and upon additional ablation of MiD49 and MiD51, mitochondrial connectivity is comparable to DRP1-null cells. Furthermore, confirming MiDs role in DRP1 recruitment, re-expression of MiD51 in cells deficient for all DRP1 adaptors was sufficient to recruit DRP1 to the mitochondria

(Osellame *et al*., 2016), and re-expression of either MiD49 or MiD51 in Fis1/MFF-null cells restored DRP1 recruitment to the MOM (Loson *et al*., 2013). These findings suggest that the DRP1 receptors can function both independently and in concert to regulate DRP1 recruitment and fission.

These reports raise the question of the role MiD proteins play. If they function as a “canonical” positive regulator of fission, such as MFF, why does MiD overexpression result in increased DRP1 recruitment, but lead to elongated mitochondria? Loson *et al* observe that upon MiD overexpression, there is an increase in the inhibitory S637 phosphorylation modification of DRP1 (Loson *et al*., 2013). By observing mitochondrial morphology with increasing MiD51 expression, Palmer *et al* demonstrate that increasing MiD51 levels inactivates DRP1 at the mitochondria, resulting in fusion (Palmer *et al*., 2013), and as mentioned above, MiD proteins can associate with oligomer-deficient DRP1, and MiD51 inhibits DRP1 GTPase activity (Liu and Chan, 2015; Osellame *et al*., 2016). Thus, an emerging notion of the role of the MiD proteins is to sequester low order structures of inactivated DRP1 on the mitochondrial surface, and the expression/activity of the MiD proteins is an important factor to regulate mitochondrial fusion/fission. Indeed, it has been suggested that the MiD proteins act as a “scaffold” for the recruitment of DRP1, since MiDs form rings around the mitochondria in DRP1-null cells (Palmer *et al*., 2011), implying that DRP1 is dispensable for MiD complex assembly on the MOM.

A recent report offers an elegant mechanism as to how MiD proteins confer this inhibitory effect on mitochondrial fission. Yu *et al* propose a more complex system

of interactions between DRP1 and the adaptor proteins, demonstrating that MiD proteins facilitate the interaction between DRP1 and MFF, acting as a “molecular bridge”, and that the expression level is critical in regulating DRP1-MFF binding (Yu *et al*., 2017). They show that MFF overexpression increases DRP1-mediated fission, agreeing with previous findings (Otera *et al*., 2010), however, knockout of the MiD proteins greatly reduced MFF-mediated recruitment of DRP1, suggesting that MiD proteins promote the MFF-DRP1 interaction. Conversely, MFF knockdown did not affect MiD overexpression-inducing mitochondrial elongation and DRP1 recruitment. The authors confirm the interaction between DRP1, MiD and MFF by co-immunoprecipitation, and upon knockout of both MiD proteins, MFF binding to DRP1 is dramatically reduced, whereas MFF knockdown had no effect on the MiD-DRP1 interaction. In alternative experiments, increasing levels of MiD decrease DRP1 binding to MFF in a dose-dependent manner, and likewise, upon increasing MFF protein levels, the DRP1-MiD interaction is decreased in a dose-dependent manner. Using sequential co-immunoprecipitations, Yu *et al.* determine that DRP1-MiD-MFF exist as a trimeric complex, where DRP1 is bound to MiD, and MFF is associated with MiD (Yu *et al*., 2017). In ~71% of cases, the trimeric complex is formed, in ~21% of cases DRP1 is bound to MiD in the absence of MFF. At much lower levels, MFF binds directly to DRP1 (~3%), and MiD binds MFF in the absence of DRP1 (~5%) (see Figure 1.10C D).

This model offers an explanation to the observations that both overexpression and knockdown of MiD induces fusion, and that close association between

receptors regulate mitochondrial dynamics (Elgass *et al*., 2015; Osellame *et al*., 2016). Indeed, live cell imaging confirmed a high degree of co-localisation of MiD49, MiD51, DRP1 and MFF at pre-fission sites. Intriguingly, MiD foci were observed to coalesse and fuse at fission sites before fission (Elgass *et al.*, 2015), moreover, FRET and close proximity biotinylation experiments show a close association between MiD51, DRP1 and MFF (Osellame *et al.*, 2016). These reports suggest that DRP1 adaptor proteins interact at pre-fission sites and cooperatively mediate fission.

MiD49 protein levels are regulated by the mitochondrial ubiquitin ligase MARCH5; upon mitochondrial stress and apoptosis stimuli, MARCH5-mediated degradation of MiD49 by the proteasome promotes fission, indicating that loss of MiD49 is required for stress induced mitochondrial fragmentation (Xu *et al*., 2016b). Indeed, other reports highlight the importance of the MiD proteins in cell stress. MiD overexpression exacerbates CCCP induced fragmentation (Loson *et al*., 2013), and double knockout of MiD49 and MiD51 conferred resistance to cytochrome c release and fragmentation upon CCCP treatment and apoptotic stimuli (Osellame *et al*., 2016).

This section highlights the importance of regulating appropriate fusion and fission, and the PTMs that mediate mitochondrial dynamics to ensure mitochondrial function, alter morphology, safe-guard mitochondrial integrity, protect against cell death or initiate apoptosis. Figure 1.10 summarises the major concepts of mitochondrial dynamics.

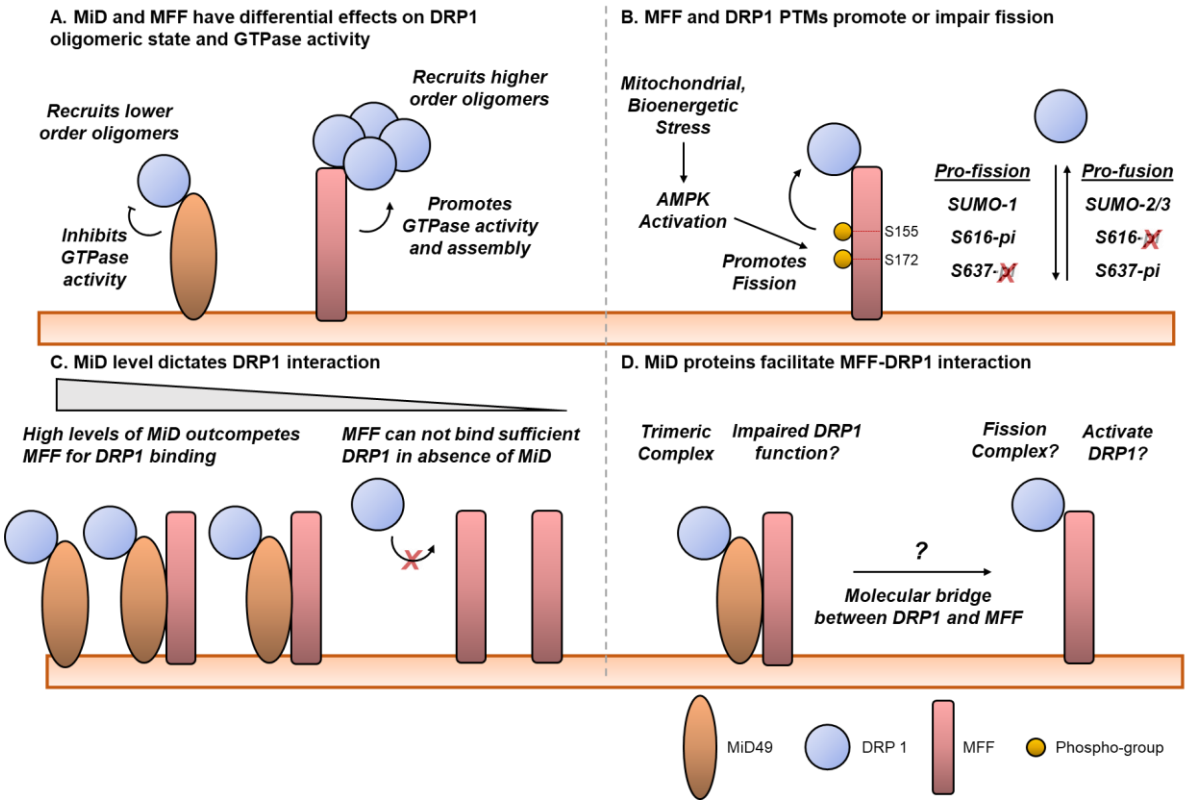

Figure 1.10 Summary of mitochondrial fission

Schematic illustrating the layers of regulation of mitochondrial fission. **A** MiD49 and MiD51 can bind lower order DRP1 oligomers (dimers) and inhibit DRP1 GTPase activity. MFF favours binding to higher order oligomers and enhances DRP1 GTPase activity. **B** MFF and DRP1 undergo PTM to alter function. MFF is phosphorylated at S155 and S172 by AMPK to promote fission during bioenergetic stress, and DRP1 is phosphorylated at S616 and S637, having differential effects on fission. DRP1 is also SUMOylated by SUMO-1 to promote stable association with the MOM, whereas SUMO-2/3 sequesters DRP1 in the cytosol. **C** MiD, DRP1 and MFF form various complexes, with the majority of the complexes being trimeric, whereas only a small proportion of MFF directly binds DRP1 in absence of MiD. **D** The MiD proteins facilitate the interaction between DRP1 and MFF. The mechanism of transition from an inactive trimeric complex to an active fission assembly of DRP1 and MFF is unclear.

1.4 SUMO regulation of mitochondria

SUMOylated conjugates have been identified in the mitochondrial fraction (Prudent *et al*., 2015; Zunino *et al*., 2007, 2009), indicating multiple mitochondrial proteins are SUMOylated. SUMO-1 overexpression localises to fission sites and promotes fission (Harder *et al*., 2004), a phenotype that is reversed upon SENP5 expression (Zunino *et al*., 2007). Zunino *et al* also show that SENP5 is responsible for deconjugating mitochondrial proteins and reducing SUMO-1 and DRP1 recruitment to fission sites. This mitochondrial elongation phenotype was also observed by targeting SENP5 to the MOM, and could be replicated by silencing MAPL, the mitochondrial SUMO E3 ligase (Prudent *et al*., 2015). DRP1 constantly cycles from the cytosol to the MOM, and SUMO-1-DRP1 conjugation increases under apoptotic stimuli and is stabilised on the MOM (Wasiak *et al*., 2007). Conversely, SUMO-2/3 conjugation sequesters DRP1 in the cytosol, mediated by SENP3, and overexpression of SENP3 promotes DRP1 SUMO-2/3 deconjugation and mitochondrial fission (Guo *et al*., 2013), demonstrating that the SENP enzymes differentially regulate DRP1 SUMOylation and function, and moreover, that the SUMO pathway regulates mitochondrial dynamics.

As previously mentioned, SUMOylation of DRP1 by SUMO-1 via the action of MAPL promotes fission under apoptotic stimuli (Prudent *et al*., 2015). Mono-SUMO-1 stabilises DRP1 (Harder *et al*., 2004), which is antagonised by SENP5. Indeed, SENP5 overexpression reduces DRP1 levels (Zunino *et al*., 2007). MAPL mediated DRP1 SUMOylation stabilises ER-mitochondrial contact sites and is required for Ca^{2+} transfer from ER to mitochondria, cristae remodelling and

cytochrome c release under apoptotic conditions (Prudent *et al*., 2015). On the other hand, SUMO-2/3 conjugated DRP1 abrogates fission, a modification reversed by SENP3. During OGD, SENP3 levels are reduced, promoting a significant increase in global SUMO-2/3 conjugation. DRP1-SUMO-2/3 does not localise to the mitochondria, but upon reperfusion, SENP3 levels recover, deSUMOylating DRP1, promoting translocation to the MOM and inducing fission, cytochrome c release and apoptosis. Moreover, SUMO-deficient DRP1 increases mitochondrial fragmentation, and binds to MFF to a greater extent compared with wildtype DRP1, indicating that completely abolishing SUMOylation of DRP1 enhances the MFF-DRP1 interaction (Guo *et al*., 2013, 2017). Indeed, a DRP1 GTPase inactive mutant K38A has increased SUMO-3 conjuagtion (Figueroa-Romero *et al*., 2009), suggesting that inactive DRP1 is SUMOylated by SUMO-2/3 and sequestered in the cytosol, and deSUMOylation is required for translocation, agreeing with previous hypothess of DRP1 regulation (Guo *et al*., 2013, 2017). How this model fits with the findings that SUMO-1 is stabilised at the MOM is yet to be resolved.

1.5 The mitochondrial stress response

The dynamic and plastic nature of the mitochondrial network confers a high degree of adaptability and sensitivity to changing metabolic demands and cellular stress, and the concerted mechanisms of fusion, fission and transport act to adapt mitochondrial morphology and motility to restore homeostasis (Ferree and Shirihai, 2012; Labbé *et al*., 2014; Youle and Van Der Bliek, 2012).

Cellular stress can be acute or chronic in duration, and intrinsic or extrinsic in nature. Intrinsic stressors include genetic mutations (genomic or mtDNA), metabolite/nutrient deprivation or oversupply, oxidative stress and calcium overload, and extrinsic stressors include UV irradiation, toxins, mitochondrial ETC inhibitors and infections. As previously mentioned, many pathways converge at the mitochondria, so any disruption or stress to these will elicit a mitochondrial stress response to attempt to restore homeostasis (Eisner *et al*., 2018).

The link between fusion/fission, mitochondrial morphology and bioenergetic stress is reviewed in Eisner *et al*., 2018; Labbé *et al*., 2014; Tilokani *et al*., 2018. I will discuss briefly some mitochondrial stressors and the impact on mitochondrial morphology.

1.5.1 Nutrient stress

Nutrient or growth factor depletion induces the catabolic process of autophagy (a process of degradation involving the sequestration of cytoplasm and organelles destined for lysosomal delivery) as a means to restore and recycle components (Dikic and Elazar, 2018). During starvation of glucose, amino acids and growth

factors, mitochondria elongate, which maintains ATP levels, preserves mitochondria from degradation and supports cell viability (Gomes *et al*., 2011; Rambold *et al*., 2011). The extent of elongation is additive with combinations of nutrient depletion, with more severe starvation conditions causing a more rapid and complete elongation phenotype. Upon re-introduction of nutrients, this phenotype is reversed (Rambold *et al*., 2011), indicating that changes in mitochondrial dynamics are transient. Interestingly, inhibiting this fusion behaviour reduces ATP levels, the mitochondria become targets for degradation, and cell death ensues, suggesting that mitochondrial elongation during nutrient stress is a protective response (Gomes *et al*., 2011).

Conversely, nutrient excess has the opposite effect on mitochondrial morphology. High glucose and fatty acid treatment of β-cells arrests fusion, promotes fission and eventual apoptosis, which can be reversed by inhibiting fission (Molina *et al*., 2009). Primary cardiovascular cells respond in a similar way to prolonged hyperglycaemic conditions, with increased mitochondrial fragmentation, oxidative stress and cell death (Yu *et al*., 2008). The skeletal muscle of mice fed a high fat and high sugar diet have increased oxidative stress, smaller and swollen mitochondria and reduced expression of pro-fusion proteins. Remarkably, antioxidant treatment restored the mitochondrial structure and integrity. Moreover, the authors report reduced mtDNA content and reduced expression of subunit 1 and 3 of complex IV of the ETC (Bonnard *et al*., 2008).

1.5.2 Ischemic stress

It is well established that following ischemic insult, which deprives tissue of oxygen and glucose (such as during a heart attack or stroke), mitochondria are susceptible to dysfunction. *In vivo* studies of brain ischemia have shown that mitochondrial respiration is impaired, coupled with reduced activity of complexes of the ETC (Allen *et al*., 1995; Almeida *et al*., 1995; Anderson and Sims, 1999). *In vitro* studies of primary neurons have confirmed mitochondrial dysfunction during OGD. 1hr OGD reduces complex I activity, ATP levels are depleted, $\Delta\psi m$ is reduced, oxidative stress is increased, accompanied with increased cell death (Almeida *et al*., 2002). Wappler *et al* observed morphological changes to the mitochondria of primary neurons following OGD and undertook a comprehensive study of the fission and fusion protein levels. 1hr ODG resulted in larger and more swollen mitochondria, but with no change in the levels of Mfn1/2, OPA1, DRP1 or Fis1. However, following 3hrs ODG, the mitochondria remained large and swollen, and the cristae folds became unstructured. This was accompanied with decreased DRP1 and Mfn2 protein levels, whereas Mfn1 levels increased (Wappler *et al*., 2013). Another study investigating the effects of OGD on primary neurons showed that 90 minutes of OGD induces similar mitochondrial dysfunction, with mitochondria appearing punctate and significantly shorter. No difference in mRNA levels of Mfn1/2, DRP1, Fis1 or OPA1 were detected, however, after OGD insult, OPA1 processing was observed to favour smaller isoforms, indicative of inhibited fusion. The alterations in OPA1 processing were also mirrored in *in vivo* studies of ischemic insult to mouse brain (Baburamani *et*

al., 2015).

1.5.3 Mitochondrial inhibitors

As previously discussed, various stressors are used to induce mitochondrial stress and apoptosis. CCCP is a mitochondrial uncoupler, which dissipates the membrane potential, and ETC inhibitors, such as rotenone and antimycin A, are also used to reduce mitochondrial function and ATP levels. These are extreme mitochondrial stressors, and treatment at high concentrations cause mitochondrial fragmentation and eventual cell death, by inhibition and degradation of the fusion proteins (Leboucher *et al*., 2012; Park *et al*., 2014; Pyakurel *et al*., 2015), and activation of the fission machinery (Prudent *et al*., 2015; Toyama *et al.*, 2016). All the DRP1 receptors seem to play a role in mitochondrial fragmentation following depolarisation; Fis1/MFF double-null cells are very resistant to CCCP induced fragmentation, which can be rescued by MiD overexpression (Loson *et al*., 2013). Agreeing with these results, single receptor-null cells have some resistance to CCCP, but successive loss of the receptors conferred addition resistance, with MiD49/MiD51-null and MiD49/MiD51/MFF-null cells exhibiting the greatest protection to CCCP induced mitochondrial fragmentation (Osellame *et al*., 2016).

However, lower doses (10 or 20μM) of antimycin A, a complex III inhibitor, induced hyperfusion, whereas at higher doses (50 or 100μM), cells underwent rapid fragmentation and cell death (Park *et al.*, 2014). This finding highlight that the severity of the insult dictates the response, and when possible, the

mitochondria will undergo SIMH as a protective response, and if the insult is too great, fission will be activated to promote mitophagy and cell death.

Other stresses which have been shown to induce mitochondrial elongation and SIMH are inhibition of transcription or translation, and UV irradiation. The mitochondrial ability to fuse preserves mitochondrial integrity, maintains ATP levels and confers resistance to apoptosis under such stresses (Tondera *et al*., 2009).

1.6 AMP-activated Protein Kinase (AMPK)

1.6.1 AMPK activation

Cells constantly need to balance energy demand with nutrient availability and the ability to generate ATP. During times of high energy demand, ATP levels decrease, and the cell needs to restore the energy supply. Conversely, during times of low energy expenditure, ATP levels will increase, and the cell can undertake energy demanding processes. The equilibrium between these nucleotides can be described by the following equation: 2ADP ↔ AMP + ATP, and thus, falling energy levels are represented as an increase in either the ADP/ATP or AMP/ATP ratios (Hardie, 2016). The key regulator of matching energy demand with energy availability is the AMP-activated protein kinase (AMPK) (Herzig and Shaw, 2018; Kim *et al*., 2016), which has been referred to as the cells “fuel gauge” (Kahn *et al*., 2005). AMPK is a serine/threonine protein kinase, consisting of three subunits; a catalytic α subunit, and two regulatory

subunits, β and γ. There are two α subunits (α1/α2), two β subunits (β1/β2) and three γ (γ1/γ2/γ3), where different combinations can form 12 isoforms of AMPK, with potentially different cellular localisations and functions, although little is known of the different isoform functions (Ross *et al*., 2016). Although all combinations of subunit can form the heterotrimeric complex, there is evidence suggesting that certain combinations are favoured in vivo and under different energy expenditure conditions; for example, the α2/β2/γ3 complex is the predominant complex activated under high-intensity exercise *in vivo* (Birk and Wojtaszewski, 2006).

AMPK is regulated by binding to adenosine phosphates (adenosine 5'mono, di, or tri phosphate (AMP, ADP, ATP)) within the γ subunit. The critical residue for AMPK activation is threonine 172 in the α subunit, and its phosphorylation/dephosphorylation state determines AMPK activation. Binding of AMP activates AMPK by three mechanisms: 1) promotion of phosphorylation at T172, 2) protection against dephosphorylation and 3) allosteric activation of activated AMPK. ADP also induces AMPK activation by the first two mechanisms, whereas ATP binding promotes dephosphorylation (Davies *et al*., 1995; Oakhill *et al*., 2012; Xiao *et al*., 2011). AMPK activation is reviewed in Hardie, 2016.

The major upstream of AMPK is liver kinase B1 (LKB1) (Hawley *et al*., 2003; Woods *et al*., 2003), however, there is still residual AMPK α T172 phosphorylation in $LKB1^{-/-}$ cells (Hawley *et al*., 2003), suggesting additional kinases. Ca^{2+}/Calmodulin-dependent protein kinase kinase-β (CAMKKβ) was subsequently identified as an alternative kinase of AMPK (Hawley *et al*., 2005;

Woods *et al*., 2005). CAMKKβ therefore adds an additional Ca^{2+}-mediated pathway, coupling AMPK activation to intracellular Ca^{2+} concentrations.

1.6.2 AMPK function

The effect of AMPK activation is to restore energy homeostasis by 1) stimulating catabolic processes to generate ATP and 2) inhibition of anabolic processes to reduce ATP demand. Examples of processes to increase ATP include increased glucose and fatty acid uptake, glycolysis, fatty acid oxidation and activation of autophagy. AMPK inactivates multiple biosynthetic pathways, such as inhibiting fatty acid and lipid synthesis, gluconeogenesis, and global protein synthesis, reviewed in Hardie, 2011; Herzig and Shaw, 2018; Oakhill *et al*., 2012.

1.6.3 AMPK and mitochondria

As AMPK is a major energy sensor of the cell, and since mitochondria are sites of OXPHOS, generating the majority of ATP, it is therefore not surprising that AMPK regulates mitochondrial function. *In vivo* studies show that AMPK activation promotes mitochondrial biogenesis and muscle adaptation under energy stress (Bergeron *et al*., 2001; Garcia-Roves *et al*., 2008; Tanner *et al*., 2013; Zong *et al.*, 2002). A major target of AMPK is peroxisome proliferator-activated receptor-γ co-activator-1α (PGC-1α), a positive regulator of mitochondrial biogenesis, which upon AMPK phosphorylation has enhanced activity (Fernandez-Marcos and Auwerx, 2011; Jäger *et al*., 2007). PGC-1α promotes the expression and activity of many transcription factors, for example, nuclear respiratory factors (NRF) and estrogen-related receptor α (ERRα) (Mootha *et al*., 2004; Schreiber *et al*., 2004). In concert with these factors, PGC-

1α orchestrates expression of genes involved in enhancing mitochondrial biogenesis and respiration (Austin and St-Pierre, 2012).

Another way AMPK affects mitochondrial biology is through activating autophagy and mitophagy. AMPK phosphorylates the primary mediator of autophagy, unc-51-like kinase 1 (ULK1), which is involved in the early stages of autophagy initiation (Gwinn *et al*., 2008; Zachari and Ganley, 2017). Phosphorylated ULK1 translocates to damaged mitochondria, where it promotes recruitment of the autophagosome required for mitochondrial degradation (Tian *et al*., 2015; Wu *et al*., 2014). The link between AMPK-ULK1 and mitochondria was established when it was observed that ULK1 deficient mice accumulate mitochondria in maturing reticulocytes, MEF ULK1-null cells have increased mitochondrial mass (Kundu *et al*., 2008) and both AMPK-null and ULK1-null cells have increased mitochondrial number and increased levels of the mitophagy adaptor p62 (Egan *et al*., 2011).

A third mechanism through which AMPK affects mitochondrial function is via phosphorylation of MFF at S155 and S172 during mitochondrial uncoupling and membrane depolarisation, which is necessary for stress induced fission (Toyama *et al*., 2016), as discussed in 1.3.5. AMPK regulation of mitochondria is reviewed in Hardie, 2011; Herzig and Shaw, 2018; Thornton, 2017.

1.6.4 AMPK and OGD

Due to its diverse roles in many signalling pathways, it is not surprising that AMPK has become a target for therapeutic benefit. OGD causes massive energy failure, and as a result a rapid increase in AMPK activation (Culmsee *et al*., 2001; Mungai *et al*., 2011; Rousset *et al*., 2015). *In vitro* OGD of primary neurons showed that

AMPK activation is triggered within 5 minutes, and peaks at 60 minutes. This study chemically manipulated AMPK activity by either sustaining or inhibiting AMPK activation post-OGD. Remarkably, reducing AMPK activation abolishes cell death, whereas prolonged activation enhances cell death. Moreover, pre-conditioning with the AMPK inhibitor prior to OGD exacerbated cell death (Rousset *et al*., 2015). These findings echo *in vivo* findings showing that AMPK activation before ischemic insult to the brain of mice reduces infarct size, cell death and improves neurological function, thus suggesting that AMPK activation is a protective response (Jiang *et al*., 2014). These findings contradict earlier studies, which found that inhibition of AMPK during ischemia, either by pharmacological inhibition or AMPK-α2 knockout in mice, reduces infarct size in the brain, whereas AMPK activation exacerbates stroke pathology (Li *et al*., 2007; McCullough *et al*., 2005). It is clear that AMPK has a major role in cellular pathology during ischemic insult, and further investigations are required to delineate the pathways involved.

1.7 Mitochondria in neurons

The human brain constitutes approximately 2% of total body mass, yet consumes ~20% of O_2 (Attwell and Laughlin, 2001; Mink *et al*., 1981). The majority of ATP generated in neurons is by OXPHOS (Rangaraju *et al*., 2014), which powers the many energy intensive functions within a neuron, such as restoration of ionic balance following action potentials, maintaining resting potentials, neurotransmitter release and recycling, vesicle packaging and trafficking (Attwell and Laughlin, 2001; Lennie, 2003). This imposes a huge demand on neuronal mitochondria. Moreover, neurons are extremely polarised, and their unique architecture poses extreme challenges on mitochondria. For example, a single human dopaminergic neuron has a very complex axonal arbour, with multiple layers of branching and up to 4.5m of processes and 1-2.4 million synapses (Bolam and Pissadaki, 2012). This imposes several challenges for the neuron: Firstly, they need to match the energy demands of the synapses and branches with an adequate supply of ATP to ensure their health and stability. Secondly, since it's proposed the majority of the biosynthetic machinery resides in the soma (Amiri and Hollenbeck, 2008), how does the neuron organise mitochondrial supply to the periphery. This is especially a challenge for extremely large neurons, where the commute from the soma to the periphery is longer than the half-life of many mitochondrial proteins, so how are these mitochondria "re-supplied"? (Misgeld and Schwarz, 2017). There is mounting evidence that mitochondrial fission and fusion is required to maintain mitochondrial supply to neurites, and is required for synaptic function and neuronal health.

1.7.1 Mitochondria fusion in neurons

Fusion and fission dynamics are vital for neuronal function. For reasons already mentioned in section 1.2.2, fusion allows the mixing of contents and complementation, and fission allows segregation and removal of damage, particularly important for post-mitotic, high energy demanding neurons. Indeed, ~82% of fusion occurs between mobile and stationary mitochondria (Cagalinec *et al*., 2013), suggesting that mobility is required for fusion, and may be a mechanism to “replenish” docked mitochondria.

Defective fusion caused by Mfn2 mutations (which cause CMT2A disease) induce aggregation of mitochondria, disrupted mitochondrial distribution and impaired mitochondrial transport along axons (Baloh *et al.*, 2007; Detmer *et al*., 2008; Misko *et al*., 2010). *In vivo* loss of Mfn2 in dopamine neurons leads to fragmented mitochondria and reduces mitochondrial transport events and velocity in axons and dendrites (Pham *et al*., 2012), and Mfn2 is required for maintaining axonal integrity, since Mfn loss leads to lack of mitochondrial supply to distal axons, leading to their degeneration (Lee *et al*., 2012). Interestingly, Mfn1 and OPA1 knockout did not affect mitochondrial trafficking to the same extent as Mfn2, and Mfn2 has been implicated in regulating the Miro-Milton complex (Misko *et al*., 2010; Pham *et al*., 2012), which may explain the greater susceptibility to Mfn2 loss.

1.7.2 Mitochondrial fission in neurons

Primary neurons lacking DRP1 have reduced synapses and neurite number, demonstrating fission is required for the formation of synapses and neuronal

process integrity (Ishihara *et al*., 2009). DRP1 depletion in Purkinje cells results in neuronal degeneration, mitochondrial elongation, accumulation of ROS, decreased ETC activity and progressively become swollen aggregates in the soma. Remarkably, the swollen mitochondrial phenotype and cell death could be reversed by treatment with antioxidants, indicating that oxidative stress is a major factor in mitochondrial dysfunction (Kageyama *et al*., 2012). MFF is required for maintaining axonal size; upon MFF knockdown, axonal mitochondria increase in size, which increase mitochondrial Ca^{2+} buffering capacity, leading to decreased neurotransmitter release and reduced axonal branching (see Figure 1.11AB). MFF also regulates mitochondria entering the axon, since the larger mitochondria in the soma were slower to enter the axon (Lewis *et al*., 2018). Impaired fission depletes the axons and dendrites of mitochondria, therefore deprives the neuronal processes of the ATP and Ca^{2+} buffering capacity the mitochondria provide. Dendritic mitochondria are required for neurite, synapse and dendritic branch formation during development (Fukumitsu *et al*., 2015; Ishihara *et al*., 2009; Lee *et al*., 2004) and also for stimulation induced spine formation (Li *et al*., 2004).

1.7.3 Mitochondria in axons versus dendrites

Mitochondria within the axons and dendrites exhibit different morphologies. Axonal mitochondria are small, punctate and sparsely distributed, whereas dendritic mitochondria are more elongated and occupy a greater volume of the process (Chang *et al*., 2006; Lewis *et al*., 2018). The significance and mechanism of the differential mitochondrial size in neuronal compartments is unclear.

Cagalinec *et al* reveal an intriguing behaviour of axonal mitochondria to regulate their size; in ~85% of fusion-fission cycles, fusion precedes fission, and fission precedes fusion, therefore most mitochondria undergo cyclic fusion-fission events and the rates of fusion and fission are equal. However, small mitochondria favour successive fusion, and larger mitochondria are more likely to undergo successive fission events (non-cyclic). This “self-correcting” behaviour avoids extremes of mitochondrial size. Furthermore, upon increasing mitochondrial fusion by expressing Mfn2, a concomitant increase in fission balanced mitochondrial size. Likewise, expressing a dominant negative mutant of Mfn2 decreases the fusion rate, and the cell responds by decreasing the fission rate, with little effect on mitochondrial size (Cagalinec *et al*., 2013). Whether a similar mechanism occurs in dendrites is yet to be determined. MFF regulates axonal mitochondria, but surprisingly, given the wide cellular distribution of MFF in both axons and dendrites, Lewis *et al* report no effect on the dendritic mitochondria upon MFF knockdown. These data raise the question of what the mechanism of regulating mitochondrial size in axons versus dendrites is, and is there compartment-specific regulation of MFF? Interestingly, DRP1 knockdown reduced the sensitivity of large mitochondria to undergo non-cyclic fission, with no change in the fission/fusion rate (Cagalinec *et al*., 2013). Could this account for the difference observed between the axons and dendrites in the Lewis *et al* report? Could the greatly impaired fission upon MFF depletion be too much for the cells to correct by reducing fusion, and would inhibiting fusion to such an extent be even more detrimental to the cell?

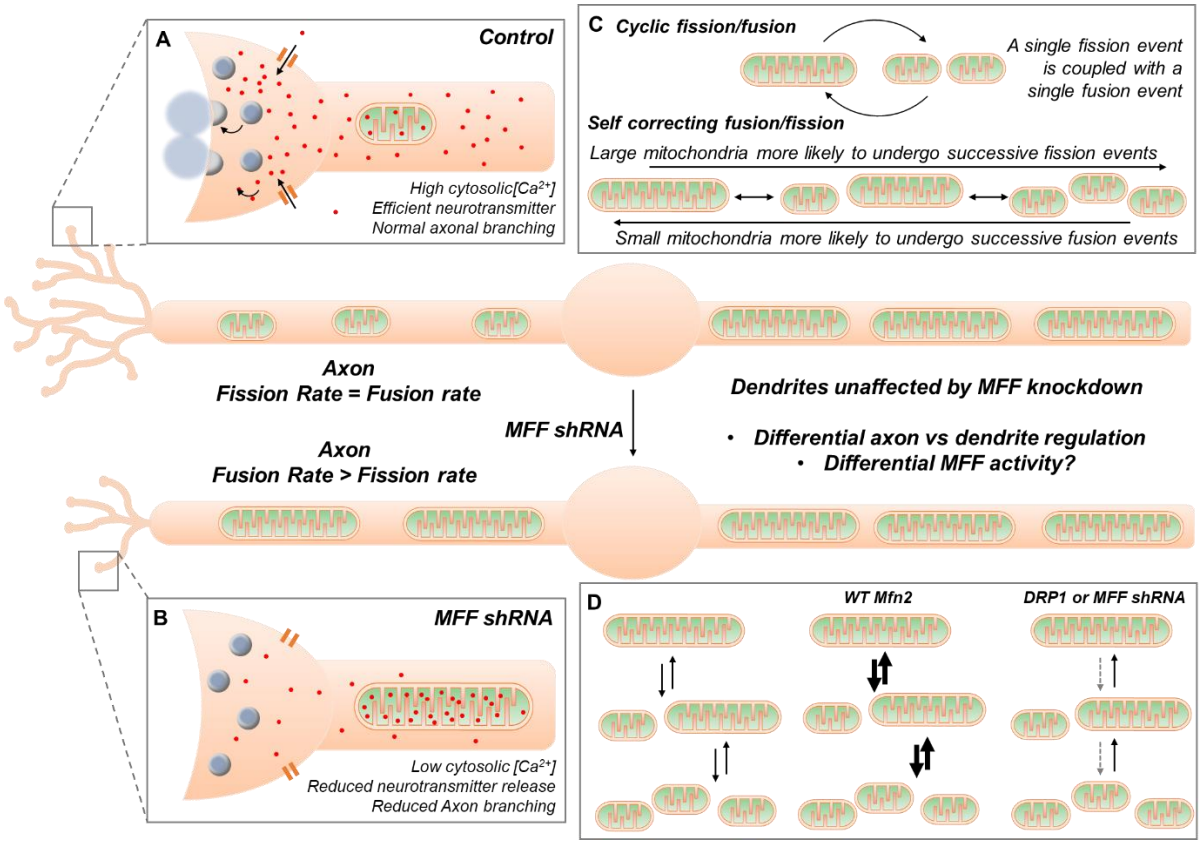

Figure 1.11 Regulation of mitochondrial size in neurons

Schematic of mitochondrial size regulation in neurons based on reports by Cagalinec *et al*. and Lewis *et al.* **A** Axonal mitochondria are small and punctate, their size mediated by MFF, mediating neurotransmitter release and axonal branching. Upon MFF knockdown (**B**) axonal mitochondria increase in size. The enlarged mitochondria have increased Ca^{2+} buffering capacity, which decreases cytosolic Ca^{2+} concentations, decreasing neurotransmitter release and axonal branching. No effect was observed in dendrites upon MFF loss. (**C**) Most mitochondria undergo cyclic fusion-fission events, therefore have balanced rates. But larger mitochondria undergo non-cyclic, successive fission events to correct their size, whereas small mitochondria undergo successive fusion events. This “self-correcting behaviour” avoids extremes in mitochondrial size. **D** manipulating mitochondrial dynamics results in a compensatory adjustment of the

opposing rate. However, under certain conditions i.e. DRP1 and MFF knockdown, it seems that the self-correcting behaviour is insufficient to resolve the change in mitochondrial size.

1.8 Mitochondrial dynamics and disease

The importance of the fusion/fission balance on mitochondrial integrity and health, and the adaptability and plasticity that it bestows on mitochondrial dynamics during stress, is underscored by human disease as a result of disruption of mitochondrial biology.

Mitochondrial diseases are a set of heterogenous disorders associated with disrupted OXPHOS efficiency and mitochondrial function, arising from mutations of either nuclear or mtDNA. Due to the heteroplasmic nature and stochastic mechanism of mtDNA distribution, the clinical symptoms are diverse and can manifest at any age, often involving multiple tissues of high energy demand, such as the heart, brain and muscles. It is estimated that 1 in 5000 people in the UK are affected by mitochondrial disease (Schaefer *et al*., 2008). Common symptoms include cardiomyopathy, encephalopathy, early onset-dementia, deafness, blindness, neuronal atrophy, seizures, developmental delay, poor growth and myopathy (Jameson and Morris, 2011; Lax *et al*., 2017). Mutations in the ETC subunits, mtDNA transcription and translation machinery, mitochondrial tRNAs and mitochondrial dynamics proteins have all been linked to mitochondrial disease.

1.8.1 Fusion

Mfn2 mutations have been linked to Charcot-Marie-tooth disease type 2A (CMT2A) (Polke *et al*., 2011), which involves slow and progressive degeneration of the peripheral neurons, mostly affecting the extremities. The defect in mitochondrial trafficking in Mfn-deficient neurons may account for the fact that Mfn2 has been linked to CMT disease, where longer axons are preferentially affected, and therefore perhaps more dependent on long distance transport. As previously mentioned, OPA1 mutations are linked to degeneration of the optic nerve, leading to eventual blindness (Alexander *et al*., 2000; Delettre *et al*., 2000), with over 100 mutations associated with the disease (Han *et al*., 2006). A study in mice found that homozygous mutations is embryonically lethal, and heterozygous mice at 12 months of age had decreased OXPHOS activity, loss of cristae structure, increased oxidative stress, mtDNA loss, progressive cardiomyopathy resulting in abnormal cardiac function, and progressive blindness (Han *et al*., 2006). OPA1 has therefore become a target for therapy; Varanita *et al* demonstrate that mild overexpression (~1.5-fold increase) is protective against various insults *in vivo* (Varanita *et al*., 2015). For example, following ischemic insult, cell death in the heart and infarct size in the brain was significantly reduced. Moreover, OPA1 overexpression decreased susceptibility to *in vivo* models of liver damage and muscle atrophy by reducing cytochrome c release and ROS generation. Similar work shows that OPA1 can reverse motor symptoms, respiratory deficits and increase lifespan in mouse models of mitochondrial disease, and show that OPA1 is important for regulating cristae structure,

ameliorating cell death and stabilising OXPHOS complexes, highlighting that OPA1 is a targetable component of mitochondrial dynamics during mitochondrial disease (Civiletto *et al*., 2015; Varanita *et al.*, 2015).

1.8.2 Fission

One case of human mutant DRP1 mutation has been reported in a new-born. The patient exhibited little spontaneous movement and reflexes were poor, with poor visual fixation. She had high concentrations of lactate in the blood and spinal fluid, typical of a mitochondrial disease. She remained unresponsive, did not thrive and had little developmental progress, and died suddenly aged 37 days (Waterham *et al*., 2015).

Autosomal recessive mutations of MFF, causing a truncation and loss of the transmembrane domain of MFF, were identified to cause Leigh-like syndrome in infants. The patients became symptomatic within the first year of life, exhibited developmental delay, microcephaly, and progressively developed spasticity and optic and peripheral neuropathy (Koch *et al*., 2016; Shamseldin *et al*., 2012). Chen *et al.* generated MFF mutant homozygous mice, which have neuromuscular defects, cardiomyopathy and fibrosis, eventually leading to heart failure and die at an average age of 13 weeks. Cardiomyocytes from MFF mutant mice have decreased mtDNA levels, ETC complex activity and increased oxidative stress. Remarkably, the authors combined the MFF mice with mutations of Mfn1 and 2, which rescued the cardiomyopathy, mitochondrial defects, oxidative stress and enhanced life span by ~60% (Chen *et al.*, 2015).

This study demonstrates that balanced fusion and fission are vital for survival and tissue function, and by extension, understanding the mechanism of mitochondrial dynamics, and how they can be manipulated, can offer therapeutic benefit.

1.8.3 Neurodegeneration

Neurodegenerative diseases are broadly associated with mitochondrial dysfunction, increased oxidative stress, neuronal cell death and impaired proteostasis (Briston and Hicks, 2018; Selfridge *et al*., 2013). The major neurodegenerative diseases, Alzheimer's disease (AD) and Parkinson's disease (PD) are characterised by accumulation of amyloid-β, phosphorylated-tau and α-synuclein, respectively (Briston and Hicks, 2018).

The protein aggregates associated with AD and PD are detrimental to mitochondrial function; amyloid-β localises to mitochondria in the brains of human AD patients and is internalised by the mitochondrial import machinery (Hansson Petersen *et al*., 2008). Transgenic-mouse strains of amyloid-β and tau pathology exhibit reduced mitochondrial membrane potential, increased oxidative stress and impaired OXPHOS activity (Rhein *et al*., 2009), possibly through amyloid-β and phosphorylated-tau interacting with mitochondrial proteins and inhibiting mitochondrial import (Cenini *et al*., 2016; Manczak and Reddy, 2012). Likewise, pathologic α-synuclein localises to the mitochondria in both *in vivo* and *in vitro* studies, which inhibits complex I activity and induces oxidative stress (Chinta *et al*., 2010; Devi *et al*., 2008). α-synuclein was recently shown to interact with mitochondrial import machinery, disrupting mitochondrial protein import and causing oxidative stress and reduced membrane potential (Di Maio *et al*., 2016).

In addition, unpublished work from the Henley lab indicate that SENP3 levels increase in PD brain patients, and DRP1 decreases in AD samples, indicating a potential disruption in the SUMO pathway and altered mitochondrial fission proteins under pathological conditions. These studies demonstrate that pathological proteins associated with neurodegeneration disrupt mitochondrial function, and a greater understanding of the relationship between mitochondrial dysfunction and neurodegeneration could potentially offer therapeutic benefit.

As mentioned in section 1.2.2, the PINK1/parkin pathway targets dysfunctional mitochondria for degradation by mitophagy, and rare mutations in PINK1 and parkin cause early onset autosomal recessive PD (Kitada *et al*., 1998; Valente *et al*., 2004). Thus, disruption of the PINK1/parkin pathway will impair the protective effect and quality control this pathway confers, highlighting the importance of maintaining a healthy population of mitochondria, and the critical process of mitophagy for neuronal health. PINK1$^{-/-}$ mice show impaired mitochondrial function at 3-4 months, whereas a similar impairment was observed in wild-type mice only at 24 months of age. Furthermore, this report demonstrated that loss of PINK1 exacerbates susceptibility of cortical mitochondria to H_2O_2-induced respiratory impairment (Gautier *et al*., 2008). There are mixed reports of parkin mutant mice, with some evidence of mitochondrial dysfunction, decreased respiration and increased oxidative stress (Palacino *et al*., 2004), whereas others report no overt phenotype (Perez and Palmiter, 2005). Studies have shown that additional stress to parkin mutant mice, such as crossing with PolG mutant (which accumulates mtDNA mutations) or exhaustive exercise results in increased

inflammation, mitochondrial dysfunction and dopaminergic cell death (Pickrell *et al*., 2015; Sliter *et al*., 2018). These reports highlight that disruption of mitophagy increases mitochondrial susceptiblity to damage and dysfunction, and this results in loss of dopaminergic neurons.

Aims

Preliminary data from the Henley lab suggested that MFF is a SUMO substrate. With the wealth of evidence that PTMs regulate mitochondrial dynamics proteins, and that mitochondrial morphology is inextricably linked to cellular health, this warranted further investigation. Indeed, DRP1 function has been shown to be regulated by SUMOylation following stress (Guo *et al*., 2013; Prudent *et al*., 2015), and since MFF is the major DRP1 receptor, I thought it reasonable that the receptors are also likely highly regulated by PTM.

My project aims were to address the following questions:

- Where is MFF SUMOylated?
- How is MFF SUMOylation regulated?
- What is the function of MFF SUMOylation in mitochondrial morphology?

Chapter 2 Materials and Methods

2.1 Materials

All reagents were purchased from Sigma-Aldrich unless otherwise stated.

2.1.1 Bacterial reagents

<u>*E. Coli* bacterial strain</u>

DH5α – supE44 Δlac Φ80 lacZΔ M15 hsdR17 recA1 endA1 gyrA96 thi-1 relA1 u169

Competent DH5α (Thermo Fisher) were used for cloning and amplification of DNA, and were made in house as described in Inoue *et al*., 1990.

Bacterial growth media and agar plates

Bacteria were grown in Luria Bertani (LB) broth prepared in house (University of Bristol central stores) for cloning and DNA amplification purposes. Agar plates were prepared using LB and 1.5% (w/v) agar and kept at 4°C. LB and agar plates were supplemented with appropriate antibiotics; ampicillin (100µg/ml) or kanamycin (25µg/ml).

2.1.2 Molecular Biology reagents

Enzymes

All restriction enzymes and buffers for site directed mutagenesis and cloning were supplied by New England Biolabs (NEB) and stored at -20°C. T4 DNA ligase to ligate vectors and inserts was from Takara (BioWhittaker). Calf Intestinal Alkaline Phosphatase (CIP) was from NEB.

Catalytically active domain of ubiquitin specific peptidase 2 (USP2) was a kind

gift from P. Murphy from the R. Hay lab (University of Dundee). The catalytically active domain of SENP1 was from A. Nishimune. Both were aliquoted and stored at -20°C.

Polymerase Chain Reaction (PCR) kit

PCR reagents (Polymerase, 10x buffer, dNTPs and $MgSO_4$) were from the KOD Hot Start DNA Polymerase kit from Merck Millipore.

Plasmid DNA purification

Thermo Scientific GeneJET™ plasmid Miniprep kit (#K0503) and Midiprep kit (#K0481) were used for plasmid DNA purification purposes

RNA extraction and cDNA synthesis

RNeasy mini kit RNA extraction kit was obtained from Qiagen (#74104) and cDNA RevertAid First Strand kit (Thermo Scientific #K1621) was from Thermo Fisher Scientific.

Plasmids used

- pcDNA3.1 (Invitrogen)
- pECFP-C1 (Clontech)
- Mito DS-Red (pxlg-px-wpre construct, from K. Wilkinson)
- GST-MFF (pEBG construct from Guo *et al*., 2017)
- GST-DRP1 receptors (pEBG construct from Guo *et al*., 2017)
- FLAG-SUMO (pCMV construct, Henley Lab)
- YFP-SUMO-ΔGG (From F. Melchior)
- HA-ubiquitin (Henley Lab)
- Myc-MiD49 (mouse MiD49, pEBG construct from C. Guo)

Oligonucleotide primers for Site Directed mutagenesis of MFF

All oligonucleotides were purchased from Sigma-Aldrich and resuspended in 1xTE (10mM Tris-HCl pH8.0, 1mM EDTA).

Table 1 Oligonucleotide primers used for Site-Directed Mutagenesis

Protein and mutation	Primer sequence	Vector	Tag (N/C terminus)
MFF K151R	ATCCGAGCAGTTGGCAGACTA**AGA**A GAGAGCGGTCTATGAGTGAA (For) TTCACTCATAGACCGCTCTCT**TCT**TAG TCTGCCAACTGCTCGGAT (Rev)	pEBG-GST pECFP	GST (N) CFP (N)
MFF E153A	GCAGTTGGCAGACTAAAAAGA**GCG**C GGTCTATGAGTGAAAATGCT (For) AGCATTTTCACTCATAGACCG**CGC**TC TTTTTAGTCTGCCAACTGC (Rev)	pEBG-GST pECFP	GST (N) CFP (N)
MFF S155A	GGCAGACTAAAAAGAGAGCGG**GCT**A TGAGTGAAAATGCTGTTCGC (For) GCGAACAGCATTTTCACTCAT**AGC**CC GCTCTCTTTTTAGTCTGCC (Rev)	pEBG-GST pECFP	GST (N) CFP (N)
MFF S155D	GGCAGACTAAAAAGAGAGCGG**GAT**A TGAGTGAAAATGCTGTTCGC (For) GCGAACAGCATTTTCACTCAT**ATC**CC GCTCTCTTTTTAGTCTGCC(Rev)	pEBG-GST pECFP	GST (N) CFP (N)
MFF 2SA	GGACAGCTGGTCAGAAATGAT**GCT**CT GTGGCACAGATCAGATTC (For) GAATCTGATCTGTGCCACAG**AGC**ATC ATTTCTGACCAGCTGTCC (Rev)	pECFP (S155A)	CFP (N)
MFF 2SD	GGACAGCTGGTCAGAAATGAT**GAT**CT GTGGCACAGATCAGATTC (For) GAATCTGATCTGTGCCACAG**ATC**ATC ATTTCTGACCAGCTGTCC (Rev)	pECFP (S155D)	CFP (N)

2.1.3 Electronic Equipment

For cell culture, laminar hoods were from Holten LaminAir and incubators were from RS Biotech. Bacterial shaking incubator was from Brunswick Scientific. Benchtop microcentrifuges were form Eppendorf and Biofuge. Low speed centrifuges were from Jouan and Hettick. Power pack electrophoresis system was from Bio-Rad Laboratories. Thermal cycler PCR machine was from MJ Research PTC-2000. X-Ray film developer (SRX-101A) was obtained from Konica. Dissection microscopes for dissection were from Leica. MACS-VA500-Micro Aerophilic workstation for OGD was from dw Scientific. Heat block was from Eppendorf, water bath from Grant and UV transilluminator from BioDoc-It™ Imaging System. For sonicating cells, Microson Ultrasonic Cell Disrupter was used. Imaging was carried out using a Leica SP5-II confocal laser scanning microscope attached to a Leica DMI 6000 inverted epifluorescence microscope.

2.1.4 Cell culture reagents

Glassware and plasticware

Pipette tips (10 to 1000µl) were obtained from StarLabs, and gel loading tips from Fisher. 5, 10, 25mL stripettes were from CellStar. 1.5mL microcentrifuge tubes were purchased from Eppendorf and 0.5mL thin-walled PCR tubes were purchased from StarLabs. 15mL and 50mL conical Falcon tubes, 6-well dishes and T75 vented flasks were CellStar. 25mm glass coverslips and glass slides were obtained from VWR International.

HEK293T cells

Human Embryonic Kidney cells (HEK293T) cells were from the European Collection of Cell Cultures (ECACC), maintained in 1% DMSO and stored in liquid nitrogen for long term storage.

MEF cells

Mouse Embryonic Fibroblasts (MEF), wildtype and MFF-null, were a kind gift from D. Chan, reported in Loson *et al*., 2013, maintained in 1% DMSO and stored in liquid nitrogen for long term storage.

Complete media and reagents

HEK293T and MEF cells were maintained in Dulbecco's Modified Eagle's Medium (DMEM) media (with phenol red) containing 4.5g/L glucose (Lonza), 10% heat-inactivated foetal bovine serum (FBS, Sigma), 2mM L-glutamine (Gibco) and 1000U penicillin and 0.1mg streptomycin (Gibco). Used to maintain stocks of HEK293T and MEF cells. 10x phosphate buffered saline (PBS), sterile cell culture grade water, 0.05% trypsin-EDTA and L-Glutamine were obtained from Gibco. Lipofectamine 2000 was from Invitrogen. Poly L and D lysine were from Sigma.

Neuronal plating media

Neurobasal media (Gibco), 5mM glutamax (Gibco), 5% horse serum (Sigma), 1% penicillin/streptomycin (Sigma), 10% B27 (Gibco).

Neuronal feeding media

Neurobasal media, 1% penicillin/streptomycin, 2mM glutamine (Gibco), 10% B27.

2.1.5 Protein biochemistry reagents

30% v/v acrylamide was from Geneflow, cOmplete™ Protease tablets were obtained from Roche and dissolved in 1mL distilled water to prepare a 50x stock and stored at 4°C. Polyvinylidene difluoride (PVDF) immobilin membrane (0.45µM pore) was obtained from Millipore and filter paper was from GE Healthcare Life Sciences. PageRuler protein ladder (10-180kDa #26616) was from Thermo Fisher. Non-fat milk powder from the Co-operative own brand was used for blocking. Enhanced Chemiluminescence (ECL) solutions Supersignal® West Pico and West Femto ECL were from Thermo Scientific. Lumnata™ Crescendo and Luminata™ Forte were from Merck Millipore. CL-Xposure™ X-ray film was from Thermo Scientific and used to develop blots by ECL in a hypercassette™ from Amersham biosciences. Fixer and developer solutions were obtained from Fixaplus. GFP-Trap beads were from Chromotek and GST beads were from GE Healthcare Life Sciences.

2.1.6 Recipes of commonly used solution

The following solutions were prepared in house

Phosphate buffered saline (PBS)

137mM NaCl, 10mM Na_2HPO_4, 2.7mM KCl, 2mM K_2HPO_4, pH 7.4

Phosphate buffered saline with Tween (PBS-T)

137mM NaCl, 10mM Na_2HPO_4, 2.7mM KCl, 2mM K_2HPO_4, pH 7.4, 0.001% Tween-20

2x Laemmli sample buffer

4% SDS, 10% glycerol, 125mM Tris pH 6.4, 10% 2-β-mercaptoethanol (β-ME), 0.004% bromophenol blue

Immunoprecipitation/pulldown buffer

20mM Tris (pH 7.4), 137mM NaCl, 1% Triton X-100, 10% glycerol, 25mM β-glycerophosphate, 2mM Na-pyrophosphate, 20mM N-ethylmaleimide, 2mM EDTA, pH adjusted when cold using NaCl to 7.5±0.02. Stored at 4°C.

10-12% resolving poly-acrylamide gel

375mM Tris-HCL pH 8.8, 10% or 12% acrylamide, 0.1% SDS, 0.1% APS and 0.01% TEMED

5% stacking gel

125mM Tris-HCL pH 6.8, 5% acrylamide, 0.1% SDS, 0.1% APS, 0.01% TEMED

Transfer buffer

50mM Tris, 40mM glycine and 20% methanol in ddH2O

Running buffer

25mM Tris, 250mM glycine and 0.1% SDS

Fixed cell imaging reagents

Stock solution of 16% Formaldehyde was obtained from Electron Microscopy Sciences and Fluoromount-G™ mount media with DAPI was from Thermo Fisher.

Primary Antibodies

Table 2 lists primary antibodies used for Western blotting (WB) and immunocytochemistry (ICC), concentrations, supplier, preparation and use (WB or ICC). For WB, antibodies were prepared in either 2% BSA or 2.5% milk in PBS-T, and for ICC, antibodies were prepared in 3% BSA in 1x PBS.

Secondary Antibodies

For Western blotting, HRP-conjugated anti-mouse (raised in Goat), anti-goat (raised in Rabbit), anti-rabbit (raised in Goat) and anti-rat (raised in Rabbit) were obtained from Sigma-Aldrich and used at a dilution of 1:10,000 in 2.5% milk or 2% BSA in PBS-T.

All secondary antibodies for ICC were Cy2, Cy3 and Cy5 (raised in Donkey) were from Jackson ImmunoResearch and used at 1:400 in 3% BSA in 1x PBS

Table 2 List of antibodies for Western blotting and immunocytochemistry

Protein	Dilution	Supplier	Catalogue number	Species	Preparation
AMPK-pi (T172)	1:1,000	Cell Signalling	2535S	Rabbit	BSA
p-(S/T) AMPK substrate motif	1:10,000	Cell Signalling	5759S	Rabbit	BSA
Ankyrin G (ICC)	1:500	UC Davis/NIH NeuroMab facility	75-146	Mouse	BSA
Beta actin	1:20,000	Sigma	A5441	Rabbit	BSA
DRP1	1:1,000	BD Bio Science	611113	Mouse	Milk
DRP1 (ICC)	1:400	BD Bio Science	611113	Mouse	BSA
FLAG	1:1,000	Sigma	F3165	Mouse	Milk
GFP	1:20,000	Chromotech	pabg-1-100	Rat	Either
GFP (ICC)	1:1000	Abcam	13970	Chicken	BSA
GST	1:10,000	GE Healthcare	27457701V	Goat	Either
HA	1:4,000	Sigma	H3663	Mouse	Milk
MiD49	1:500	Proteintech	16413-1-AP	Rabbit	Milk
MFF	1:500	Santa Cruz	SC-398731	Mouse	Milk
Myc	1:1,000	Santa Cruz	SC-40	Mouse	Milk
SENP 3	1:1,000	Cell Signalling	5591S	Rabbit	BSA
SUMO-1	1:1,000	Cell Signalling	4930S	Rabbit	BSA
SUMO-2/3	1:1,000	Cell Signalling	4971S	Rabbit	BSA
Ubiquitin (P4D1)	1:1,000	Cell Signalling	3936	Mouse	Milk

2.2 Methods

2.2.1 Cell culture of HEK293T and MEF cells

All cell culture was performed in sterile laminar flow cabinets and cells were maintained in humidified incubators at 37°C, 5% CO_2 and 95% O_2. HEK293T and MEF cells were maintained in complete media and grown in T75 ventilated flasks.

2.2.2 Passaging of cells

Cells were passaged regularly when they reached ~90-100% confluency, by gentle washing with pre-warmed sterile 1x PBS, and incubated in 1mL 0.05% trypsin-EDTA for 3-5 minutes at 37°C, followed by addition of an equal volume of complete media and gentle pipetting and agitation to detach the cells. Cells were pelleted by centrifugation at 1500rcf for 2 minutes, trypsin aspirated, and cells resuspended in complete culture media by gentle trituration and plated in a new culture T75 flask at 1:10 or 1:20 in 10mL complete culture media.

2.2.3 Plating cells

For transfection experiments, 6cm plastic dishes coated in PLL were used to aid adhesion. Dishes were incubated with 2mL 0.1mg/mL PLL, diluted in sterile water, for at least 1hr at 37°C and washed three times with sterile water. HEK293T cells were passaged as described above, and an aliquot of cell suspension was counted using a haemocytometer. $1.5x10^6$ cells were plated in 4mL transfection media (complete media lacking antibiotics) per dish and incubated overnight.

MEF cells were seeded in 6-well dishes with one 25mm glass cover slips at the bottom. PLL was used to aid adhesion to the glass (as above). Following

passaging, cells were counted, and $10x10^5$ cells were plated in 1.5mL complete media per well and left overnight to adhere to the glass.

2.2.4 Haemocytometer counting cells

Following trypsinisation and resuspension, 20µL of cells were diluted in 180µL 0.4% Trypan Blue (Gibco). The cell mixture was pipetted into a haemocytometer chamber and the average number of live cells counted to determine the concentration of cells. Cell suspension was then diluted in media and plated accordingly.

2.2.5 Total protein cell lysis

For total protein lysate, cells were plated in 6-well dishes and grown until confluency. Cells were washed once in 1x PBS, 300µL 1x Sample Laemmli buffer was added and cells scraped into Eppendorf tubes, sonicated and boiled at 95°C for 10 minutes. Samples were then stored at -20°C.

2.2.6 HEK293T Transfection

On the day of transfection, cells were inspected to ensure confluency of ~60-70%. Cells underwent one media change to 4mL transfection media at least 30 minutes before transfection. For a single transfection, 2.5µg DNA was used, for a double transfection, 1.5µg of each construct was used. DNA was added to 500µL plain DMEM in a 1.5mL Eppendorf, and Lipofectamine® 2000 was added at 1.5µL x µg of DNA. DNA-Lipofectamine mixture was vortex briefly and incubated at room temperature for 30 minutes. The mixture was added dropwise to the dish, with gentle swirling and left in the incubator for 48hrs.

2.3 Primary Neuronal Culture

Primary rat hippocampal neurons were cultured on PDL-coated glass cover slips, plated in 2mL plating media for the first 24hrs. Media was changed to 3mL feeding media and neurons were left for two weeks in humidified incubators at 37°C, 5% CO_2 and 95% O_2.

2.3.1 Preparation of glass coverslips

25mm glass coverslips were submerged in nitric acid and incubated overnight with gentle agitation at room temperature. The nitric acid was carefully removed, and coverslips were washed with distilled water; three quick washes followed by three 30-minute washes. The coverslips were carefully transferred to a 140mm plastic cell culture dish and sterilised in 70% ethanol for at least 2 hours with gentle agitation at room temperature. The coverslips were then given three quick washes and three 30 minute washes with sterile cell culture grade water, carried out in a cell culture hood. The coverslips were stored in cell culture grade water at room temperature until further use.

2.3.2 PDL coating and borate buffer

Borate buffer was used in conjunction with PDL to aid adherence to the glass coverslip. Borax and boric acid powders were diluted in sterile cell culture grade water to 1mM borax and 5mM boric acid and filtered through a sterile filter vacuum system with 0.2µm pore membrane.

Sterile coverslips were carefully placed at the bottom of a well of 6-well dish (one cover slip per well) and PDL was dissolved in borate buffer to a concentration of

1mg/mL and 2mL added to each well, enough to cover the glass cover slip. Coverslips were incubated in PDL overnight at 37°C. Coverslips were then washed three times in sterile cell culture grade water to remove borate buffer and residual PDL.

2.3.3 Rat embryonic brain dissociation

Pregnant E18 Wistar rats were deeply anaesthetised using isoflurane with pure oxygen flow until heart failure and then humanely sacrificed using cervical dislocation or decapitation under Home Office Schedule 1 regulations. The embryonic sac was dissected out and placed in Hank's Buffered Salt Solution (HBSS) (Gibco) at room temperature. Embryos were immediately removed from their sacks and decapitated. Under a dissection microscope, the brains were removed from severed heads using sharp, sterile dissection forceps. The meninges, cerebellum and midbrain were discarded, and the individual hippocampi were dissected out of the cortex.

After isolation of the hippocampus, the following steps were carried out using aseptic techniques in a sterile laminar flow hood. The dissected hippocampus was transferred to sterile 15ml falcon tubes and washed three times with 10mL HBSS. Hippocampi were incubated in 10ml HBSS containing 0.005% trypsin-EDTA for 9 minutes at 37°C. The trypsinised tissue was washed three times in 10mL HBSS, then washed once in 1mL plating media to inactivate any residual trypsin. The hippocampal cell suspension was gently pipetted up and down several times using a 1ml pipette to dissociate hippocampal cells. The hippocampal cell suspension was diluted with 4ml plating media and cells counted

using a haemocytometer. 80,000 hippocampal cells were plated into each 6-well dish.

2.3.4 Neuronal transfection

DIV 14 hippocampal neurons were washed by briefly (<1 minute) placing into a 6-well dish with pre-warmed plain neurobasal media to remove antibiotics and debris. Coverslips were then placed into a new 6-well dish with fresh pre-warmed feeding media without antibiotics (1mL/dish) and placed in the incubator. DNA was prepared in plain 100µL neurobasal media (1µg of CFP-MFF construct and 1µg Mito DS-Red), and Lipofectamine was prepared in a separate Eppendorf tube in plain 100µL neurobasal media (at 1.5µL x µg of DNA). Each tube was vortexed for 5 seconds and left at room temperature for 5 minutes. Lipofectamine was added to the DNA tube and vortexed again for 5 seconds and left at room temperature for 30 minutes.

Following incubation, DNA-Lipofectamine mixture was added dropwise to the coverslips and left to incubate in the incubator for 60 minutes. Following this, coverslips were carefully removed, briefly washed again in the plain neurobasal media and replaced back into their original media. Cells were left for 2 days until fixation.

2.4 Western blotting

2.4.1 SDS-PAGE

Sodium dodecyl sulphate-polyacrylamide gel electrophoresis (SDS-PAGE) was used to resolve proteins based on molecular weight. Resolving gel was prepared within 1.5mm glass plates and filled with ~7.5mL 10% or 12% acrylamide resolving gel solution and 2mL 100% ethanol was added on top to ensure level polymerisation. Once gel had polymerised, ethanol was removed by washing with distilled water and then ~2mL 5% stacking gel was added and either a 10-lane or 15-lane comb was inserted to form the wells of the gel. Once stacking gel had polymerised, the comb was removed and the gel inserted into a Bio-Rad power pack electrophoresis system. The tank was filled with SDS-PAGE running buffer and samples were loaded into the wells. 5µl pre-stained protein molecular weight was also loaded. Electrophoresis was initially carried out at 80V to allow samples to clear the stacking gel and to ensure level running of the samples. Power was then increased to 150-180V to resolve proteins.

2.4.2 Transfer

Once proteins had been sufficiently resolved, the proteins within the poly-acrylamide gel were carefully removed from the glass plates and transferred to an Immobilin-PVDF membrane, activated with 100% methanol for several minutes and equilibrated for at least 5 minutes in transfer buffer. All transfers were carried out using wet transfer, and sponges and filter paper were pre-soaked in transfer buffer before assembly. The gel and membrane were sandwiched between filter paper (three each side) and sponges within a transfer cassette.

Transfer was carried out at 400mA for 90 minutes and cooled with an ice pack and constant stirring with a magnetic flea at the bottom of the transfer tank.

2.4.3 Immunoblotting

Once transfer was complete, membranes were blocked in either 4% BSA or 5% milk in PBS-T. Membranes were then incubated in primary antibody, diluted in 2% BSA or 2.5% milk (Table 2) overnight at 4°C with gentle rotation. Blotting solution matched the solution of the primary antibody. Following primary antibody incubation, membranes were washed three times in PBS-T for ten minutes each at room temperature. Membranes were then incubated with secondary antibody at a dilution of 1:10,000 at room temperature for 1hr in either 2% BSA or 2.5% milk.

2.4.4 Chemiluminescence detection

Following secondary incubation, membranes were washed three times for ten minutes each with PBS-T. Membranes were dried of excess PBS-T and incubated for 1 minute at room temperature with the appropriate ECL substrate: Pierce™ West Pico, Luminata™ Crescendo, Luminata™ Forte, SuperSignal™ West Femto. Excess ECL was removed and membrane was placed between acetate sheets within a developing cassette. In a dark room, the membrane was exposed to X-ray film and developed in a medical X-ray film processer. Films were scanned as TIF files and ImageJ software was used for densitometry analysis.

2.5 Immunoprecipitations

2.5.1 Cell lysis

In order to retain the labile SUMO on MFF, without disrupting non-covalent interactions, N-ethylmaleimide (NEM) was added to lysis buffer to inhibit deSUMOylating enzymes. Addition of β-glycerophosphate and Na-pyrophosphate inhibits phosphatases, based on a previous method (Guo *et al*., 2013) (20mM Tris (pH 7.4), 137mM NaCl, 1% triton X-100, 10% glycerol, 25mM β-glycerophosphate, 2mM Na-pyrophosphate, 20mM NEM, 2mM EDTA, pH adjusted when cold using NaCl to 7.5±0.02. Stored at 4°C). On day of the experiment, 1x protease inhibitor cocktail (Roche) was added. For experiments investigating SUMO and ubiquitin, lysis buffer was also supplemented with 0.1% SDS. HEK293T cells were washed once in 1x PBS and lysed in 500µL ice cold lysis buffer. Cells were scraped and collected into 1.5mL Eppendorf tubes and lysed on ice for 30-45 mins. For investigating SUMO and ubiquitin (lysed in buffer with 0.1% SDS) samples were briefly sonicated with five short (~2 seconds) sonications on output 3. Lysate was centrifuged for 20 minutes at 16,000g at 4°C to precipitate insoluble material. Supernatant was collected and kept on ice. 20µL (4%) input taken and added at 1:1 to 2x Laemmli sample buffer. Inputs were boiled at 95°C for 10 minutes.

2.5.2 Pull Downs

GST-tagged proteins were isolated on 20µL glutathione-Sepharose 4B (GE Healthcare), CFP-tagged proteins were isolated on 6µL GPT-TRAP® beads (Chromotek). Beads were washed twice in 1mL wash buffer (lysis buffer without

NEM, SDS and protease inhibitors) by centrifugation at 1500rcf for 2 minutes and aspirating wash buffer. After washing, beads were equally split into fresh Eppendorf tubes. Supernatant was incubated with beads at 4°C for 90 minutes with slow rotation. Beads were washed three times in 500µL wash buffer by placing on a rotating wheel at 4°C for 3-5 minutes. After final wash supernatant was removed and 40µL 2x Laemmli sample buffer added to samples and boiled at 95°C for 10 minutes.

2.6 Molecular biology methods

2.6.1 Bacterial transformation

Chemically competent DH5α E.coli were stored at -80°C and used for transformation and amplification of plasmid DNA. When E.coli had thawed (on ice) 1μL of DNA was incubated with 10μL E.coli (for DNA amplification purposes) 40μL E.coli was incubated with 4μL PCR product (i.e. from a site directed mutagenesis PCR reaction or ligation) on ice for 30 minutes. E.coli was then heat shocked at 42°C for 45 seconds, then cooled on ice for a further 2 minutes. 200μL plain LB broth was added to the bacteria. If the antibiotic resistance was kanamycin, bacteria were incubated for 1hr at 37°C to allow expression of genes for antibiotic resistance. To spread bacteria on agar plates, LB broth and bacteria were added to pre-warmed plates and spread evenly using a disposable L-shaped cell spreader. Agar plates were incubated at 37°C overnight with the lid face down to avoid condensation occurring on the agar.

2.6.2 Bacterial amplification and DNA purification

For PCR product screening purposes, single colonies on the LB agar plates were picked and grown in 3mL LB broth (supplemented with appropriate antibiotic) at 37°C overnight in a shaking incubator. To extract and purify plasmid DNA, Thermo Scientific GeneJET™ plasmid Miniprep kit was used according to manufacturer's instructions and eluted in 50μL elution buffer.

For DNA plasmid amplification, single colonies were picked and added to 100mL LB broth (with appropriate antibiotic) and incubated at 37°C overnight in a shaking incubator. DNA was extracted and purified using Thermo Scientific GeneJET™

plasmid Midiprep kit according to manufacturer's instructions, eluted in 500µL elution buffer.

To determine the concentration of plasmid DNA, a NanoDrop ND-1000 (LabTech) was used to measure absorbance at 260nm. PCR plasmids were screened for successful site-directed mutagenesis by using Eurofins MWG Services with standard forward and reverse primers available from Eurofins MWG. DNA was stored at 4°C, or -20°C for long term storage.

2.6.3 Polymerase Chain Reaction (PCR)

KOD Hot Start DNA Polymerase kit was used for PCR reactions. Hot KOD polymerase was purified from *Thermococcus kodakaraensis*. Table 3 lists the components for each PCR reactions.

Table 3 Components of PCR reactions

Component	Volume (µL)	Final concentration	Stock concentration
10x Buffer	5	1x	10x
dNTP mix	5	0.2mM	2mM
$MgSO_4$	3	1.5mM	25mM
DMSO	2.5	5%	100%
Template DNA	10	0.2ng/µL	1ng/µL
Forward primer	1.5	0.3µM	10µM
Reverse primer	1.5	0.3µM	10µM
Sterile water	20.5	-	-
KOD Hot Start Polymerase	1	0.02 units/µL	1 units/µL

PCR thermocycler setup was carried out with the settings in Table 4. For GST-MFF and CFP-MFF constructs, the number of repeats was 22-24 cycles and an extension time of 320 seconds. For amplification from cDNA for cloning purposes, 34 cycles were used and an extension time of 5 seconds.

Table 4 PCR thermocycler settings

Step	Temperature (°C)	Time (Seconds)	Process
1	95	120	Activates Polymerase
2	95	20	Denature DNA
3	55	10	Anneal Primers
4	70	320/*5*	Extension
5	Repeat steps 2-4, 22-24/*34* cycles		
6	70	320/*5*	Final extension
7	10	600	Cooling. Anneal DNA

For site directed mutagenesis, once PCR product had cooled, 1µL Dpn1 was added for 1-2hrs at 37°C, which digests methylated DNA to remove original template DNA, and then PCR product was transformed into bacteria.

2.6.4 PCR product and vector digestion purification

For cloning purposes to ensure successful PCR and digestion, DNA was purified using GeneJET™ Gel extraction kit (#K0691) using manufacturer's protocol. Briefly, binding buffer was added at a 5:1 ratio, vortexed briefly, added to the purification column and centrifuged at 16,000rcf for 1 minute in a benchtop centrifuge. Flow-through was discarded and wash buffer was added to the column and centrifuged. Flow-through discarded and wash step was repeated. DNA was

eluted in 25µL dH2O. 5µL was run on a 1.5% agarose gel at 135 volts for 20 minutes and imaged using a UV transilluminator to assess success and quantity of digested products and to establish whether the vector is linear following digestion.

2.6.5 RNA extraction

RNA was extracted from HEK293T cells using Qiagen RNeasy mini kit as per manufacturer's instructions. RNAse free microcentrifuge tubes and filter tips were used and all equipment and surfaces were made RNAse free using RNAseZap™ decontamination solution (Invitrogen). Briefly, a confluent 6cm dish of HEK293T cells was scraped into 600µl RLT buffer supplemented with β-mercaptoethanol and centrifuged at 16,000rcf. Supernatant was precipitated using an equal volume of 70% ethanol and transferred to a RNeasy Mini Spin column. Column was washed and RNA eluted into an RNAse free microcentrifuge tube with 25µL RNase-free water. RNA concentration was measured by Nanodrop at 280nm.

2.6.6 cDNA synthesis

cDNA was synthesised from HEK293T cell RNA using RevertAid First Strand kit (Thermo Scientific) according to manufactures protocol. The following table lists the components and concentrations used, made up to a final volume of 20µL with nuclease-free water. The solution was mixed by pipetting and heated to 42°C for 1hr. Reaction was halted by heating to 70°C for 5 minutes to inactivate the polymerase. cDNA concentration was measured by Nanodrop at 260nm.

Table 5 Components of the RevertAid cDNA synthesis reaction

Component	Volume	Final Concentration	Stock concentration
Template RNA	As needed	0.05µL/µL	-
Primers	1µL	5µM	100µM
Reaction Buffer	4µL	1x	5x
RNase inhibitor	1µL	1units/µL	20units/µL
dNTP Mix	2µL	0.5mM	10mM
Reverse Transcriptase	1µL	10units/µL	200units/µL
Nuclease-free Water	As required to make up to 20µL	-	-

2.6.7 Restriction digestion for ligation

Restriction digestion was carried out according to table 6. Reaction was made up to 100µL and incubated at 37°C for 2hrs. BamH1 and HindIII were used for cloning into pECFP-C1 and for cloning into pcDNA3.1.

Table 6 Components of PCR Product and vector digestion reaction

Component	Volume (µL) (PCR product)	Volume (µL)/amount (Vector)
CutSmart buffer	10	10
BamH1	2	2
HindIII	2	2
CIP	-	2
PCR Product	25	-
Vector	-	2µg
dH_2O	Up to 100	Up to 100

2.6.8 Ligation

Digested vector and inserts were ligated at an approximate insert:vector ratio of 3:1, to ensure excess of insert, determined by resolving in agarose gel and imaged with a UV transilluminator. Digested products were appropriately diluted in dH_2O to make a 1:1 mix by volume. 1µL of vector was added to 1µL of insert and mixed with 2µl T4 ligase solution 1 (Takara). Ligation mixture was incubated at room temperature for 30 minutes.

2.6.9 Cloning

Generating CFP-MFF mutants

The GST-MFF (human isoform 1), made in the Henley lab as previously reported (Guo *et al*., 2017) was used to generate MFF mutants listed in Table 1 by site-directed mutagenesis, and the above techniques were used to clone into BamH1/HindIII sites of pECFP-C1 to generate CFP-MFF constructs. Briefly, inserts from the GST-MFF constructs and pECFP-C1 were digested as per Table 6, purified using GeneJET™ Gel extraction kit and ligated according to 2.6.8, followed by a further purification step, transformation into bacteria, miniprep prepared of plasmid DNA, followed by sequencing.

Generating human MiD51-HA

RNA was extracted from HEK293T cells (2.6.5) and cDNA synthesised (2.6.6). KOD Hot Start DNA Polymerase PCR was used to generate and amplify an insert that will incorporate a HA-tag at the C terminus of MiD51, and the cloning sites HindIII/BamHI for ligation into pcDNA3.1. For amplification from cDNA, 34 cycles were used and an extension time of 5 seconds. The following primers were used:

Forward primer

GTGAAGCTTGCCACCATGGCAGGCGCTGGTGAGCGCAAA

Reverse primer

CACGGATCCCTAAGCGTAATCTGGAACATCGTATGGGTACGTCTGCAGCA

GCACCTCTGGCTC

Following PCR thermocycling, a purification step cleaned the DNA product and 5µL was resolved on agarose gel to determine the success of the PCR reaction. This was followed by restriction digestion of inserts and pcDNA3.1 vector (2.6.7) and another purification step and resolved on agarose gel to establish relative ratio. Insert and vector were ligated at room temperature for 30 minutes (2.6.8) with insert in ~3-fold excess. Ligation mixture was then transformed into bacteria, colonies picked, DNA minipreped and sequenced.

2.7 *In vitro* deSUMOylation and deubiquitination assay

The catalytically active domain of SENP1 and USP2 were used to enzymatically remove SUMO and ubiquitin from MFF, respectively. See Figure 2.1 for details. Multiple (12-15) 6cm dishes of HEK293T cells expressing wildtype CFP-MFF (3 dishes expressing CFP for negative control) were lysed on ice and pooled in lysis buffer (2.5.1) containing 0.1% SDS and 20mM NEM. Lysate was sonicated and insoluble debris cleared by centrifugation at 16,000rcf at 4ºC for 20 minutes. Supernatant was collected and incubated with GFP-TRAP beads for 90 minutes at 4ºC with gentle rotation. Beads were washed in 1mL wash buffer (150mM NaCl, 50mM tris pH7.4, 5mM MgCl2) by gentle centrifugation (2 minutes at 1,500rcf at

4ºC), aspiration of media, and gentle rotation for 5 minutes in 1mL wash buffer, repeated three times. This step removed unbound material and also removed SDS and NEM, which would inhibit the enzymes. Beads were equally separated into four tubes, and a final concentration of 500nM USP2 and 100nM SENP1 were added to the tubes for 2hrs at 37ºC, with occasional agitation. Samples were boiled in 2x sample buffer at 95ºC for 10 minutes, ready for SDS-PAGE. See Figure 2.1 for schematic.

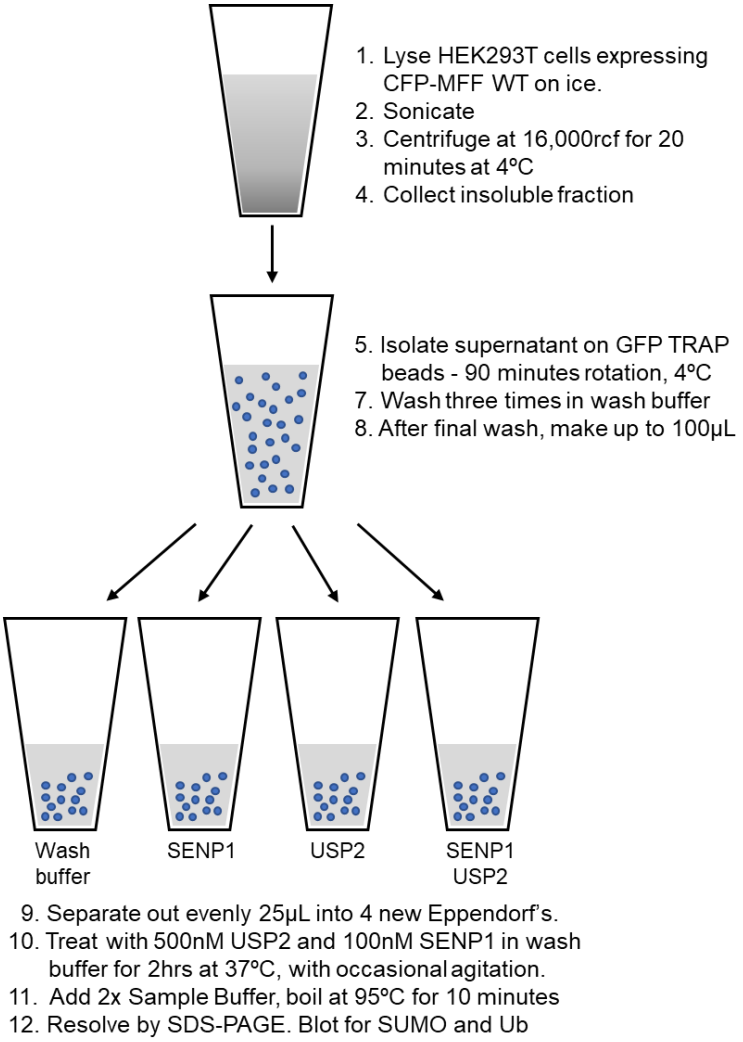

Figure 2.1 Schematic of *in vitro* deSUMOylation and deubiquitination assay

Workflow illustrating the *in vitro* assay. See text for details.

2.8 Oxygen/Glucose deprivation (OGD)

Stock media was prepared as follows: 25mM HEPES, 137mM NaCl, 5mM KCl, 1.5mM $CaCl_2$, 1.5mM $MgCl_2$. For OGD, media was supplemented with 25mM sucrose to maintain osmolarity, for control media, 25mM glucose was added. Media was then filter sterilised and kept at 4°C. A MACS-VA500-microaerophilic-workstation (from dw Scientific) was used to perform OGD experiments. The workstation was maintained at 37°C under anerobic conditions of 95% N_2 and 5% CO_2. The night before OGD experiments, media and PBS were left to deoxygenate in the workstation. Cell were placed in the workstation and washed once in deoxygenated media then incubated in OGD media for 1-2hr. (2mL for 6-well dishes, 3mL for 6cm dishes). For control cells, the same procedure was carried out with pre-warmed control media in a laminar flow hood and incubated in a humidified incubator at 37°C, 5% CO_2 and 95% O_2. After incubation, cells were carefully washed twice in ice cold deoxygenated 1x PBS and lysed in 200µL/well (50mM tris pH 7.4, 150mM NaCl, 0.5% triton X-100, 1% SDS, 20mM NEM, protease inhibitors). Cells were left on ice for 15 minutes to lyse, scraped into Eppendorf tubes, briefly sonicated (5 times ~2 seconds, output 3), left on ice for a further 15 minutes and then centrifuged at 16,000rcf for 20 minutes to pellet insoluble material. Supernatant was then collected and boiled with an equal volume of 2x sample buffer. For pulldown experiments, samples were processed as described in section 2.5.2.

2.9 Imaging

Imaging of MEF cells and primary neurons was carried out using a Leica SP5-II confocal laser scanning microscope attached to a Leica DMI 6000 inverted epifluorescence microscope. Images were captured using a 63x HCX PL APO CS oil-immersion objective, with either 512x512 (MEF) or 1024x1024 (neurons) pixel resolution and optical zoom of 3x (MEF) and 1x (neurons) at 400Hz. Z-stacks were taken with 0.25µm (MEF) and 0.5µM (neurons) incremental steps. DAPI was excited using a 50mW 405nm diode laser, Cy2 was excited using 150mW Ar laser (488nm), Cy3 and Mito DS-Red using 20mW solid state yellow laser (561nm) and Cy5 and mitotracker deep-red using a 20mW Red He/Ne (633nm). All the parameters were kept constant for a complete set of experiments.

2.9.1 Immunocytochemistry

MEF cells were pre-treated with Mitotracker deep-red (Invitrogen #M22426) for 45 minutes prior to fixation. Mitotracker was prepared in complete media and added dropwise to the cells to a final concentration of 100nM. Neuronal mitochondria were already expressing Mito DS-Red. To preserve mitochondrial morphology, cells were fixed by adding formaldehyde dropwise to the culture media to a final concentration of 2% formaldehyde and incubated for 12-15 minutes at 37°C. Cells were washed once in 1x PBS to remove debris and media, permeabilised with 0.1% Triton X-100 (in 1x PBS) for 3-4 minutes, then washed in 1x PBS a further two times. Cells were incubated for 3-4 minutes in 100mM glycine (in 1x PBS) to quench any unreacted PFA. To block non-specific binding,

cells were incubated in 3% BSA (in 1x PBS) for 20 minutes at room temperature. Primary antibody was prepared in 3% BSA and spotted on parafilm on the bench (~80µL) and coverslips were carefully inverted on the primary antibody and left to incubate for 60 minutes at room temperature. Coverslips were carefully placed back in the culture dishes and washed three times with 1x PBS and then inverted onto drops of secondary antibody (prepared in 3% BSA) for 45 minutes at room temperature. Coverslips were washed four times and mounted on glass microscope slides using 20µL Fluoromount-G (containing DAPI).

2.9.2 DRP1 colocalisation analysis

With the help of Dr Stephen Cross of the Wolfson Bioimaging facility, I generated a cytoplasmic mask to designate the area for DRP1-mitotracker colocalisation analysis, which would remove the nuclei and non-cytoplasmic regions. This would therefore avoid overestimating colocalisation, since poorly stained, non-cell regions would give a positive colocalisation value, and an automated system would avoid manually designating the cytoplasmic region, making analysis more objective. Using the DRP1 stain channel the following workflow was used:

- Segmentation of the nuclei using the following steps: median filter of radius 2-pixels. Applied global threshold to binarise the image (Otsu method), removed holes in the binarized image, identified nuclei as connected regions to have a 2D area larger than 50µm^2, using the MorphoLibJ library.
- To identify the extent of the cell: median filter applied with radius 2-pixels. Applied global intensity threshold to binarise image (Huang method), combined the binarised nuclear and cytoplasmic images to get a complete

binary image of the cell. Applied another median filter (2-pixel radius). Applied fill holes as before and used distance-based watershed transform to split any adjacent cells. Cells had a minimum 2D area larger than 400µm^2 to be identified.

- Subtracted the nucleus from the whole cell to yield the cytoplasmic region. Cytoplasmic objects identified as before, using connected foreground-labelled pixels. Cytoplasm detected area must be larger than 50µm^2

The 2 channels were filtered with a 2D Gaussian filter (radius 1-pixel) to remove noise and normalised to the full 8-bit intensity range. Mander's colocalisation coefficient was calculated between the DRP1 channel and mitotracker channel within the cytoplasmic mask

Plugin is archived in S. Cross, (2019, January 4) "ModularImageAnalysis" (Version 0.7.22) Zenodo http://doi.org/10.5281/zenodo.2531668

2.9.3 Developing an ImageJ macro to analyse mitochondrial morphology

In order to analyse the mitochondrial network of MEF cells, I generated an objective macro which yields information on quantifiable parameters of mitochondrial morphology. I was inspired by a method developed by Valente and colleagues, which describes a simple macro in conjunction with ImageJ software (Valente *et al*., 2017), termed Mitochondrial Network Analysis (MiNA). Their method uses a pre-processing step, which includes local contrast enhancement, background subtraction, unsharp mask and median filter, all available in ImageJ. This pre-processing step helps to enhance the quality of the image by increasing the sharpness, brightness in dim areas and reducing noise. Next, the image is

converted to a binary image by using IsoData thresholding. The binary image is then skeletonised, generating a 1-pixel wide outline of the entire mitochondrial network. From this, two groups of objects are identified; Networks, being structures with at least one junction, and individuals, being objects with no junctions, further categorised into rods, puncta, and large/round. The macro then outputs various parameters, for example the mean length of rods/network branches, number of branches per network.

When I used the macro on my images, I found that the pre-processing steps did not detect all mitochondria, and the skeleton did not sufficiently represent the original image. As part of the macro interface, adjustments to the pre-processing steps can be altered, however, in my hands, none of these changes improved how the skeletonised image reflected the nature of the original image. I therefore decided to adapt the pre-processing steps to better reproduce the mitochondrial morphology. Moreover, this report used pre-determined descriptors of structures and pre-determined output parameters, some of which are difficult to interpret, i.e. length of rods/network branches, and did not provide information on the individual structures.

I used similar pre-processing steps as in the Valente *et al,* 2017 report, with minor adjustments and additions. details the steps incorporated in the macro, using a wildtype MEF cell as an example. Firstly, the confocal z-stack is projected to a single image (max intensity), local contrast enhanced (blocksize=125 histogram bins=256 maximum slope=2), background subtracted (radius 10, with sliding paraboloid). Following this, two filters were applied: median filter (radius 1 pixel),

unsharp filter (0.4 sigma radius, 0.7 mask weight). I incorporated a plug-in called "Tubeness" (sigma 0.2), originally described for visualising blood vessels (Sato *et al*., 1998). I found that without using this plug-in, the skeleton struggled to detect smaller, dimmer mitochondria, and also failed to detect detail or connected mitochondria that were separate objects, or fragmented many structures that were in fact a single structure (see Figure 2.2 for comparison of performance of MiNA and my adapted approach). As can be seen in Figure 2.2, the pre-processed image more faithfully represents the raw confocal image.

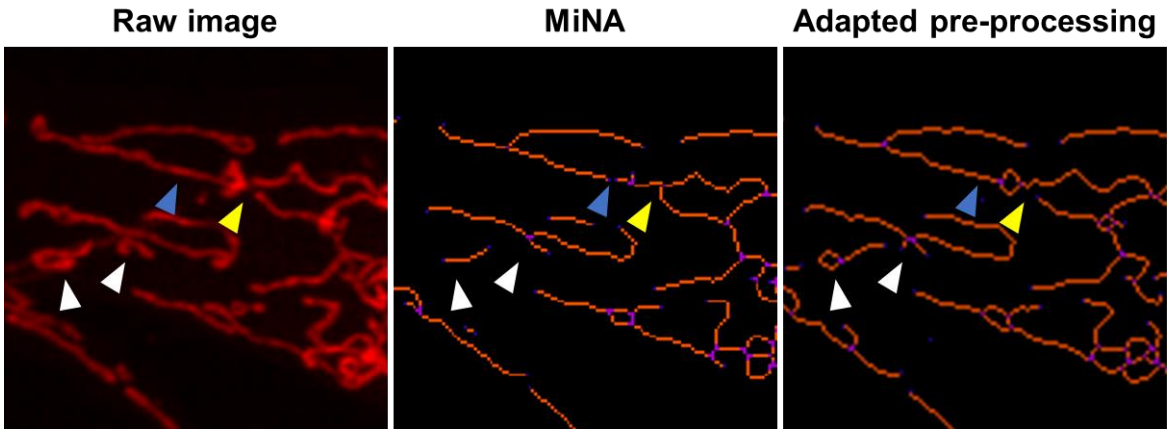

Figure 2.2 Comparison of MiNA and my adapted image processing workflow

An example of the skeleton generated from the MiNA workflow and my adapted workflow. Using identical filters and contrast enhancement parameters, my adapted version, with the addition of the Tubeness tool, outperforms MiNA. Indicated are examples where MiNA fails to detect detail, but the adapted version does (white arrows). MiNA also connects some structures that are separated, whereas my version separates such structures (yellow arrows), and MiNA also fragments some mitochondria, whereas the mitochondrial structure is retained in my workflow (blue arrows).

Figure 2.3. Figure legend overleaf

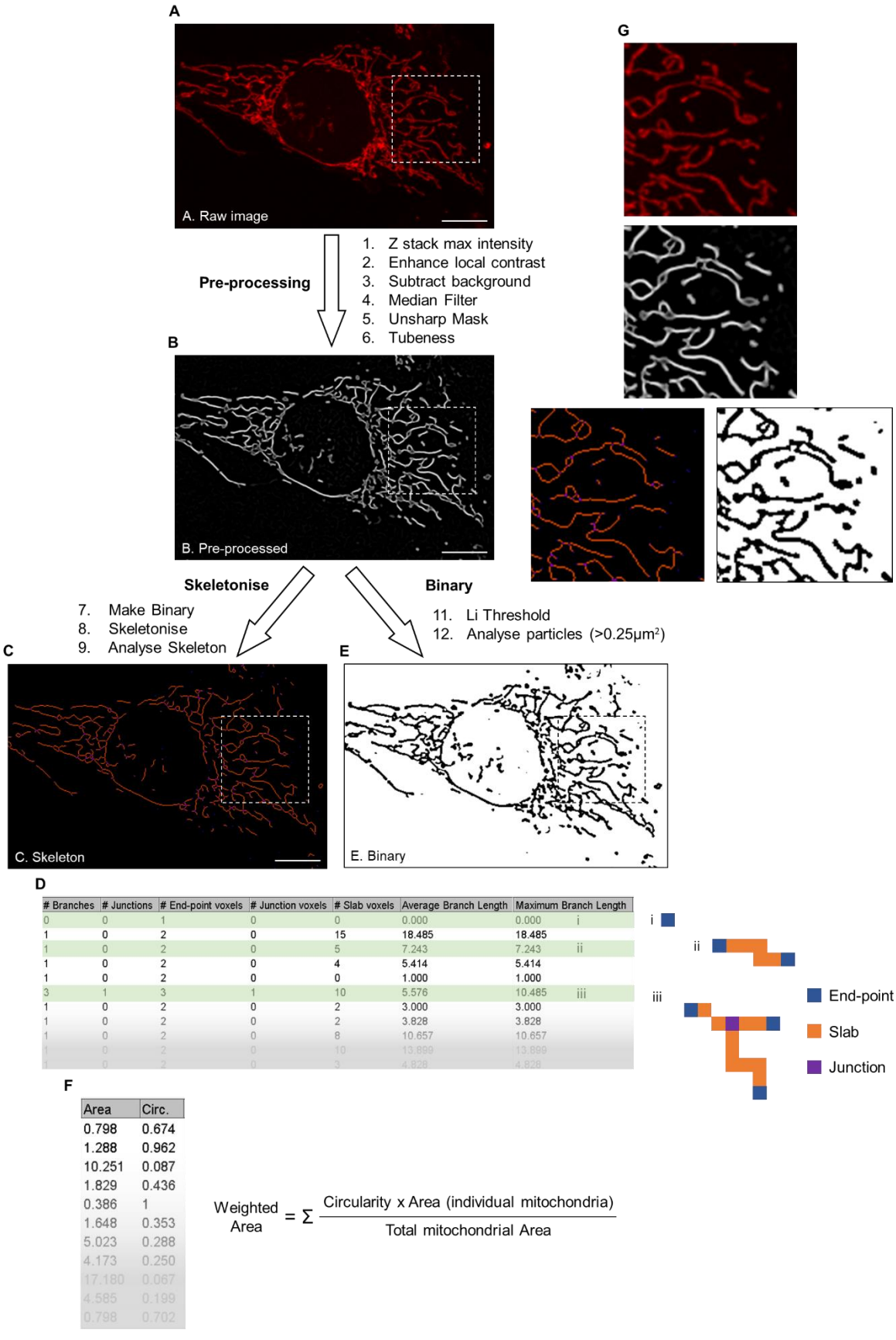

# Branches	# Junctions	# End-point voxels	# Junction voxels	# Slab voxels	Average Branch Length	Maximum Branch Length	
0	0	1	0	0	0.000	0.000	i
1	0	2	0	15	18.485	18.485	
1	0	2	0	5	7.243	7.243	ii
1	0	2	0	4	5.414	5.414	
1	0	2	0	0	1.000	1.000	
3	1	3	1	10	5.576	10.485	iii
1	0	2	0	2	3.000	3.000	
1	0	2	0	2	3.828	3.828	
1	0	2	0	8	10.657	10.657	
1	0	2	0	10	13.899	13.899	
1	0	2	0	3	4.828	4.828	

Area	Circ.
0.798	0.674
1.288	0.962
10.251	0.087
1.829	0.436
0.386	1
1.648	0.353
5.023	0.288
4.173	0.250
17.180	0.067
4.585	0.199
0.798	0.702

$$\text{Weighted Area} = \Sigma \frac{\text{Circularity x Area (individual mitochondria)}}{\text{Total mitochondrial Area}}$$

Figure 2.3 Workflow of ImageJ macro to analyse mitochondrial morphology

Schematic of the steps taken to analyse the mitochondrial morphology of MEF cells. **A** Confocal images were pre-processed (see text for details), generating a black and white image representing the mitochondrial structures (**B**). The processed image is then skeletonised (**C**) or Li threshold (**E**) applied to generate an 8-bit binary image. Scale bar 10μm. The skeleton is then analysed by using the ImageJ "Analyse skeleton" plug-in, generating a table of branch information for analysis (**D**). Highlighted are three examples, illustrating how the end, slab and junction pixels are allocated (i-iii). The binary image from **E** is analysed using the "Analyse objects" plug-in (>0.25μm^2), giving a table of area and corresponding circularity descriptors (**F**). A weighted average of circularity was caluclated from the summation of circularity multiplied by area, divided by total area. **G** Enlargements of raw, pre-processed, skeleton and binary image.

2.9.4 Branch analysis

Following pre-processing the image was binarised and skeletonised (ImageJ “make binary” and “skeletonise”). This generates a 1-pixel outline which allocates three types of pixel, based on the immediate neighbours: end pixels have either 1 or 0 neighbours, slab pixels have 2 neighbours, whereas junctions have 3 or 4 neighbours (C D). I used ImageJ’s in-built “analyse skeleton” which generates a table of information on the branches and pixels (D). Also highlighted are examples of a 1 branch structure with no junctions (Dii) and a larger structure with 1 junction and 3 branches (Diii). From the table of branch information, I extracted 5 parameters:

1) *Mean number of branches per network*: Mean number of branches within structures containing ≥2 branches and ≥1 junction.
2) *Mean mitochondrial length*: Extracted from the average branch length, which is the length between two endpoints, an end-point and junction, or two junctions. I only considered structures with ≥1 branch and non-zero lengths (an example is illustrated in Di, which will be excluded in this parameter).
3) *Maximum number of branches in a single network*: The largest number of branches in a single structure. Frequently the majority of mitochondria exist within a few large, continous structures, and these will be weighted the same as small structures when a mean average is taken (as in parameter 1), therefore smaller structures will skew the mean, giving an under-representation.

4) *Maximum mitochondria length in a single network*: Calculated from the longest mitochondria, either within a network or an isolated structure. As explained above, the “maximum” parameters were included to capture information of the very large structures, which would be “averaged-out” with the smaller structures when calculating the mean.
5) *Free end index*: The number of free end pixels divided by the total number of pixels, expressed as a percentage. It is a measure of the connectivity of the mitochondria; fewer free ends corresponds to a more connected network, and *vice versa*.

2.9.5 Circularity analysis

I calculated the mitochondrial circularity as a descriptor of the shape of the mitochondria. A value of 1 represents a perfect circle, whereas values approaching 0 indicate increasingly elongated, elaborate structures. The pre-processed image (B) was processed with Li thresholding (E) and ImageJ’s “analyse objects” plug-in was used to calculate each objects area and circularity (F). To overcome the problem of small objects being weighted equally as larger objects, I calculated each objects circularity as a proportion of the total mitochondrial area. I multiplied each objects circularity by its area, divided by the total mitochondrial area, and summed all these values (see equation in F). I only considered objects with area >0.25μm^2, as anything below this size is likely to be background or debris and not a mitochondrion.

By using the branch parameters and weighted circularity parameter, I will get a sense of the degree of branching, the length of mitochondria, the size and

complexity of very large structures, the shape of mitochondria and the connectivity.

2.9.6 Analysing neuronal mitochondrial area

The mitochondria in neuronal processes are simpler in architecture compared to MEF cells, since they often exist as single entities which can easily be discerned by eye. I therefore used a simpler method to quantify mitochondrial area in neurons. I max projected the z-stack into a single image (max intensity) and used the ImageJ plug-in “Tubeness” (sigma 0.2405) to better define the mitochondria, (as discussed in 2.9.3). Images were then binarised by Li thresholding (see Figure 2.4). The axonal initial segment was stained with ankyrin-G, which was used to differentiate between the axons and dendrites. Using the free hand tracer, axons and dendrites were carefully traced to include mitochondria within a single neurite. This typically excluded the first 20-30μm of the neurite, where the mitochondria were very clustered or multiple neurites extended from the cell body. In some instances, multiple dendrites (typically 2-3) were analysed for a single cell. Only one axon of a cell was analysed. Objects within the traced area were then analysed by using the plug-in “Analyse objects”, which generates a table of area. Mean average area was calculated from all objects of a size >0.25μm^2.

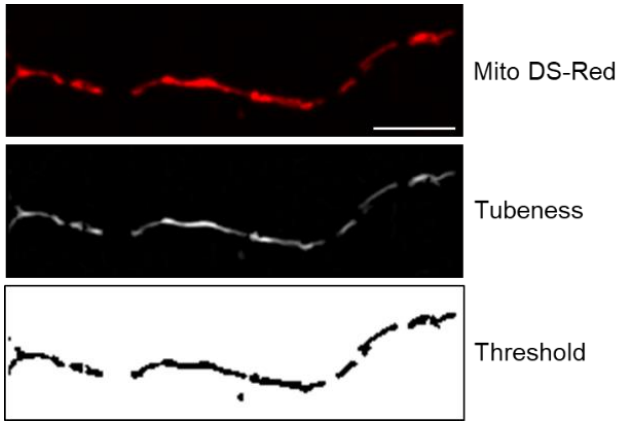

Figure 2.4 Image processing of neuronal mitochondria

Example of the tubness and thresholding of confocal images of neuronal dendritic mitochondria. DIV 14 hippocampal neurons was transfected with Mito DS-Red for 2 days. Neurons were fixed and stained for ankyrin-G and imaged by confocal imaging with 0.5µm steps. Z-stacks were compressed (max intensity) and processed with tubeness and Li threshold. Scale bar 10µm.

2.9.7 Analysing neuronal density

I used the “Simple Neurite Tracer” plug-in to trace the neurite analysed, which calculates the length of the neurite. I then calculated the density of mitochondria by dividing the number of objects detected (from section 2.9.6) by the length of the neurite. I was aware not to use mitochondrial occupancy (mitochondrial area/neurite area) in the analysis of density, since the size of mitochondria will impact on this parameter, which is already calculated in section 2.9.6. Instead, I analysed the number of mitochondrial objects per distance unit, therefore is independent of size.

This generated a large number of objects detected per cell; for axons an average of approximately 60 mitochondria were detected along a total length of ~400µm, and for dendrites ~84 mitochondria along approximately a total of 680µm processes were analysed. A mean average area and density for mitochondria in axons and dendrites was calculated per cell, and 6-8 neurons were analysed per condition, per experiment.

2.9.8 Statistical analysis

All graphs were prepared, and statistical analysis performed using Graphpad Prism version 7.0. Figure legends indicate number of independent repeats. Statistical analysis was only carried out on experiments that were performed at least three independent times. Data is presented as mean values +/- standard deviation (S.D). Unpaired t test and one-way ANOVA followed by Tukey's *post hoc* test to correct for multiple comparisons was used in chapters 3 and 4 for Western blot analysis. In chapter 5, I tested for normal distribution using the D'Agostino and Pearson normality test; if not normally distributed, I carried out the non-parametric Mann-Whitney test. If data was normally distributed, I carried out an unpaired t test. Figure legends state the p values, data considered significant if $p<0.05$.

Chapter 3 Characterising MFF SUMOylation

3.1 Introduction

Although SUMOylation has typically been thought to occur exclusively in the nucleus, there is a growing body of evidence that extra-nuclear proteins are also SUMOylated. The first SUMO substrate identified was the RAN-GTPase-activating protein RanGAP1, a primarily cytosolic protein, which upon SUMOylation shuttles to the nuclear pore complex (Matunis *et al*., 1996) . Since then, multiple cytosolic proteins have been identified as SUMO substrates. In yeast for example, SUMOylation of septins is under tight regulation and only occurs during mitosis (Johnson and Blobel, 1999). SUMOylation of the glucose transporters GLUT1 and GLUT4 decreases and increases basal protein levels, respectively, having opposing effects on glucose transport (Giorgino *et al*., 2000). The kainate receptor subunit GluR6 is SUMOylated in response to stimulation, which is then internalised in a SUMO-dependent manner (Martin *et al*., 2007). These reports underscore the dynamic nature of SUMOylation, and the varied roles SUMO plays in many cellular contexts outside the nucleus (Watts, 2004).

SUMOylation has also been shown to regulate mitochondrial protein function, and thus impact mitochondrial dynamics. SUMO-1 positive puncta were detected at mitochondrial fission sites, and SUMO-1 overexpression enhances mitochondrial fission (Harder *et al*., 2004), whereas SENP5 overexpression reverses this phenotype (Zunino *et al*., 2007) demonstrating global SUMOylation levels impact mitochondrial dynamics. DRP1 is SUMOylated by SUMO-1 and SUMO-2/3, with opposing effects on function; SUMO-1 stabilises DRP1 at mitochondrial-ER contact sites and promotes Ca^{2+} signalling and apoptosis (Prudent *et al*., 2015),

whereas DRP1-SUMO-2/3 is sequestered in the cytosol, and is recruited to the MOM upon deSUMOylation by SENP3 (Guo *et al.*, 2013, 2017).

Two PTMs have been identified for MFF to date; AMPK phosphorylation at S155 and S172 promotes fission under bioenergetic stress (Toyama *et al*., 2016) and ubiquitination by parkin (Gao *et al*., 2015; Lee *et al*., 2019).

3.2 Aims

With the wealth of evidence that many PTMs regulate mitochondrial proteins, fusion and fission, and SUMOylation and SENPs are known to regulate mitochondrial fusion and fission, I reasoned that the DRP1 receptors are also likely highly regulated to affect their function. However, it isn't known whether these proteins are targets for SUMOylation. Preliminary observations from the Henley lab identified a molecular weight shift of GST-MFF, often observed following PTM such as SUMOylation.

The aims of this chapter are:

- To confirm previous observations that MFF is a potential SUMO substrate.
- To identify the site(s) of MFF SUMOylation.
- To define how MFF SUMOylation is regulated.

3.3 Results

3.3.1 MFF is a novel SUMO substrate

To confirm previous preliminary observations made in the Henley lab that MFF may be a SUMO substrate, and to assess if any of the other DRP1 receptors are SUMOylated, I conducted a GST-pulldown experiment of all four DRP1 receptors in HEK293T cells co-expressing GST-tagged receptor with either FLAG-SUMO-1 or FLAG-SUMO-2. Figure 3.1 shows that MFF is the only DRP1 receptor SUMOylated, by both SUMO isoforms. The FLAG signal demonstrates that MFF is modified by both isoforms, which display a similar pattern; a major band can be observed at ~140kDa, and higher molecular weight species appear above. This finding validates previous observations made in the lab. My interpretation of this pattern is that MFF is either poly-SUMOylated, and the higher molecular weight species are a result of increasing lengths of SUMO chains, and/or is mono SUMOylated at multiple sites. Furthermore, the mono-SUMOylated species of MFF can be detected in the input, suggesting that MFF is a highly SUMOylated substrate.

When a protein is SUMOylated, this can alter how it is resolved by SDS-PAGE, and the expected ~11kDa shift does not always correspond to what is observed. I expressed GST-MFF +/-SUMO-1 or SUMO-2 in bacteria, and I detect a band at ~130kDa (See appendix Figure 8.1). I predict this band to represent mono SUMOylated-MFF, since bacteria are unlikely to generate poly-SUMO chains, supporting the view that the major band at 140kDa observed in Figure 3.1 is a mono-SUMO species.

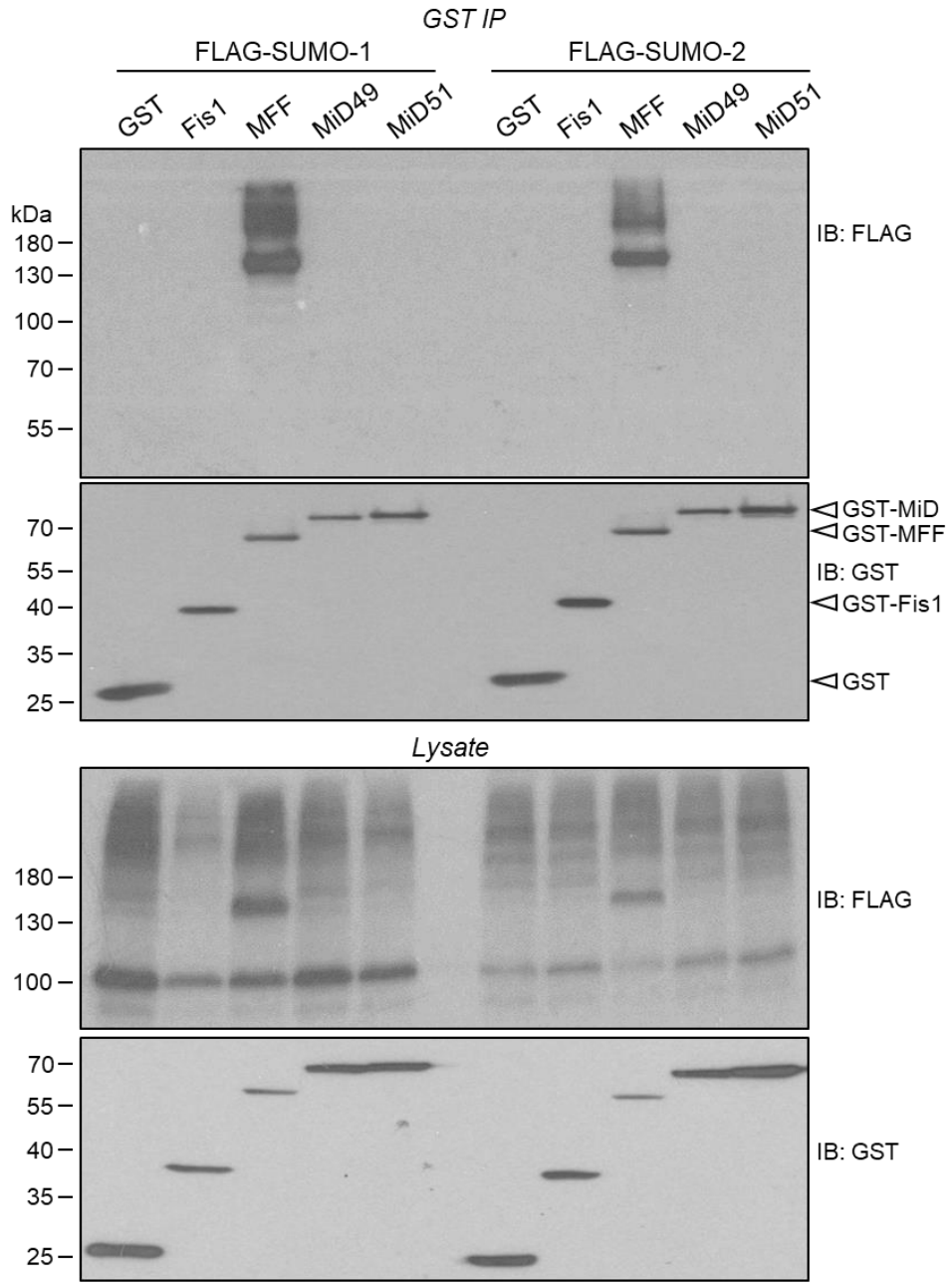

Figure 3.1 MFF is a novel SUMO substrate

HEK293T cells were transiently co-transfected with GST fusion constructs of the four DRP1 receptors (Fis1, MFF, MiD49, MiD51) and either FLAG-SUMO-1 or FLAG-SUMO-2 for 48hrs. GST-pulldowns were carried out on lysate and resolved by SDS-PAGE. Blots were probed for FLAG and GST. 4% input taken before IP to assess FLAG and GST-receptor expression.

3.3.2 MFF is SUMOylated at lysine 151

To identify the SUMOylated lysine residue(s) of MFF, I analysed the human MFF isoform 1 sequence using the online program SUMOplot™, which identifies SUMO consensus sites, based on the consensus SUMO motif ψKxD/E. Three lysines were identified as having a high probability of SUMOylation; K114, K151 and K319 (Figure 3.2A). Lysine 151 had the highest score (Figure 3.2B), so I generated a putative SUMOylation-deficient mutant (K151R) by site directed mutagenesis in a CFP-MFF construct of MFF human isoform 1. I conducted a simple experiment where I lysed HEK293T cells expressing CFP-MFF WT or CFP-MFF K151R in buffer +/-2% SDS, previously used to identify modified proteins (Rocca *et al*., 2017). The SDS will assist in retaining covalent modification by inhibiting deconjugation (i.e. deSUMOylating, deubiquitinating enzymes), whereas in the buffer without SDS, these enzymes will still be active. Moreover, this will confirm that the modification observed in Figure 3.1 is covalent modification. Figure 3.2C shows that in buffer containing SDS, the modification is maintained on wildtype MFF, as evidenced by the molecular weight shift and increasing molecular weight species above a major SUMO band, agreeing with Figure 3.1. No higher molecular weight band was observed when the SDS was omitted and no molecular weight shift was observed for the K151R mutant under denaturing conditions, demonstrating that K151R is the site responsible for this modification. It is noteworthy that a high exposure is required to detect the higher molecular weight species. This indicates that the majority of MFF exists in a non-modified state (CFP + MFF: 28kDa + 38kDa = ~66kDa), and a small pool of CFP-

MFF is modified, as seen for other substrates (Martin *et al*., 2007). Furthermore, the size of the modifications on WT MFF are substantial, resolving higher than 200kDa. I interpret this to mean that K151 is a site of extensive modification.

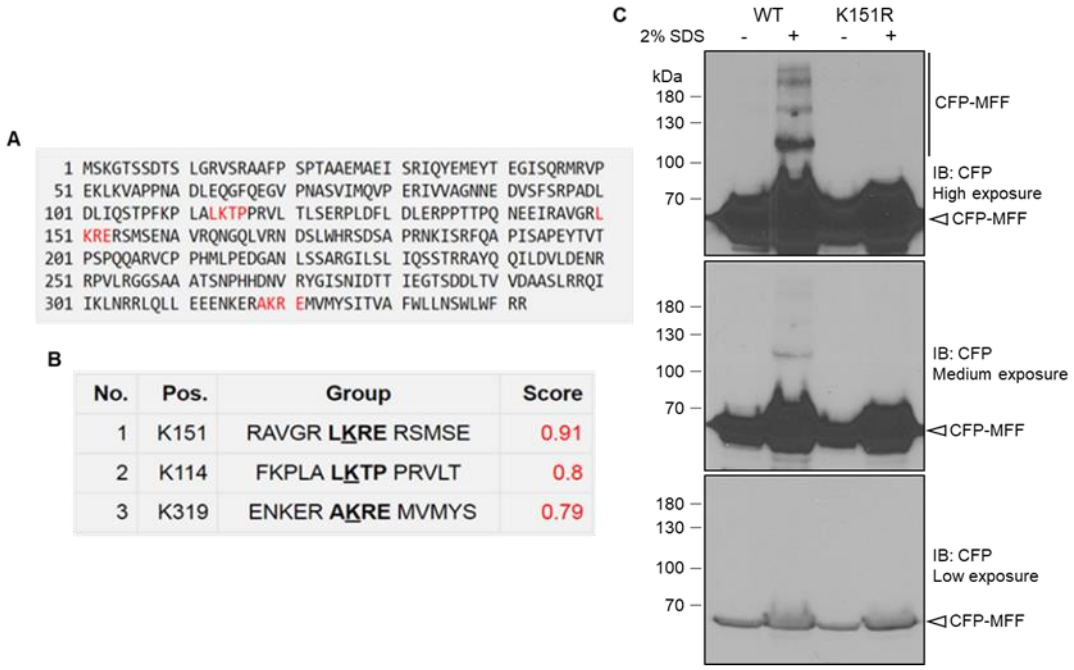

Figure 3.2 MFF is modified at K151

A The human sequence of MFF isoform 1 (Uniprot: Q9GZY8-1) was submitted to SUMOplot™, identifying SUMOylation consensus motifs based on the amino acid sequence ψKxD/E. **B** K151 was identified as containing the highest probability consensus sequence. **C** HEK293T cells expressing CFP-MFF (WT) or CFP-MFF (K151R) were lysed in buffer +/-2% SDS. Total lysate was resolved by SDS-PAGE and probed for CFP. Representative of two independent experiments.

It cannot be stated from the above experiment that the molecular weight shift is exclusively due to SUMOylation, since it has been reported that MFF is subject to other modifications, such as ubiquitination (Gao *et al*., 2015; Lee *et al*., 2019). The experiment only demonstrates modification occurring within a SUMO consensus motif. To definitively confirm MFF is SUMOylated at K151, I assessed endogenous SUMOylation of CFP-MFF WT and CFP-MFF K151R by carrying out CFP immunoprecipitations and probing for endogenous SUMO-1 and SUMO-2/3. I also generated a second putative SUMO mutant, E153A, which disrupts the SUMO consensus motif by removing the acidic residue in the +2 position. Figure 3.3 shows that SUMOylation of the K151R and E153A mutants is abolished. The endogenous SUMO pattern exhibits a poly-SUMOylation pattern, and generates a major species at ~110kDa, with increasing chains forming above, which corresponds to the pattern observed in Figure 3.1 and Figure 3.2. The observed difference in size of the major species between endogenous and overexpressed FLAG-SUMO (Figure 3.1 vs Figure 3.2 and 3.3) of ~140 vs ~110kDa, respectively, may be due to the FLAG tag, which affects how the proteins are resolved.

Together, the above data confirm that MFF is poly-SUMOylated by SUMO-1 and SUMO-2/3, and that K151 is the only SUMO site of MFF. Moreover, the majority of MFF exists in a non-SUMOylated state, and a small proportion exist as mono and poly-SUMOylated forms of MFF.

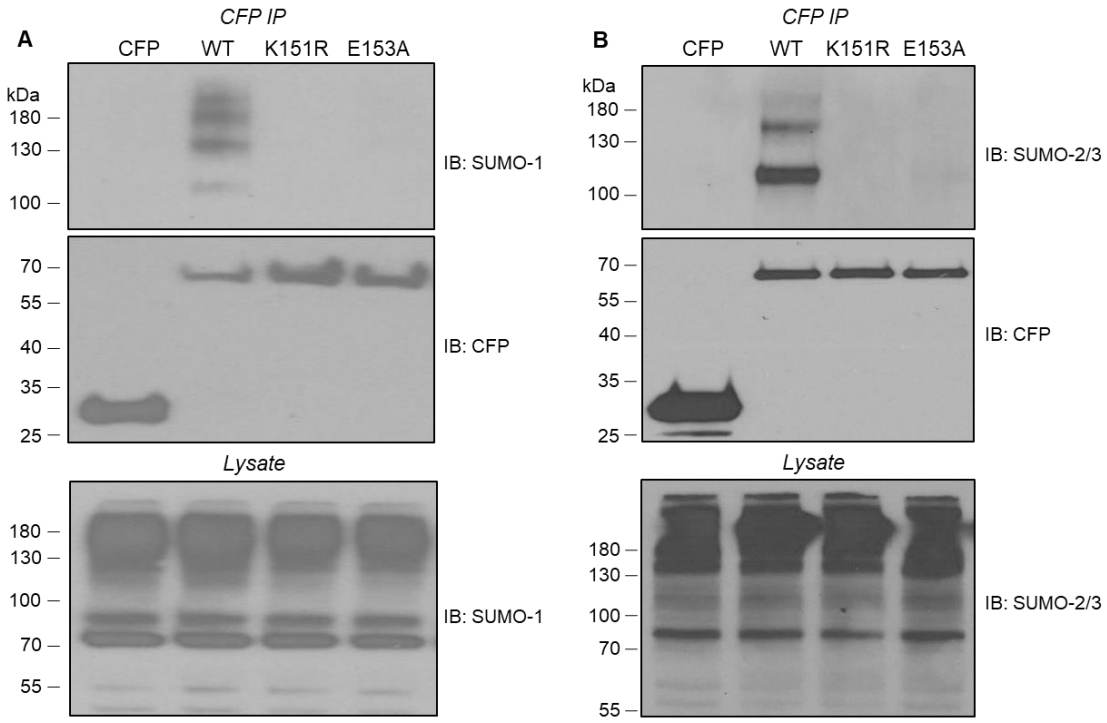

Figure 3.3 MFF is SUMOylated by endogenous SUMO at K151

HEK293T cells were transiently transfected with CFP wildtype (WT) or putative SUMO-deficient mutants (K151R and E153A). Cells were lysed and supernatant subjected to CFP immunoprecipitation. CFP immunoprecipitates were resolved by SDS-PAGE and probed for endogenous SUMO-1 (**A**) (IP and blot shown here was performed by L. Lee) and SUMO-2/3 (**B**). Representative blots of three independent experiments.

3.3.3 MFF K151R has reduced ubiquitination

Since SUMO can form hybrid chains with ubiquitin, and MFF has previously been shown to be ubiquitinated (Gao *et al*., 2015; Lee *et al*., 2019), I next established the ubiquitination state of the SUMO mutant. I carried out CFP-immunoprecipitation from HEK cells co-expressing CFP-MFF (WT or K151R) and HA-ubiquitin. Figure 3.4A shows that wildtype MFF is poly-ubiquitinated, exhibiting a similar pattern to SUMOylation of increasing ubiquitin chain length, agreeing with previous findings (Lee *et al*., 2019). K151R also displays the same poly-SUMOylation pattern, but overall ubiquitination is reduced by ~60% (Figure 3.4B). I reasoned this reduction could be due to two possibilities; 1) K151 is a direct site of ubiquitination, along with at least one other site or 2) K151 is not a direct site of ubiquitination but is required to promote ubiquitination on another site. Indeed, SUMO can act as a signal for promoting ubiquitination by recruiting a SUMO targeted ubiquitin ligase (STUbL), demonstrating significant cross-talk and interplay between the SUMO and ubiquitin system, reviewed in Sriramachandran and Dohmen, 2014. To test this possibility, I analysed the ubiquitination state of the SUMO mutant E153A. Because ubiquitination sites do not generally conform to consensus sites as SUMOylation does, the presence of K151 in E153A allows me to investigate the effect of SUMOylation on ubiquitination, without removing a potential acceptor residue. Like K151R, E153A also exhibited reduced ubiquitination, suggesting that K151 is not a ubiquitin site, and that SUMOylation may promote ubiquitination on a separate site.

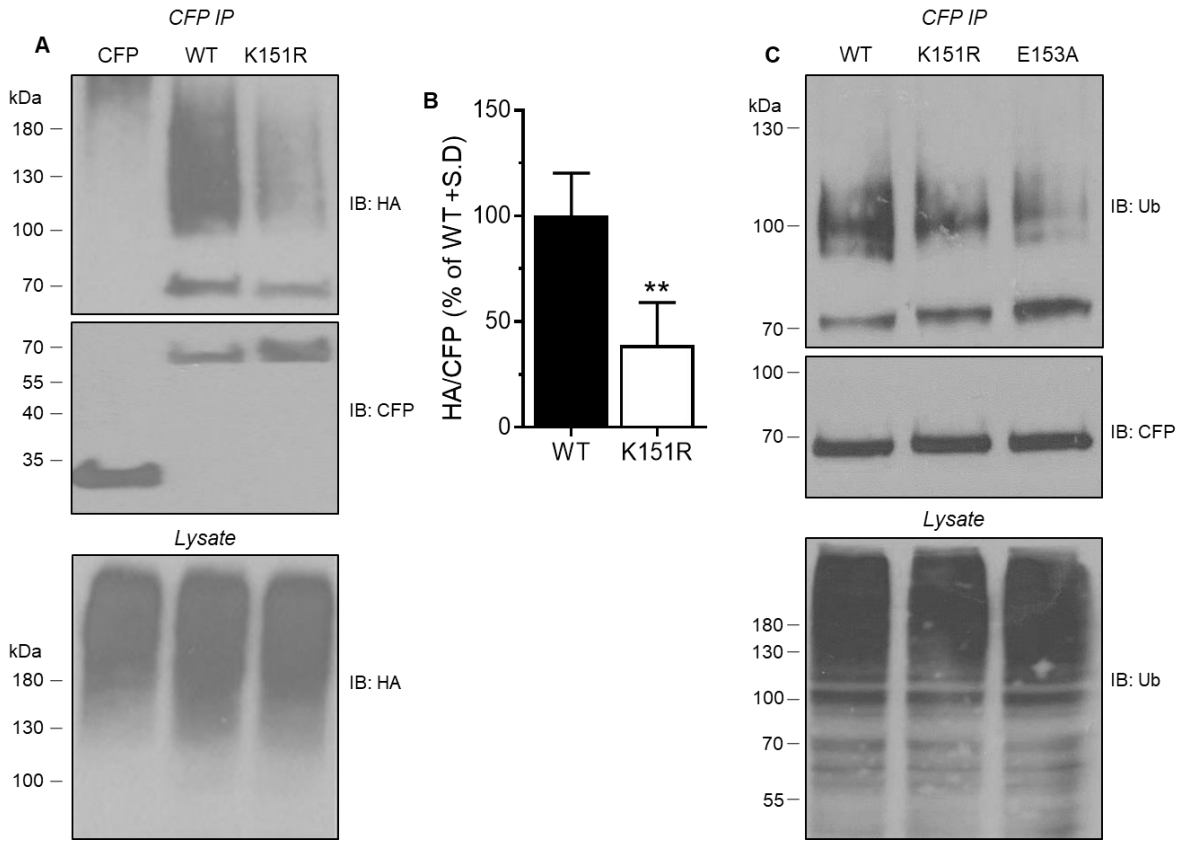

Figure 3.4 The non-SUMOylatable MFF mutant K151R has reduced ubiquitination

A HEK293T cells were transiently co-transfected for 48hrs with HA-ubiquitin and either wildtype (WT) or K151R CFP-MFF. CFP precipitates were probed for HA-ubiquitin. 4% input taken. Representative blot of 4 independent experiemnts (the IP and blot in **A** was carried out by L. Lee). **B** Quantification of total HA-ubiquitination normalised to CFP expressed as percentage of wildtype MFF. n=4, t test used to determine significance, p**<0.01. **C** Representative blot of endogenous ubiquitination of wildtype, K151R and E153A MFF. HEK293T cells were transiently transfected with indicated CFP-MFF constructs. CFP-immunoprecipitation carried out on lysate and probed for endogenous ubiquitin. Similar results were independently observed by myself and L. Lee, obtained for endogenous and overexpressed ubiquitin. E153A exhibits ~50% reduction in ubiquitination (L. Lee, unpublished data).

3.3.4 MFF is not modified by SUMO-Ubiquitin chains

To further explore the possibility that SUMO and ubiquitin form mixed chains on MFF, I used an *in vitro* assay of purified ubiquitin specific peptidase 2 (USP2), previously used to cleave ubiquitin chains (Mahul-Mellier *et al*., 2012; Shan *et al*., 2009; Stevenson *et al*., 2007) and SENP1 to cleave endogenous ubiquitin and SUMO, respectively. As expected, treatment of immunoprecipitated wildtype CFP-MFF with SENP1 completely removed both SUMO-1 and SUMO-2/3 reactive bands, and USP2 removed all ubiquitination. Treatment with SENP1 and USP2 in combination removed all SUMO and ubiquitin. However, following USP2 treatment, the majority of SUMO isoforms remained conjugated, and likewise with SENP1 treatment ubiquitination was retained (Figure 3.5). These results indicate that SUMO and ubiquitin target independent sites in MFF. However, there is an apparent discrepancy between these data; when there is no SUMOylation and ~60% reduction of ubiquitin in the K151R mutant (Figure 3.3 and Figure 3.4), but the *in vitro* assay in Figure 3.5 suggest targeting to different sites. If SUMO and ubiquitin do form mixed chains, then *in vitro* SENP1 treatment would reduce SUMO along with any conjugated ubiquitination, and USP2 treatment would have the same effect on SUMO. The fact that this is not the case indicates that SUMO and ubiquitin target independent sites.

Combining this with the observation that K151R has reduced ubiquitination suggests that SUMO on K151 promotes MFF ubiquitination, but on a separate site(s) (see Figure 3.6 for details). One possible ubiquitin site has already been identified, corresponding to K302 in isoform 1 (Gao *et al*., 2015). I also observe

reduced ubiquitination of the SUMO mutant E153A (Figure 3.4C), supporting the view that SUMOylation promotes ubiquitination.

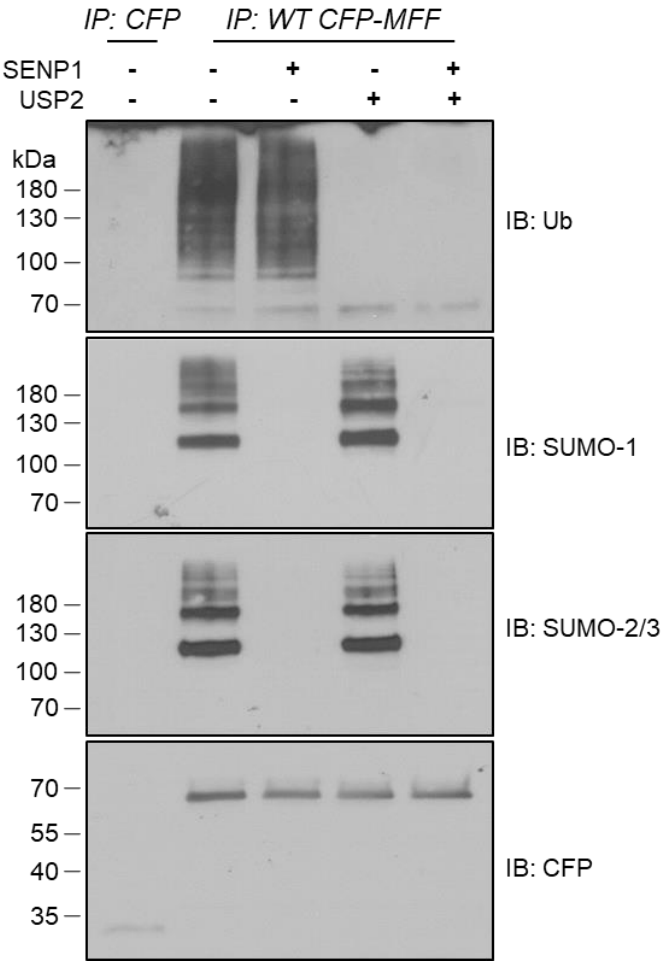

Figure 3.5 MFF is not modified by SUMO-Ubiquitin hybrid chains

CFP-MFF (WT) from transiently transfected HEK293T cells was isolated on GFP-TRAP beads, pooled and separated equally. Immunoprecipitates were washed in wash buffer (50mM Tris, 150mM NaCl, 5mM $MgCl_2$, pH 7.5) and treated with 500nM USP2, 100nM SENP1, both enzymes, or wash buffer containing no enzymes at 37ºC for 2hrs, with gentle aggitation. CFP acted as a negative control and was incubated in wash buffer. Following incubation samples were boiled in 2x sample buffer and resolved by SDS-PAGE and blotted for endogneous SUMO-1, SUMO-2/3, ubiquitin and CFP. n=2.

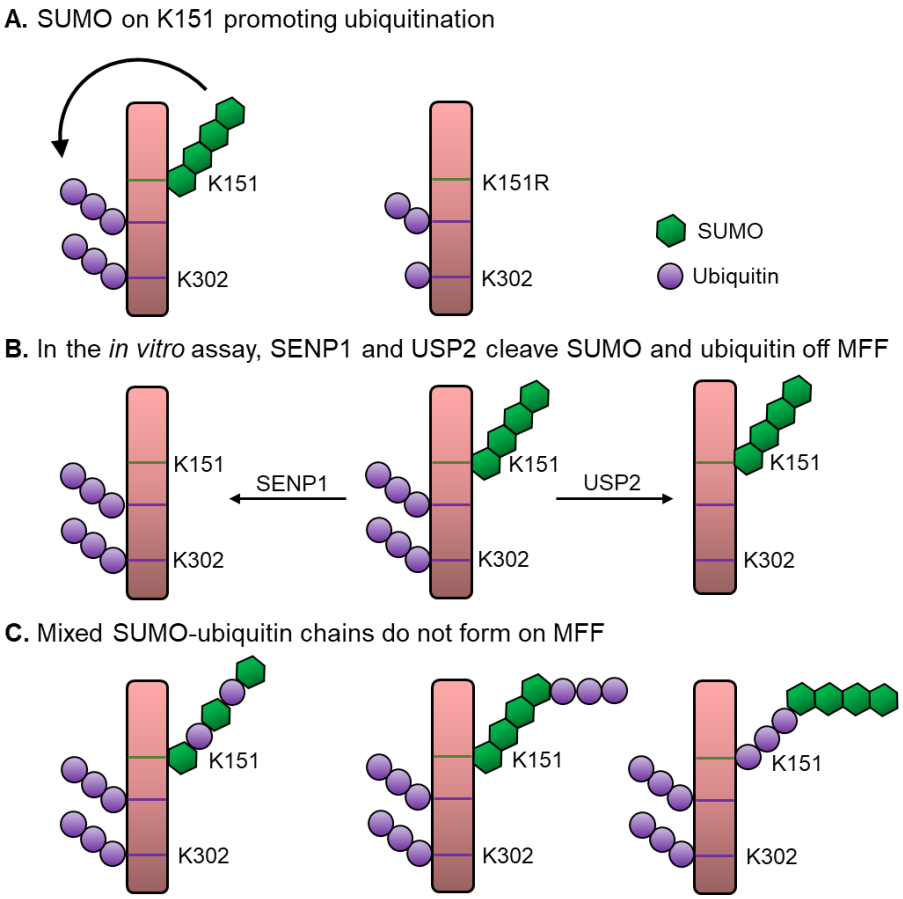

Figure 3.6 Models of SUMOylation and ubiquitination of MFF

A Based in the *in vitro* assay and immunoprecipitations, I propose a mechanism whereby SUMOylation of MFF enhances MFF ubiquitination on a site(s) other than K151. Illustrated here is one of those sites, K302, previously identified as a ubiquitin site (Gao *et al*., 2015). **B** USP2 cleaves all ubiquitin but has no/little effect on MFF SUMOylation, and SENP1 retains all ubiquitin and abolishes SUMOylation. **C** Mixed chains that unlikely occur on MFF. If this was the case, SENP1 treatment would reduce ubiquitination, and USP2 would reduce SUMO.

3.3.5 Phosphorylation of MFF enhances SUMOylation

Proteomic reports confirm that MFF is an AMPK substrate (Chen *et al*., 2019; Ducommun *et al*., 2015; Toyama *et al*., 2016), AMPK phosphorylates MFF at two sites (serine 155 and 172) which is necessary and sufficient to induce mitochondrial fragmentation (Toyama *et al*., 2016). Interestingly, S155 is in the +4 position with respect to the SUMOylation site. This region therefore conforms to a phosphorylation-dependent SUMO consensus motif (PDSM), whereby phosphorylation enhances SUMOylation (Watts *et al*., 2007). To test if SUMOylation at K151 is influenced by phosphorylation at S155, I engineered two further mutants of the original GST-MFF isoform 1 construct: a phospho-null (S155A), and a phospho-mimetic (S155D). I also generated the SUMOylation-deficient E153A mutation in the GST-MFF construct. I then performed GST-pulldown experiments and assessed modification of MFF with FLAG-SUMO-1. Figure 3.7 shows that mimicking phosphorylation at S155 enhanced SUMOylation by ~75% above wildtype levels, and more than 2-fold above the phospho-null mutant, demonstrating that this region behaves as a PDSM. The E153A mutant had significantly reduced SUMOylation, yet interestingly still retains ~10% SUMOylation.

It is important to note here that the analysis carried out in Figure 3.7 (and all similar future analysis) is the intensity of FLAG signal normalised to GST. Therefore, it is a ratio of SUMOylated species to non-SUMOylated MFF.

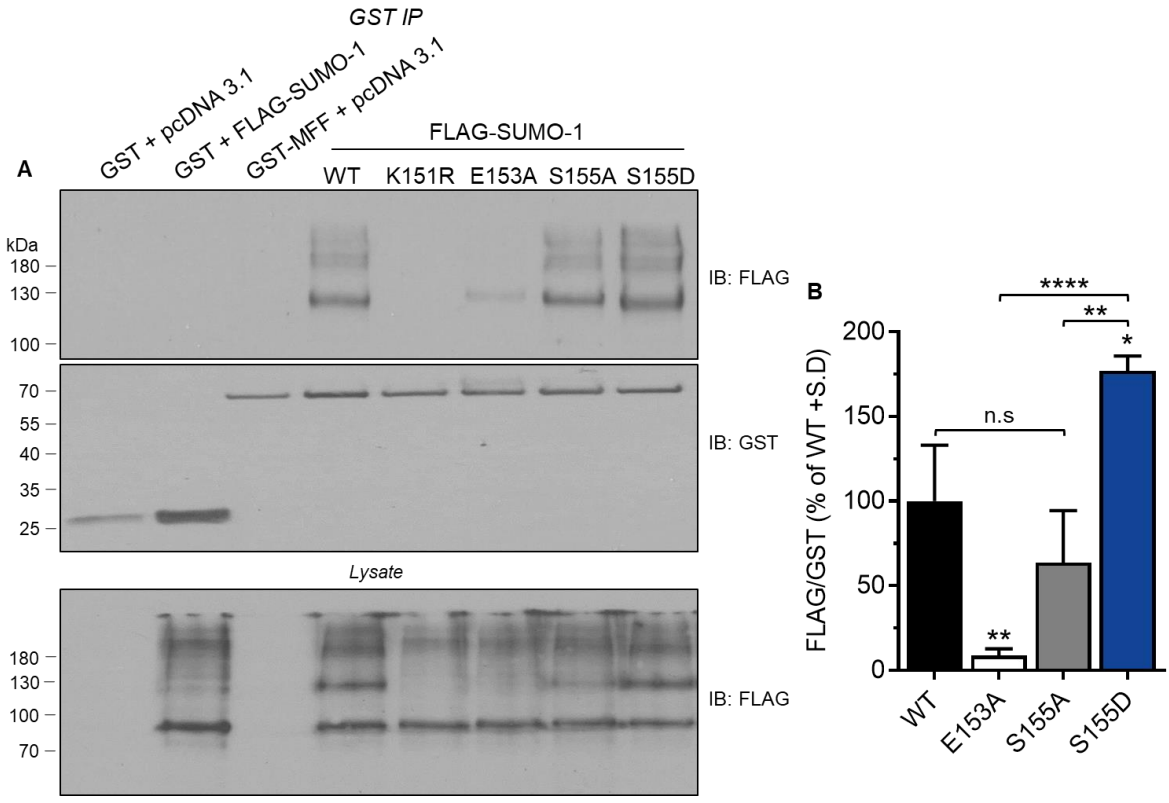

Figure 3.7 Phosphorylation at S155 enhances MFF SUMOylation

A HEK293T cells were transiently co-transfected with the indicated GST-MFF constructs and FLAG-SUMO-1 (pcDNA 3.1 acted as a negative control). GST immunoprecipitates were immunoblotted for FLAG and GST. 4% input lysates were taken and immunoblotted for FLAG. **B** Quantification of FLAG normalised to GST, represented as a percentage of wildtype MFF. One-way ANOVA followed by Tukeys post hoc test carried out to determine significance. Data generated from three independent experiments. p*<0.05, p**<0.005, p****<0.0001.

3.3.6 Phosphorylation is upstream of SUMOylation

It is well established that there is significant crosstalk between phosphorylation and SUMOylation, for example phosphorylation promotes the SUMOylation of the transcription factors NF-E2 (Su *et al*., 2012) and HSF-1 (Hietakangas *et al*., 2003), whereas phosphorylation of c-Jun and p53 inhibits SUMOylation (Müller *et al*., 2000). To establish that phosphorylation precedes SUMOylation, and to test that SUMOylation has no effect on phosphorylation at S155, I used an antibody that recognises the AMPK phosphorylation consensus site, which S155 (but not S172) conforms to. I observed no difference in phosphorylation at S155 between wildtype and K151R (Figure 3.8), indicating phosphorylation is upstream of SUMOylation.

It has been reported that AMPK phosphorylation of MFF at S155 and S172 promote fission under stress, linking the phosphorylation state of MFF to mitochondrial and bioenergetic stress (Toyama *et al*., 2016). My findings that phosphorylation promotes SUMOylation lead me to hypothesise that an increase in SUMOylation would therefore be linked to increased fission. Moreover, since AMPK is the major bioenergetic status sensor of the cell (Garcia and Shaw, 2017), this model would establish a direct link between the bioenergetic state of the cell and MFF SUMOylation.

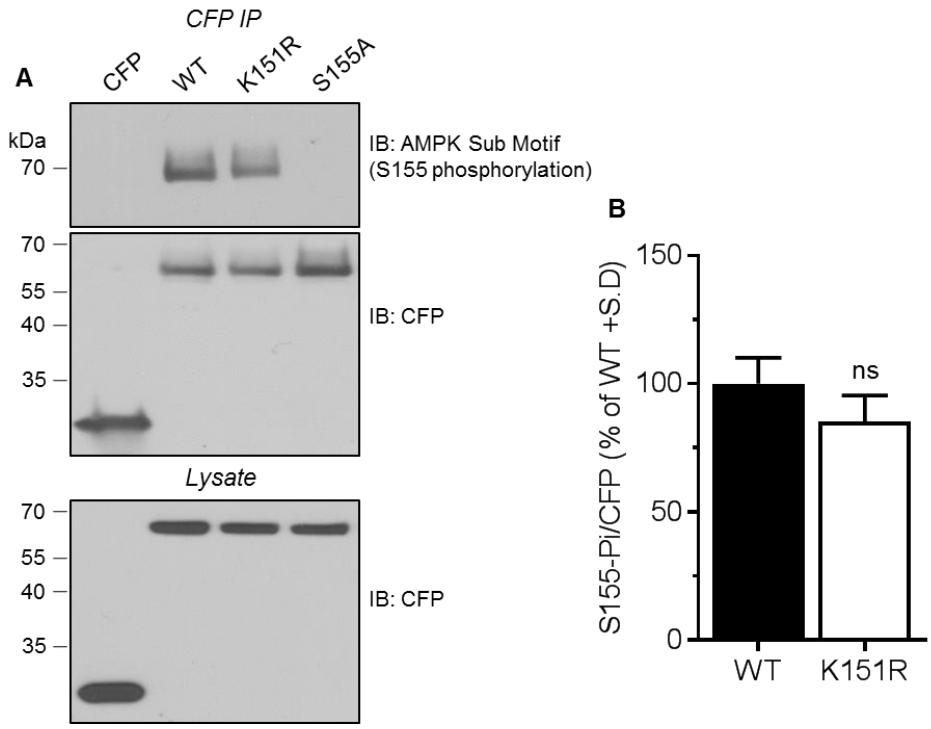

Figure 3.8 Phosphorylation is upstream of MFF SUMOylation

A HEK293T cells were transiently transfected with wildtype (WT), K151R or S155A CFP-MFF and immunoprecipitates were resolved by SDS-PAGE and probed for phosphorylation at S155 by using a specific AMPK substrate motif antibody. S155A used as a negative control to demonstrate the specificity of the antibody. **B** Quantification of WT and K151R phosphorylation at S155 normalised to CFP and represented as a percentage of WT. Unpaired Students t test used to determine significance (n=3, ns=non significant).

3.3.7 Phosphorylation and dephosphorylation of MFF at S155 and S172 have differential effects on SUMOylation

To further dissect the role of AMPK phosphorylation on MFF SUMOylation, I generated phospho-null and phospho-mimetic mutants at both reported AMPK sites, S155 and S172, within the CFP-MFF construct of MFF isoform 1. I also generated the previously reported double phospho-null and phospho-mimetics (2SA and 2SD, respectively, (Toyama *et al*., 2016)). In this set of experiments, I analysed mono-SUMOylated and higher molecular weight (MW) species separately, because in some cases the mono-SUMO species saturated before the higher MW species were detected. I therefore obtained different exposures to capture the different SUMO modified populations.

Figure 3.9 shows the total SUMOylation change (average change of mono and higher MW), and Figure 3.10 shows the quantification of the mono (arrow) and higher MW species (asterisk) separately. This type of analysis revealed that the higher MW species changes to a greater extent than the mono-species. Consistent with my previous observations in Figure 3.7, S155D enhances total MFF SUMO-1-ylation, in this case approximately 2.8-fold above WT levels, and ~3.7-fold greater than S155A. Phosphorylation at S155 had the greatest effect on the higher MW species of SUMO-1, enhancing SUMOylation by over 4-times. S155D also increases the higher MW bands for SUMO-2 by ~3.4-fold, and the SUMO-2 mono species is significantly greater than S155A. No significant change is observed between WT, S155A and 2SA in all cases. The double phospho-mimetic did not significantly increase SUMOylation levels above wildtype levels,

however it did significantly increase total levels of both isoforms above 2SA, and the high MW species of SUMO-1 above 2SA.

The phospho-mimetic at S172 had no effect on SUMOylation. However, S172A increases SUMO-1 levels above WT, S155A and 2SA, and S172A enhances the SUMO-2 mono species above S155A and 2SA. Interestingly, a similar increase in total SUMO-2 is detected for S155D and 2SD, whereas 2SD significantly reduced SUMO-1 levels compared to S155D.

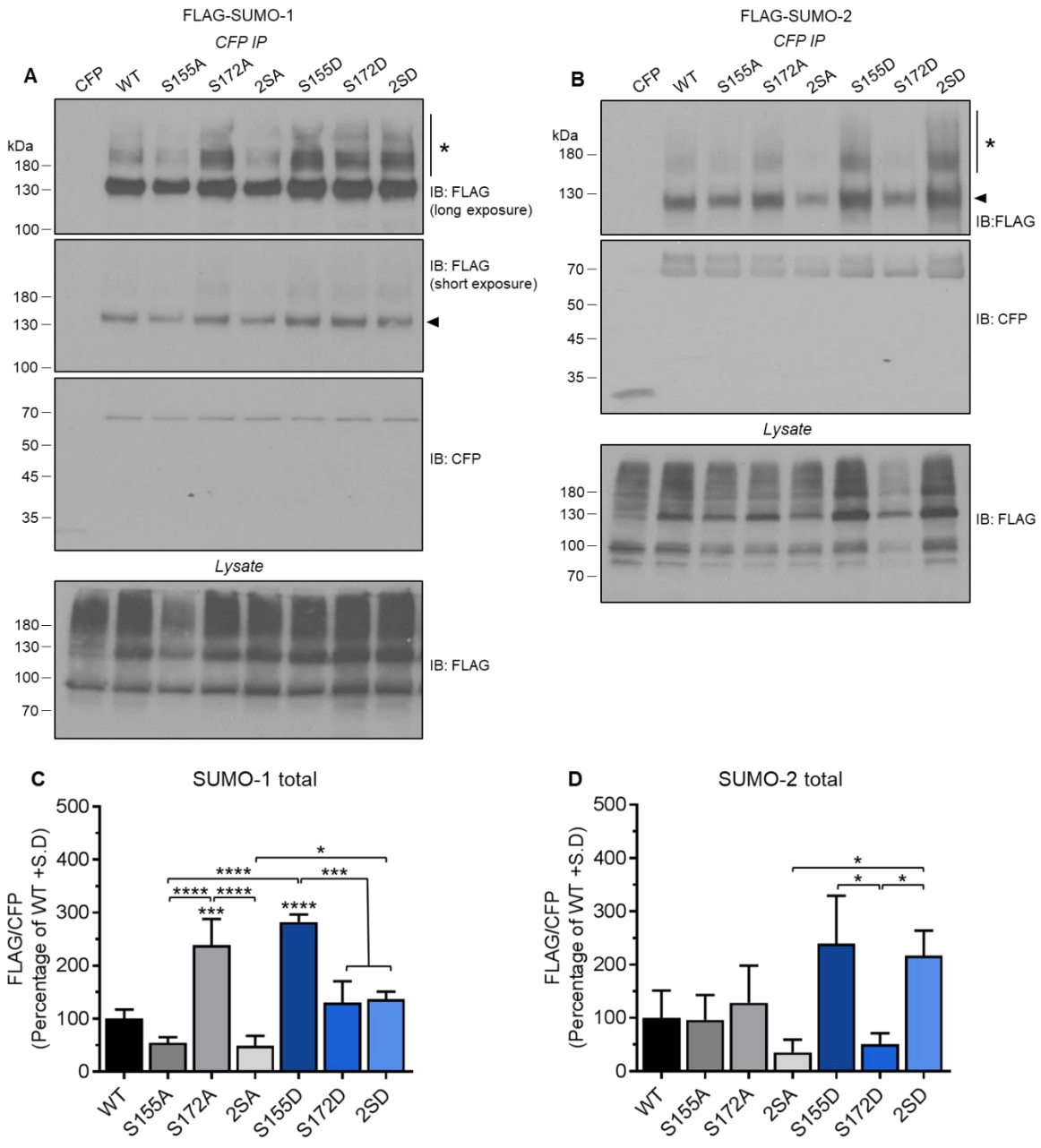

Figure 3.9 MFF phosphorylation differentially regulates SUMOylation

A-B HEK293T cells were transiently co-transfected with the indicated CFP-MFF constructs and either FLAG-SUMO-1 (**A**) or FLAG-SUMO-2 (**B**). CFP immunoprecipitates were resolved by SDS-PAGE and probed for FLAG and CFP. 4% input probed for FLAG. **C-D** Quantification of total FLAG signal (average change of mono-species and higher MW species (arrow and asterix, respectively) normalised to

CFP and expressed as a percentage of wildtype. n=5 (SUMO-1) and n=3 (SUMO-2). One-Way ANOVA carried out and Tukey's *post hoc* test used to determine significance. p*<0.05, p***<0.0005, p****<0.0001.

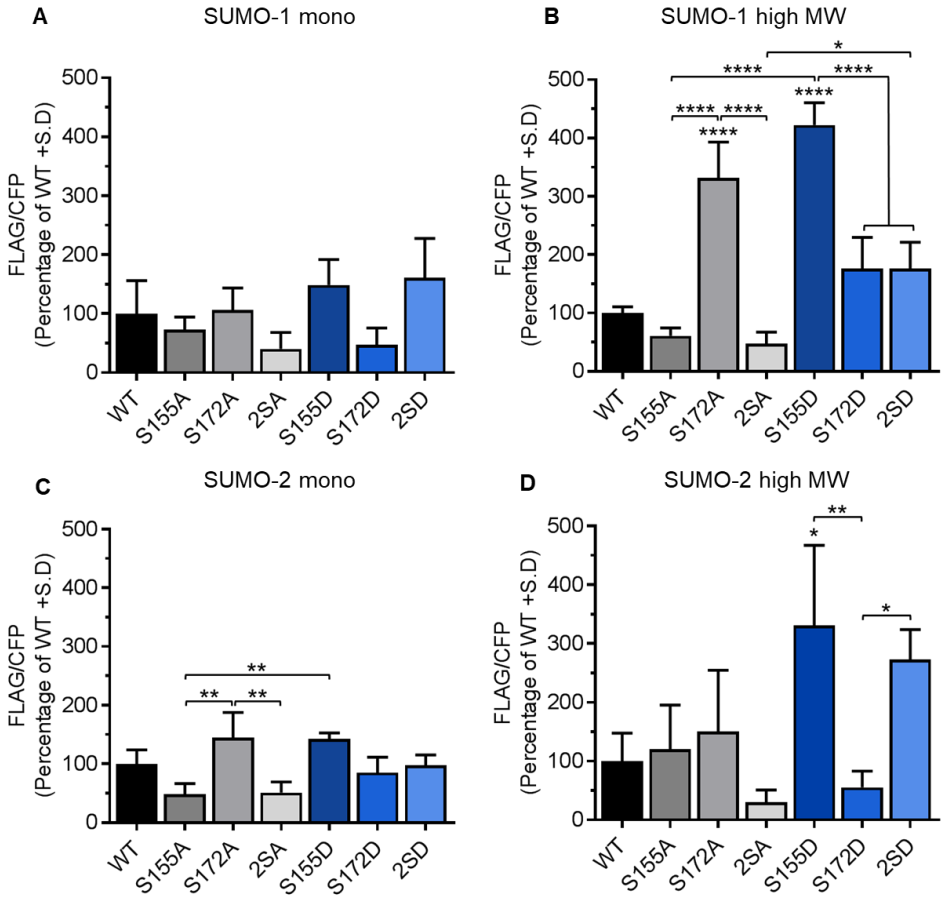

Figure 3.10 Quantification of mono and higher molecular species of MFF phospho-mutants

Graphs showing the individual quantification of the mono (**A, C**) and higher MW (**B, D**) SUMO populations from Figure 3.9, expressed as a percentage of wildtype normalised to CFP. n=5 (SUMO-1) n=3 (SUMO-2). One-Way ANOVA carried out and Tukey's post hoc test used to determine significance. p*<0.05, p**<0.001, p****<0.0001.

3.3.8 Phosphorylation at the AMPK sites enhances SUMOylation

Following the observations made in Figure 3.9, I selected the double phospho-null 2SA and double-phospho mimetic 2SD as a means to modify MFF SUMOylation for the following reasons:

1. Both sites have been shown to be phosphorylated by AMPK under stress (Chen *et al*., 2019; Detmer and Chan, 2007; Ducommun *et al*., 2015; Toyama *et al*., 2016), thus I reasoned that using the double mutants will be more physiologically relevant and will represent two extreme states of MFF; 2SD representing MFF under mitochondrial stress and a pro-fission state, whereas 2SA represents MFF under basal conditions.
2. They have opposite effects on SUMOylation, thus is a method to investigate the extremes of MFF SUMOylation.
3. Even though other mutants enhance SUMOylation (i.e. S172A, S155D), with the double phospho-mutants, I am able to directly determine the phosphorylation state of each site, ruling out any confounding issues potentially resulting from altered phosphorylation at one site as a consequence of mutation of the other. Indeed, since no antibody is available to detect phosphorylation at S172 in MFF isoform 1, I therefore am unable to determine whether compensatory changes to the phosphorylation state of S172 are occuring.

I therefore reassessed the effect of wildtype, 2SA and 2SD mutation on MFF SUMOylation in further experiments. Figure 3.11 shows that 2SA significantly reduces SUMO-1 by ~50%, and the 2SD mutant has significantly enhanced SUMOylation of both isoforms; a ~50% increase in total SUMO-1 and ~2.6-fold increase in total SUMO-2. The mono and high MW species show a similar trend.

Figure 3.11. Figure legend overleaf

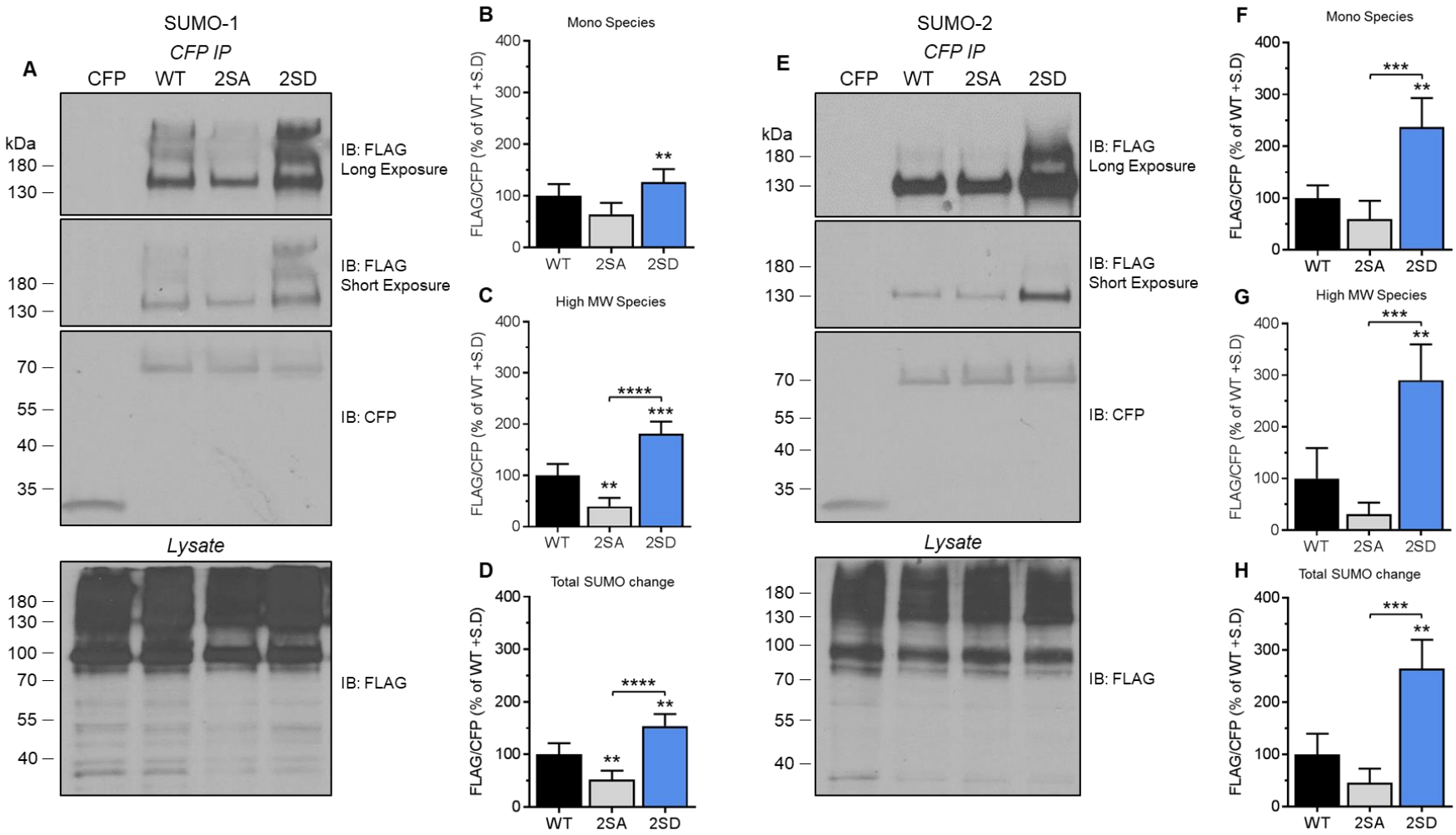

Figure 3.11 Phosphorylation of the two MFF AMPK sites S155 and S172 enhances MFF SUMOylation

HEK293T cells were transfected with wildtype, 2SA or 2SD CFP-MFF constructs and either FLAG-SUMO-1 or FLAG-SUMO-2. CFP immunoprecipitates were resolved by SDS-PAGE and probed for FLAG and CFP (blot in **A**=SUMO-1, **E**=SUMO-2). The mono SUMO species (**B, F**) and the higher MW species (**C, G**) were analysed individually and total SUMO change calculated as a mean average of the mono and higher MW species (**D, H**). Different exposures of the FLAG blots were required to detect the mono SUMO species and the higher MW species. Data represented as a percentage of WT +S.D. n=5 (SUMO1), n=4 (SUMO-2). One-Way ANOVA carried out and Tukey's *post hoc* test used to determine significance. p*<0.05, p**<0.001, p***<0.0005, p****<0.0001.

3.4 Discussion

The aim of this chapter was to confirm and characterise the SUMOylation of MFF, to identify where it is SUMOylated and how it is regulated. My key findings are:

Key findings

- MFF is a novel SUMO substrate, occurring at a single site, K151
- MFF exists in multiple SUMO states, mono- and poly-SUMOylated
- The SUMO-deficient mutant K151R has reduced ubiquitination
- *In vitro* deconjugation of SUMO has no effect on ubiquitin, and ubiquitin deconjugation has no effect on SUMOylation
- MFF SUMOylation is mediated by a PDSM, and phosphorylation occurs upstream of SUMOylation
- S155 has a greater effect on promoting SUMOylation. S172 alone has no effect on SUMOylation

SUMOylation of MFF

In this chapter I identified that MFF is heavily modified at K151 (Figure 3.2). Many previously identified SUMO substrates have distinct band shifts corresponding to sequential addition of SUMO molecules, such as with HIF-1α (Matic *et al*., 2008). Mono-SUMO events are generally considered to regulate protein interactions or compete with ubiquitin (Ulrich, 2008). With MFF, I observe a “smear” of modification above a prominent mono-SUMO species, indicating that MFF exists in multiple SUMO states. Moreover, the increasing molecular weight species are

observed for both SUMO-1 and SUMO-2/3, and since SUMO-1 poly-SUMOylation occurs at very low efficiency, if at all (Matic *et al*., 2010), the SUMO-1 observed in the higher molecular weight species is likely due to terminating SUMO-2/3 chains. It is feasible that MFF is modified at K151 by multiple different chain lengths, and possibly different branch structures as well, although mass spectrometry analysis would confirm the architecture of the SUMO chains.

Because SUMO can form hybrid chains with ubiquitin, and since MFF had previously been reported to be ubiquitinated (Gao *et al*., 2015; Lee *et al*., 2019), I wished to establish the nature of the SUMO chain, and whether the SUMO modification I was observing was potentially due to SUMO being incorporated into ever increasing ubiquitin chains. I ruled out this possibility, and infer that the modification on K151, observed in Figure 3.2C, is due to pure SUMO chains, based on three lines of evidence: Firstly, the band shift is completely abolished in the K151R mutation (Figure 3.2C). Secondly, the *in vitro* experiment suggests non-hybrid chains, and thirdly, both K151R and E153A mutation have abolished and significantly reduced SUMOylation, respectively, and comparable reduction in ubiquitination. The presence of K151 in the E153A mutant means it can still be ubiquitinated, since ubiquitination does not conform to a consensus sequence as SUMO does. Therefore, I conclude that SUMOylation is the major modification at K151, and ubiquitination occurs on separate sites.

Very few proteins have been identified as poly-SUMO substrates, and so there is little evidence of what the role of large SUMO chains on proteins could be. PML-SUMO aids the formation of NBs (Hattersley *et al*., 2011), poly-SUMO chains

recruits RNF4 and the proteasome for ubiquitination and initiates degradation (Lallemand-Breitenbach *et al*., 2008; Tatham *et al*., 2008) and SUMO-2/3 chains recruit CENP-E during mitosis (Zhang *et al*., 2008b). Since MFF is both mono and poly-SUMOylated, investigating the role of each of these SUMO species in turn will be the basis for further work.

Role of AMPK in MFF SUMOylation

Many proteins, mainly transcription factors, are regulated by a PDSM, with only a small amount of substrate SUMOylated at any given time. However, since the S155A and 2SA mutants retain ~50% SUMOylation, MFF phosphorylation is not essential for MFF SUMOylation, rather, it acts to enhance SUMOylation above 'basal' levels. These data raise a number of interesting questions; primarily what is the significance of MFF basal SUMOylation? and what is the function of enhancing SUMOylation upon AMPK phosphorylation? Furthermore, is the increase in SUMOylation due to more MFF proteins becoming SUMOylated, or are previously SUMOylated MFF proteins becoming more SUMOylated? These possibilities may not be exclusive, and while it is difficult to state conclusively, the profile of SUMO signal is similar between conditions, suggesting that there is a shift from previously non-SUMOylated MFF to SUMOylated MFF. Moreover, there is a greater increase in the higher molecular weight species compared to the mono species (Figure 3.11 B, C vs F, G) suggesting a shift to favour poly-SUMOylation (See schematic Figure 3.12).

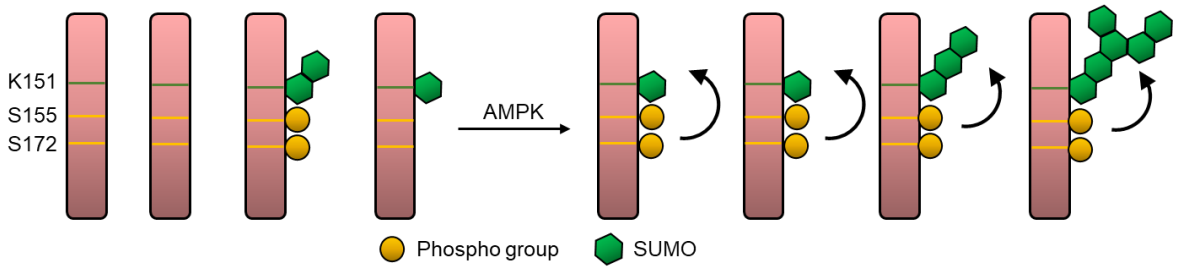

Figure 3.12 Model of AMPK phosphorylation enhancing MFF SUMOylation

The majority of MFF exists in a non-SUMOylated state, with some basal phosphorylation and SUMOylation. AMPK phosphorylates MFF at two sites, S155 and S172, previously shown to promote mitochondrial fission (Toyama *et al*., 2016). This phosphorylation enhances the SUMOylation state of MFF, including both the mono SUMOylated species and the higher MW species, although higher MW species are favoured. It is important to bear in mind that both SUMO-1 and SUMO-2/3 are increased following phosphorylation, and that many possible poly-SUMO chains, and potentially branched chains, could be formed.

To show definitively the involvement of AMPK in MFF SUMOylation, I carried out preliminary experiments using AMPK-α subunit null HEK cells (Thomas *et al*., 2018) and tested the SUMOylation state of WT MFF (see appendix Figure 8.2). These preliminary results show that in the AMPK α-null cells, SUMOylation of MFF is impaired, however, further repeats are required to confirm this.

Does SUMOylation promote ubiquitination via a STUbL?

How does blocking SUMOylation reduce ubiquitination? I propose a model whereby SUMO on MFF enhances ubiquitination on an alternative site via a STUbL (see Figure 3.6). One possible candidate for such a mechanism is parkin. We and others have reported that MFF is a parkin target, since parkin knockdown increases MFF levels (Gao *et al*., 2015; Lee *et al*., 2019). The report by Gao *et al*. identified one site of MFF ubiquitination, whereas our data show there are at least three (Lee *et al*., 2019). Gao *et al* also used CCCP or overexpressed parkin to detect ubiquitination, but under our conditions we observed endogenous ubiquitin on MFF. These differences could be due to the different isoforms used (we used isoform 1 whereas the Gao *et al* report used isoform 2), which have different propensities of parkin recruitment. Parkin knockdown reduces total ubiquitination by ~40% on wildtype MFF, whereas the K151R mutant was insensitive to further reduction in ubiquitination in the absence of parkin (Lee *et al*., 2019), suggesting that parkin may require the SUMO on K151 to promote ubiquitination on an alternative site. This exciting possibility warrants further investigation.

To investigate ubiquitination of MFF further, I generated a K302R mutant, corresponding to the ubiquitin site identified by Gao *et al*, and a combination mutant of K151R and K302R (2KR), to determine if both sites are ubiquitin acceptors. My rationale was that if the K302R mutation abolishes ubiquitination, the remaining ubiquitin on K151R is on K302, and K302 is the only ubiquitin site. However, if this is not the case, then MFF contains multiple ubiquitin sites.

My data show that all these mutants retain ubiquitination, albeit to a lesser extent than WT, demonstrating that MFF isoform 1 has at least three ubiquitin sites (see Figure 2f in Lee *et al*., 2019, published work in appendix).

Nonetheless, the possibility that SUMO and ubiquitin compete to conjugate at K151 cannot be excluded. The blot in Figure 3.2 shows that MFF is heavily modified at K151. Moreover, K151R retains approximately half the ubiquitination compared to wild type. Assuming equal stoichiometry of SUMO and ubiquitin, if this hypothesis were correct, I would expect to see higher bands appearing in the K151R condition under denaturing conditions, which would correspond to ubiquitination. However, even at high exposure, no such bands were detected. It is therefore reasonable to suggest that the signal detected in Figure 3.2 is primarily due to SUMOylation. Moreover, the E153A mutant has significantly reduced SUMOylation (Figure 3.7), and similar levels of ubiquitination to K151R, further supporting the hypothesis that MFF-SUMO promotes ubiquitination. To decipher the complex relationship between SUMO and ubiquitin further, and the structure of the poly-SUMO chains, mass spectrometry analysis should be carried out on WT vs K151R MFF, although due to time limitations, this was beyond the scope of the work presented here.

MFF isoforms

As discussed in Figure 1.9, the MFF gene encodes multiple splice isoforms. One exon junction of human isoform 1 lies very close to the S172 site, changing the amino acid sequence following the AMPK site. It cannot be said that the AMPK sites which do not conform to the AMPK optimal sequence are necessarily less

phosphorylated, since the S172 site still contains much of the AMPK motif consensus sequence. Moreover, isoform 2 has the same number of AMPK motif elements as isoform 1, and has been shown to be phosphorylated (Toyama *et al*., 2016). Additionally, all isoforms contain the perfect AMPK site at S155, which will recruit AMPK. I show that phosphorylation at S155 has the greatest effect on SUMOylation, and S172D alone had no effect. However, I do observe that combining these phosphorylation events has differential effects on SUMOylation; S172D has reduced SUMO-1-ylation compared to S155D, at similar levels to 2SD. Conversely, 2SD has enhanced SUMO-2-ylation, similar to S155D levels, and significantly greater than S172D.

Differential effects of phosphorylation at S155 and S172

I speculate that phosphorylation at S172 has differential roles in regulating SUMO; it negatively regulates SUMO-1, whereas it has no effect on SUMO-2 (see Figure 3.13). Additionally, S172A significantly increased higher MW SUMO-1 species over 3-fold compared to wildtype. Could this be due to compensatory phosphorylation at S155? It is clear that S155 phosphorylation has the greatest effect on promoting SUMOylation, but could the double phosphorylation event that occurs upon AMPK activation concurrently regulate SUMOylation? Indeed, distal phosphorylation sites have been demonstrated to regulate SUMOylation for kainate receptors (Chamberlain *et al*., 2012; Konopacki *et al*., 2011; Martin *et al*., 2007) and STAT1 (Vanhatupa *et al*., 2008).

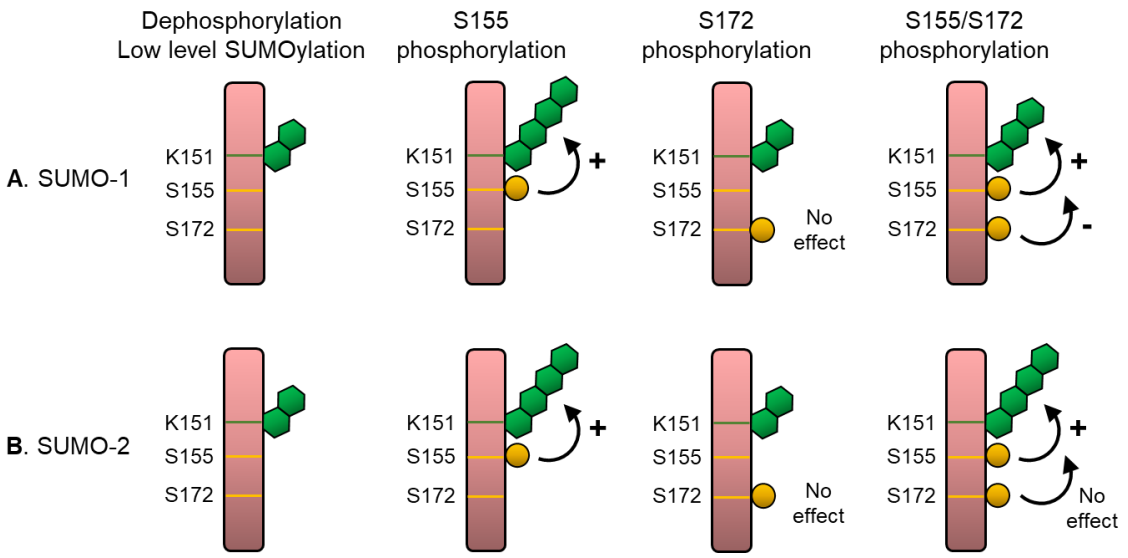

Figure 3.13 Phosphorylation at S155 and S172 have differential effects on MFF SUMOylation

Based on the SUMO profiles of the various phosphorylation mutants, I predict that phosphorylation at S172 has a negative effect on promoting SUMO-1, whereas it has no effect on SUMO-2. S172 phosphorylation has no effect in the absence of S155 phosphorylation. When both sites are phosphorylated, SUMOylation is enhanced, but SUMO-1 levels are reduced compared to S155 phosphorylation alone.

Summary

My data so far leads to a model whereby AMPK phosphorylation enhances MFF SUMOylation, and since AMPK activation and phosphorylation of MFF has been shown to be involved in fission (Toyama *et al*., 2016), I therefore hypothesise that the increase in SUMOylation has a role in mitochondrial fission. In the next chapter I investigate the role of SUMOylation in MFF function.

Chapter 4 Investigating the function of MFF SUMOylation

4.1 Introduction

MFF is the major DRP1 receptor involved in mitochondrial fission (Loson *et al*., 2013; Otera *et al*., 2010), although all the DRP1 receptors can function independently to recruit DRP1 (Osellame *et al*., 2016). Indeed, MiD49 and MiD51 localise with DRP1 and MFF at pre-fission sites (Elgass *et al*., 2015), and MFF and DRP1 were detected in a proximity biotinylation assay with MiD51, indicating close association between MiD51, DRP1 and MFF (Osellame *et al*., 2016). The role of the MiD proteins is still not clear; knock-down of MiD proteins induces mitochondrial elongation, but overexpression of MiD49 or MiD51 promotes DRP1 recruitment, but counter-intuitively elongates the mitochondrial network as well (Loson *et al*., 2013; Palmer *et al*., 2011, 2013). These results do not indicate that the MiD proteins behave as “canonical” DRP1 receptors, where one would expect overexpression to promote fission, and conversely knockdown to lead to unopposed fusion, as seen when manipulating MFF or DRP1 expression levels (Gandre-Babbe and van der Bliek, 2008; Loson *et al*., 2013; Otera *et al*., 2010).

Overexpression of the MiD proteins enhances the inhibitory phosphorylation modification at S637 on DRP1 (Loson *et al*., 2013). This report suggests that the MiD proteins regulate mitochondrial morphology by binding to inactive DRP1 and sequestering it on the MOM. A recent report offers an intriguing explanation to the complex nature of the MiD protein function, suggesting that MiD proteins facilitate the MFF-DRP1 interaction, by functioning as a “molecular bridge” between MFF and DRP1 (Yu *et al*., 2017). MFF can bind to MiD proteins in the absence of DRP1, however reduction of MiD levels reduces MFF binding to DRP1, and

overexpression has the same effect. They hypothesise that intermediate levels of MiD facilitate direct MFF-DRP1 binding, and low levels can not promote this interaction, whereas high levels sequester DRP1, in effect “out-competing” MFF for DRP1 binding. Thus, this elegant hypothesis provides an explanation for the apparently contradictory findings of MiD protein function, and adds increasing complexity to the regulation of receptor-receptor and receptor-DRP1 interactions. The implication is that to dissect the molecular steps of mitochondrial fission, it is necessary to consider the mitochondrial fission machinery as a complex of DRP1, in active or inactive states, and different DRP1 receptors having different capacities for DRP1 binding, depending on other DRP1 receptors.

The mitochondrial network is inextricalbly linked to various cellular stresses. Mitochondrial fragmentation and cell death occur upon treatment with mitochondrial uncouplers or ETC inhibitors, such as CCCP and rotenone (Griparic *et al*., 2007; Otera *et al*., 2010; Toyama *et al*., 2016), and oxygen-glucose deprivation (OGD) (Guo *et al*., 2013; Sanderson *et al*., 2015). Increasing global SUMO-2/3 levels is cytoprotective in response to ischemia and OGD (Datwyler *et al*., 2011; Yang *et al*., 2008) and Guo *et al*. report the increased global SUMO-2/3 levels are coupled with a decrease in levels of the deSUMOylating enzyme SENP3. Increased SUMOylation of DRP1 by SUMO-2/3 during OGD sequesters DRP1 in the cytosol, and upon restoration of oxygen and glucose levels (reperfusion) SENP3 levels recover and this leads to cytochrome c release, mediated by deSUMOylation of DRP1 by SENP3 and trafficking to the MOM (Guo *et al*., 2013).

These reports highlight that protein SUMOylation is a key factor in cellular responses to stress, and can have profound effects on mitochondrial morphology and cellular health. I therefore wondered how SUMOylation of MFF alters its interaction with DRP1 and MiD protiens, and how MFF SUMOylation is affected following cell stress.

4.2 Aims

Following the characterisation of MFF SUMOylation, and identifying enhanced SUMOylation in response to phosphorylation, I next investigated the effects of SUMOylation of MFF on binding to DRP1 and MiD proteins. Utilising the SUMOylation-deficient mutant K151R and the double phosphorylation mutants (2SD and 2SA) as a method to regulate MFF SUMOylation levels, this chapter addressed the following:

- To investigate the binding of DRP1 to MFF, to test if SUMOylation correlates with DRP1 binding.
- Examine MiD binding to investigate if SUMOylation impacts the MiD-MFF interaction.
- If SUMOylation of MFF does affect the pre-fission complex, what is the mechanism?
- To test the effect of SUMOylation of MFF following OGD stress.

4.3 Results

4.3.1 MFF SUMOylation promotes DRP1 binding

MFF is reported to be major DRP1 receptor (Otera *et al*., 2010), so I initially investigated if the non-SUMOylatable K151R MFF mutant still effectively bound to DRP1. I transfected WT and K151R CFP-MFF into HEK293T cells and co-immunoprecipitated endogenous DRP1. Binding to K151R is significantly decreased, displaying approximately 41% binding compared to WT (Figure 4.1) suggesting that SUMOylation of MFF promotes binding to DRP1. This agrees with the hypothesis stated at the end of section 3.4, whereby phosphorylation by AMPK promotes SUMOylation, which then enhances DRP1 binding and subsequent mitochondrial fission (See schematic in Figure 4.2). At this point, I do not know how SUMO on MFF promotes the binding to DRP1, and I do not know whether it is a direct interaction. It is possible there is a weak interaction between MFF and DRP1, and between SUMO and DRP1. Therefore the simple model in Figure 4.2 illustrates DRP1 bound arbitrarily to SUMOylated-MFF, but I cannot state that SUMO has a direct ability to bind to DRP1.

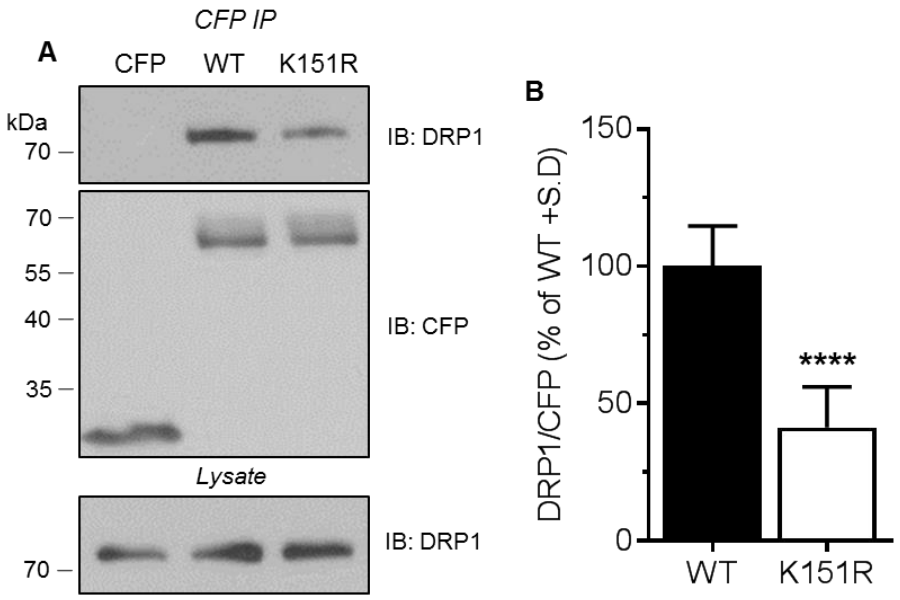

Figure 4.1 Non-SUMOylatable MFF displays reduced DRP1 binding

A HEK293T cells were transiently transfected with CFP-MFF wildtype or K151R. CFP co-immunoprecipitates were resolved by SDS-PAGE and probed for endogenous DRP1. **B** Quantification of DRP1 binding to MFF, normalised to CFP and expressed as a percentage of WT +/- S.D. t test used to determine significance, n=6, p****<0.0001.

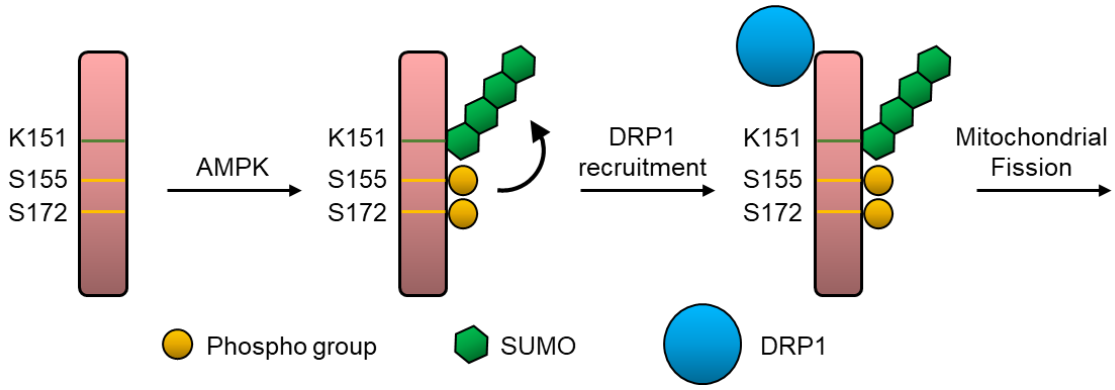

Figure 4.2 SUMO-MFF mediated model of DRP1 recruitment

Model of phosphorylation dependent SUMOylation of MFF facilitating the recruitment of DRP1 and subsequent fission of the mitochondria. Upon bioenergetic stress, activated AMPK phosphorylates MFF at S155 and S172, which subsequently enhances MFF SUMOylation. This SUMOylation can then promote MFF's ability to bind to DRP1. Position of DRP1 binding to MFF with respect to SUMO on MFF is unkown.

4.3.2 MFF phosphorylation null and mimetic mutants have reduced DRP1 binding

Following the observation that DRP1 binding to K151R is reduced, I next investigated the binding of DRP1 to the phosphorylation mutants. Surprisingly, DRP1 binding to 2SA and 2SD was ~63% and ~48% compared to WT, similar to K151R-DRP1 binding levels (Figure 4.3). According to my hypothesis (Figure 4.2) enhanced SUMOylation follows AMPK phosphorylation, leading to DRP1 recruitment and fission. The K151R and 2SA binding data agree with this hypothesis, however, one would expect enhanced DRP1 binding to 2SD. Therefore, these results suggest that the level of MFF SUMOylation does not directly correlate with DRP1 binding.

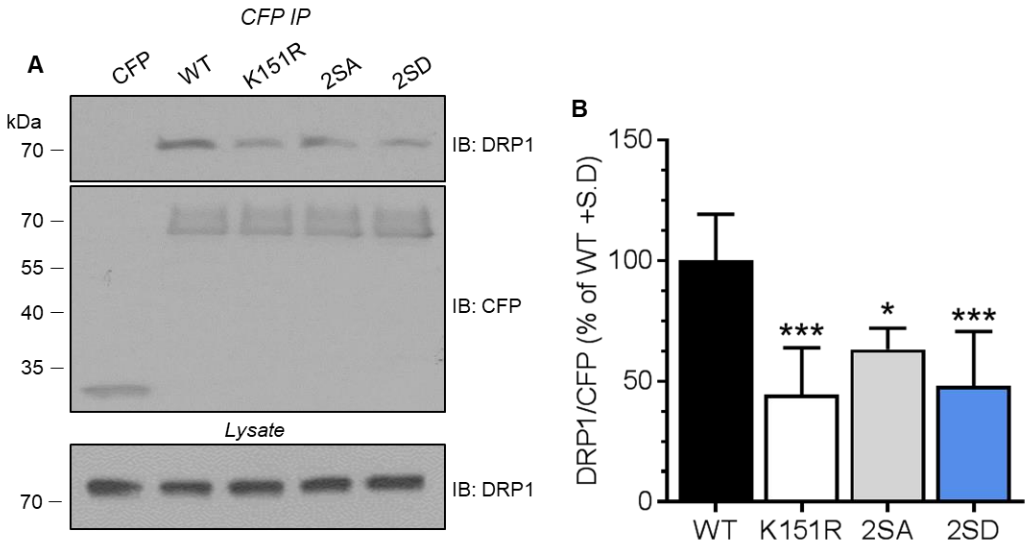

Figure 4.3 MFF SUMO and phosphorylation mutants reduce DRP1 binding

A HEK293T cells were transiently transfected with the indicated CFP-MFF constructs. CFP immunoprecipitates were resolved by SDS-PAGE and probed for endogenous DRP1. **B** Quantification of DRP1 binding. Data expressed as a percentage of wildtype control and normalised to CFP. One way ANOVA and Tukey's post hoc test carried out to determine significance. Data generated from 6 independent experiments, p*<0.05, p***<0.0005. No significant difference found between K151R, 2SA, 2SD.

4.3.3 MiD49 contains a SUMO interacting motif

As outlined above, MiD proteins (MiD49, MiD51), DRP1 and MFF are localised at pre-fission foci on the MOM (Elgass *et al*., 2015; Osellame *et al*., 2016) and MiD proteins promote the binding to MFF and DRP1 (Yu *et al*., 2017). These reports prompted me to investigate a potential role of the MiD proteins to offer an explanation to the DRP1 binding data in Figure 4.3. I wondered whether SUMOylation of MFF has a role in regulating the MFF-MiD interaction, and whether any of the DRP1 receptors contain a SUMO interacting motif (SIM) which could mediate this interaction. I used a non-conjugatable form of SUMO lacking the di-glycine di-peptide (ΔGG), which in effect behaves as “free” SUMO i.e. that can bind via a SIM, but not covalently conjugate to the target protein. I observed MiD49 binding to SUMO-1-ΔGG, suggestive of a non-covalent interaction between MiD49 and SUMO-1, whereas non of the other DRP1 receptors interacted with SUMO-ΔGG (Figure 4.4).

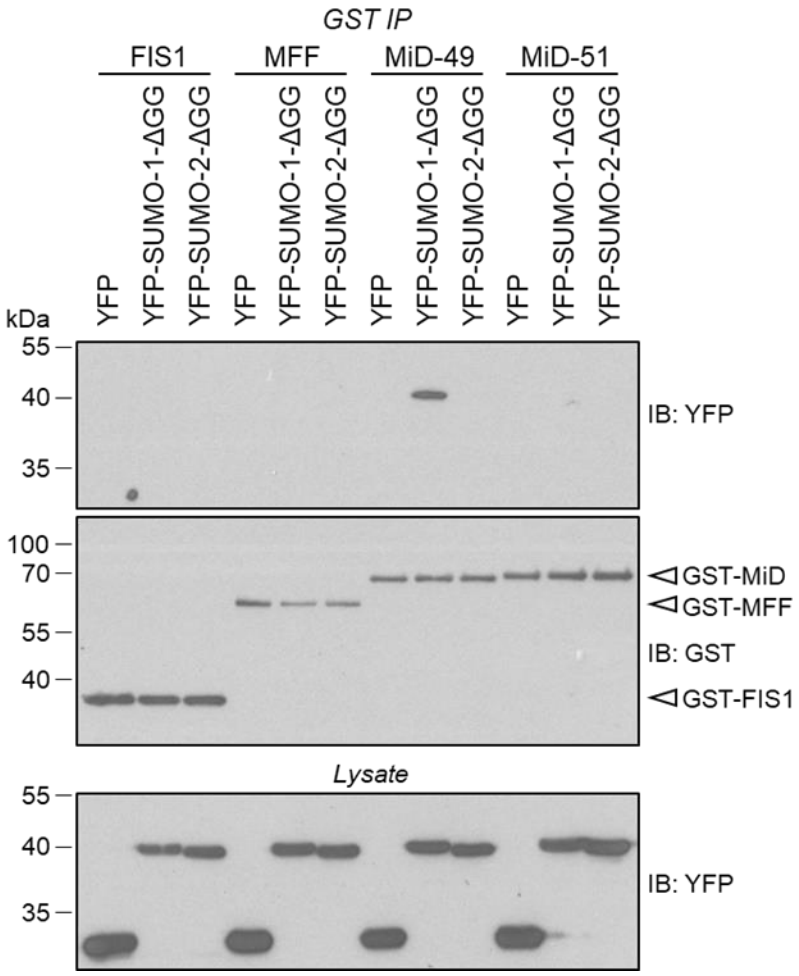

Figure 4.4 MiD49 contains a SIM

HEK293T cells were transiently co-transfected with human GST-FIS1, GST-MFF, GST-MiD49 (mouse) or GST-MiD51 (mouse), and either YFP, YFP-SUMO1-ΔGG or YFP-SUMO2-ΔGG. GST pulldown carried out on supernatant and samples were blotted for YFP and GST. n=1 for all receptors. Individual repeat of just MiD49 confirms interaction with SUMO-1 (see appendix 8.4).

4.3.4 MFF phosphorylation reduces MiD49 binding

The exciting result of MiD49 non-covalently interacting with SUMO-1 offered the possibility that SUMOylation of MFF may enhance its interaction with MiD49 via the SIM. In this case the increased MFF SUMOylation, in response to phosphorylation, could increase association between MFF and DRP1-MiD49, thus increasing the amount of trimeric complexes? I tested the binding of the MFF mutants to endogenous MiD49 in HEK293T cells and detected a ~three-fold increase of MiD49 binding to 2SA compared to 2SD (150.2% vs 43.8%) (Figure 4.5A, B). I also tested binding between MiD and K151R, and observe enhanced binding to myc-MiD49 and MiD51-HA (Figure 4.5C and D). If MiD49 was binding to SUMOylated MFF via a SUMO-SIM interaction, I would expect reduced binding to K151R, and 2SD to bind more than 2SA. Unexpectedly, I observed the reverse, and from this I conclude that SUMOylating MFF impairs the MiD interaction.

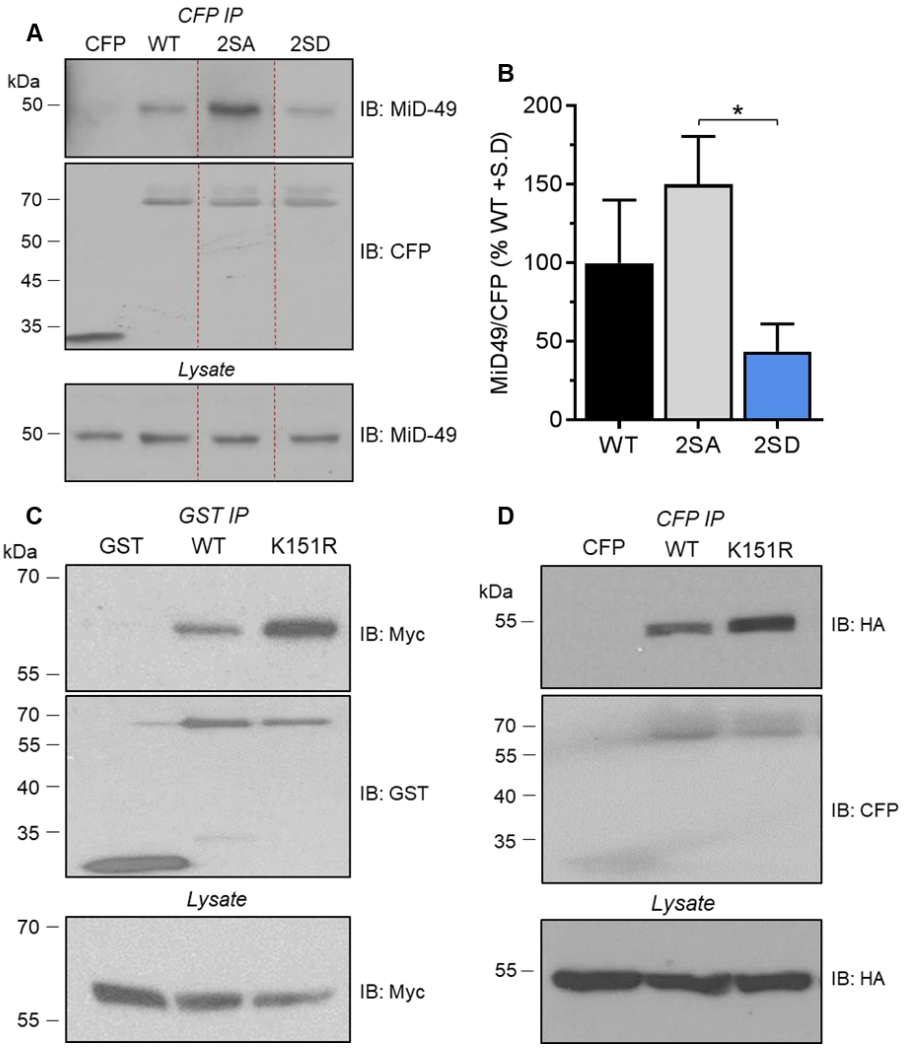

Figure 4.5 MFF phosphorylation and SUMOylation reduces MiD49 binding

A HEK293T cells were transfected with wildtype, 2SA or 2SD CFP-MFF constructs for 2 days. CFP immunoprecipitations carried out on lysate, resolved by SDS-PAGE and blotted for endogenous MiD49. Dotted lines indicate splicing from a larger blot. **B** Quantification of MiD49 binding normalised to CFP. One-Way ANOVA followed by Tukey's post hoc test used to determine significance. n=3, p*<0.05. **C-D** HEK293T cells were transfected with GST or CFP-MFF wildtype and K151R and either myc-MiD49 (**C**) or MiD51-HA (**D**). GST/CFP pulldowns carried out on lysate, resolved by SDS-PAGE and blotted for either myc or HA. Representative of two independent experiments.

Comparing Figure 4.3B and Figure 4.5B, there is an altered ratio of MiD49/DRP1 binding to 2SA and 2SD. The phosphorylation mutants both bind DRP1 to similar levels, however, within the complex of DRP1-MiD49-MFF, there is proportionally more MiD49 to DRP1 (~2.5-fold) within the 2SA complex compared to 2SD. Since K151R also has enhanced MiD binding (approximatey 2.6-fold compared to WT, based on experiments with myc-MiD49 (Figure 4.5C)), I hypothesise that SUMOylation reduces the binding between MFF and MiD49, altering the ratio of MiD49 within the pre-fission complex, illustrated in Figure 4.6. highlights that pulldowns of the mutants show similar amounts of DRP1 binding, but exhibit altered MiD49 binding.

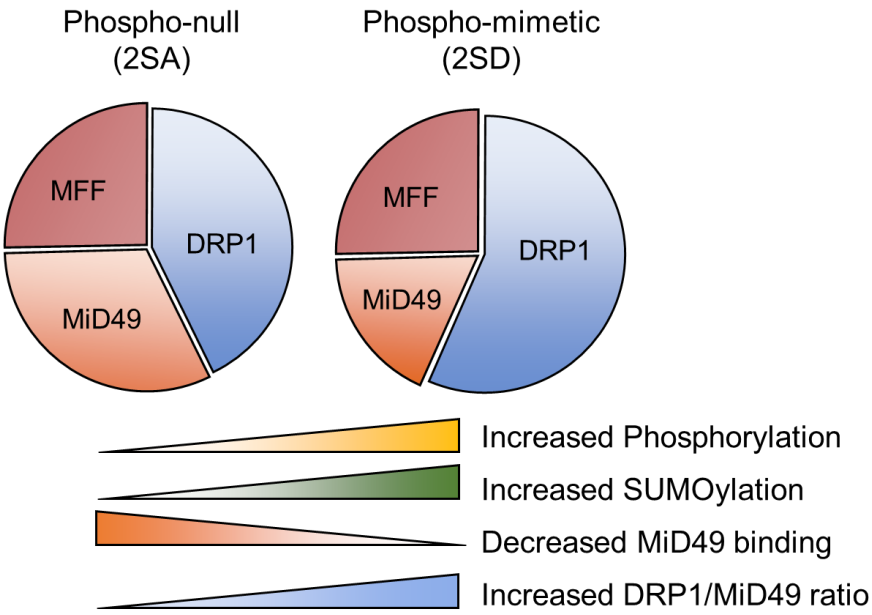

Figure 4.6 Conceptual representation of ratios of fission proteins within pre-fission complexes under differential MFF PTM's

Pie charts represent comparative ratios of MiD49 and DRP1 bound to MFF within the trimeric complex under different MFF PTM's. 2SA and 2SD mutants have comparable DRP1 binding, however 2SD has reduced MiD49 binding compared to 2SA. Therefore, there is a change in the abundance of MiD49 within the trimeric complexes, where 2SD MFF will associate with comparatively lower amounts of MiD49 than 2SA. This leads to an increase in the DRP1/MiD49 ratio, which could conceptually lead to enhanced fission, if proportionally more DRP1 is bound to MFF and not MiD49 within this complex.

4.3.5 Oxygen/Glucose deprivation enhances global SUMO-2/3 conjugation, decreases SENP3 levels, and enhances MFF SUMOylation

To test the effect of metabolic stress on SUMOylation in general, and SUMOylation of MFF, I used OGD to model ischemia, as has previously been used to induce mitochondrial dysfunction and fragmentation (Almeida *et al*., 2002; Guo *et al*., 2013; Sanderson *et al*., 2015). After challenging HEK cells with 1hr OGD, SENP3 levels decrease ~50% (Figure 4.7A, C) and global SUMO-2/3 conjugation is increased ~70% (Figure 4.7B, D), in agreement with previous findings (Guo *et al*., 2013). Many different time points have previously been used to induce mitochondrial dysfunction following OGD challenge, from 5 minutes to 3hr (Almeida *et al*., 2002; Rousset *et al*., 2015; Wappler *et al*., 2013). OGD insult to primary neurons activates AMPK very rapidly (within 5 minutes), which persists for up to 1.5hr (Rousset *et al*., 2015). With the evidence linking AMPK activation and SUMO changes occurring after OGD, and that prolonged stress at 3hr induces greater mitochondrial dysfunction than 1hr OGD, I investigated whether SUMOylation of MFF is sensitive to a more prolonged OGD treatment. I transfected HEK293T cells with wildtype CFP-MFF and challenged with 2hr OGD. SUMO-1 conjugation to MFF increased (almost doubling, Figure 4.7C) following OGD, although further repeats will be required to confirm this.

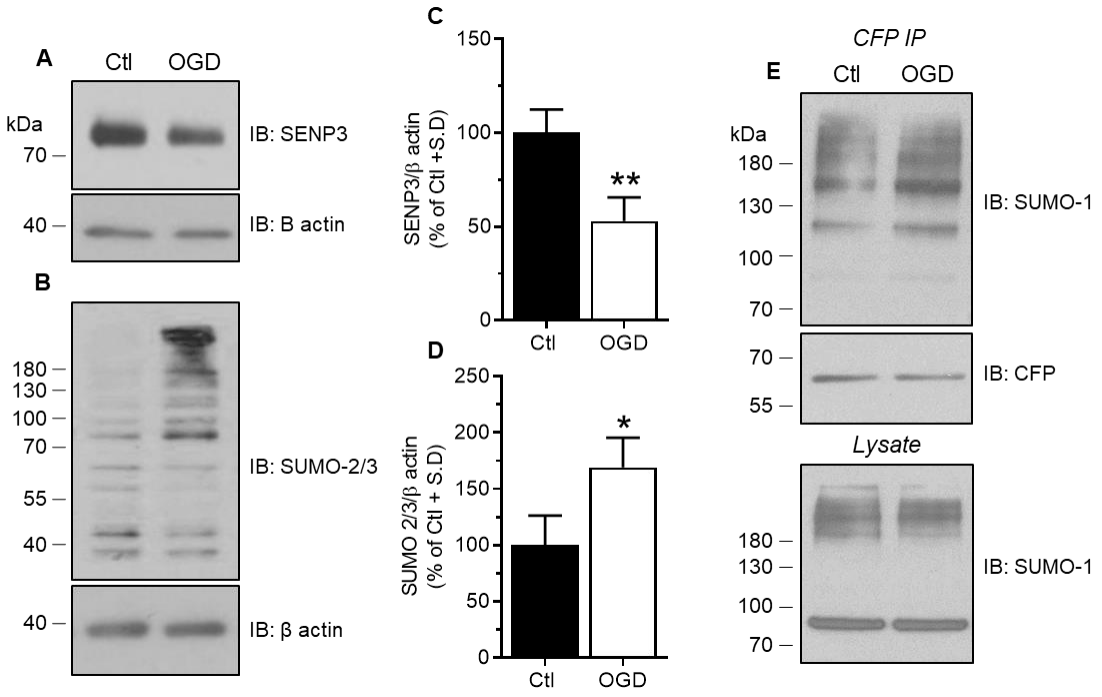

Figure 4.7 Oxygen/Glucose deprivation increases global SUMO-2/3 conjugation, decreases SENP3 levels and increases SUMO-1 conjugation to MFF

HEK293T cells were challenged with OGD for 1 hr, lysed and total protein probed for SENP3 (**A**) and SUMO-2/3 levels (**B**). Quantification of total SENP3 protein levels (**C**) and SUMO-2/3 levels (**D**) normalised to β actin and expressed as a percentage of control. n=3, p*<0.01, p**<0.01. **E** HEK293T cells were transfected with wildtype CFP-MFF for 2 days. 2hrs prior to lysis cells were challenged with OGD (performed by N. Rawlings). CFP-immunoprecipitates were probed for SUMO-1 (representative of 2 independent experiments).

4.3.6 MFF SUMOylation promotes DRP1 binding under mitochondrial stress

Following the observation that global SUMOylation increases following OGD stress (Figure 4.7B) and that MFF SUMOylation increases under OGD (Figure 4.7E), I hypothesised that the increase in the SUMOylation state of MFF under stress promotes DRP1 binding, thus facilitating mitochondrial fission, as outlined in Figure 4.2. To test this hypothesis, I investigated DRP1 binding to wildtype and K151R MFF following mitochondrial depolarisation with rotenone. Figure 4.8 shows the effects of rotenone for 1hr, which has previously been used to induce AMPK-mediated MFF phosphorylation and mitochondrial fission (Toyama *et al*., 2016). DRP1 binds to the K151R mutant at a reduced level compared to wildtype MFF (as previously demonstrated in section 4.3.1), and this difference is exacerbated upon rotenone treatment from ~50% binding under control conditions to <15% after treatment. This suggests that the ability of MFF to be SUMOylated under mitochondrial stress (ETC inhibition) facilitates the increase in DRP1 binding. Unfortunately, due to time limitations, I could not carry out sufficient repeats for statistical analysis. Nonetheless, I observed a comparable trend in two similar experiments using either rotenone (250ng/mL for 15 minutes) or CCCP (20μM for 30 minutes) and believe this is a potentially important result that would form the basis for further investigation.

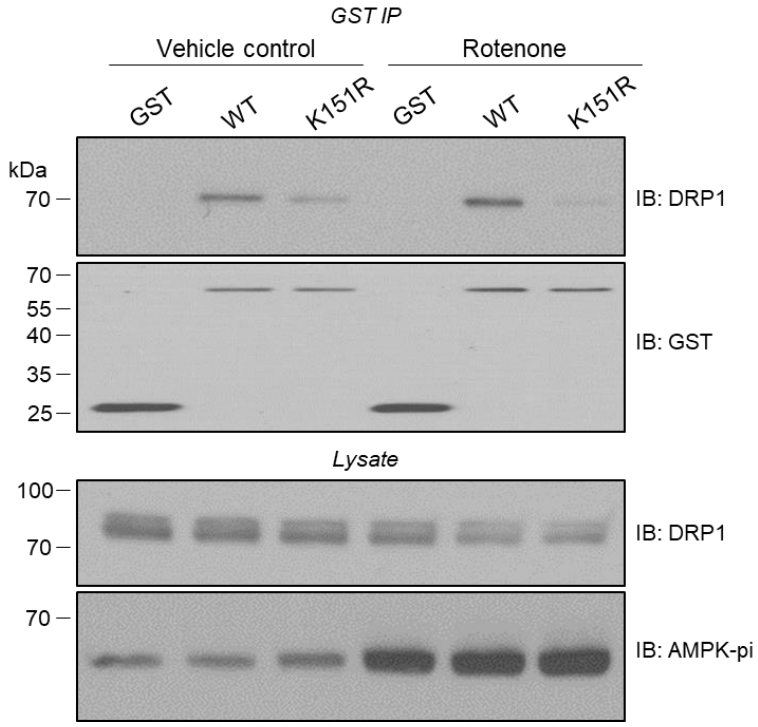

Figure 4.8 DRP1 binding to MFF wildtype and K151R during rotenone treatment

HEK293T cells were transiently transfected with GST-MFF wildtype or K151R for 48hrs. 1hr prior to lysis, cells were treated with 250ng/mL rotenone (DMSO acted at vehicle control). Cells were lysed and GST-pulldown carried out on lysate, resolved by SDS-PAGE and blotted for endogenous DRP1 and GST. Lysate probed for DRP1 and AMPK activation.

4.4 Discussion

In this chapter my aim was to biochemically investigate the function of MFF SUMOylation. My key findings are:

- K151R, 2SA and 2SD MFF mutants have reduced DRP1 binding
- SUMOylation is a negative regulator of MiD binding
- MFF 2SA has enhanced MiD binding compared to 2SD
- MiD49 contains a SIM
- SUMO-2/3 conjugation increases and SENP3 decreases following OGD
- SUMO-1 conjugation to MFF increases following OGD
- Under mitochondrial stress using ETC inhibitors, DRP1 binding is further reduced to K151R compared to control conditions

SUMOylation and DRP1 binding

My finding that the MFF mutants K151R, 2SA and 2SD all have reduced binding to DRP1 was initially perplexing. Although the reduced K151R and 2SA binding agrees with the hypothesis presented in Figure 4.2, the reduced DRP1-MFF (2SD) interaction does not. Toyama *et al* show that 2SD fragments mitochondria without stress (I confirmed the findings of Toyama *et al*. that the 2SD mutant induces decreased mitochondrial size in neuronal dendrites compared to 2SA (See appendix Figure 8.3)), and so it has since been assumed that the MFF phosphorylation increases DRP1 binding capacity. However, what the Toyama *et al* report failed to demonstrate was an increased interaction, since they only report

mitochondrial imaging data. They also show that using cells depleted of endogenous Fis1, MFF and MiD51, the phospho-deficent MFF mutant can recruit DRP1 to comparable levels as wildtype MFF, but fails to increase recruitment under stress. This is in line with my data, since the experiments in Figure 4.3 were carried out under basal conditions and 2SA can bind to DRP1. However, since endogenous MiD49 was still present, it is possible that what Toyama *et al* observed is not direct recruitment of DRP1 to MFF, but altered interactions between the re-expressed MFF and endogenous MiD49, and consequent differences in the capacity of this complex for DRP1 recruitment and its ability to proceed to fission.

What is further perplexing is that all mutants have reduced DRP1 binding compared to wildtype. Could “restricting” MFF to the extremes of SUMOylation and phosphorylation only allow observation of a sub-set of interactions, whereas wildtype MFF can occupy all states, and therefore the higher DRP1 binding is observed? Potentially, maximal binding of DRP1 to MFF may require switching between the PTM states of MFF, something which each of the mutants are deficient in. Moreover, this raises the question of the different states i.e. PTMs of DRP1 binding to the three mutants. Figure 4.3 shows total DRP1, but does not inform on whether the interacting DRP1 is phosphorylated at S616, S637 or SUMOylated. This could account for the observed no differences in total DRP1 binding, but it is possible that I co-immunoprecipitated more active DRP1 with 2SD, and more inhibited DRP1 with 2SA and K151R. Repeats of the experiments

and blotting for phosphorylated forms of DRP1 as a proportion of total DRP1, and using a SUMOylation-deficient mutant of DRP1 will be for future work.

Roles of MiD proteins

My data indicate that the canonical “binary” model of increased DRP1 binding to mitochondrial receptors leads to increased fission is an over simplification. DRP1 continuously cycles between the cytosol and puncta on the MOM (Wasiak *et al*., 2007). This suggests a very dynamic system, regulated by PTMs of DRP1 which alter its stability at the MOM. Indeed, individual puncta of DRP1 and the DRP1 receptors MiD49, MiD51 and MFF show a high degree of co-localisation at pre-fission sites. Intriguingly, during live cell imaging experiments, MiD foci were observed to undergo cycles of constriction and relaxation before complete fission (Elgass *et al*., 2015), suggesting that these are “primed” sites and that a fission stimulus can rapidly elicit fission. Moreover, MFF and MiD proteins localise in puncta even in the absence of DRP1 (Otera *et al*., 2010; Palmer *et al*., 2011). Therefore, current data in the literature support a model of complex DRP1-receptor interactions in regulating the pre-fission complex, and my data suggest that PTMs of the receptors can alter pre-fission complexes.

Yu *et al.* offer an explanation for the apparent discrepency in observations of knockdown and overexpressed MiD proteins, both of which cause mitochondrial elongation (Yu *et al*., 2017). In essence, these findings point to a model where the abundance of MiD proteins confers a biological outcome; too much MiD protein and they sequester DRP1. Too little MiD protein leads to inadequate pre-fission complexe formation, and an inability for MFF to efficiently bind DRP1. Of

course, in a biologial setting under basal conditions the MiD protein levels are relatively stable. But could proximity of the proteins in relation to each other confer such a biological response?

I show that MiD49 binding to MFF 2SA and K151R is higher than 2SD, and predict that the MFF-DRP1 interaction is mediated by decreased binding to or displacement of MiD proteins from MFF-DRP1, regulated by SUMOylation. This incorporates the observations that DRP1 is inhibited by MiD proteins, and that displacing MiD from MFF-DRP1 promotes fission. Upon inspection of the DRP1 and MiD49 binding data, it is clear that even though MFF 2SA and 2SD bind to similar amounts of DRP1, more MiD49 is incorporated in the 2SA complex (see Figure 4.6). One can start to build a model whereby DRP1 is sequestered by MiD in a pre-fission complex, and then following a fission stimulus, MFF becomes phosphorylated and then SUMOylated, MiD is displaced and “hands-over” DRP1 to MFF. The increase in direct MFF-DRP1 binding then represents a fission competent complex (Figure 4.9).

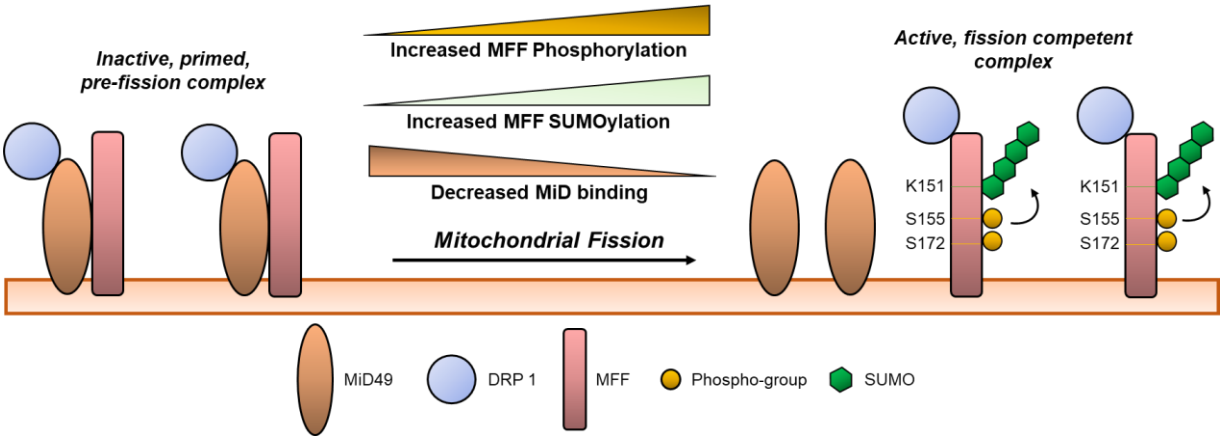

Figure 4.9 Model of mitochondrial fission: Does MFF SUMOylation act as a molecular switch?

Based on previously published data and my own findings, I propose a model of mitochondrial division which is regulated by MFF SUMOylation:

1. Pre-fission complexes consist of DRP1 bound to MiD proteins, which is bound to non-phosphorylated/non-SUMOylated MFF.
2. AMPK phosphorylation of MFF at S155 and S172 enhances SUMOylation.
3. Increased SUMOylation displaces MiD from the complex, resulting in a high proportion of DRP1 bound to MFF. SUMO-MFF bound to DRP1 represents a fission competent complex.

What this model does not address is the state of DRP1 and how it is removed from MiD and binds to MFF. One possibility is via the SUMO-1 interacting motif I identified on MiD49. DRP1 was elegantly shown to cycle from the cytosol to the MOM, with a half-time of ~50 seconds residency at mitochondria (Wasiak *et al*., 2007). DRP1-SUMO-1 is stabilised at MOM under apoptotic conditions (Prudent *et al*., 2015; Wasiak *et al*., 2007), so could the SIM on MiD49 be binding to the

cycling DRP1, and thus offer a mechanism of recruiting specifically SUMOylated DRP1 to pre-fission sites? Generating a MiD49 SIM mutant and investigating DRP1 recruitment under basal and stress conditions would reveal a possible SUMO regulated mechanism of DRP1 recruitment. Moreover, Figure 4.9 examines MiD49, since that is what was mainly investigated in Figure 4.5, yet there are two MiD proteins, both of which were demonstrated to facilitate the DRP1-MFF interaction (Yu *et al*., 2017), and in FRET analysis MiD51 is in closer proximity to MFF and DRP1 compared to MiD49 (Elgass *et al*., 2015). Osellame *et al*. elegantly show that MiD51 and MFF have antagonising effects in an *in vitro* experiment on DRP1 GTPase activity; MFF + DRP1 enhance GTPase activity above DRP1 alone. MiD51 + DRP1 reduce DRP1 activity compared to just DRP1. But interestingly when all three are together, they exhibit similar activity to MiD51 + DRP1, with the addition of MFF having no effect. This demonstrates that MFF and MiD51 function to alter DRP1 activity, and when together, MiD51 can supress MFF (Osellame *et al*., 2016). This supports the concept that DRP1 receptors can work cooperatively to impact the function of DRP1, and highlights the potential importance of MFF SUMOylation to remove inhibitory MiD binding from pre-fission complexes to allow fission to proceed. Figure 4.5D indicates an increase in MiD51 binding to K151R, which fits with the model of increasing SUMOylation promoting fission. Future experients will confirm the interaction between MFF SUMO/phosphorylation mutants and MiD51, and how MiD51 will fit into the model in Figure 4.9.

MFF SUMOyaltion and stress

I observe during 1hr OGD that SENP3 levels decrease and SUMO-2/3 conjugation increases, agreeing with previous findings (Guo *et al*., 2013). I also detect an increase in SUMO-1 conjugation to MFF after 2hrs of OGD, indicating that an increase in SUMOylation is related to bioenergetic stress. Unfortunately, I do not have an accompanying blot showing AMPK activation increase under OGD, although AMPK activation after 2hrs OGD is well characterised (Mungai *et al*., 2011; Rousset *et al*., 2015). OGD induces severe mitochondrial dysfunction, exhibited by a reduction in complex I activity, ATP levels are depleted, $\Delta\psi m$ is reduced, oxidative stress is increased, followed by cell death (Almeida *et al*., 2002). Following 1hr of OGD, Wappler *et al* observe large and more swollen mitochondria, but with no change in the levels of Mfn1/2, OPA1, DRP1 or Fis1, but following 3hrs OGD, DRP1 and Mfn2 protein levels decreased whereas Mfn1 levels increased and the cristae folds were unstructured (Wappler *et al*., 2013). 90 minutes of OGD induces similar mitochondrial dysfunction in primary neurons, with mitochondria appearing more punctate. Furthermore, OPA1 processing was observed to favour smaller isoforms, indicative of inhibited fusion (Baburamani *et al*., 2015). These findings indicate that OGD has profound impacts on mitochondrial dynamics, and that increasing the duration of insult increases the detrimental effect.

Further work is required to dissect the role of MFF SUMOylation in OGD. It would be interesting to carry out OGD over a time course and analyse in parallel experiments the changes of SUMO conjugation (especially of SUMO-2/3), AMPK

activation and AMPK phosphorylation of MFF at S155, DRP1/MiD binding and mitochondrial morphology. Additionally, it would be interesting to test how MFF SUMOylation responds to reperfusion stress, since DRP1 deSUMOylation by SENP3 upon reperfusion was shown to promote fragmentation (Guo *et al*., 2013). Further work is required to reconcile the SUMOylation states of DRP1 and MFF under different stress conditions.

OGD is not the only mitochondrial stress I attempted to use to investigate MFF SUMOylation. Previous reports demonstrate a significant increase in MFF phosphorylation upon 1hr treatment with ETC inhibitors and AMPK activators (Ducommun *et al*., 2015; Toyama *et al*., 2016), and so AMPK phosphorylation-induced MFF SUMOylation would be predicted to be a stress response as well. In my hands, I could not detect an increase in SUMOylation of MFF with rotenone or CCCP at a treatment time of 1hr. The fact that I can detect an increase following 2hrs OGD may reflect different responses to stress. Moreover, I did not observe an increase in S155 phosphorylation, and in fact detected high basal MFF phosphorylation (Figure 3.8). This could be due to several possibilities; I used MFF isoform 1, whereas these reports used either mouse isoform 4 (Ducommun *et al*., 2015), or human MFF isoform 5. Additionally, I used HEK293T cells, whereas the Ducommum *et al*. report used primary mouse hepatocytes, and Toyama *et al*. used MEF cells. The HEK293T cells used here may have reduced sensitivity to stress or high basal AMPK activation, whereas the primary hepatocytes and MEF cells may be more sensitive to stress. Indeed, differences between primary cells and cell lines have been noted (Alge *et al*., 2006; Pan *et*

al., 2009). Alternatively, this could also reflect differences in the phosphorylation capacity of the different MFF isoforms. Finally, a 1hr time treatment with mitochondrial poisons such as rotenone or CCCP may be too long to observe SUMOylation. Whereas phosphorylation may persist, SUMOylation is very labile, and may occur very suddenly, carry out its function, then be deSUMOylated. It will be interesting to use shorter time treatments to try to "capture" the increased SUMO species following mitochondrial inhibition. To overcome the potential insensitivity of cell lines, future experiments will be performed using primary cells or growing cell lines in galactose instead of glucose, to shift the cells' metabolism to depend more on OXPHOS instead of glycolysis, making mitochondria more active and potentially more susceptible to mitochondrial poisons.

I have preliminary data suggesting that MFF SUMOylation is required under ETC inhibition to promote DRP1 binding (Figure 4.8). The further reduction of DRP1 to K151R under stress conditions and AMPK activation indicates that MFF SUMOylation promotes DRP1 binding, and therefore mitochondrial fission. I believe this notion agrees with my model illustrated in Figure 4.9, and offers a future line of investigation of investigating the role of MFF SUMOylation under increased AMPK activation and fission states. It would be insightful to replicate this experiment and assess MiD49 binding under stress conditions to test if SUMOylation is required for the displacement of these inhibitory proteins under mitochondrial stress conditions.

I cannot definitively rule out the possibility that it is phosphorylation, rather than SUMOylation, of MFF that is eliciting the differences in MiD binding presented in

Figure 4.5. Nonetheless, I observe an increase in MiD binding to K151R, which is still phosphorylated (Figure 3.8), implying that it is SUMOylation, and not phopshorylation, eliciting the effect. To unequivically distinguish the roles of SUMO and phosphorylation, a SUMOylation-deficient mutant could be generated in the 2SD and 2SA construct i.e. K151R/2SA and K151R/2SD, and the same experiments carried out to establish if the effects are additive, or independent of one another.

Summary

In summary, SUMOylation of MFF does not correlate directly with increased DRP1 binding, and is inversely correlated with MiD49 binding. My data contradicts the hypothesis of Toyama *et al.* that phosphorylating MFF increases DRP1 binding, and I have developed a working model of SUMOylation modulating pre-fission complex ratios of MiD49/DRP1, and that phosphorylation induced SUMOylation in fact reduces MiD binding and promotes a more direct binding of MFF to DRP1. I also have preliminary data showing that SUMO conjugation to MFF increases under stress, and that this is required for DRP1 binding under mitochondrial stress conditions.

Chapter 5 Exploring the role of MFF SUMOylation in Mitochondrial Morphology

5.1 Introduction

The mitochondrial network is highly responsive to the metabolic state of the cell and dynamically reacts to a wide range of chemical, metabolic, environemntal, infectious and genetic stressors. Understanding how the mitochondrial network responds to challenge, and the pathways that orchestrate them, will further our understanding of these dynamic organelles, and shed light on the transition from physiological to pathological mitochondrial behaviour (Eisner *et al*., 2018). Defining how the morphology of the mitochondrial network changes is a key research goal, but attempts to define mitochondrial morphology often fall short of capturing the true nature of the mitochondrial network. A common approach is to use fluorescence confocal microscopy of fixed cells, providing a “snap shot” of the mitochondria, and then scoring the morphology into groups, such as long, short, tubular, circular, collapsed, net-like etc. However, arbitary and subjective descriptions fequently fail to reflect the nature of the mitochondria, they are open to interpretation, and there is little consistency in the literature on what constitutes the different morphological groups. Furthermore, a single cell will exhibit many different types of mitochondrial morphology at any given time, so how does one decide? Some investigations employ a morphometric analyse approach, for example Loson *et al*. used mitochondrial length/interconnectivity, by measuring the number of discrete mitochondria and dividing by total mitochondrial area (Loson *et al*., 2013). Although perhaps better than the subjective scoring approach, is this a valid method to determine length/connectivity, and how useful is such a description? The analysis was only carried out in the periphery of the

MEF cell, where the mitochondria can be easily discerned, therefore introduces a level of subjectivity and may disregard other information.

More recently, automated methods have been developed to rapidly generate high-throughput categorisation from wide-field images of morphology, motion and membrane potential (Leonard *et al*., 2015; Zahedi *et al*., 2018). This approach removes observer bias and generates complex data sets from a vast number of cells that can be scaled to large pharmacological/toxicological evaluation. However, it still categorises cells based on morphology descriptions (rod, puncta, network, large/round, swollen), and thus its ability to identify subtle changes in mitochondrial morphology and the application to confocal or high-resolution imaging in smaller scale experiments is questionable. Other reports have quantified the mitochondrial network, such as number and length of individual branches, thus in principal describing the mitochondrial network changes in numerical terms (Peng *et al*., 2011; Song *et al*., 2008; Sukhorukov *et al*., 2012).

Given these caveats, to analyse the effect of MFF SUMOylation on mitochondrial morphology, I decided to use a more objective method which aimed to more fully represent the true nature of the mitochondrial structure. A recent report by Valente and colleagues developed a simple method to be used on confocal images and ImageJ software to analyse the mitochondrial network (Valente *et al*., 2017). I adapted the Valente approach (see material and methods section 2.9.3) to better represent my raw images of the mitochondrial network and carried out my own analysis of the network on wildtype and MFF-null MEF cells.

Due to the exceptional size and complexity of neuronal architecture, coupled with the high energy requirement of these cells, the mitochondria face an extreme challenge in meeting the neurons bioenergetic demand. Neuronal morphology requires long distance trafficking of healthy and functional mitochondria to distal dendrites and axon terminals, reviewed in Misgeld and Schwarz, 2017. Intriguingly, mitochondria in axons and dendrites exhibit different sizes; in general, mitochondria in axons are small and punctate with a sparse distribution, whereas in dendrites they are longer, more tubular and occupy more of the dendritic length (Chang *et al*., 2006; Lewis *et al*., 2018). However, the significance and regulation of this difference is not well understood. The rates of fusion and fission events in axons are regulated to maintain the mitochondria at an optimal size; longer mitochondria are more likely to undergo a fission event, whereas short mitochondria are more likely to undergo fusion, thus avoiding extremes of mitochondrial length in the axon (Cagalinec *et al*., 2013).

The significance and mechanism of the differential mitochondrial size in neuronal compartments is unclear. However, recent work has reported that MFF is responsible for maintaining axonal mitochondrial size (Lewis *et al*., 2018). MFF-knockdown increases the size of axonal mitochondria, which increase mitochondrial Ca^{2+} buffering capacity, leading to decreased neurotransmitter release and axonal branching (Lewis *et al*., 2018). Surprisingly, given the wide cellular distribution of MFF, Lewis *et al* report no effect on the dendritic mitochondria upon MFF knockdown. These data raise the question of what is the

mechanism of regulating mitochondrial size in axons vs dendrites, and is there compartment-specific regulation of MFF?

5.2 Aims

Fusion and fission maintain mitochondrial size in neurons, and my biochemical findings suggest SUMOylated MFF promotes fission. To explore this further, I developed a simple ImageJ macro, based on a previous methodology (Valente *et al*., 2017), to objectively quantify the mitochondrial morphology of mouse embryonic fibroblasts (MEF) deficient in MFF (previously described in Loson *et al*., 2013), as a background to characterise wildtype MEF vs MFF-null MEFs. I also wished to investigate the role of MFF SUMOylation in neuronal mitochondrial morphology. My specific aims were to:

- Quantify DRP1 co-localisation with mitochondria in WT vs MFF-null MEF cells.
- Objectively quantify the mitochondrial morphology in MEF WT vs MFF-null using the new ImageJ macro.
- Determine the effects of the SUMOylation-deficient mutant K151R on mitochondrial morphology and DRP1 recruitment by generating wildtype and K151R rescue MEF cells and reassess mitochondrial morphology and DRP1 recruitment.
- Using transient transfection, investigate the effects of WT and K151R MFF on mitochondrial morphology in the axons and dendrites of primary hippocampal neurons.

5.3 Results

5.3.1 MFF recruits/stabilises DRP1 at mitochondria

Using MEF cells null for all isoforms of MFF (a kind gift from D. Chan, see Figure 5.1C), I assessed DRP1 recruitment to the mitochondria using mitotracker and fixed staining for endogenous DRP1. In WT MEF cells, DRP1 is predominantly cytosolic, with a small proportion of large, bright puncta colocalising with the mitochondria. In the absence of MFF, DRP1 recruitment is significantly impaired, and the remaining DRP1-mitochondrial puncta are fewer in number, and display reduced size and intensity (Figure 5.1A), agreeing with previous observations (Loson *et al*., 2013; Otera *et al*., 2010). I quantified the co-localisation of DRP1 with mitotracker using the Manders co-efficient. The MFF-null MEF cells exhibit ~50% reduction in co-localisation (Figure 5.1B).

The MFF-null MEFs also exhibit a much more elongated, tubular network, compared to wildtype cells, where the mitochondria exist as shorter, more fragmented structures, as previously reported (Loson *et al*., 2013; Otera *et al*., 2010). I then proceeded to objectively analyse the network using the parameters described in the methods section.

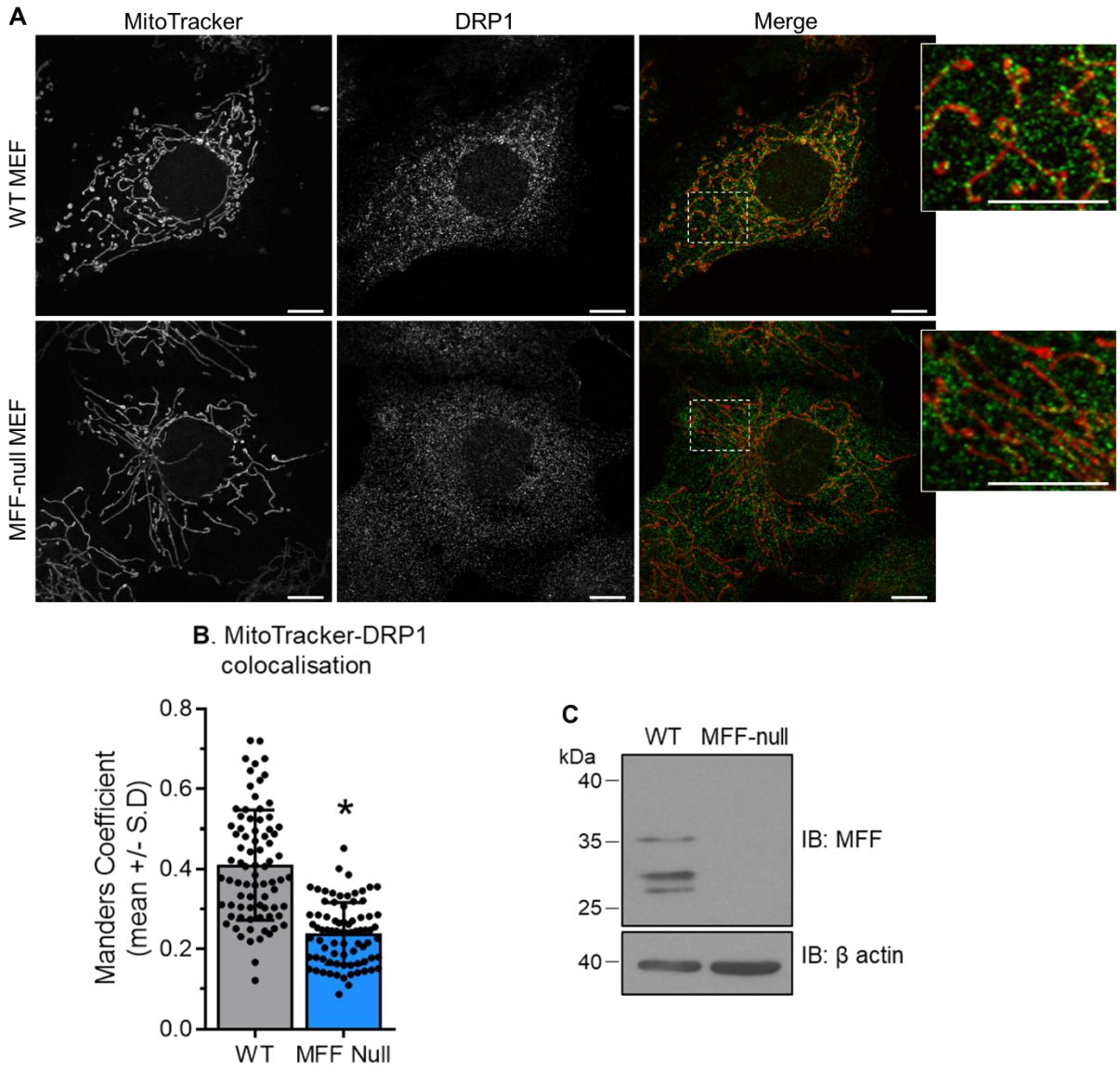

Figure 5.1 MFF is required for DRP1-mitochondrial recruitment

A MEF cells were incubated with far red mitotracker for 30 minutes before fixation and stained for endogenous DRP1. Insets are enlargements of highlighted areas. 10µm scale bar. **B** Manders co-efficient of DRP1-mitotracker co-localisation. Unpaired t-test used to determine significance, p*<0.0001. Data expressed as the Manders co-efficent ±S.D and generated from three independent experiments (n=79 cells WT, n=80 cells MFF-null). **C** MFF blot of total lysate, showing MEF MFF-null cells are complete knock-outs for all MFF isofoms.

5.3.2 MFF is required to maintain mitochondrial morphology

I analysed the mitochondrial morphology of WT vs MFF-null cells using the macro I developed (see 2.9.3 for details). Figure 5.2 shows that the average branch number is doubled in the absence of MFF with ~20 branches, compared with WT cells which have approximately 10 branches. The length of the mitochondria also increased in MFF-null cells to ~1.8µm, whereas in WT cells the average mitochondria length is ~1.4µm. Considering the extremes of these parameters, the largest structures identified in MFF-null cells was ~160 branches and 17µm in length, compared to ~60 branches for WT and 11µm. As expected, I detected a significant decrease of ~38% in the free-end index in the absence of MFF, demonstrating greater connectivity of the mitochondrial network. Moreover, the weighted circularity index is significantly reduced by approximately 41%, indicating more elaborate and less uniform structures.

Lenti-viral expression of wildtype CFP-MFF in the MFF-null cells restored the DRP1 recruitment, confirming that the impaired DRP1 recruitment phenotype is due to loss of MFF. The CFP-MFF was localised across the mitochondria, and was also observed as bright puncta, which often co-localised with DRP1 puncta, agreeing with previous findings (Otera *et al*., 2010). This was accompanied by a restoration of the mitochondrial morphology (insufficient data for analysis). Furthermore, this shows that the CFP-MFF isoform 1 is functional and sufficient to recruit DRP1. Taken together, these data show that MFF plays a major role in regulating the recruitment/stabilisation of DRP1, and consequent regulation of mitochondrial morphology. MFF is required to maintain the length and number of

branches, and mitochondria become more connected and elaborate in overall shape in the absence of MFF.

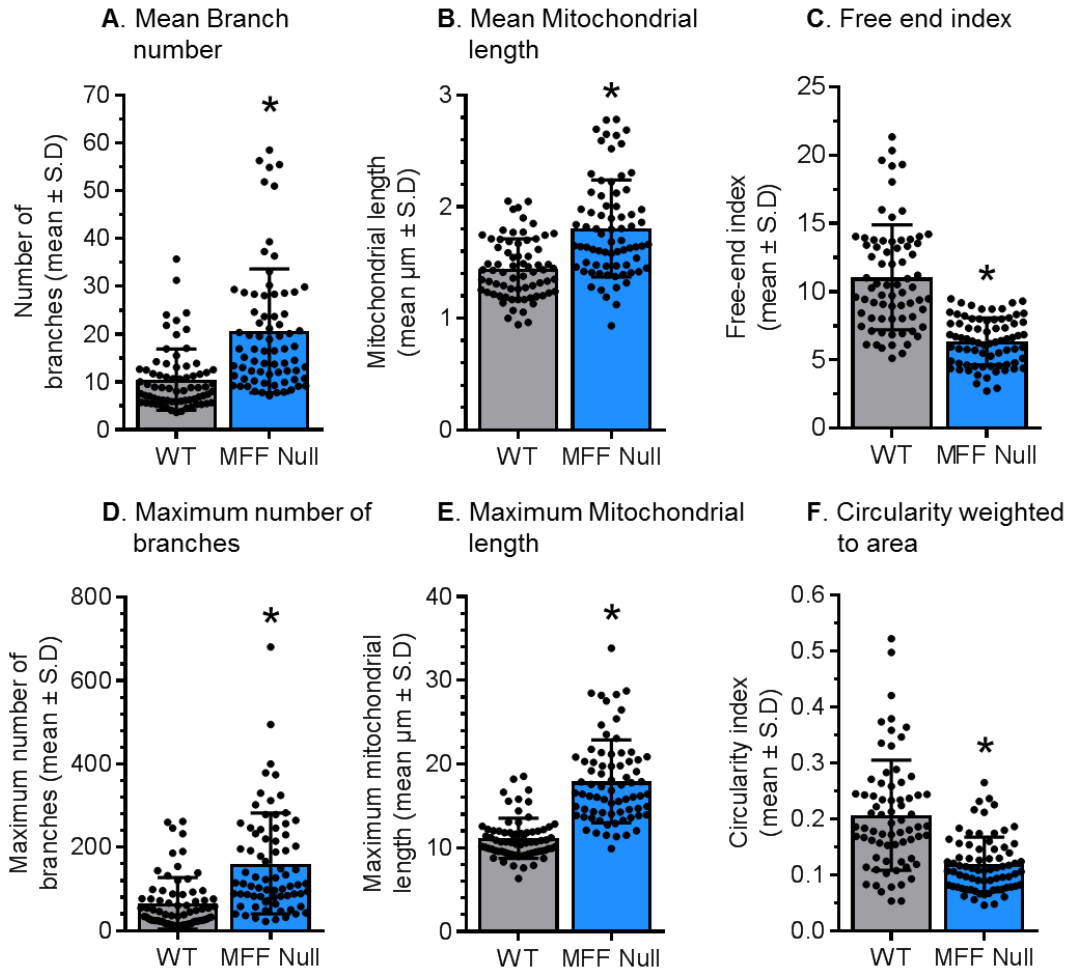

Figure 5.2 MFF is required to maintain mitochondrial morphology

The following morphological parameters were used to assess mitochondrial morphology of wildtype vs MFF-null MEFs: **A** Mean number of branches per network. **B** Mean mitochondrial length. **C** Free end index . **D** Maximum number of branches. **E** Maximum mitochondria length. **A, C-F**: Mann-Whitney non-parametric test (data not normally distributed. n=71 cells WT, n=74 cells MFF-null). **B**: Students unpaired t-test (n=79 cells WT, n=79 cells MFF-null). Data gathered from three independent experiments and expressed as mean values ±S.D. p*<0.0001.

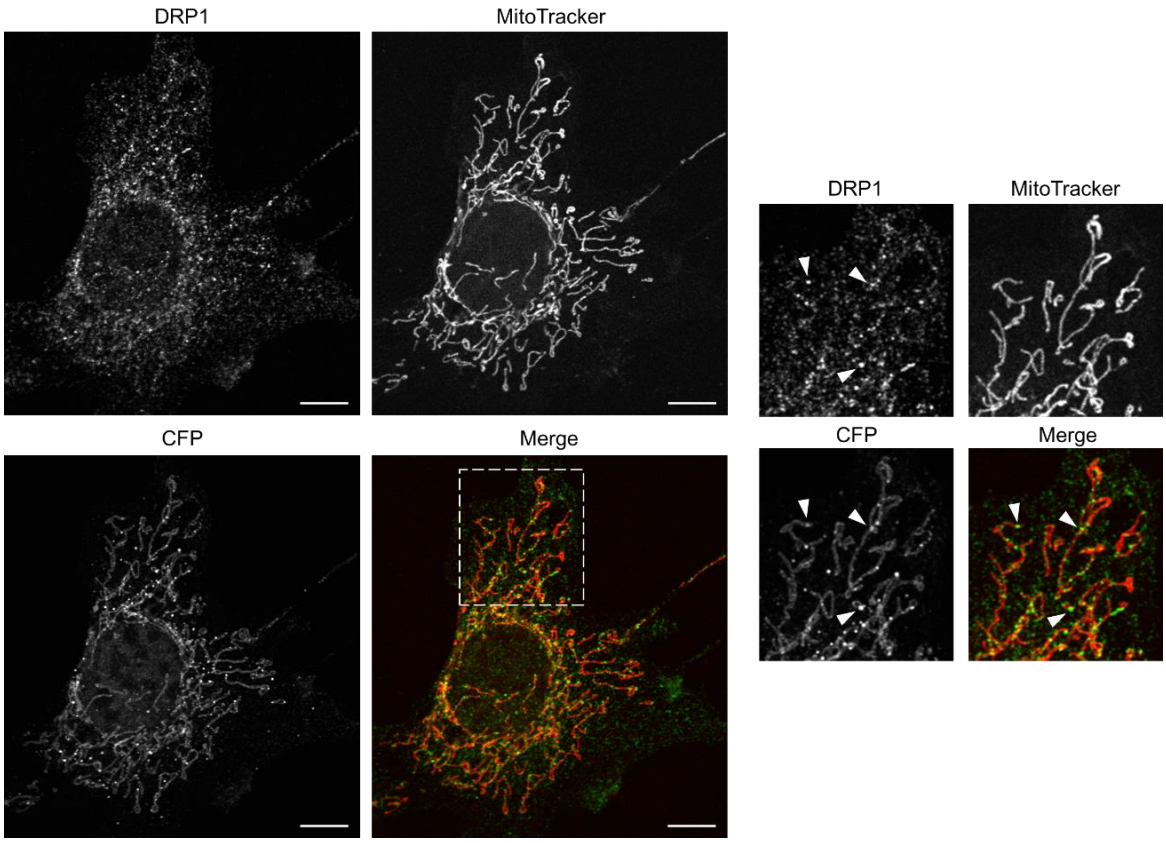

Figure 5.3 CFP-MFF isoform 1 rescues MFF deficient MEFs

MFF-null MEFs were infected with CFP-MFF isoform 1 using lenti virus. Cells were treated with mitotracker far red for 30 minutes, fixed and stained for endogenous DRP1 and GFP. Right panels show zoom of highlighted area, arrows indicate sites of CFP-MFF and DRP1 puncta co-localisation. Scale bar 10µm.

I believe the macro I have developed here is a more robust, objective and improved representation of the mitochondrial network. Unfortunately, due to time constraints, insufficient data was gathered for the rescue experiments of WT vs K151R MFF, but the preliminary data in Figure 5.3 is promising and demonstrates that the CFP-MFF construct is functional. In future experiments, this type of analysis can be carried out on MFF-null cells expressing wildtype or K151R, the

consideration being similar expression levels between WT and K151R, at approximately endogenous MFF levels.

5.3.3 MFF SUMOylation is required to maintain mitochondrial size and distribution in dendrites

Mitochondrial size differs between the axon and dendrites; axonal mitochondria are more punctate and sparsely distributed, whereas dendritic mitochondria can be extremely long in length and occupy a greater percentage of the dendrite (Chang *et al*., 2006; Lewis *et al*., 2018). Using the tubeness and thresholding method described in materials and methods, I carried out my own analysis of the mitochondria in primary hippocampal neurons by transfection of neurons with the mitochondrial-targeted fluorescent protein Mito DS-Red and staining for the axon with ankyrin-G (Figure 5.4A). In the axons I observe round, sparse mitochondria of on average ~1μm^2 in area and approximately 1 mitochondrion every 5μm. In the dendrites the mitochondria are much longer, reaching an average area of ~2.6 μm^2, but with a comparable density along the dendrite (Figure 5.4D, E). My analysis of the mitochondria are in close agreement with previous findings (Chang *et al*., 2006).

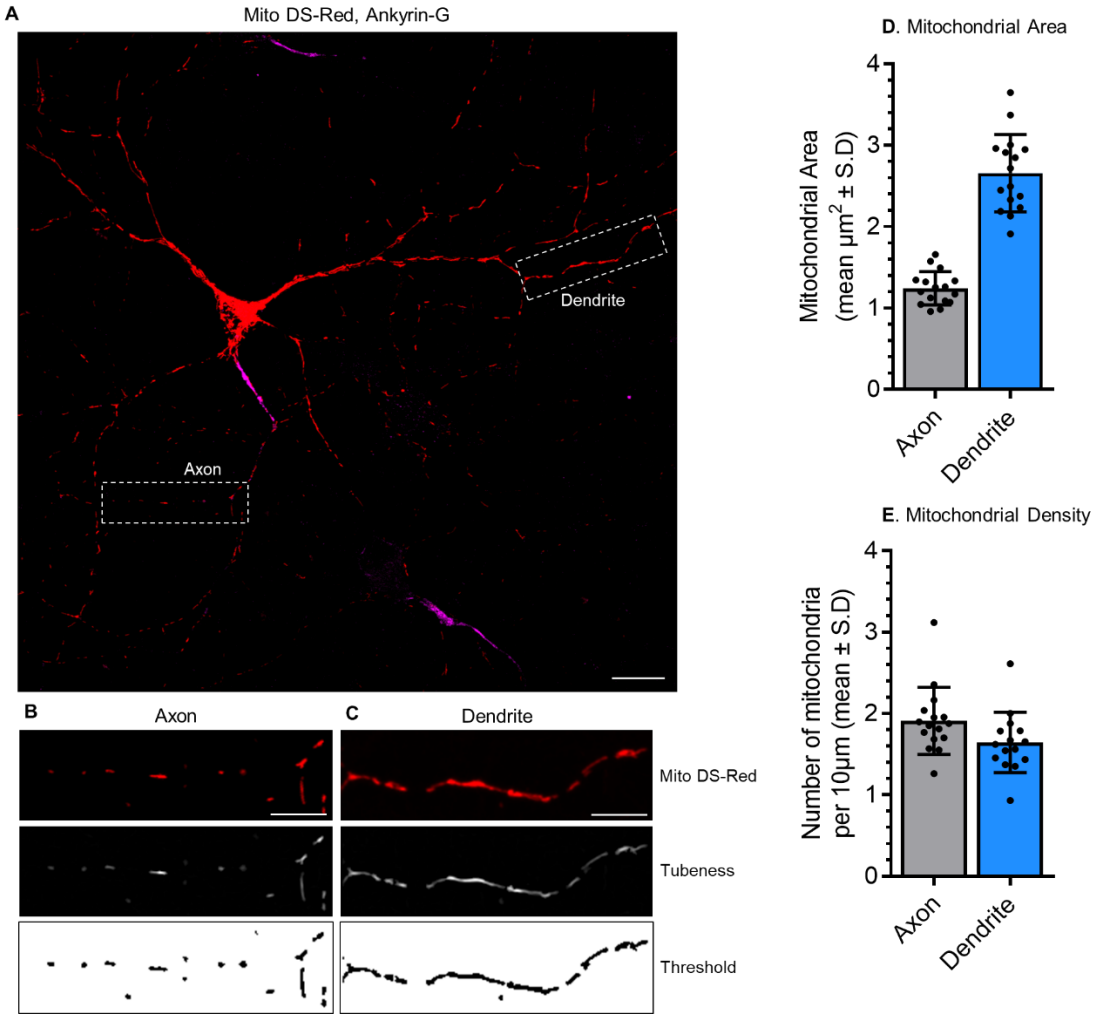

Figure 5.4 Differential mitochondrial size in axons and dendrites of primary hippocampal neurons

A Representative confocal image of a DIV 14 primary hippocampal neuron transfected with Mito DS-Red (red) and stained for the axonal initial segment with ankyrin-G (magenta). Scale bar 20µm. Expanded fields of the highlighted axon (**B**) and dendrite (**C**) show the raw image, processed image following tubeness analysis and threshold image. Scale bar 10µm. Mitochondrial area (**D**) and density (**E**) of axon and dendrites show mean values +/- S.D. Data gathered from 16 neurons from two independent cultures. Average number of approximately 64 axonal mitochondria and 350µm per cell, averge approximately 70 dendritic mitochondria along ~470µm per cell.

To test whether SUMOylation influences mitochondrial morphology in neurons, I transiently transfected primary hippocampal neurons with the CFP-MFF WT or K151R mutant along with Mito DS-Red. Both CFP-MFF constructs localise to mitochondria in both axons and dendrites (Figure 5.5A, B). Enlargements in the right-hand panels show GFP, mito DS-Red and merge. I analysed the area and density of mitochondria and observed a significant increase in dendritic mitochondrial size between wildtype and K151R MFF expressing cells, approximately 3.25µm^2 to 4µm^2, respectively. In WT expressing cells the dendritic mitochondrial density is 1.31 mitochondria/10µm, whereas it is significantly reduced to 1.17 mitochondria/10µm in the SUMO mutant expressing cells, a percentage decrease of approximately 12%. Axonal mitochondrial area and density are comparable between WT and K151R (Figure 5.5E, F).

Figure 5.5. Figure legend overleaf

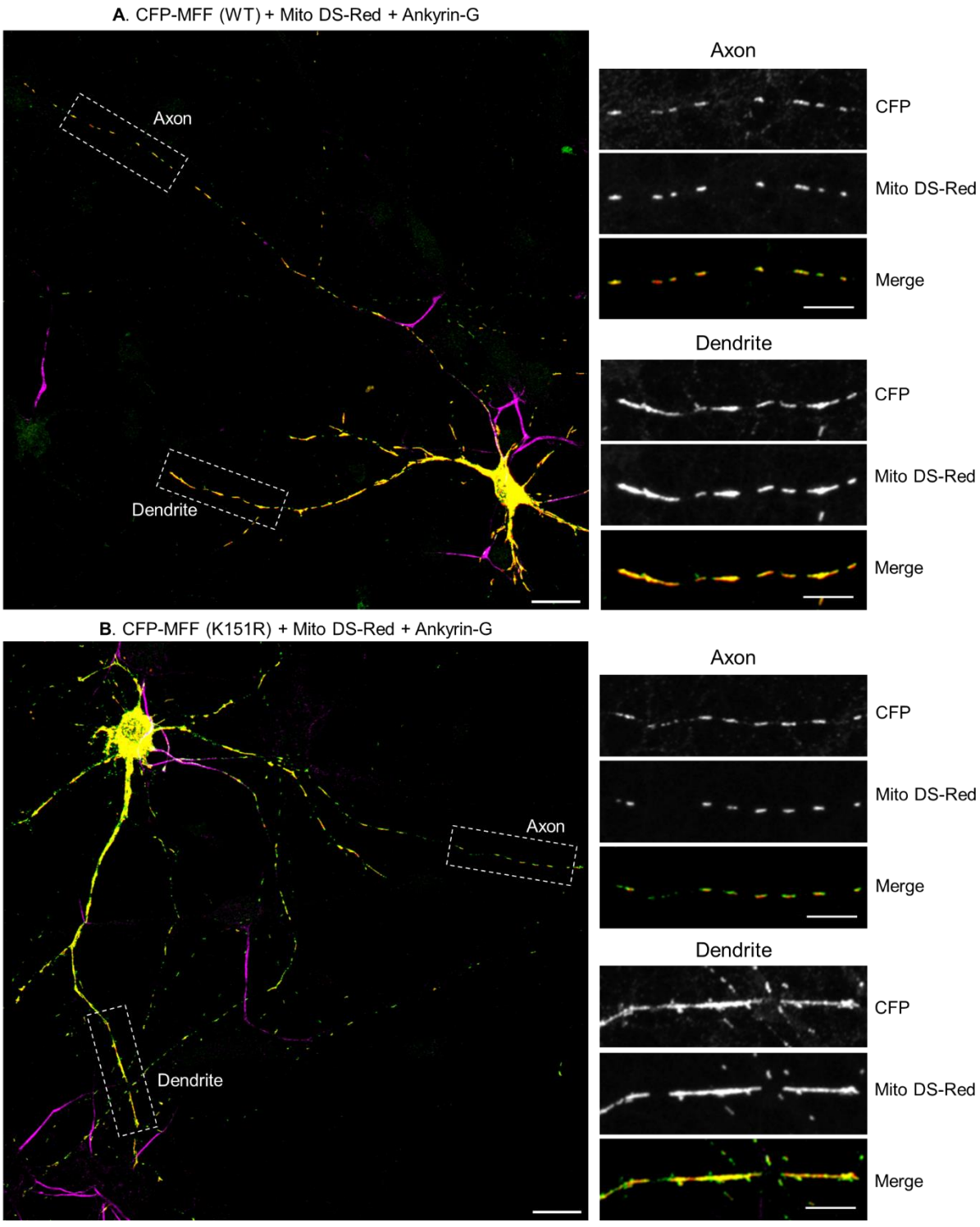

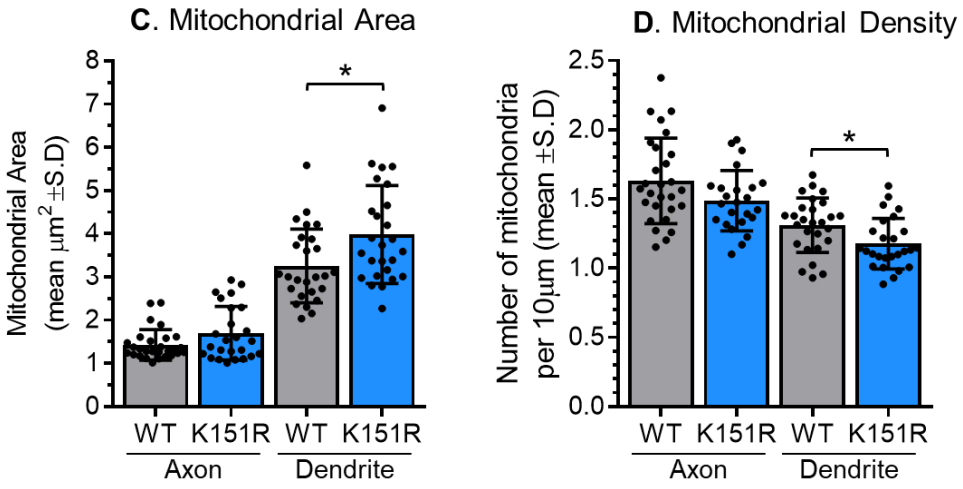

Figure 5.5 MFF SUMOylation is required to maintain dendritic mitochondrial size and distribution

DIV 14 hippocampal neurons were co-transfected for two days with **A** 1µg CFP-MFF wildtype or **B** K151R, and 1µg Mito DS-Red. Following fixation, neurons were stained for ankyrin-G (magenta) and GFP (green) to enahnce CFP signal. Scale bar 20µm. Enlargements show axonal and dendritic sections, scale bar 10µm. Mitochondrial area (**C**) and mitochondrial density (**D**) analysed for axons and dendrites. Data gathered from four independent cultures, 6-8 cells analysed per condition, per experiment (n=26 WT, n=26 K151R. Average for axons per cell: 61 mitochondria, 400µm. Average for dendrites per cell: 85 mitochondria, 680µm. p*<0.05).

5.4 Discussion

In this chapter I present an improved method to quantitatively analyse mitochondrial morphology, based on more useful parameters and less subjective descriptions. Although, due to time constraints, insufficient data was gathered for rescue experiments to assess mitochondrial morphology upon expression of the non-SUMOylatable K151R MFF mutant under basal and stressed conditions, preliminary observations of CFP-MFF wildtype indicate that this construct can rescue the MFF-null mitochondrial phenotype. Furthermore, I analysed the mitochondrial size in axons and dendrites in primary hippocampal neurons, and investigated the effect of SUMO-deficient MFF on mitochondrial morphology in neurons. My key findings for the analysis of MFF-deficient MEF cells and neuron mitochondrial analysis are:

Key findings

- MFF promotes recruitment/stabilty of DRP1 to mitochondria
- MFF decreases mitochondrial length and branch number
- MFF increases the numebr of free ends and increases circularity
- Axonal mitochondria are shorter and more sparsely distributed, whereas dendritic mitochondria are longer and occupy a greater volume of the neurite
- MFF-SUMO mutant K151R increases the size and decreases the density of dendritic mitochondria, with no effect on axonal mitochondria

MFF promotes DRP1 recruitment/stability of DRP1 at mitochondria

My findings of reduced DRP1 colocalisation with mitochondria in the absence of MFF agree with many previous observations (Gandre-Babbe and van der Bliek, 2008; Loson *et al*., 2013; Otera *et al*., 2010). However, is this decrease in colocalisation a recruitment deficiency, or a result of reduced DRP1 stabilty at mitochondria? Is MFF required for one, or both? Could the loss of MFF decrease the half-life of DRP1 at the MOM, therefore reduce its stability, with no impact on DRP1 binding to MOM? Conversley, is MFF responsible for the initial recruitment of DRP1 to the MOM, and loss of MFF thus reduces DRP1 associating with the MOM in the first place? All four of the DRP1 receptors play a role in DRP1 recruitment and mitochondrial morphology, although to different extents (Loson *et al*., 2013; Osellame *et al*., 2016), and when MFF is dislocalised to the plasma membrane, DRP1 colocalises at the plasma membrane, indicating that MFF alone is sufficient to recruit DRP1 (Otera *et al*., 2010). I observe smaller and dimmer mitochondrial DRP1 puncta in MFF-null cells, as previously reported (Loson *et al*., 2013), suggesting that MFF helps to promote the stability of DRP1. Taken together, is seems that MFF can both promote DRP1 recruitment and increase the size and intensity of DRP1 puncta, although further experiments such as FRAP and live cell imaging to assess the cycling behaviour and half-life of DRP1 at the MOM in MFF ablated cells will be required to conclusively establish this.

MFF and mitochondrial morphology

Mitochondrial morphology is inextricably linked to mitochondrial function, appropriate responses to metabolic demand and cellular health. The importance of mitochondrial dynamics is underscored by mutations in proteins responsible for fusion, fission and mitophagy resulting in disease (Eisner *et al*., 2018). To fully assess the intricate, and sometimes subtle changes that occur under different stress states, robust methods are required to faithfully represent the nature of mitochondrial morphology, without introducing observer bias or subjectivity. In this chapter I analysed mitochondrial morphology of WT and MFF-null MEFs. The effect of MFF on mitochondrial morphology is well characterised, therefore this offered an opportunity to develop an imaging method and see how it correlates with previous observations. Depletion of MFF has been stated to cause “formation of closed mitochondrial networks” and the network “had fewer free ends” (Otera *et al*., 2010) or “mitochondria in MFF-null cell lines are severly elongated and interconnected” and “have long or net-like mitochondria relative to wildtype” (Loson *et al*., 2013). Indeed, this is what I also observe, but as previously mentioned, such decriptions are subjective and therefore their validiity is open to question. Using a macro of ImageJ plug-ins, I assessed six parameters of mitochondrial morphology. As discussed in the methods section, there are various steps involved in the pre-processing to generate a sharp image. I was satisfied that the skeleton faithfully represented the mitochondrial morphology, and was effective at separating objects and connecting structures, especially in larger structures.

MFF reduces the number of branches within networks by ~50% and there is almost a 30% increase in the length of mitochondria. Lack of MFF also generates more extreme lengths and branched structures; 17µm and ~160 branches compared to 11µm and ~60 branches in wildtype cells. Finally, the number of free ends is reduced by approximately 38% and the circularity is also reduced by ~41%. With such quantitative detail, one can build a picture of what the “average” mitochondria in the MFF-null and wildtype cells look like i.e. how many branches the networks have, how long the mitochondria are, the number of free ends etc… Based on these findings, it is clear that MFF promotes fission and suppresses extreme fusion, which when unopposed results in extreme lengths of mitochondria. In addition, the increased branch number and reduced free end index (greater connectivity) implies that MFF has roles in regulating mitochondrial architecture as well. Unopposed fusion also leads to branching of networks, resulting in more elaborate and less uniform structures, and so MFF prevents such excessive branched structures.

Rescue experiments

As mentioned in section 5.3.2, I tried rescue experiments in the MFF-null MEF background with CFP-MFF WT and K151R constructs. Unfortunately, due to time constraints I could not fully characterise these cells. However, preliminary experiments were promising, demonstrating that the CFP-WT MFF expressing cells did increase DRP1 recruitment to the mitochondria, and exhibited a reduced mitohondrial elongation phenotype. For future experiments, generating a stable cell line of MFF wildtype and SUMOylation-deficient mutant in the MFF-null MEF

cells will be a very useful tool for dissecting how MFF-SUMOylation affects mitochondrial morphology. Such experients can be carried out under basal and stressed conditions, and if carried out in conjunction with biochemical analysis of DRP1 and MiD interaction, as discussed in Chapter 4, will provide a coherent and systematic analysis of the role of SUMOylation of MFF under basal and stress conditions. It is worth noting that since MFF is a pro-fission protein, overexpression or under-expression compared to endogenous levels will alter the mitochondrial morphology. Therefore, care should be taken to ensure even expression of wildtype and K151R MFF, which is often difficult to achieve with transfection, so the use of viral titrations should be used for the generation of a stable cell line.

Axonal versus dendritic regulation of mitochondria

Knockdown of MFF leads to unopposed fusion events in the axon, resulting in a dramatic increase in mitochondrial length and occupancy along the axon (Lewis *et al*., 2018). What is surprising from this report is that MFF is present in both axons and dendrites, so could this be a result of compartment-specific regulation of MFF? Is MFF more active in axons, and in dendrites less active, or dispensible? I observe that K151R expression increases dendritic mitochondrial size and reduces density, with no effect on the mitochondria in axons. An increase in mitochondrial size agrees with my biochemical data, since K151R has reduced binding to DRP1 and enhanced MiD binding, which will inhibit DRP1 function and compete with MFF for DRP1 binding, leading to enlarged mitochondria. However, this does not explain why K151R expression only affects dendritic mitochondria.

The Lewis *et al* report identified that MFF is important for axons and not dendrites, whereas my data show that MFF SUMOylation is imortant for dendrites and not axons. In close agreement with my findings, Toyama *et al*. observe fragmented mitochondria upon phospho-mimetic MFF expression in the dendrites, whereas the phospho-null MFF had no effect (Toyama *et al*., 2016). They did not report any findings regarding the axons. I carried out preliminary experiments and observe a similar trend in the dendrites, and no effect on the axons (See appendix Figure 8.3). K151R trafficked to both compartments, so this is not due to differential MFF-SUMO localisation. Taken together, this shows that complete depletion of MFF only affects axons, whereas PTM of MFF by SUMO or phosphorylation primarily affects dendrites. I hypothesise that this could be a result of three, not necessarily exclusive, factors: firstly, MFF SUMOylation has different roles or is differentially regulated in the two compartments, secondly, MFF SUMOylation is dispensable for axonal mitochondria, thirdly, axons have a greater capacity for self-correcting mitochondrial size.

Elegant experiments by Cagalinec *et al*. demonstrate the cyclic nature of fusion and fission events in primary cortical neuronal axons, where ~85% of fusion events are followed by fission, and *vice versa.* Therefore matching the rates of fusion and fission prevent extremes of axonal mitochondrial size (Cagalinec *et al*., 2013). The authors identify a “self-correcting” mechanism to regulate mitochondrial size, which involves fusion followed by fusion if mitochondria are too small, whereas if mitochondria are too large, fission would be followed by a subsequent fission event, with the rate of fission exponentially increasing with

mitochondrial length (Cagalinec *et al*., 2013). This self-correcting mechanism will maintain a homogenous population of mitochondria in the axon. This mechanism can perhaps offer an explanation as to why I do not detect any change in axonal mitochondria upon expressing MFF. The fusion rate could be reduced to match the fission rate of K151R expression. Whether a similar rate-matching mechanism occurs in dendrites to maintain mitochondrial size is unknown. Indeed, upon DRP1 depletion by siRNA, the fusion/fission rate was not altered (Cagalinec *et al*., 2013), but reduced the sensitivity of large mitochondria to undergo non-cyclic fission. Could the greatly impaired fission upon DRP1 and MFF depletion in axons be such a drastic decrease in fission efficiency that the cells cannot correct for it? Indeed, would inhibiting fusion to such an extent be even more detrimental to the cell? The K151R MFF mutant can still bind to ~50% DRP1 compared to wildtype, and so is unlikely to be as drastic as complete loss of MFF, and so in axons, the self-correcting mechanism may compensate. Carrying out live cell imaging experiments in the axons and dendrites will provide evidence of the effects on fusion and fission rates with WT vs K151R MFF expressing neurons.

Chang *et al*. demonstrate that modulating neuronal activity has profound effects on mitochondrial morphology. Interestingly, axonal and dendritic mitochondria respond in opposite directions; following 24hr TTX treatment (a blocker of voltage-gated sodium channels) mitochondria in axons had reduced occupancy, whereas dendritic mitochondria had increased occupancy, accompanied with increased length (Chang *et al*., 2006). What this study demonstrates is that different mechanisms regulate mitochondrial size between the axons and dendrites. Such

differences may explain why the Lewis *et al*. report, and my own findings, observe differences in axons vs dendrites upon modulation of MFF, highlighting the possibility that MFF is differentially regulated in the different compartments. My finding that SUMOylation of MFF is important in the dendrites and not the axons offers the possibility that PTM of the mitochondrial fission machinery is regulated differently in the different neurite types. It would be interesting to test the modulation of synaptic activity on MFF SUMOylation and see if MFF-SUMO conjugation is altered, and how this corresponds to the changes observed by Chang *et al*.

K151R reduces dendritic mitochondrial density

I also observe a small but significant decrease in the density of mitochondria along the dendritic processes, but no effect was detected in axons (Figure 5.5F) Is this difference due to altered trafficking or docking? Without live cell imaging I cannot state one or the other, but differences in the axon and dendrite can provide some indication. The Miro-Milton complex is responsible for mitochondrial trafficking, and is sensitive to Ca^{2+} concentrations, where high concentrations cause complex rearrangement which inhibit movement (Schwarz, 2013; Sheng and Cai, 2012). Once paused, proteins such as syntaphilin in the axon can anchor mitochondria to microtubules, however, syntaphilin is absent in the dendrites (Kang *et al*., 2008). So, could the axonal mitochondria be more resistant to changes in movement due to increased anchoring of syntaphilin, whereas dendritic mitochondria are more sensitive and more easily trafficked? In addition, positioning of mitochondria is important for the development of dendritic spines

following stimulation, and promoting fission enhances spine formation (Fukumitsu *et al*., 2015; Li *et al*., 2004). So, conceptually, if inhibition of fission be expression of K151R reduced spine density, then the mitochondria would potentially be more sparsely distributed, since there are less spines to supply with ATP. Of course, this is speculation, and imaging of the spines with a post-synaptic maker such as post-synaptic density-95 would reveal how the mitochondria are positioned with respect to spines. Moreover, larger mitochondria have a greater Ca^{2+} buffering capacity, as reported for axonal mitochondria (Lewis *et al*., 2018). So the elongated mitochondria of K151R expressing cells could therefore reduce synaptic activity and spine formation, and therefore have an impact on the positioning of mitochondria. Future work to unravel these observations should include staining of post-synaptic markers and assessing mitochondrial localisation to these sites, coupled with Ca^{2+} imaging to establish the buffering capacity of the elongated mitochondria.

Comparing Figure 5.4D, E with Figure 5.5E, F shows that when neurons were transfected with WT MFF, mitochondrial area and density increase compared to untransfected neurons. It is well established that MFF is a pro-fission protein, in cell lines and primary neurons (Gandre-Babbe and van der Bliek, 2008; Lewis *et al*., 2018; Loson *et al*., 2013; Otera *et al*., 2010). The discrepency between my observations of MFF expression in neurons and those of others could be due to time/efficiency of expression. Future expriments would involve knockdown of endogenous MFF, followed by rescue experiments with wildtype and K151R MFF

back to endogenous levels. This will remove any background MFF which may mask the function of the re-expressed MFF constructs.

Summary

MFF is the major DRP1 fission receptor, having roles in DRP1 recruitment/stability at the MOM, and in reducing the length of mitochondria and the number of branches in networks. MFF SUMOylation is involved in regulating neuronal mitochondrial size and density, however this is limited to dendrites. These findings highlight the important role of regulating MFF SUMOylation and its potential implications for synaptic activity, and dendritic spine and branch formation.

Chapter 6 General Discussion

6.1 Summary of Research

The aims of the work presented in this thesis were to establish:

- where and when MFF is SUMOylated
- the regulatory pathways involved
- the functional outcomes of this modification

The initial approaches I took were to use biochemical methods, site directed mutagenesis and immunoprecipitations to identify the site(s) of SUMOylation. Following this, I aimed to determine how this modification affects DRP1 binding and MiD binding, previously characterised interactors of MFF. I propose a mechanism of sequential fission steps incorporating MFF SUMOylation as a key mechanism regulating mitochondrial fission. Furthermore, I show that SUMO-deficient MFF is required to maintain mitochondrial size and density in dendrites, but intriguingly not in axons. Together, my data indicate that SUMOylation of MFF is a pro-fission PTM with roles in maintaining compartment-specific mitochondrial size and distribution in neurons. Outlined below is a summary of my key findings, with respect to previous literature and suggestions for future work.

6.1.1 Regulation of MFF SUMOylation

I identified a single site at K151 responsible for SUMO conjugation to MFF, and show that MFF is mono and poly-SUMOylated, which are completely abolished in the K151R mutant (Figure 3.2). Interestingly, K151R, and another SUMOylation mutant E153A, also exhibit reduced ubiquitination. However, using an *in vitro* assay, I established that K151 is unlikely to be a direct ubiquitination site, and that

the interplay between SUMO and ubiquitin may be via a STUbL mechanism, whereby the SUMO chain recruits a ubiquitin ligase that ubiquitinates MFF at a separate site. Parkin has previously been show to ubiquitinate MFF during mitophagy (Gao *et al*., 2015) but parkin knockdown had no effect on K151R (Lee *et al*., 2019). Unpublished observations by L. Lee show that parkin can non-covalently interact with SUMO-1 and SUMO-2/3, indicative of a SIM, so parkin may ubiquitinate MFF via a STUbL mechanism. Moreover, MFF still retained ubiquitin after parkin knockdown, indicating that other ubiquitin ligases modify MFF (Lee *et al*., 2019). Of possible candidates, MARCH5 ubiquitinates many mitochondrial proteins (Karbowski *et al*., 2007; Nakamura *et al.*, 2006; Yonashiro *et al*., 2006), and RNF4 has been shown to act as a STUbL on poly-SUMOylated substrates such as PML (Tatham *et al*., 2008), so would be a logical focus for future work.

Since parkin knockdown had no effect on K151R, we initially interpreted these data to suggest that parkin acts at this site. However, my evidence suggests that the ubiquitin ligase(s) utilise the SUMO chain of K151 to ubiquitinate another site. This observation raised the interesting questions:

- Would it follow that increasing SUMOylation increases ubiquitination?
- What role would this pathway have?

The ubiquitin-K63 link is observed on MFF, which is reduced in the absence of parkin, but interestingly, MFF lacks the major degradative signal of K48-ubiquitin linkages (Lee *et al*., 2019 (appendix, figure 4BC)). This finding suggests that the substantial ubiquitin modifications on MFF are atypical, with potentially non-

degradative roles (Komander and Rape, 2012). Exploring the nature of the ubiquitin modifications with different antibodies and by mass spectrometry would reveal new functions and the architecture of MFF PTMs.

The K151 region conforms to the well characterised PDSM, whereby phosphorylation at S155 by AMPK promotes SUMOylation, of both the mono and poly-SUMO species. However, the phospho-null S155D and 2SA still retain some SUMOylation, demonstrating that phosphorylation is not obligatory for SUMO conjugation. This indicates that SUMOylation is not an “all or nothing” event, rather, I suggest that phosphorylation shifts the balance towards conjugation. Another important focus for future research will be to determine the phosphatases and deSUMOylating enzymes involved. In initial work, I showed that global SUMO-2/3 levels are inversely related to SENP3 levels during OGD, and SUMO-1 (and presumably SUMO-2/3) levels of conjugation of MFF increase, hinting that SENP3 is responsible, but this will require further investigation.

6.1.2 MFF SUMOylation as a stress response

I observed that MFF SUMOylation is enhanced following phosphorylation at S155. This site, along with S172, have previously been identified as AMPK sites (Chen *et al*., 2019; Ducommun *et al*., 2015; Toyama *et al*., 2016), suggesting that an increase in MFF SUMOylation upon phosphorylation is a stress response. Indeed, SUMOylation of DRP1 increases following various stress insults (Guo *et al*., 2013; Prudent *et al*., 2015; Wasiak *et al*., 2007), and global SUMO-2/3 conjugation increases upon stress (Saitoh and Hinchey, 2000).

To test the hypothesis that SUMOylation of MFF is a stress response, I

investigated DRP1 binding to wildtype and K151R following mitochondrial depolarisation with rotenone. Figure 4.8 shows the effects of rotenone for 1hr, which has previously been used to induce AMPK-mediated MFF phosphorylation and fission (Toyama *et al*., 2016). Rotenone treatment induces a further reduction in binding between DRP1 and K151R compared to wildtype, agreeing with my hypothesis that increased SUMOylation following stress and AMPK activation promotes mitochondrial fission. I believe this is a potentially important result that would form the basis for further investigation.

At the 1hr time point previously used to induce MFF phosphorylation, mitochondria have already undergone fragmentation and it has been reported that MFF remains phosphorylated (Toyama *et al*., 2016). However, I was unable to replicate this observation to detect an increase in MFF phosphorylation nor a concomitant increase in SUMOylation upon rotenone or CCCP treatment. Importantly, however, an increase in MFF conjugation by SUMO-1 was observed under OGD stress (Figure 4.7E). This could be due to differences in the stressors used and the activation of different pathways, or the rate at which the mitochondria respond. Moreover, this could reflect the labile nature of SUMOylation, and not be due to a lack of SUMOylation. Consistent with what is known about SUMOylation of many other proteins (Hay, 2004) it seems likely that a transient increase in MFF SUMOylation may occur after stress, carry out a cellular function, and then be deSUMOylated, as has been shown for the NF-κB essential modulator (NEMO), a regulatory unit in the NF-κB signalling pathway. In response to genotoxic stress, NEMO is SUMOylated and trafficks to the

nucleus. NEMO is then deSUMOylated and subsequently ubiquitinated, which is important for nuclear export and activation of NF-κB (Hay, 2004; Huang *et al*., 2003). This study demonstrates that SUMOylation of NEMO is transient and stress can induce sequential PTMs. Future experiments should investigate a "time-window" early in AMPK-activation to capture the peak of the MFF-SUMOylation increase.

6.1.3 MFF SUMOylation – fine tuning the fission rate?

DRP1 exists in a SUMOylated and deSUMOylated state, and continuously cycles from the cytosol to the MOM, where SUMOylation of DRP1 by SUMO-1 stabilises DRP1 during apoptotic stress and promotes its association with the MOM (Harder *et al*., 2004; Wasiak *et al*., 2007), whereas DRP1 modification by SUMO-2/3 during OGD prevents MOM association (Guo *et al*., 2013). Thus, a theme emerges of basal SUMOylation having a role in constitutive regulation, and certain stimuli shift the balance between the SUMO conjugated state and non-SUMO state, inducing an enhanced/reduced biological effect. Such a mechanism could occur for SUMO regulation of MFF, whereby MFF exists in multiple SUMOylated states (mono and poly-SUMOylated), and the shift to SUMOylated species elicits the enhanced biological response of increased fission. Importantly, as mentioned, this is not an "all or nothing" process, since I observe SUMOylation even of the phospho-null mutant, the SUMO state of MFF can be considered as an increasing "scale" of SUMOylation which fine-tune the fission rate.

The "SUMO enigma" is the observation that only a small proportion of available substrate is SUMOylated at a given time, but SUMO mutants can have large

effects on protein function. It is proposed that SUMOylation can alter protein interaction/complex formation, but not be required to maintain the new interaction (Hay, 2005). My findings suggest that the shift to SUMO conjugation leads to disassociation of MiD proteins from pre-fission complexes, which relieves the inhibition on DRP1, and promotes fission, and so SUMO induces reorganisation of the pre-fission complex into a fission-competent complex. The proposed mechanism presented in Figure 6.1 and bullet-pointed below is a testable hypothesis that incorporates and attempts to reconcile my findings with previous literature. Note the additions made compared to Figure 1.10.

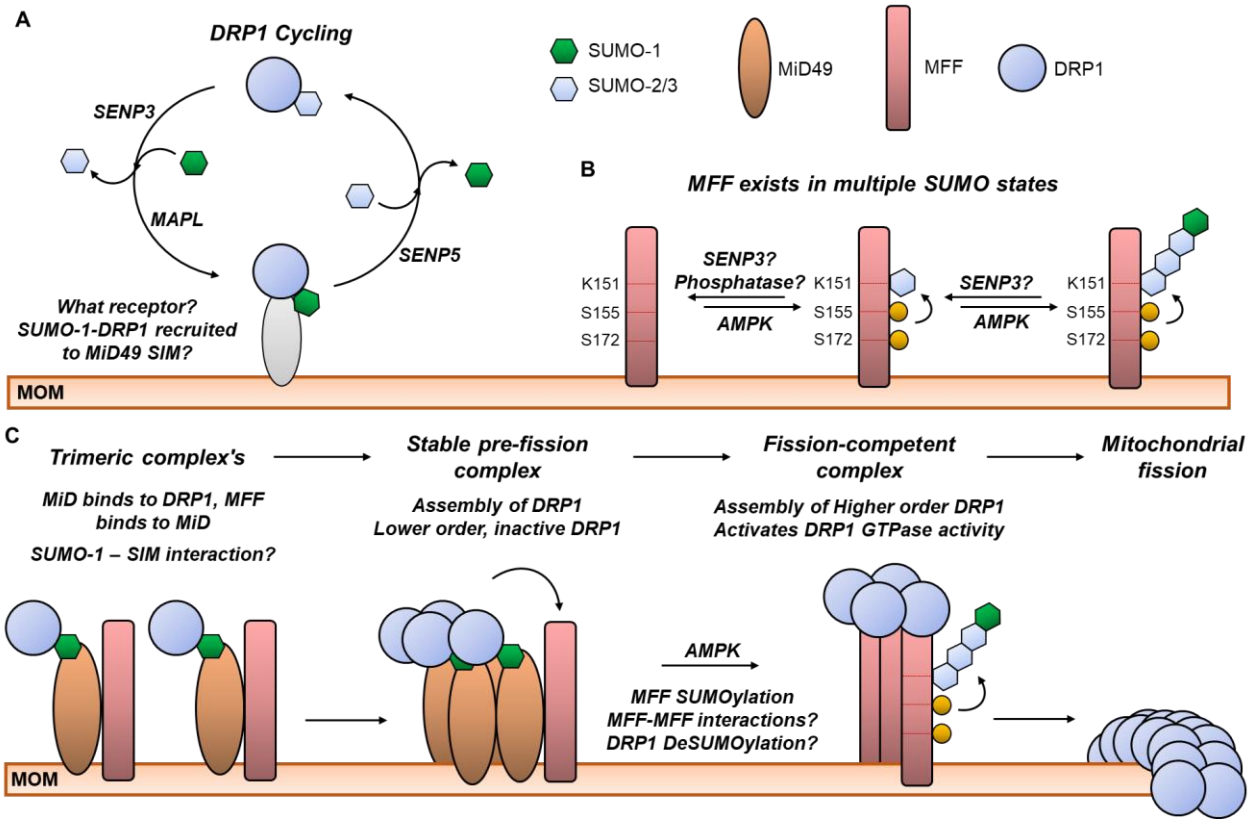

Figure 6.1 Conceptual SUMO-regulation of mitochondrial fission

Schematic of mitochondrial fission, regulated by SUMOylation of DRP1 and MFF, incorporating the findings presented in this thesis. **A** DRP1 cycling is mediated, in part, by SUMOylation. SUMO-1-DRP1 is stabilised at the MOM. Is this mediated by the SIM on MiD49? **B** MFF exists in multiple SUMO and non-SUMO states. AMPK phosphorylation promotes SUMOylation of mono and poly-SUMO species. What are the deSUMOylating SENP(s) and phosphatase(s)? **C** DRP1 receptors interact in pre-fission complexes. The trimeric complex of DRP1-MiD-MFF is the major complex. Is DRP1 SUMOylated in this complex? MiDs can sequester inactive DRP1 at the MOM (illustrated here is MiD49, yet both MiD proteins can sequester DRP1), and upon AMPK phosphorylation of MFF and increased SUMOylation, MiD is dissociated and DRP1 assembles onto MFF, which promotes fission. Does DRP1 undergo PTM between MiD binding and MFF binding?

Steps in the hypothesis of SUMO-mediated mitochondrial fission:

- DRP1 cycles from the cytosol to the MOM. SUMO-1 stabilises DRP1 at the MOM. SENP5 deconjugates SUMO-1, inhibiting fission (Harder *et al*., 2004; Wasiak *et al*., 2007; Zunino *et al*., 2007, 2009).
- SUMO-2/3 conjugation sequesters DRP1 in the cytosol, deconjugation by SENP3 promotes fission (Guo *et al*., 2013, 2017).
- Although MFF is primarily non-SUMOylated, it can be modified in multiple different ways (mono, poly-SUMO, ubiquitin chains etc).
- AMPK phosphorylation at S155 and S172 enhances SUMOylation of both SUMO isoforms and both mono and poly-SUMO modifications.
- Under basal conditions, DRP1-MiD-MFF exist as a trimeric complex (Yu *et al*., 2017), with MiD proteins inhibiting DRP1 GTPase activity (Osellame *et al*., 2016), and may act to promote DRP1 assembly (Palmer *et al*., 2011).
- Upon MFF SUMOylation, the MiD proteins dissociate from the complex, and there is a “hand-over” of DRP1 to MFF (Yu *et al*., 2017).
- MFF promotes higher order assembly of DRP1 and activates its GTPase activity (Palmer *et al*., 2011).

6.1.4 MFF SUMOylation in neurons

I show that MFF SUMOylation is required for maintaining mitochondrial size and density in dendrites, but not in axons, demonstrating that under basal conditions, SUMOylation regulates mitochondrial dynamics. As discussed in 5.4, this finding

raises three possibilities; firstly, MFF SUMOylation has different roles or is differentially regulated in the two compartments; secondly, MFF SUMOylation is dispensable for axonal mitochondria; thirdly, axons have a greater capacity for self-correcting mitochondrial size, which is MFF SUMOylation-independent. These possible explanations may not be exclusive. However, they differ from the report of Lewis *et al*, who show that MFF is necessary for axonal mitochondria, but is dispensable for regulating dendritic mitochondrial size (Lewis *et al*., 2018). On the other hand, Toyama *et al* observe that expression of wildtype and phosphomimetic MFF (2SD) reduce the area of dendritic mitochondria, whereas 2SA has no effect. They do not report whether similar effects were observed in axons (Toyama *et al*., 2016). Therefore, to more extensively corroborate my findings, I carried out transient over-expression of 2SA and 2SD in primary neurons and observed a similar trend, where 2SD decreases dendritic mitochondrial area compared to 2SA, and no change was observed in axons (see appendix Figure 8.3).

Cagalinec *et al* identified axonal mitochondria size self-regulation, whereby large mitochondria are more likely to undergo successive fission, whereas small mitochondria are more likely to under multiple rounds of fusion (Cagalinec *et al*., 2013). To my knowledge, no such study has investigated a similar mechanism in dendrites. But the fact that the axon vs. dendrite mitochondrial size differs, the fusion and fission machinery must be differentially regulated. My findings indicate a dependence on MFF SUMOylation in dendritic mitochondria, and whether MFF SUMOylation is dispensable for axons, or whether they have a greater self-

correcting mechanism, is yet to be determined. An interesting and practical way to address this question is with live cell imaging to follow fusion and fission events, as Cagalinec *et al* performed, to see if MFF K151R expression alters the fusion and fission rates in dendrites.

It is difficult to deduce a reason for the reduced mitochondrial density in K151R expressing neurons, since trafficking and mitochondrial morphology are coupled (Saotome *et al*., 2008). Further work is required to investigate the Ca^{2+} buffering capacity, trafficking, spine density and dendritic branch formation, all of which have been shown to be regulated by mitochondria dynamics, to determine whether MFF SUMOylation regulates these processes, and thus has an impact on mitochondrial density (Fukumitsu *et al*., 2015; Li *et al*., 2004).

6.1.5 Mitochondrial morphology analysis

I have presented here a workflow to quantitatively analyse mitochondrial morphology. I used MFF-null MEF cells to test this approach, with the aim of generating a wildtype and K151R rescue cell line. Unfortunately, due to time constraints, insufficient data for the K151R rescue was generated, however, preliminary observations of wildtype GFP-MFF expressing cells showed that DRP1 recruitment to the MOM was increased. As discussed in 5.4, MFF promotes fission and suppresses aberrant fusion, which if unopposed results in extreme lengths of mitochondria. MFF also has roles in regulating mitochondrial architecture, by decreasing branch number. Generating wildtype and K151R (and other mutants) rescue cells in the MFF-null background and carrying out the same analysis, coupled with live-cell imaging of DRP1 fluorescence recovery, will

dissect how the PTMs of MFF affect overall mitochondrial morphology and DRP1 recruitment.

6.1.6 MFF and disease

Rare mutations of MFF result in a truncation of the protein that lacks the transmembrane domain, causing Leigh-like syndrome in infants who exhibit developmental delay, microcephaly, and progressively developed spasticity and optic and peripheral neuropathy (Koch *et al*., 2016; Shamseldin *et al*., 2012). Whether this is specific loss of axonal mitochondrial regulation, leading to reduced neurotransmitter release and axonal branching, as previously shown using MFF knockdown (Lewis *et al*., 2018), remains to be confirmed. I have generated one of these patient mutations (E153Afs*5 – a frameshift causes a premature stop codon at amino acid 158), and so investigating mitochondrial morphology and dynamics in primary neurons with this construct will be the basis for future work, to hopefully provide insight to the pathogenesis of this disease.

An investigation into the binding of DRP1 to MFF demonstrated that using a short 10 amino acid peptide can specifically disrupt the DRP1-MFF interaction. Treatment of SH-SY5Y cells and primary neurons with this peptide induces an increase in oxidative stress, mitochondrial depolarisation, a dose-dependent decrease in oxygen consumption and reduces mitochondrial mobility in neurons by ~40% (Kornfeld *et al*., 2018). Interestingly, disruption of the DRP1-MFF interaction accelerated survival decline in a mouse model of Huntington's disease. This is in contrast to similar work which showed that inhibition of the Fis1-DRP1 interaction is beneficial in a model of amyotrophic lateral sclerosis

(Joshi *et al*., 2018). This suggests that MFF-mediated fission is necessary in neurodegenerative disease, whereas Fis1 mediated fission is detrimental. Therefore, could modulating the DRP1-MFF interaction by adjusting SUMOylation offer therapeutic benefit? If promoting MFF binding to DRP1 enhances mitochondrial mobility, mitochondrial function and reduces oxidative stress, then it follows that enhancing SUMOylation would confer a similar protective effect. Moreover, pathological proteins associated with AD and PD have been implicated in disrupting mitochondrial function (Briston and Hicks, 2018), and unpublished data from the Henely lab indicate SENP3 levels are increased in PD brains and DRP1 levels are decreased in AD brains, suggesting disrupted SUMOylation and mitochondrial dynamics under pathological conditions.

Future work will investigate how MFF-SUMOylation is affected in various disease contexts (treatment with amyloid-β, α-synuclein, OGD), whether SUMOylation of MFF has a role under these conditions, and whether it can be targeted to rescue mitochondrial dysfunction.

6.2 Outstanding Questions

The model presented in Figure 6.1 raises many questions, several of which are:

- What enzymes are required for MFF deSUMOylation?
- What are the PTM of DRP1 when bound directly to MFF in the fission competent complex? Do they regulate the switch from a pre-fission complex to a fission-competent one?
- Does the SUMO on MFF directly recruit DRP1, thus promote binding?
- Does phosphorylation of MFF have roles beyond promoting SUMOylation? What is the significance of S172 reducing MFF-SUMO-1 (Figure 3.13), does S172 phosphorylation have a different role to S155 phosphorylation?
- What role does the SIM on MiD49 have?
- Since 2SA MFF still retains some SUMOylation, what is the significance of this “basal” SUMOylation?
- Does phosphorylation and/or SUMOylation alter MFF structure/MFF-MFF interactions to promote DRP1 binding and to reduce MiD binding?

Additionally, more broad questions regarding the role of MFF SUMOylation:

- Why does MFF SUMOylation only affect dendritic mitochondria?
- Does increasing SUMOylation increase parkin-mediated ubiquitination, and thus have a role in mitophagy?
- Would decreasing MFF SUMOylation promote fusion?
- Is there an inter-organelle function of MFF SUMOylation?
- Could manipulation of MFF SUMOylation be targeted for therapeutic benefit?

6.3 Future Work

Future work would address the outstanding questions outlined in Figure 6.1.

The PTM state of DRP1

Antibodies against phosphorylation of DRP1 at S616 and S637 and DRP1 phosphorylation and SUMOylation mutants (S637A/D, S616A/D, 4KR) are available to investigate the PTM state of DRP1. Carrying out immunoprecipitations and assessing them as a proportion of total DRP1 bound to the MFF mutants will reveal the PTM and activity state of DRP1 in the complexes. Furthermore, generating phospho-null and phospho-mimetics with the addition of the K151R mutation will help to delineate the contribution of phosphorylation and SUMOylation to MFF function.

MFF deSUMOylation and dephosphorylation pathway

Since OGD increases SUMO-2/3 levels and decreases SENP3 levels, with effects on DRP1 SUMOylation (Guo *et al*., 2013, 2017), it is possible that the increase in MFF SUMOylation following OGD is due to reduced SENP3 levels. Carrying out knockdown and overexpression of the different SENPs and investigating SUMO-1 and SUMO-2/3 conjugation to MFF will reveal the deSUMOylation pathway. Likewise, investigation into the phosphatases involved in the dephosphorylation of MFF would inform on the negative regulation of MFF-SUMO signalling. This will add greater insight into the cell signalling pathways and regulation of MFF, since SENPs are sensitive to different stresses (Stankovic-Valentin *et al*., 2016). To definitively determine the roles of SUMOylation and phosphorylation, phosphorylation mutants (2SA and 2SD) should be generated in combination with

the SUMO-deficient K151R mutant. This will delineate potential differences in the function of MFF SUMOylation and phosphorylation. Moreover, combinations of S155 and S172 phosphorylation mutants (i.e. S155D and S172A, S155A and S172D) and investigation into DRP1 and MiD49 binding would address potential differences between these phosphorylation sites, as has been demonstrated for DRP1 S616 and S637 (Cereghetti *et al*., 2008).

***In vitro* assays**

The *in vitro* deSUMOylation assay will be a useful tool to specifically remove SUMO without the need for mutation. Isolating deSUMOylated MFF onto beads and investigating binding to DRP1 and MiD proteins (either endogenous or overexpressed) would definitively reveal the dependence of SUMO on these interactions. Likewise, bacterial expression can be used to investigate direct binding. However, bacteria can only generate the mono SUMO species of MFF (appendix Figure 8.1), but this would provide a simplified system to investigate the direct binding between DRP1 and MiD proteins, and also identify any differences between the mono and poly-SUMOylated MFF. Manipulation of SENP6 has been used to increase and decrease poly-SUMO chains (Hattersley *et al*., 2011). Similar experiments could be used to investigate the role of the SUMO chain of MFF.

SUMO-SIM interactions in fission

DRP1 contains putative SIM motifs (appendix Figure 8.5) the capacity for non-covalent SUMO interaction. Disruption of these SIM motifs by mutagenesis and interrogation of the binding to SUMOylated MFF will establish whether DRP1

binds directly to the SUMO on MFF. Unfortunately, there is no structure of MFF available, and so it is difficult to predict the DRP1-MFF interface. A structure has recently been solved for DRP1 binding to MiD49, which shows extensive contact between the two proteins, with DRP1 contacting four MiD49 proteins (Kalia *et al*., 2018). Although beyond the scope of this thesis, structural modelling could inform on the steric possibility of the SIM on MiD49 recruiting DRP1-SUMO. Also, mutation of the SIM on MiD49 and investigation of ability to bind to DRP1 will elucidate whether the MiD-DRP1 interaction is SUMO-SIM dependent. For predicted SIMs on MiD49, see appendix Figure 8.5.

Investigating MFF-SUMOylation, DRP1 and MiD binding, and fission

As previously discussed, carrying out parallel experiments of DRP1 binding, AMPK activation, MFF phosphorylation and SUMOylation changes during different stressors (i.e. CCCP, rotenone, OGD) over different time courses will reveal how MFF SUMOylation is regulated and links to DRP recruitment and mitochondrial morphology changes. Shorter time points should be carried out when using mitochondrial depolarisation reagents, since after longer time points, SUMOylation may have already been deconjugated.

Generating stable cell lines in the previously characterised MFF-null cells of the various MFF mutants will be a powerful tool for future experiments. Investigating the effects on mitochondrial polarisation, ATP levels, oxygen consumption and DRP1 cycling, in parallel with the experiments mentioned above, will provide a comprehensive understanding of the effects of MFF PTM on mitochondrial function. The work throughout this thesis has focused on MFF SUMOylation

promoting fission, but conversely, would decreasing SUMOylation of MFF promote fusion, and increase the association with MiD proteins? Future work will investigate MFF SUMOylation and the fission complex balance under stress that promotes mitochondrial fusion.

MFF SUMOylation in neurons

To further investigate mitochondrial dynamics in neurons, knockdown of endogenous MFF followed by rescue with MFF mutants (SUMO, phosphorylation and disease mutant) should be carried out. This will be a more conclusive experimental set-up than the overexpression experiments presented in this thesis, since silencing of endogenous MFF will remove any residual effect it may play on fission. Live cell imaging of neurons and assessing mobility, localisation to synapses, and fusion-fission rates, will reveal the role of MFF PTMs. Furthermore, similar experiments could be carried out under stress conditions (i.e. OGD, mitochondrial depolarisation, amyloid beta, α-synuclein) and expression of the disease MFF mutant (E153Afs*5) to investigate how MFF modifications and known disease mutants play a role in mitochondrial stress response in neurons.

MFF at ER-mitochondrial contact sites?

Finally, the mitochondria form significant contact with the endoplasmic reticulum (ER), where the ER can wrap around the mitochondria at pre-fission sites, which reduces the mitochondrial diameter and is predicted to aid formation of the DRP1 helix (Friedman *et al*., 2011). These ER-mitochondrial contact sites are important of lipid and Ca^{2+} homeostasis (Wu *et al*., 2018). ER-mitochondrial contact sites are maintained by protein “tethers” between the ER and mitochondrial outer

membranes, termed ER-mitochondria encounter structure (ERMES), and these contacts are not transient events, but highly regulated (Murley and Nunnari, 2016). MFF localises to these ER-mitochondrial contact pre-fission sites, in a DRP1 independent manner (Friedman *et al*., 2011). Could MFF be involved in ER tethering, like the Fis1-Bap31 interaction (Iwasawa *et al*., 2011), and could the large SUMO and ubiquitin chains facilitate these interactions? Mass spectrometry of MFF wildtype vs SUMO mutant would reveal new avenues of investigation, and potentially identify non-mitochondrial protein interactions.

6.4 Conclusions

In conclusion, the work presented here provides new insight into the regulation of mitochondrial dynamics. I have shown that the previous finding of MFF phosphorylation promoting DRP1 binding is incorrect and present a model of MFF SUMOylation regulating pre-fission complexes by reducing binding to the inhibitory MiD proteins. This work highlights the complex nature of PTM regulation of mitochondrial proteins, and its potential influence on protein complex function and mitochondrial morphology. Additionally, I show that MFF SUMOylation is important to regulate dendritic mitochondrial size and density, with no effect on axonal mitochondria, suggesting differential roles or regulation of MFF SUMOylation in neuronal compartments. I propose a testable model of MFF-SUMO mediated mitochondrial division, which will be the basis for future work.

Chapter 7 References

Alavi, M. V, Bette, S., Schimpf, S., Schuettauf, F., Schraermeyer, U., Wehrl, H.F., Ruttiger, L., Beck, S.C., Tonagel, F., Pichler, B.J., et al. (2007). A splice site mutation in the murine Opa1 gene features pathology of autosomal dominant optic atrophy. Brain *130*, 1029–1042.

Alexander, C., Votruba, M., Pesch, U.E., Thiselton, D.L., Mayer, S., Moore, A., Rodriguez, M., Kellner, U., Leo-Kottler, B., Auburger, G., et al. (2000). OPA1, encoding a dynamin-related GTPase, is mutated in autosomal dominant optic atrophy linked to chromosome 3q28. Nat. Genet. *26*, 211–215.

Alge, C.S., Hauck, S.M., Priglinger, S.G., Kampik, A., and Ueffing, M. (2006). Differential protein profiling of primary versus immortalized human RPE cells identifies expression patterns associated with cytoskeletal remodeling and cell survival. J. Proteome Res. *5*, 862–878.

Allen, K.L., Almeida, A., Bates, T.E., and Clark, J.B. (1995). Changes of Respiratory Chain Activity in Mitochondrial and Synaptosomal Fractions Isolated from the Gerbil Brain After Graded Ischaemia. J. Neurochem. *64*, 2222–2229.

Almeida, A., Allen, K.L., Bates, T.E., and Clark, J.B. (1995). Effect of Reperfusion Following Cerebral Ischaemia on the Activity of the Mitochondrial Respiratory Chain in the Gerbil Brain. J. Neurochem. *65*, 1698–1703.

Almeida, A., Delgado-Esteban, M., Bolaños, J.P., and Medina, J.M. (2002). Oxygen and glucose deprivation induces mitochondrial dysfunction and oxidative stress in neurones but not in astrocytes in primary culture.

Amiri, M., and Hollenbeck, P.J. (2008). Mitochondrial biogenesis in the axons of vertebrate peripheral neurons. Dev. Neurobiol. *68*, 1348–1361.

Anderson, M.F., and Sims, N.R. (1999). Mitochondrial Respiratory Function and Cell Death in Focal Cerebral Ischemia. J. Neurochem. *73*, 1189–1199.

Attwell, D., and Laughlin, S.B. (2001). An Energy Budget for Signaling in the Grey Matter of the Brain. J. Cereb. Blood Flow Metab. *21*, 1133–1145.

Austin, S., and St-Pierre, J. (2012). PGC1α and mitochondrial metabolism - emerging concepts and relevance in ageing and neurodegenerative disorders. J. Cell Sci. *125*, 4963–4971.

Baburamani, A.A., Hurling, C., Stolp, H., Sobotka, K., Gressens, P., Hagberg, H., and Thornton,

C. (2015). Mitochondrial Optic Atrophy (OPA) 1 Processing Is Altered in Response to Neonatal Hypoxic-Ischemic Brain Injury. Int. J. Mol. Sci. *16*, 22509–22526.

Baloh, R.H., Schmidt, R.E., Pestronk, A., and Milbrandt, J. (2007). Altered axonal mitochondrial transport in the pathogenesis of Charcot-Marie-Tooth disease from mitofusin 2 mutations. J. Neurosci. *27*, 422–430.

Bender, A., Krishnan, K.J., Morris, C.M., Taylor, G.A., Reeve, A.K., Perry, R.H., Jaros, E., Hersheson, J.S., Betts, J., Klopstock, T., et al. (2006). High levels of mitochondrial DNA deletions in substantia nigra neurons in aging and Parkinson disease. Nat. Genet. *38*, 515–517.

Bergeron, R., Ren, J.M., Cadman, K.S., Moore, I.K., Perret, P., Pypaert, M., Young, L.H., Semenkovich, C.F., and Shulman, G.I. (2001). Chronic activation of AMP kinase results in NRF-1 activation and mitochondrial biogenesis. Am. J. Physiol. Endocrinol. Metab. *281*, E1340-1346.

Bernier-Villamor, V., Sampson, D.A., Matunis, M.J., and Lima, C.D. (2002). Structural basis for E2-mediated SUMO conjugation revealed by a complex between ubiquitin-conjugating enzyme Ubc9 and RanGAP1. Cell *108*, 345–356.

Birk, J.B., and Wojtaszewski, J.F.P. (2006). Predominant α2/β2/γ3 AMPK activation during exercise in human skeletal muscle. J. Physiol. *577*, 1021–1032.

Boddy, M.N., Howe, K., Etkin, L.D., Solomon, E., and Freemont, P.S. (1996). PIC 1, a novel ubiquitin-like protein which interacts with the PML component of a multiprotein complex that is disrupted in acute promyelocytic leukaemia. Oncogene *13*, 971–982.

Boddy, M.N., Duprez, E., Borden, K.L., Freemont, P.S., Howe, K., Boddy, M.N., Solomon, E., The, H. de, Hay, R.T., and Freemont, P.S. (1997). Surface residue mutations of the PML RING finger domain alter the formation of nuclear matrix-associated PML bodies. J. Cell Sci. *110*, 2197–2205.

Bohren, K.M., Nadkarni, V., Song, J.H., Gabbay, K.H., and Owerbach, D. (2004). A M55V polymorphism in a novel SUMO gene (SUMO-4) differentially activates heat shock transcription factors and is associated with susceptibility to type I diabetes mellitus. J. Biol. Chem. *279*, 27233–27238.

Bolam, J.P., and Pissadaki, E.K. (2012). Living on the edge with too many mouths to feed: Why dopamine neurons die. Mov. Disord. *27*, 1478–1483.

Bonnard, C., Durand, A., Peyrol, S., Chanseaume, E., Chauvin, M.-A., Morio, B., Vidal, H., and Rieusset, J. (2008). Mitochondrial dysfunction results from oxidative stress in the skeletal muscle

of diet-induced insulin-resistant mice. J. Clin. Invest. *118*, 789–800.

Briston, T., and Hicks, A.R. (2018). Mitochondrial dysfunction and neurodegenerative proteinopathies: Mechanisms and prospects for therapeutic intervention. Biochem. Soc. Trans. *46*, 829–842.

de Brito, O.M., and Scorrano, L. (2008). Mitofusin 2 tethers endoplasmic reticulum to mitochondria. Nature *456*, 605–610.

Cagalinec, M., Safiulina, D., Liiv, M., Liiv, J., Choubey, V., Wareski, P., Veksler, V., and Kaasik, A. (2013). Principles of the mitochondrial fusion and fission cycle in neurons. J. Cell Sci. *126*, 2187–2197.

Calvo, S.E., Clauser, K.R., and Mootha, V.K. (2016). MitoCarta2.0: An updated inventory of mammalian mitochondrial proteins. Nucleic Acids Res. *44*, 1251–1257.

Castillo-Lluva, S., Tatham, M.H., Jones, R.C., Jaffray, E.G., Edmondson, R.D., Hay, R.T., and Malliri, A. (2010). SUMOylation of the GTPase Rac1 is required for optimal cell migration. Nat. Cell Biol. *12*, 1078–1085.

Cenini, G., Rub, C., Bruderek, M., and Voos, W. (2016). Amyloid β-peptides interfere with mitochondrial preprotein import competence by a coaggregation process. Mol. Biol. Cell *27*, 3257–3272.

Cereghetti, G.M., Stangherlin, A., de Brito, O.M., Chang, C.R., Blackstone, C., Bernardi, P., and Scorrano, L. (2008). Dephosphorylation by calcineurin regulates translocation of Drp1 to mitochondria. Proc. Natl. Acad. Sci. *105*, 15803–15808.

Chamberlain, S.E.L., González-González, I.M., Wilkinson, K.A., Konopacki, F.A., Kantamneni, S., Henley, J.M., and Mellor, J.R. (2012). SUMOylation and phosphorylation of GluK2 regulate kainate receptor trafficking and synaptic plasticity. Nat. Neurosci. *15*, 845–852.

Chang, C.-R., and Blackstone, C. (2007). Cyclic AMP-dependent protein kinase phosphorylation of Drp1 regulates its GTPase activity and mitochondrial morphology. J. Biol. Chem. *282*, 21583–21587.

Chang, D.T.W., Honick, A.S., and Reynolds, I.J. (2006). Mitochondrial Trafficking to Synapses in Cultured Primary Cortical Neurons. J. Neurosci. *26*, 7035–7045.

Chen, H., Detmer, S.A., Ewald, A.J., Griffin, E.E., Fraser, S.E., and Chan, D.C. (2003). Mitofusins Mfn1 and Mfn2 coordinately regulate mitochondrial fusion and are essential for embryonic

development. J. Cell Biol. *160*, 189–200.

Chen, H., Chomyn, A., and Chan, D.C. (2005). Disruption of Fusion Results in Mitochondrial Heterogeneity and Dysfunction. J. Biol. Chem. *280*, 26185–26192.

Chen, H., Ren, S., Clish, C., Jain, M., Mootha, V., McCaffery, J.M., and Chan, D.C. (2015). Titration of mitochondrial fusion rescues Mff-deficient cardiomyopathy. J. Cell Biol. *211*, 795–805.

Chen, Z., Lei, C., Wang, C., Li, N., Srivastava, M., Tang, M., Zhang, H., Choi, J.M., Jung, S.Y., Qin, J., et al. (2019). Global phosphoproteomic analysis reveals ARMC10 as an AMPK substrate that regulates mitochondrial dynamics. Nat. Commun. *10*, 104.

Chinta, S.J., Mallajosyula, J.K., Rane, A., and Andersen, J.K. (2010). Mitochondrial alpha-synuclein accumulation impairs complex I function in dopaminergic neurons and results in increased mitophagy in vivo. Neurosci. Lett. *486*, 235–239.

Cho, D.-H., Nakamura, T., Fang, J., Cieplak, P., Godzik, A., Gu, Z., and Lipton, S.A. (2009). S-nitrosylation of Drp1 mediates beta-amyloid-related mitochondrial fission and neuronal injury. Science *324*, 102–105.

Civiletto, G., Varanita, T., Cerutti, R., Gorletta, T., Barbaro, S., Marchet, S., Lamperti, C., Viscomi, C., Scorrano, L., and Zeviani, M. (2015). Opa1 overexpression ameliorates the phenotype of two mitochondrial disease mouse models. Cell Metab. *21*, 845–854.

Cogliati, S., Enriquez, J.A., and Scorrano, L. (2016). Mitochondrial Cristae: Where Beauty Meets Functionality. Trends Biochem. Sci. *41*, 261–273.

Collavin, L., Gostissa, M., Avolio, F., Secco, P., Ronchi, A., Santoro, C., and Del Sal, G. (2004). Modification of the erythroid transcription factor GATA-1 by SUMO-1. Proc. Natl. Acad. Sci. *101*, 8870–8875.

Cribbs, J.T., and Strack, S. (2007). Reversible phosphorylation of Drp1 by cyclic AMP-dependent protein kinase and calcineurin regulates mitochondrial fission and cell death. EMBO Rep. *8*, 939–944.

Culmsee, C., monnig, J., Kemp, B.E., and Mattson, M.P. (2001). AMP-Activated Protein Kinase is Highly Expressed in Neurons in the Developing Rat Brain and Promotes Neuronal Survival Following Glucose Deprivation. J. Mol. Neurosci. *17*, 45–58.

Datwyler, A.L., Lättig-Tünnemann, G., Yang, W., Paschen, W., Lee, S.L.L., Dirnagl, U., Endres, M., and Harms, C. (2011). SUMO2/3 conjugation is an endogenous neuroprotective mechanism.

J. Cereb. Blood Flow Metab. *31*, 2152–2159.

Davies, S.P., Helps, N.R., Cohen, P.T., and Hardie, D.G. (1995). 5'-AMP inhibits dephosphorylation, as well as promoting phosphorylation, of the AMP-activated protein kinase. Studies using bacterially expressed human protein phosphatase-2C alpha and native bovine protein phosphatase-2AC. FEBS Lett. *377*, 421–425.

Delettre, C., Lenaers, G., Griffoin, J.M., Gigarel, N., Lorenzo, C., Belenguer, P., Pelloquin, L., Grosgeorge, J., Turc-Carel, C., Perret, E., et al. (2000). Nuclear gene OPA1, encoding a mitochondrial dynamin-related protein, is mutated in dominant optic atrophy. Nat. Genet. *26*, 207–210.

Desterro, J.M., Thomson, J., and Hay, R.T. (1997). Ubch9 conjugates SUMO but not ubiquitin. FEBS Lett. *417*, 297–300.

Desterro, J.M., Rodriguez, M.S., and Hay, R.T. (1998). SUMO-1 modification of IkappaBalpha inhibits NF-kappaB activation. Mol. Cell *2*, 233–239.

Detmer, S.A., and Chan, D.C. (2007). Functions and dysfunctions of mitochondrial dynamics. Nat. Rev. Mol. Cell Biol. *8*, 870–879.

Detmer, S.A., Velde, C. Vande, Cleveland, D.W., and Chan, D.C. (2008). Hindlimb gait defects due to motor axon loss and reduced distal muscles in a transgenic mouse model of Charcot–Marie–Tooth type 2A. Hum. Mol. Genet. *17*, 367–375.

Devi, L., Raghavendran, V., Prabhu, B.M., Avadhani, N.G., and Anandatheerthavarada, H.K. (2008). Mitochondrial import and accumulation of α-synuclein impair complex I in human dopaminergic neuronal cultures and Parkinson disease brain. J. Biol. Chem. *283*, 9089–9100.

Dikic, I., and Elazar, Z. (2018). Mechanism and medical implications of mammalian autophagy. Nat. Rev. Mol. Cell Biol. *19*, 349–364.

Dorn, G.W. (2018). Evolving Concepts of Mitochondrial Dynamics. Annu. Rev. Physiol. *81*, 1–17.

Duan, G., and Walther, D. (2015). The roles of post-translational modifications in the context of protein interaction networks. PLoS Comput. Biol. *11*, e1004049.

Ducommun, S., Deak, M., Sumpton, D., Ford, R.J., Núñez Galindo, A., Kussmann, M., Viollet, B., Steinberg, G.R., Foretz, M., Dayon, L., et al. (2015). Motif affinity and mass spectrometry proteomic approach for the discovery of cellular AMPK targets: Identification of mitochondrial fission factor as a new AMPK substrate. Cell. Signal. *27*, 978–988.

Durcan, T.M., Tang, M.Y., Pérusse, J.R., Dashti, E.A., Aguileta, M.A., McLelland, G., Gros, P., Shaler, T.A., Faubert, D., Coulombe, B., et al. (2014). USP 8 regulates mitophagy by removing K 6-linked ubiquitin conjugates from parkin. EMBO J. *33*, 2473–2491.

Egan, D.F., Shackelford, D.B., Mihaylova, M.M., Gelino, S., Kohnz, R.A., Mair, W., Vasquez, D.S., Joshi, A., Gwinn, D.M., Taylor, R., et al. (2011). Phosphorylation of ULK1 (hATG1) by AMP-activated protein kinase connects energy sensing to mitophagy. Science. *331*, 456–461.

Eisner, V., Picard, M., and Hajnóczky, G. (2018). Mitochondrial dynamics in adaptive and maladaptive cellular stress responses. Nat. Cell Biol. *20*, 755–765.

Elgass, K.D., Smith, E.A., LeGros, M.A., Larabell, C.A., and Ryan, M.T. (2015). Analysis of ER-mitochondria contacts using correlative fluorescence microscopy and soft X-ray tomography of mammalian cells. J. Cell Sci. *128*, 2795–2804.

Elliott, H.R., Samuels, D.C., Eden, J.A., Relton, C.L., and Chinnery, P.F. (2008). Pathogenic Mitochondrial DNA Mutations Are Common in the General Population. Am. J. Hum. Genet. *83*, 254–260.

Eskiw, C.H., Dellaire, G., Mymryk, J.S., and Bazett-Jones, D.P. (2003). Size, position and dynamic behavior of PML nuclear bodies following cell stress as a paradigm for supramolecular trafficking and assembly. J. Cell Sci. *116*, 4455–4466.

Fernandez-Marcos, P.J., and Auwerx, J. (2011). Regulation of PGC-1α, a nodal regulator of mitochondrial biogenesis. In American Journal of Clinical Nutrition, pp. 884–890.

Ferree, A., and Shirihai, O. (2012). Mitochondrial dynamics: The intersection of form and function. Adv. Exp. Med. Biol. *748*, 13–40.

Figueroa-Romero, C., Iñiguez-Lluhí, J.A., Stadler, J., Chang, C.-R., Arnoult, D., Keller, P.J., Hong, Y., Blackstone, C., and Feldman, E.L. (2009). SUMOylation of the mitochondrial fission protein Drp1 occurs at multiple nonconsensus sites within the B domain and is linked to its activity cycle. FASEB J. *23*, 3917–3927.

Flotho, A., and Melchior, F. (2013). Sumoylation: a regulatory protein modification in health and disease. Annu. Rev. Biochem. *82*, 357–385.

Francy, C.A., Alvarez, F.J.D., Zhou, L., Ramachandran, R., and Mears, J.A. (2015). The mechanoenzymatic core of dynamin-related protein 1 comprises the minimal machinery required for membrane constriction. J. Biol. Chem. *290*, 11692–11703.

Friedman, J.R., and Nunnari, J. (2014). Mitochondrial form and function. Nature *505*, 335–343.

Friedman, J.R., Lackner, L.L., West, M., DiBenedetto, J.R., Nunnari, J., and Voeltz, G.K. (2011). ER tubules mark sites of mitochondrial division. Science *334*, 358–362.

Fu, C., Ahmed, K., Ding, H., Ding, X., Lan, J., Yang, Z., Miao, Y., Zhu, Y., Shi, Y., Zhu, J., et al. (2005). Stabilization of PML nuclear localization by conjugation and oligomerization of SUMO-3. Oncogene *24*, 5401–5413.

Fukumitsu, K., Fujishima, K., Yoshimura, A., Wu, Y.K., Heuser, J., and Kengaku, M. (2015). Synergistic action of dendritic mitochondria and creatine kinase maintains ATP homeostasis and actin dynamics in growing neuronal dendrites. J. Neurosci. *35*, 5707–5723.

Galanty, Y., Belotserkovskaya, R., Coates, J., Polo, S., Miller, K.M., and Jackson, S.P. (2009). Mammalian SUMO E3-ligases PIAS1 and PIAS4 promote responses to DNA double-strand breaks. Nature *462*, 935–939.

Gandre-Babbe, S., and van der Bliek, A.M. (2008). The Novel Tail-anchored Membrane Protein Mff Controls Mitochondrial and Peroxisomal Fission in Mammalian Cells. Mol. Biol. Cell *19*, 2402–2412.

Gao, J., Qin, S., and Jiang, C. (2015). Parkin-induced ubiquitination of Mff promotes its association with p62/SQSTM1 during mitochondrial depolarization. Acta Biochim. Biophys. Sin. (Shanghai). *47*, 522–529.

Garcia, D., and Shaw, R.J. (2017). AMPK: Mechanisms of Cellular Energy Sensing and Restoration of Metabolic Balance. Mol. Cell *66*, 789–800.

Garcia-Roves, P.M., Osler, M.E., Holmström, M.H., and Zierath, J.R. (2008). Gain-of-function R225Q mutation in AMP-activated protein kinase gamma3 subunit increases mitochondrial biogenesis in glycolytic skeletal muscle. J. Biol. Chem. *283*, 35724–35734.

Gautier, C.A., Kitada, T., and Shen, J. (2008). Loss of PINK1 causes mitochondrial functional defects and increased sensitivity to oxidative stress. Proc. Natl. Acad. Sci. U. S. A. *105*, 11364–11369.

Gawlowski, T., Suarez, J., Scott, B., Torres-Gonzalez, M., Wang, H., Schwappacher, R., Han, X., Yates, J.R., Hoshijima, M., Dillmann, W., et al. (2012). Modulation of dynamin-related protein 1 (DRP1) function by increased O-linked-β-N-acetylglucosamine modification (O-GlcNAc) in cardiac myocytes. J. Biol. Chem. *287*, 30024–30034.

Gegg, M.E., Cooper, J.M., Chau, K.Y., Rojo, M., Schapira, A.H.V., and Taanman, J.W. (2010). Mitofusin 1 and mitofusin 2 are ubiquitinated in a PINK1/parkin-dependent manner upon induction of mitophagy. Hum. Mol. Genet. *19*, 4861–4870.

Giorgino, F., Robertis, O. de, Laviola, L., Montrone, C., Perrini, S., McCowen, K.C., and Smith, R.J. (2000). The sentrin-conjugating enzyme mUbc9 interacts with GLUT4 and GLUT1 glucose transporters and regulates transporter levels in skeletal muscle cells. Proc. Natl. Acad. Sci. *97*, 1125–1130.

Glancy, B., Hartnell, L.M., Malide, D., Yu, Z.-X., Combs, C.A., Connelly, P.S., Subramaniam, S., and Balaban, R.S. (2015). Mitochondrial reticulum for cellular energy distribution in muscle. Nature *523*, 617–620.

Golebiowski, F., Matic, I., Tatham, M.H., Cole, C., Yin, Y., Nakamura, A., Cox, J., Barton, G.J., Mann, M., and Hay, R.T. (2009). System-wide changes to sumo modifications in response to heat shock. Sci. Signal. *2*, 1–14.

Gomes, L.C., Benedetto, G. Di, and Scorrano, L. (2011). During autophagy mitochondria elongate, are spared from degradation and sustain cell viability. Nat. Cell Biol. *13*, 589–598.

Gray, M.W., Burger, G., and Lang, B.F. (1999). Mitochondrial Evolution. Science. *283*, 1476–1481.

Griparic, L., Van Der Wel, N.N., Orozco, I.J., Peters, P.J., and Van Der Bliek, A.M. (2004). Loss of the Intermembrane Space Protein Mgm1/OPA1 Induces Swelling and Localized Constrictions along the Lengths of Mitochondria. J. Biol. Chem. *279*, 18792–18798.

Griparic, L., Kanazawa, T., and van der Bliek, A.M. (2007). Regulation of the mitochondrial dynamin-like protein Opa1 by proteolytic cleavage. J. Cell Biol. *178*, 757–764.

Grönholm, J., Vanhatupa, S., Ungureanu, D., Väliaho, J., Laitinen, T., Valjakka, J., and Silvennoinen, O. (2012). Structure-function analysis indicates that sumoylation modulates DNA-binding activity of STAT1. BMC Biochem. *13*, 1–12.

Guo, C., Hildick, K.L., Luo, J., Dearden, L., Wilkinson, K.A., and Henley, J.M. (2013). SENP3-mediated deSUMOylation of dynamin-related protein 1 promotes cell death following ischaemia. EMBO J. *32*, 1514–1528.

Guo, C., Wilkinson, K.A., Evans, A.J., Rubin, P.P., and Henley, J.M. (2017). SENP3-mediated deSUMOylation of Drp1 facilitates interaction with Mff to promote cell death. Sci. Rep. *7*, 43811.

Guo, D., Li, M., Zhang, Y., Yang, P., Eckenrode, S., Hopkins, D., Zheng, W., Purohit, S., Podolsky, R.H., Muir, A., et al. (2004). A functional variant of SUMO4, a new IκBα modifier, is associated with type 1 diabetes. Nat. Genet. *36*, 837–841.

Guzzo, C.M., Berndsen, C.E., Zhu, J., Gupta, V., Datta, A., Greenberg, R.A., Wolberger, C., and Matunis, M.J. (2012). RNF4-dependent hybrid SUMO-ubiquitin chains are signals for RAP80 and thereby mediate the recruitment of BRCA1 to sites of DNA damage. Sci. Signal. *5*, ra88.

Gwinn, D.M., Shackelford, D.B., Egan, D.F., Mihaylova, M.M., Mery, A., Vasquez, D.S., Turk, B.E., and Shaw, R.J. (2008). AMPK Phosphorylation of Raptor Mediates a Metabolic Checkpoint. Mol. Cell *30*, 214–226.

Hales, K.G., and Fuller, M.T. (1997). Developmentally Regulated Mitochondrial Fusion Mediated by a Conserved, Novel, Predicted GTPase. Cell *90*, 121–129.

Han, J., Thompson-Lowrey, A.J., Reiss, A., Mayorov, V., Jia, H., Biousse, V., Newman, N.J., and Brown, M.D. (2006). OPA1 mutations and mitochondrial DNA haplotypes in autosomal dominant optic atrophy. Genet. Med. *8*, 217–225.

Hansson Petersen, C.A., Alikhani, N., Behbahani, H., Wiehager, B., Pavlov, P.F., Alafuzoff, I., Leinonen, V., Ito, A., Winblad, B., Glaser, E., et al. (2008). The amyloid β-peptide is imported into mitochondria via the TOM import machinery and localized to mitochondrial cristae. Proc. Natl. Acad. Sci. U. S. A. *105*, 13145–13150.

Harder, Z., Zunino, R., and McBride, H. (2004). Sumo1 Conjugates Mitochondrial Substrates and Participates in Mitochondrial Fission. Curr. Biol. *14*, 340–345.

Hardie, G. (2011). AMP-activated protein kinase-an energy sensor that regulates all aspects of cell function. Genes Dev. *25*, 1895–1908.

Hardie, G. (2016). Regulation of AMP-activated protein kinase by natural and synthetic activators. Acta Pharm. Sin. B *6*, 1–19.

Hattersley, N., Shen, L., Jaffray, E.G., and Hay, R.T. (2011). The SUMO protease SENP6 is a direct regulator of PML nuclear bodies. Mol. Biol. Cell *22*, 78–90.

Haun, F., Nakamura, T., Shiu, A.D., Cho, D.-H., Tsunemi, T., Holland, E.A., La Spada, A.R., and Lipton, S.A. (2013). S-Nitrosylation of Dynamin-Related Protein 1 Mediates Mutant Huntingtin-Induced Mitochondrial Fragmentation and Neuronal Injury in Huntington's Disease. Antioxid. Redox Signal. *19*, 1173–1184.

Hawley, S.A., Boudeau, J., Reid, J.L., Mustard, K.J., Udd, L., Mäkelä, T.P., Alessi, D.R., and Hardie, D.G. (2003a). Complexes between the LKB1 tumor suppressor, STRAD alpha/beta and MO25 alpha/beta are upstream kinases in the AMP-activated protein kinase cascade. J. Biol. *2*, 1–16.

Hawley, S.A., Boudeau, J., Reid, J.L., Mustard, K.J., Udd, L., Mäkelä, T.P., Alessi, D.R., and Hardie, D.G. (2003b). Complexes between the LKB1 tumor suppressor, STRADα/β and MO25α/β are upstream kinases in the AMP-activated protein kinase cascade. J. Biol. *2*, 1–16.

Hawley, S.A., Pan, D.A., Mustard, K.J., Ross, L., Bain, J., Edelman, A.M., Frenguelli, B.G., and Hardie, D.G. (2005). Calmodulin-dependent protein kinase kinase-β is an alternative upstream kinase for AMP-activated protein kinase. Cell Metab. *2*, 9–19.

Hay, R.T. (2004). Modifiying NEMO. Nat. Cell Biol. *6*, 89–91.

Hay, R.T. (2005). SUMO: a history of modification. Mol. Cell *18*, 1–12.

Hendriks, I.A., and Vertegaal, A.C.O. (2016). A comprehensive compilation of SUMO proteomics. Nat. Rev. Mol. Cell Biol. *17*, 581–595.

Hendriks, I.A., D'Souza, R.C.J., Yang, B., Verlaan-de Vries, M., Mann, M., and Vertegaal, A.C.O. (2014). Uncovering global SUMOylation signaling networks in a site-specific manner. Nat. Struct. Mol. Biol. *21*, 927–936.

Hendriks, I.A., Lyon, D., Young, C., Jensen, L.J., Vertegaal, A.C.O., and Nielsen, M.L. (2017). Site-specific mapping of the human SUMO proteome reveals co-modification with phosphorylation. Nat. Struct. Mol. Biol. *24*, 325–336.

Hendriks, I.A., Lyon, D., Su, D., Skotte, N.H., Daniel, J.A., Jensen, L.J., and Nielsen, M.L. (2018). Site-specific characterization of endogenous SUMOylation across species and organs. Nat. Commun. *9*, 1–17.

Herzig, S., and Shaw, R.J. (2018). AMPK: Guardian of metabolism and mitochondrial homeostasis. Nat. Rev. Mol. Cell Biol. *19*, 121–135.

Hewitt, V.L., and Whitworth, A.J. (2017). Mitochondrial Fission and Fusion. In Parkinson's Disease: Molecular Mechanisms Underlying Pathology, pp. 77–111.

Hickey, C.M., Wilson, N.R., and Hochstrasser, M. (2012). Function and regulation of SUMO proteases. Nat. Rev. Mol. Cell Biol. *13*, 755–766.

Hietakangas, V., Ahlskog, J.K., Jakobsson, A.M., Hellesuo, M., Sahlberg, N.M., Holmberg, C.I., Mikhailov, A., Palvimo, J.J., Pirkkala, L., and Sistonen, L. (2003). Phosphorylation of serine 303 is a prerequisite for the stress-inducible SUMO modification of heat shock factor 1. Mol. Cell. Biol. *23*, 2953–2968.

Hietakangas, V., Anckar, J., Blomster, H.A., Fujimoto, M., Palvimo, J.J., Nakai, A., and Sistonen, L. (2006). PDSM, a motif for phosphorylation-dependent SUMO modification. Proc. Natl. Acad. Sci. U. S. A. *103*, 45–50.

Hong, Y., Rogers, R., Matunis, M.J., Mayhew, C.N., Goodson, M., Park-Sarge, O.K., and Sarge, K.D. (2001). Regulation of Heat Shock Transcription Factor 1 by Stress-induced SUMO-1 Modification. J. Biol. Chem.

Hoppins, S., Lackner, L., and Nunnari, J. (2007). The Machines that Divide and Fuse Mitochondria. Annu. Rev. Biochem. *76*, 751–780.

Hsu, K.-S., and Kao, H.-Y. (2018). PML: Regulation and multifaceted function beyond tumor suppression. Cell Biosci. *8*, 1–21.

Huang, C., Han, Y., Wang, Y., Sun, X., Yan, S., Yeh, E.T.H., Chen, Y., Cang, H., Li, H., Shi, G., et al. (2009). SENP3 is responsible for HIF-1 transactivation under mild oxidative stress via p300 de-SUMOylation. EMBO J. *28*, 2748–2762.

Huang, T.T., Wuerzberger-Davis, S.M., Wu, Z.H., and Miyamoto, S. (2003). Sequential Modification of NEMO/IKKγ by SUMO-1 and Ubiquitin Mediates NF-κB Activation by Genotoxic Stress. Cell *115*, 565–576.

Huang, Y., Xu, B., Zhou, X., Li, Y., Lu, M., Jiang, R., and Li, T. (2015). Systematic characterization and prediction of post-translational modification cross-talk. Mol. Cell. Proteomics *14*, 761–770.

Inoue, H., Nojima, H., and Okayama, H. (1990). High efficiency transformation of Escherichia coli with plasmids. Gene *96*, 23–28.

Ishihara, N., Nomura, M., Jofuku, A., Kato, H., Suzuki, S.O., Masuda, K., Otera, H., Nakanishi, Y., Nonaka, I., Goto, Y.-I., et al. (2009). Mitochondrial fission factor Drp1 is essential for embryonic development and synapse formation in mice. Nat. Cell Biol. *11*, 958–966.

Iwasawa, R., Mahul-Mellier, A.-L., Datler, C., Pazarentzos, E., and Grimm, S. (2011). Fis1 and Bap31 bridge the mitochondria–ER interface to establish a platform for apoptosis induction. EMBO J. *30*, 556–558.

Jäger, S., Handschin, C., St-Pierre, J., and Spiegelman, B.M. (2007). AMP-activated protein kinase (AMPK) action in skeletal muscle via direct phosphorylation of PGC-1alpha. Proc. Natl. Acad. Sci. U. S. A. *104*, 12017–12022.

James, D.I., Parone, P.A., Mattenberger, Y., and Martinou, J.-C. (2003). hFis1, a novel component of the mammalian mitochondrial fission machinery. J. Biol. Chem. *278*, 36373–36379.

Jameson, E., and Morris, A.A.M. (2011). Mitochondrial disease – a review. Paediatr. Child Health (Oxford). *21*, 80–83.

Ji, W.K., Hatch, A.L., Merrill, R.A., Strack, S., and Higgs, H.N. (2015). Actin filaments target the oligomeric maturation of the dynamin GTPase Drp1 to mitochondrial fission sites. Elife *4*, 1–25.

Jiang, T., Yu, J.-T., Zhu, X.-C., Wang, H.-F., Tan, M.-S., Cao, L., Zhang, Q.-Q., Gao, L., Shi, J.-Q., Zhang, Y.-D., et al. (2014). Acute metformin preconditioning confers neuroprotection against focal cerebral ischaemia by pre-activation of AMPK-dependent autophagy. Br. J. Pharmacol. *171*, 3146–3157.

Johnson, E.S., and Blobel, G. (1997). Ubc9p Is the Conjugating Enzyme for the Ubiquitin-like Protein Smt3p. J. Biol. Chem. *272*, 26799–26802.

Johnson, E.S., and Blobel, G. (1999). Cell cycle-regulated attachment of the ubiquitin-related protein SUMO to the yeast septins. J. Cell Biol. *147*, 981–994.

Johnson, E.S., Schwienhorst, I., Dohmen, R.J., and Blobel, G. (1997). The ubiquitin-like protein Smt3p is activated for conjugation to other proteins by an Aos1p/Uba2p heterodimer. EMBO J. *16*, 5509–5519.

Joshi, A.U., Saw, N.L., Vogel, H., Cunnigham, A.D., Shamloo, M., and Mochly-Rosen, D. (2018). Inhibition of Drp1/Fis1 interaction slows progression of amyotrophic lateral sclerosis. EMBO Mol. Med. *10*, 1–17.

Kageyama, Y., Zhang, Z., Roda, R., Fukaya, M., Wakabayashi, J., Wakabayashi, N., Kensler, T.W., Reddy, P.H., Iijima, M., and Sesaki, H. (2012). Mitochondrial division ensures the survival of postmitotic neurons by suppressing oxidative damage. J. Cell Biol. *197*, 535–551.

Kageyama, Y., Hoshijima, M., Seo, K., Bedja, D., Sysa-Shah, P., Andrabi, S.A., Chen, W., Höke, A., Dawson, V.L., Dawson, T.M., et al. (2014). Parkin-independent mitophagy requires D rp1 and maintains the integrity of mammalian heart and brain. EMBO J. *33*, 2798–2813.

Kahn, B.B., Alquier, T., Carling, D., and Hardie, D.G. (2005). AMP-activated protein kinase:

Ancient energy gauge provides clues to modern understanding of metabolism. Cell Metab. *1*, 15–25.

Kalia, R., Wang, R.Y.-R., Yusuf, A., Thomas, P. V., Agard, D.A., Shaw, J.M., and Frost, A. (2018). Structural basis of mitochondrial receptor binding and constriction by DRP1. Nature *558*, 401–405.

Kang, J., Gocke, C., and Yu, H. (2006). Phosphorylation-facilitated sumoylation of MEF2C negatively regulates its transcriptional activity. BMC Biochem. *7*, 1–14.

Kang, J.-S., Tian, J.-H., Pan, P.-Y., Zald, P., Li, C., Deng, C., and Sheng, Z.-H. (2008). Docking of Axonal Mitochondria by Syntaphilin Controls Their Mobility and Affects Short-Term Facilitation. Cell *132*, 137–148.

Karbowski, M., Arnoult, D., Chen, H., Chan, D.C., Smith, C.L., and Youle, R.J. (2004). Quantitation of mitochondrial dynamics by photolabeling of individual organelles shows that mitochondrial fusion is blocked during the Bax activation phase of apoptosis. J. Cell Biol. *164*, 493–499.

Karbowski, M., Neutzner, A., and Youle, R.J. (2007). The mitochondrial E3 ubiquitin ligase MARCH5 is required for Drp1 dependent mitochondrial division. J. Cell Biol. *178*, 71–84.

Kashatus, J.A., Nascimento, A., Myers, L.J., Sher, A., Byrne, F.L., Hoehn, K.L., Counter, C.M., and Kashatus, D.F. (2015). Erk2 phosphorylation of Drp1 promotes mitochondrial fission and MAPK-driven tumor growth. Mol. Cell *57*, 537–551.

Kerscher, O. (2007). SUMO junction-what's your function? New insights through SUMO-interacting motifs. EMBO Rep. *8*, 550–555.

Kim, J., Yang, G., Kim, Y., Kim, J., and Ha, J. (2016). AMPK activators: Mechanisms of action and physiological activities. Exp. Mol. Med. *48*, 224–236.

Kitada, T., Asakawa, S., Hattori, N., Matsumine, H., Yamamura, Y., Minoshima, S., Yokochi, M., Mizuno, Y., and Shimizu, N. (1998). Mutations in the parkin gene cause autosomal recessive juvenile parkinsonism. Nature *392*, 605–608.

Koch, J., Feichtinger, R.G., Freisinger, P., Pies, M., Schrödl, F., Iuso, A., Sperl, W., Mayr, J.A., Prokisch, H., and Haack, T.B. (2016). Disturbed mitochondrial and peroxisomal dynamics due to loss of MFF causes Leigh-like encephalopathy, optic atrophy and peripheral neuropathy. J. Med. Genet. *53*, 270–278.

Koirala, S., Guo, Q., Kalia, R., Bui, H.T., Eckert, D.M., Frost, A., and Shaw, J.M. (2013).

Interchangeable adaptors regulate mitochondrial dynamin assembly for membrane scission. Proc. Natl. Acad. Sci. *110*, 1342–1351.

Komander, D., and Rape, M. (2012). The Ubiquitin Code. Annu. Rev. Biochem. *81*, 203–229.

Konopacki, F.A., Jaafari, N., Rocca, D.L., Wilkinson, K.A., Chamberlain, S., Rubin, P., Kantamneni, S., Mellor, J.R., and Henley, J.M. (2011). Agonist-induced PKC phosphorylation regulates GluK2 SUMOylation and kainate receptor endocytosis. Proc. Natl. Acad. Sci. U. S. A. *108*, 19772–19777.

Kornfeld, O.S., Qvit, N., Haileselassie, B., Shamloo, M., Bernardi, P., and Mochly-Rosen, D. (2018). Interaction of mitochondrial fission factor with dynamin related protein 1 governs physiological mitochondrial function in vivo. Sci. Rep. *8*, 1–9.

Koshiba, T., Detmer, S.A., Kaiser, J.T., Chen, H., McCaffery, J.M., and Chan, D.C. (2004). Structural basis of mitochondrial tethering by mitofusin complexes. Science *305*, 858–862.

Kundu, M., Lindsten, T., Yang, C.Y., Wu, J., Zhao, F., Zhang, J., Selak, M.A., Ney, P.A., and Thompson, C.B. (2008). Ulk1 plays a critical role in the autophagic clearance of mitochondria and ribosomes during reticulocyte maturation. Blood *112*, 1493–1502.

Kysela, D.T., Brown, P.J.B., Huang, K.C., and Brun, Y. V. (2013). Biological Consequences and Advantages of Asymmetric Bacterial Growth. Annu. Rev. Microbiol. *67*, 417–435.

Labbé, K., Murley, A., and Nunnari, J. (2014). Determinants and Functions of Mitochondrial Behavior. Annu. Rev. Cell Dev. Biol. *30*, 357–391.

Lallemand-Breitenbach, V., Jeanne, M., Benhenda, S., Nasr, R., Lei, M., Peres, L., Zhou, J., Zhu, J., Raught, B., and de Thé, H. (2008). Arsenic degrades PML or PML–RARα through a SUMO-triggered RNF4/ubiquitin-mediated pathway. Nat. Cell Biol. *10*, 547–555.

Lamoliatte, F., Caron, D., Durette, C., Mahrouche, L., Maroui, M.A., Caron-Lizotte, O., Bonneil, E., Chelbi-Alix, M.K., and Thibault, P. (2014). Large-scale analysis of lysine SUMOylation by SUMO remnant immunoaffinity profiling. Nat. Commun. *5*, 1–11.

Lane, N. (2015). The Vital Question. Why is life the way it is? (Profile Books LTD).

Lane, N., and Martin, W. (2010). The energetics of genome complexity. Nature *467*, 929–934.

Lax, N.Z., Gorman, G.S., and Turnbull, D.M. (2017). Review: Central nervous system involvement in mitochondrial disease. Neuropathol. Appl. Neurobiol. *43*, 102–118.

Leboucher, G.P., Tsai, Y.C., Yang, M., Shaw, K.C., Zhou, M., Veenstra, T.D., Glickman, M.H., and Weissman, A.M. (2012). Stress-Induced Phosphorylation and Proteasomal Degradation of Mitofusin 2 Facilitates Mitochondrial Fragmentation and Apoptosis. Mol. Cell *47*, 547–557.

Lee, D., and Kim, J.-E. (2018). PDI-mediated S-nitrosylation of DRP1 facilitates DRP1-S616 phosphorylation and mitochondrial fission in CA1 neurons. Cell Death Dis. *9*, 869–882.

Lee, J.Y., Kapur, M., Li, M., Choi, M.C., Choi, S., Kim, H.J., Kim, I., Lee, E., Taylor, J.P., and Yao, T.P. (2014). MFN1 deacetylation activates adaptive mitochondrial fusion and protects metabolically challenged mitochondria. J. Cell Sci. *127*, 4954–4963.

Lee, L., Seager, R., Nakamura, Y., Wilkinson, K.A., and Henley, J.M. (2019). Parkin-mediated ubiquitination contributes to the constitutive turnover of mitochondrial fission factor (Mff). PLoS One *14*, e0213116.

Lee, S., Sterky, F.H., Mourier, A., Terzioglu, M., Cullheim, S., Olson, L., and Larsson, N.-G. (2012). Mitofusin 2 is necessary for striatal axonal projections of midbrain dopamine neurons. Hum. Mol. Genet. *21*, 4827–4835.

Lee, Y., Jeong, S.-Y., Karbowski, M., Smith, C.L., and Youle, R.J. (2004). Roles of the mammalian mitochondrial fission and fusion mediators Fis1, Drp1, and Opa1 in apoptosis. Mol. Biol. Cell *15*, 5001–5011.

Legros, F., Lombès, A., Frachon, P., and Rojo, M. (2002). Mitochondrial Fusion in Human Cells Is Efficient, Requires the Inner Membrane Potential, and Is Mediated by Mitofusins. Mol. Biol. Cell *13*, 4343–4354.

Lennie, P. (2003). The cost of cortical computation. Curr. Biol. *13*, 493–497.

Leonard, A.P., Cameron, R.B., Speiser, J.L., Wolf, B.J., Peterson, Y.K., Schnellmann, R.G., Beeson, C.C., and Rohrer, B. (2015). Quantitative analysis of mitochondrial morphology and membrane potential in living cells using high-content imaging, machine learning, and morphological binning. Biochim. Biophys. Acta *1853*, 348–360.

Lewis, T.L., Kwon, S.K., Lee, A., Shaw, R., and Polleux, F. (2018). MFF-dependent mitochondrial fission regulates presynaptic release and axon branching by limiting axonal mitochondria size. Nat. Commun. *9*, 5008.

Li, J., Zeng, Z., Viollet, B., Ronnett, G. V, and McCullough, L.D. (2007). Neuroprotective effects of adenosine monophosphate-activated protein kinase inhibition and gene deletion in stroke.

Stroke *38*, 2992–2999.

Li, Z., Okamoto, K.-I., Hayashi, Y., and Sheng, M. (2004). The Importance of Dendritic Mitochondria in the Morphogenesis and Plasticity of Spines and Synapses. Cell *119*, 873–887.

Liang, Y.-C., Lee, C.-C., Yao, Y.-L., Lai, C.-C., Schmitz, M.L., and Yang, W.-M. (2016). SUMO5, a Novel Poly-SUMO Isoform, Regulates PML Nuclear Bodies. Sci. Rep. *6*, 1–15.

Liesa, M., Palacín, M., and Zorzano, A. (2009). Mitochondrial Dynamics in Mammalian Health and Disease. Physiol. Rev. *89*, 799–845.

Lindner, A.B., Madden, R., Demarez, A., Stewart, E.J., and Taddei, F. (2008). Asymmetric segregation of protein aggregates is associated with cellular aging and rejuvenation. Proc. Natl. Acad. Sci. *105*, 3076–3081.

Liu, R., and Chan, D.C. (2015). The mitochondrial fission receptor Mff selectively recruits oligomerized Drp1. Mol. Biol. Cell *26*, 4466–4477.

Lodish, H., Berk, A., Kaiser, C.A., and Krieger, M. (2007). Molecular cell biology (W. H. Freeman).

Loson, O.C., Song, Z., Chen, H., and Chan, D.C. (2013). Fis1, Mff, MiD49, and MiD51 mediate Drp1 recruitment in mitochondrial fission. Mol. Biol. Cell *24*, 659–667.

Macdonald, P.J., Stepanyants, N., Mehrotra, N., Mears, J.A., Qi, X., Sesaki, H., and Ramachandran, R. (2014). A dimeric equilibrium intermediate nucleates Drp1 reassembly on mitochondrial membranes for fission. Mol. Biol. Cell *25*, 1905–1915.

MacVicar, T., and Langer, T. (2016). OPA1 processing in cell death and disease - the long and short of it. J. Cell Sci. *129*, 2297–2306.

Mahajan, R., Delphin, C., Guan, T., Gerace, L., and Melchior, F. (1997). A small ubiquitin-related polypeptide involved in targeting RanGAP1 to nuclear pore complex protein RanBP2. Cell *88*, 97–107.

Mahul-Mellier, A.-L., Datler, C., Pazarentzos, E., Lin, B., Chaisaklert, W., Abuali, G., and Grimm, S. (2012). De-ubiquitinating proteases USP2a and USP2c cause apoptosis by stabilising RIP1. Biochim. Biophys. Acta - Mol. Cell Res. *1823*, 1353–1365.

Di Maio, R., Barrett, P.J., Hoffman, E.K., Barrett, C.W., Zharikov, A., Borah, A., Hu, X., McCoy, J., Chu, C.T., Burton, E.A., et al. (2016). α-synuclein binds to TOM20 and inhibits mitochondrial protein import in Parkinson's disease. Sci. Transl. Med. *8*, 1–26.

Manczak, M., and Reddy, P.H. (2012). Abnormal interaction of VDAC1 with amyloid beta and phosphorylated tau causes mitochondrial dysfunction in Alzheimer's disease. Hum. Mol. Genet. *21*, 5131–5146.

Manning, G., Plowman, G.D., Hunter, T., and Sudarsanam, S. (2002). Evolution of protein kinase signaling from yeast to man. Trends Biochem. Sci. *27*, 514–520.

Martin, S., Nishimune, A., Mellor, J.R., and Henley, J.M. (2007). SUMOylation regulates kainate-receptor-mediated synaptic transmission. Nature *447*, 321–325.

Martínez-Diez, M., Santamaría, G., Ortega, Á.D., and Cuezva, J.M. (2006). Biogenesis and Dynamics of Mitochondria during the Cell Cycle: Significance of 3′UTRs. PLoS One *1*, e107.

Matic, I., van Hagen, M., Schimmel, J., Macek, B., Ogg, S.C., Tatham, M.H., Hay, R.T., Lamond, A.I., Mann, M., and Vertegaal, A.C.O. (2008). In vivo identification of human small ubiquitin-like modifier polymerization sites by high accuracy mass spectrometry and an in vitro to in vivo strategy. Mol. Cell. Proteomics *7*, 132–144.

Matic, I., Schimmel, J., Hendriks, I.A., van Santen, M.A., van de Rijke, F., van Dam, H., Gnad, F., Mann, M., and Vertegaal, A.C.O. (2010). Site-specific identification of SUMO-2 targets in cells reveals an inverted SUMOylation motif and a hydrophobic cluster SUMOylation motif. Mol. Cell *39*, 641–652.

Mattie, S., Krols, M., and McBride, H.M. (2019). The enigma of an interconnected mitochondrial reticulum: new insights into mitochondrial fusion. Curr. Opin. Cell Biol. *59*, 159–166.

Matunis, M.J., Coutavas, E., and Blobel, G. (1996). A novel ubiquitin-like modification modulates the partitioning of the Ran-GTPase-activating protein RanGAP1 between the cytosol and the nuclear pore complex. J. Cell Biol. *135*, 1457–14570.

McBride, H.M., Neuspiel, M., Wasiak, S., Chan, D.C., Chen, H., Chan, D.C., Chen, H., Detmer, S.A., Ewald, A.J., Griffin, E.E., et al. (2006). Mitochondria: More Than Just a Powerhouse. Curr. Biol. *16*, 551–560.

McCullough, L.D., Zeng, Z., Li, H., Landree, L.E., McFadden, J., and Ronnett, G. V (2005). Pharmacological inhibition of AMP-activated protein kinase provides neuroprotection in stroke. J. Biol. Chem. *280*, 20493–20502.

Mears, J.A., Lackner, L.L., Fang, S., Ingerman, E., Nunnari, J., and Hinshaw, J.E. (2011). Conformational changes in Dnm1 support a contractile mechanism for mitochondrial fission. Nat.

Struct. Mol. Biol. *18*, 20–27.

Meek, D.W., and Anderson, C.W. (2009). Posttranslational modification of p53: cooperative integrators of function. Cold Spring Harb. Perspect. Biol. *1*, a000950.

Mertins, P., Mani, D.R., Ruggles, K. V., Gillette, M.A., Clauser, K.R., Wang, P., Wang, X., Qiao, J.W., Cao, S., Petralia, F., et al. (2016). Proteogenomics connects somatic mutations to signalling in breast cancer. Nature *534*, 55–62.

Michalska, B.M., Kwapiszewska, K., Szczepanowska, J., Kalwarczyk, T., Patalas-Krawczyk, P., Szczepański, K., Hołyst, R., Duszyński, J., and Szymański, J. (2018). Insight into the fission mechanism by quantitative characterization of Drp1 protein distribution in the living cell. Sci. Rep. *8*, 1–15.

Mink, J.W., Blumenschine, R.J., and Adams, D.B. (1981). Ratio of central nervous system to body metabolism in vertebrates: Its constancy and functional basis. Am. J. Physiol. - Regul. Integr. Comp. Physiol. *10*, 203–212.

Misgeld, T., and Schwarz, T.L. (2017). Mitostasis in Neurons: Maintaining Mitochondria in an Extended Cellular Architecture. Neuron *96*, 651–666.

Mishra, P., Carelli, V., Manfredi, G., and Chan, D.C. (2014). Proteolytic cleavage of Opa1 stimulates mitochondrial inner membrane fusion and couples fusion to oxidative phosphorylation. Cell Metab. *19*, 630–641.

Misko, A., Jiang, S., Wegorzewska, I., Milbrandt, J., and Baloh, R.H. (2010). Mitofusin 2 is necessary for transport of axonal mitochondria and interacts with the Miro/Milton complex. J. Neurosci. *30*, 4232–4240.

Molina, A.J.A., Wikstrom, J.D., Stiles, L., Las, G., Mohamed, H., Elorza, A., Walzer, G., Twig, G., Katz, S., Corkey, B.E., et al. (2009). Mitochondrial networking protects beta-cells from nutrient-induced apoptosis. Diabetes *58*, 2303–2315.

Mootha, V.K., Handschin, C., Arlow, D., Xie, X., St Pierre, J., Sihag, S., Yang, W., Altshuler, D., Puigserver, P., Patterson, N., et al. (2004). Erralpha and Gabpa/b specify PGC-1alpha-dependent oxidative phosphorylation gene expression that is altered in diabetic muscle. Proc. Natl. Acad. Sci. U. S. A. *101*, 6570–6575.

Morris, J.R., Boutell, C., Keppler, M., Densham, R., Weekes, D., Alamshah, A., Butler, L., Galanty, Y., Pangon, L., Kiuchi, T., et al. (2009). The SUMO modification pathway is involved in the BRCA1

response to genotoxic stress. Nature *462*, 886–890.

Mozdy, A.D., McCaffery, J.M., and Shaw, J.M. (2000). Dnm1p GTPase-mediated mitochondrial fission is a multi-step process requiring the novel integral membrane component Fis1p. J. Cell Biol. *151*, 367–380.

Müller, S., Berger, M., Lehembre, F., Seeler, J.-S., Haupt, Y., and Dejean, A. (2000). c-Jun and p53 Activity Is Modulated by SUMO-1 Modification. J. Biol. Chem. *275*, 13321–13329.

Mungai, P.T., Waypa, G.B., Jairaman, A., Prakriya, M., Dokic, D., Ball, M.K., and Schumacker, P.T. (2011). Hypoxia Triggers AMPK Activation through Reactive Oxygen Species-Mediated Activation of Calcium Release-Activated Calcium Channels. Mol. Cell. Biol. *31*, 3531–3545.

Murley, A., and Nunnari, J. (2016). The Emerging Network of Mitochondria-Organelle Contacts. Mol. Cell *61*, 648–653.

Nacerddine, K., Lehembre, F., Bhaumik, M., Artus, J., Cohen-Tannoudji, M., Babinet, C., Pandolfi, P.P., and Dejean, A. (2005). The SUMO Pathway Is Essential for Nuclear Integrity and Chromosome Segregation in Mice. Dev. Cell *9*, 769–779.

Nakada, K., Inoue, K., Ono, T., Isobe, K., Ogura, A., Goto, Y.-I., Nonaka, I., and Hayashi, J.-I. (2001). Inter-mitochondrial complementation: Mitochondria-specific system preventing mice from expression of disease phenotypes by mutant mtDNA. Nat. Med. *7*, 934–940.

Nakamura, N., Kimura, Y., Tokuda, M., Honda, S., and Hirose, S. (2006). MARCH-V is a novel mitofusin 2- and Drp1-binding protein able to change mitochondrial morphology. EMBO Rep. *7*, 1019–1022.

Neuspiel, M., Zunino, R., Gangaraju, S., Rippstein, P., and McBride, H. (2005). Activated mitofusin 2 signals mitochondrial fusion, interferes with Bax activation, and reduces susceptibility to radical induced depolarization. J. Biol. Chem. *280*, 25060–25070.

Nunnari, J., and Suomalainen, A. (2012). Mitochondria: In sickness and in health. Cell *148*, 1145–1159.

Nussinov, R., Tsai, C.-J., Xin, F., and Radivojac, P. (2012). Allosteric post-translational modification codes. Trends Biochem. Sci. *37*, 447–455.

Oakhill, J.S., Scott, J.W., and Kemp, B.E. (2012). AMPK functions as an adenylate charge-regulated protein kinase. Trends Endocrinol. Metab. *23*, 125–132.

Olichon, A., Emorine, L.J., Descoins, E., Pelloquin, L., Brichese, L., Gas, N., Guillou, E., Delettre, C., Valette, A., Hamel, C.P., et al. (2002). The human dynamin-related protein OPA1 is anchored to the mitochondrial inner membrane facing the inter-membrane space. FEBS Lett. *523*, 171–176.

Olichon, A., Baricault, L., Gas, N., Guillou, E., Valette, A., Belenguer, P., and Lenaers, G. (2003). Loss of OPA1 perturbates the mitochondrial inner membrane structure and integrity, leading to cytochrome c release and apoptosis. J. Biol. Chem. *278*, 7743–7746.

Ono, T., Isobe, K., Nakada, K., and Hayashi, J.-I. (2001). Human cells are protected from mitochondrial dysfunction by complementation of DNA products in fused mitochondria. Nat. Genet. *28*, 272–275.

Ordureau, A., Sarraf, S.A., Duda, D.M., Heo, J.-M., Jedrychowski, M.P., Sviderskiy, V.O., Olszewski, J.L., Koerber, J.T., Xie, T., Beausoleil, S.A., et al. (2014). Quantitative Proteomics Reveal a Feedforward Mechanism for Mitochondrial PARKIN Translocation and Ubiquitin Chain Synthesis. Mol. Cell *56*, 360–375.

Osellame, L.D., Blacker, T.S., and Duchen, M.R. (2012). Cellular and molecular mechanisms of mitochondrial function. Best Pract. Res. Clin. Endocrinol. Metab. *26*, 711–723.

Osellame, L.D., Singh, A.P., Stroud, D.A., Palmer, C.S., Stojanovski, D., Ramachandran, R., and Ryan, M.T. (2016). Cooperative and independent roles of the Drp1 adaptors Mff, MiD49 and MiD51 in mitochondrial fission. J. Cell Sci. *129*, 2170–2181.

Otera, H., Wang, C., Cleland, M.M., Setoguchi, K., Yokota, S., Youle, R.J., and Mihara, K. (2010). Mff is an essential factor for mitochondrial recruitment of Drp1 during mitochondrial fission in mammalian cells. J. Cell Biol. *191*, 1141–1158.

Otera, H., Miyata, N., Kuge, O., and Mihara, K. (2016). Drp1-dependent mitochondrial fission via MiD49/51 is essential for apoptotic cristae remodeling. J. Cell Biol. *212*, 531–544.

Owerbach, D., McKay, E.M., Yeh, E.T.H., Gabbay, K.H., and Bohren, K.M. (2005). A proline-90 residue unique to SUMO-4 prevents maturation and sumoylation. Biochem. Biophys. Res. Commun. *337*, 517–520.

Palacino, J.J., Sagi, D., Goldberg, M.S., Krauss, S., Motz, C., Wacker, M., Klose, J., and Shen, J. (2004). Mitochondrial Dysfunction and Oxidative Damage in parkin-deficient Mice. J. Biol. Chem. *279*, 18614–18622.

Palmer, C.S., Osellame, L.D., Laine, D., Koutsopoulos, O.S., Frazier, A.E., and Ryan, M.T. (2011).

MiD49 and MiD51, new components of the mitochondrial fission machinery. EMBO Rep. *12*, 565–573.

Palmer, C.S., Elgass, K.D., Parton, R.G., Osellame, L.D., Stojanovski, D., and Ryan, M.T. (2013). Adaptor proteins MiD49 and MiD51 can act independently of Mff and Fis1 in Drp1 recruitment and are specific for mitochondrial fission. J. Biol. Chem. *288*, 27584–27593.

Pan, C., Kumar, C., Bohl, S., Klingmueller, U., and Mann, M. (2009). Comparative proteomic phenotyping of cell lines and primary cells to assess preservation of cell type-specific functions. Mol. Cell. Proteomics *8*, 443–450.

Park, Y.Y., Nguyen, O.T.K., Kang, H., and Cho, H. (2014). MARCH5-mediated quality control on acetylated Mfn1 facilitates mitochondrial homeostasis and cell survival. Cell Death Dis. *5*, 1172–1184.

Parone, P.A., Da Cruz, S., Tondera, D., Mattenberger, Y., James, D.I., Maechler, P., Barja, F., and Martinou, J.-C. (2008). Preventing mitochondrial fission impairs mitochondrial function and leads to loss of mitochondrial DNA. PLoS One *3*, e3257.

Peng, J.-Y., Lin, C.-C., Chen, Y.-J., Kao, L.-S., Liu, Y.-C., Chou, C.-C., Huang, Y.-H., Chang, F.-R., Wu, Y.-C., Tsai, Y.-S., et al. (2011). Automatic morphological subtyping reveals new roles of caspases in mitochondrial dynamics. PLoS Comput. Biol. *7*, e1002212.

Perez, F.A., and Palmiter, R.D. (2005). Parkin-deficient mice are not a robust model of parkinsonism. Proc. Natl. Acad. Sci. U. S. A. *102*, 2174–2179.

Pernas, L., and Scorrano, L. (2016). Mito-Morphosis: Mitochondrial Fusion, Fission, and Cristae Remodeling as Key Mediators of Cellular Function. Annu. Rev. Physiol. *78*, 505–531.

Pham, A.H., Meng, S., Chu, Q.N., and Chan, D.C. (2012). Loss of Mfn2 results in progressive, retrograde degeneration of dopaminergic neurons in the nigrostriatal circuit. Hum. Mol. Genet. *21*, 4817–4826.

Pickrell, A.M., Huang, C.H., Kennedy, S.R., Ordureau, A., Sideris, D.P., Hoekstra, J.G., Harper, J.W., and Youle, R.J. (2015). Endogenous Parkin Preserves Dopaminergic Substantia Nigral Neurons following Mitochondrial DNA Mutagenic Stress. Neuron *87*, 371–381.

Piquereau, J., Caffin, F., Novotova, M., Lemaire, C., Veksler, V., Garnier, A., Ventura-Clapier, R., and Joubert, F. (2013). Mitochondrial dynamics in the adult cardiomyocytes: Which roles for a highly specialized cell? Front. Physiol. *4*, 1–12.

Polke, J.M., Laurá, M., Pareyson, D., Taroni, F., Milani, M., Bergamin, G., Gibbons, V.S., Houlden, H., Chamley, S.C., Blake, J., et al. (2011). Recessive axonal Charcot-Marie-Tooth disease due to compound heterozygous mitofusin 2 mutations. Neurology *77*, 168–173.

Prabakaran, S., Lippens, G., Steen, H., and Gunawardena, J. (2012). Post-translational modification: nature's escape from genetic imprisonment and the basis for dynamic information encoding. WIREs Syst Biol Med.

Prudden, J., Pebernard, S., Raffa, G., Slavin, D.A., Perry, J.J.P., Tainer, J.A., McGowan, C.H., and Boddy, M.N. (2007). SUMO-targeted ubiquitin ligases in genome stability. EMBO J. *26*, 4089–4101.

Prudent, J., Zunino, R., Sugiura, A., Mattie, S., Shore, G.C., and McBride, H.M. (2015). MAPL SUMOylation of Drp1 Stabilizes an ER/Mitochondrial Platform Required for Cell Death. Mol. Cell *59*, 941–955.

Pyakurel, A., Savoia, C., Hess, D., and Scorrano, L. (2015). Extracellular regulated kinase phosphorylates mitofusin 1 to control mitochondrial morphology and apoptosis. Mol. Cell *58*, 244–254.

Rambold, A.S., Kostelecky, B., Elia, N., and Lippincott-Schwartz, J. (2011). Tubular network formation protects mitochondria from autophagosomal degradation during nutrient starvation. Proc. Natl. Acad. Sci. U. S. A. *108*, 10190–10195.

Rangaraju, V., Calloway, N., and Ryan, T.A. (2014). Activity-Driven Local ATP Synthesis Is Required for Synaptic Function. Cell *156*, 825–835.

Rhein, V., Song, X., Wiesner, A., Ittner, L.M., Baysang, G., Meier, F., Ozmen, L., Bluethmann, H., Dröse, S., Brandt, U., et al. (2009). Amyloid-β and tau synergistically impair the oxidative phosphorylation system in triple transgenic Alzheimer's disease mice. Proc. Natl. Acad. Sci. U. S. A. *106*, 20057–20062.

Rocca, D.L., Wilkinson, K.A., and Henley, J.M. (2017). SUMOylation of FOXP1 regulates transcriptional repression via CtBP1 to drive dendritic morphogenesis. Sci. Rep. *7*, 877.

Rosonina, E., Akhter, A., Dou, Y., Babu, J., and Sri Theivakadadcham, V.S. (2017). Regulation of transcription factors by sumoylation. Transcription *8*, 220–231.

Ross, F.A., MacKintosh, C., and Hardie, D.G. (2016). AMP-activated protein kinase: a cellular energy sensor that comes in 12 flavours. FEBS J. *283*, 2987–3001.

Ross, J.M., Stewart, J.B., Hagström, E., Brené, S., Mourier, A., Coppotelli, G., Freyer, C., Lagouge, M., Hoffer, B.J., Olson, L., et al. (2013). Germline mitochondrial DNA mutations aggravate ageing and can impair brain development. Nature *501*, 412–415.

Rousset, C.I., Leiper, F.C., Kichev, A., Gressens, P., Carling, D., Hagberg, H., and Thornton, C. (2015). A dual role for AMP-activated protein kinase (AMPK) during neonatal hypoxic-ischaemic brain injury in mice. J. Neurochem. *133*, 242–252.

Saitoh, H., and Hinchey, J. (2000). Functional heterogeneity of small ubiquitin-related protein modifiers SUMO-1 versus SUMO-2/3. J. Biol. Chem. *275*, 6252–6258.

Sanderson, T.H., Raghunayakula, S., and Kumar, R. (2015). Neuronal hypoxia disrupts mitochondrial fusion. Neuroscience *301*, 71–78.

Santel, A., and Fuller, M. (2000). Control of mitochondrial morphology by human mitofusin. J. Cell Sci. *114*, 867–874.

Santel, A., Frank, S., Gaume, B., Herrler, M., Youle, R.J., and Fuller, M.T. (2003). Mitofusin-1 protein is a generally expressed mediator of mitochondrial fusion in mammalian cells. J. Cell Sci. *116*, 2763–2774.

Saotome, M., Safiulina, D., Szabadkai, G., Das, S., Fransson, A., Aspenstrom, P., Rizzuto, R., and Hajnóczky, G. (2008). Bidirectional Ca2+-dependent control of mitochondrial dynamics by the Miro GTPase. Proc. Natl. Acad. Sci. U. S. A. *105*, 20728–20733.

Sato, Y., Nakajima, S., Shiraga, N., Atsumi, H., Yoshida, S., Koller, T., Gerig, G., and Kikinis, R. (1998). Three-dimensional multi-scale line filter for segmentation and visualization of curvilinear structures in medical images. Med. Image Anal. *2*, 143–168.

Schaefer, A.M., McFarland, R., Blakely, E.L., He, L., Whittaker, R.G., Taylor, R.W., Chinnery, P.F., and Turnbull, D.M. (2008). Prevalence of mitochondrial DNA disease in adults. Ann. Neurol. *63*, 35–39.

Schreiber, S.N., Emter, R., Hock, M.B., Knutti, D., Cardenas, J., Podvinec, M., Oakeley, E.J., and Kralli, A. (2004). The estrogen-related receptor alpha (ERRalpha) functions in PPARgamma coactivator 1alpha (PGC-1alpha)-induced mitochondrial biogenesis. Proc. Natl. Acad. Sci. U. S. A. *101*, 6472–6477.

Schwarz, T.L. (2013). Mitochondrial trafficking in neurons. Cold Spring Harb. Perspect. Biol. *5*, a011304.

Selfridge, J.E., Lezi, E., Lu, J., and Swerdlow, R.H. (2013). Role of mitochondrial homeostasis and dynamics in Alzheimer's disease. Neurobiol. Dis. *51*, 3–12.

Shamseldin, H.E., Alshammari, M., Al-Sheddi, T., Salih, M.A., Alkhalidi, H., Kentab, A., Repetto, G.M., Hashem, M., and Alkuraya, F.S. (2012). Genomic analysis of mitochondrial diseases in a consanguineous population reveals novel candidate disease genes. J. Med. Genet. *49*, 234–241.

Shan, J., Zhao, W., and Gu, W. (2009). Suppression of cancer cell growth by promoting cyclin D1 degradation. Mol. Cell *36*, 469–476.

Sheng, Z.-H., and Cai, Q. (2012). Mitochondrial transport in neurons: impact on synaptic homeostasis and neurodegeneration. Nat. Rev. Neurosci. *13*, 77–93.

Shin, E.J., Shin, H.M., Nam, E., Kim, W.S., Kim, J.-H., Oh, B.-H., and Yun, Y. (2012). DeSUMOylating isopeptidase: a second class of SUMO protease. EMBO Rep. *13*, 339–346.

Sliter, D.A., Martinez, J., Hao, L., Chen, X., Sun, N., Fischer, T.D., Burman, J.L., Li, Y., Zhang, Z., Narendra, D.P., et al. (2018). Parkin and PINK1 mitigate STING-induced inflammation. Nature *561*, 258–262.

Smirnova, E., Griparic, L., Shurland, D.L., and Van der Bliek, A.M. (2001). Dynamin-related protein Drp1 is required for mitochondrial division in mammalian cells. Mol. Biol. Cell *12*, 2245–2256.

Smith, L.M., Kelleher, N.L., Proteomics, T.C. for T.D., Linial, M., Goodlett, D., Langridge-Smith, P., Goo, Y.A., Safford, G., Bonilla*, L., Kruppa, G., et al. (2013). Proteoform: a single term describing protein complexity. Nat. Methods *10*, 186–187.

Song, W., Bossy, B., Martin, O.J., Hicks, A., Lubitz, S., Knott, A.B., and Bossy-Wetzel, E. (2008). Assessing mitochondrial morphology and dynamics using fluorescence wide-field microscopy and 3D image processing. Methods *46*, 295–303.

Spoel, S.H. (2018). Orchestrating the proteome with post-translational modifications. J. Exp. Bot. *69*, 4499–4503.

Sriramachandran, A.M., and Dohmen, R.J. (2014). SUMO-targeted ubiquitin ligases. Biochim. Biophys. Acta - Mol. Cell Res. *1843*, 75–85.

Stankovic-Valentin, N., Drzewicka, K., König, C., Schiebel, E., and Melchior, F. (2016). Redox regulation of SUMO enzymes is required for ATM activity and survival in oxidative stress. EMBO J. *35*, 1312–1329.

Stevenson, L.F., Sparks, A., Allende-Vega, N., Xirodimas, D.P., Lane, D.P., and Saville, M.K. (2007). The deubiquitinating enzyme USP2a regulates the p53 pathway by targeting Mdm2. EMBO J. *26*, 976–986.

Stewart, J.B., and Chinnery, P.F. (2015). The dynamics of mitochondrial DNA heteroplasmy: Implications for human health and disease. Nat. Rev. Genet. *16*, 530–542.

Stojanovski, D., Koutsopoulos, O.S., Okamoto, K., and Ryan, M.T. (2004). Levels of human Fis1 at the mitochondrial outer membrane regulate mitochondrial morphology. J. Cell Sci. *117*, 1201–1210.

Su, Y.-F., Shyu, Y.-C., Shen, C.-K.J., and Hwang, J. (2012). Phosphorylation-dependent SUMOylation of the transcription factor NF-E2. PLoS One *7*, e44608.

Suen, D.-F., Narendra, D.P., Tanaka, A., Manfredi, G., and Youle, R.J. (2010). Parkin overexpression selects against a deleterious mtDNA mutation in heteroplasmic cybrid cells. Proc. Natl. Acad. Sci. U. S. A. *107*, 11835–11840.

Sugioka, R., Shimizu, S., and Tsujimoto, Y. (2004). Fzo1, a protein involved in mitochondrial fusion, inhibits apoptosis. J. Biol. Chem. *279*, 52726–52734.

Sukhorukov, V.M., Dikov, D., Reichert, A.S., and Meyer-Hermann, M. (2012). Emergence of the Mitochondrial Reticulum from Fission and Fusion Dynamics. PLoS Comput. Biol. *8*, e1002745.

Sun, H., Leverson, J.D., and Hunter, T. (2007). Conserved function of RNF4 family proteins in eukaryotes: targeting a ubiquitin ligase to SUMOylated proteins. EMBO J. *26*, 4102–4112.

Swatek, K.N., and Komander, D. (2016). Ubiquitin modifications. Cell Res. *26*, 399–422.

Taguchi, N., Ishihara, N., Jofuku, A., Oka, T., and Mihara, K. (2007). Mitotic phosphorylation of dynamin-related GTPase Drp1 participates in mitochondrial fission. J. Biol. Chem. *282*, 11521–11529.

Tanaka, A., Cleland, M.M., Xu, S., Narendra, D.P., Suen, D.-F., Karbowski, M., and Youle, R.J. (2010). Proteasome and p97 mediate mitophagy and degradation of mitofusins induced by Parkin. J. Cell Biol. *191*, 1367–1380.

Tanner, C.B., Madsen, S.R., Hallowell, D.M., Goring, D.M.J., Moore, T.M., Hardman, S.E., Heninger, M.R., Atwood, D.R., and Thomson, D.M. (2013). Mitochondrial and performance adaptations to exercise training in mice lacking skeletal muscle LKB1. Am. J. Physiol. Endocrinol. Metab. *305*, E1018-1029.

Tatham, M.H., Jaffray, E., Vaughan, O.A., Desterro, J.M.P., Botting, C.H., Naismith, J.H., and Hay, R.T. (2001). Polymeric Chains of SUMO-2 and SUMO-3 Are Conjugated to Protein Substrates by SAE1/SAE2 and Ubc9. J. Biol. Chem. *276*, 35368–35374.

Tatham, M.H., Geoffroy, M.-C., Shen, L., Plechanovova, A., Hattersley, N., Jaffray, E.G., Palvimo, J.J., and Hay, R.T. (2008). RNF4 is a poly-SUMO-specific E3 ubiquitin ligase required for arsenic-induced PML degradation. Nat. Cell Biol. *10*, 538–546.

Thomas, E.C., Hook, S.C., Gray, A., Chadt, A., Carling, D., Al-Hasani, H., Heesom, K.J., Hardie, D.G., and Tavaré, J.M. (2018). Isoform-specific AMPK association with TBC1D1 is reduced by a mutation associated with severe obesity. Biochem. J. *475*, 2969–2983.

Thornton, C. (2017). AMPK: keeping the (power)house in order? Neuronal Signal. *1*, NS20160020.

Tian, W., Li, W., Chen, Y., Yan, Z., Huang, X., Zhuang, H., Zhong, W., Chen, Y., Wu, W., Lin, C., et al. (2015). Phosphorylation of ULK1 by AMPK regulates translocation of ULK1 to mitochondria and mitophagy. FEBS Lett. *589*, 1847–1854.

Tilokani, L., Nagashima, S., Paupe, V., and Prudent, J. (2018). Mitochondrial dynamics: overview of molecular mechanisms. Essays Biochem. *62*, 341–360.

Tondera, D., Grandemange, S., Jourdain, A., Karbowski, M., Mattenberger, Y., Herzig, S., Da Cruz, S., Clerc, P., Raschke, I., Merkwirth, C., et al. (2009). SlP-2 is required for stress-induced mitochondrial hyperfusion. EMBO J. *28*, 1589–1600.

Toyama, E.Q., Herzig, S., Courchet, J., Lewis, T.L., Loson, O.C., Hellberg, K., Young, N.P., Chen, H., Polleux, F., Chan, D.C., et al. (2016). AMP-activated protein kinase mediates mitochondrial fission in response to energy stress. Science. *351*, 275–281.

Trifunovic, A., Wredenberg, A., Falkenberg, M., Spelbrink, J.N., Rovio, A.T., Bruder, C.E., Bohlooly-Y, M., Gldlöf, S., Oldfors, A., Wibom, R., et al. (2004). Premature ageing in mice expressing defective mitochondrial DNA polymerase. Nature *429*, 417–423.

Twig, G., Elorza, A., Molina, A.J.A., Mohamed, H., Wikstrom, J.D., Walzer, G., Stiles, L., Haigh, S.E., Katz, S., Las, G., et al. (2008a). Fission and selective fusion govern mitochondrial segregation and elimination by autophagy. EMBO J. *27*, 433–446.

Twig, G., Hyde, B., and Shirihai, O.S. (2008b). Mitochondrial fusion, fission and autophagy as a quality control axis: the bioenergetic view. Biochim. Biophys. Acta *1777*, 1092–1097.

Uchimura, Y., Nakamura, M., Sugasawa, K., Nakao, M., and Saitoh, H. (2004). Overproduction of eukaryotic SUMO-1- and SUMO-2-conjugated proteins in Escherichia coli. Anal. Biochem. *331*, 204–206.

Ulrich, H.D. (2008). The fast-growing business of SUMO chains. Mol. Cell *32*, 301–305.

Uzunova, K., Göttsche, K., Miteva, M., Weisshaar, S.R., Glanemann, C., Schnellhardt, M., Niessen, M., Scheel, H., Hofmann, K., Johnson, E.S., et al. (2007). Ubiquitin-dependent proteolytic control of SUMO conjugates. J. Biol. Chem. *282*, 34167–34175.

Valente, A.J., Maddalena, L.A., Robb, E.L., Moradi, F., and Stuart, J.A. (2017). A simple ImageJ macro tool for analyzing mitochondrial network morphology in mammalian cell culture. Acta Histochem. *3*, 315–326.

Valente, E.M., Abou-Sleiman, P.M., Caputo, V., Muqit, M.M.K., Harvey, K., Gispert, S., Ali, Z., Del Turco, D., Bentivoglio, A.R., Healy, D.G., et al. (2004). Hereditary early-onset Parkinson's disease caused by mutations in PINK1. Science. *304*, 1158–1160.

Vanhatupa, S., Ungureanu, D., Paakkunainen, M., and Silvennoinen, O. (2008). MAPK-induced Ser727 phosphorylation promotes SUMOylation of STAT1. Biochem. J. *409*, 179–185.

Varanita, T., Soriano, M.E., Romanello, V., Zaglia, T., Quintana-Cabrera, R., Semenzato, M., Menabò, R., Costa, V., Civiletto, G., Pesce, P., et al. (2015). The OPA1-dependent mitochondrial cristae remodeling pathway controls atrophic, apoptotic, and ischemic tissue damage. Cell Metab. *21*, 834–844.

Verstreken, P., Ly, C. V., Venken, K.J.T., Koh, T.-W., Zhou, Y., and Bellen, H.J. (2005). Synaptic Mitochondria Are Critical for Mobilization of Reserve Pool Vesicles at Drosophila Neuromuscular Junctions. Neuron *47*, 365–378.

Vu, L.D., Gevaert, K., and De Smet, I. (2018). Protein Language: Post-Translational Modifications Talking to Each Other. Trends Plant Sci. *23*, 1068–1080.

Wai, T., and Langer, T. (2016). Mitochondrial Dynamics and Metabolic Regulation. Trends Endocrinol. Metab. *27*, 105–117.

Wakabayashi, J., Zhang, Z., Wakabayashi, N., Tamura, Y., Fukaya, M., Kensler, T.W., Iijima, M., and Sesaki, H. (2009). The dynamin-related GTPase Drp1 is required for embryonic and brain development in mice. J. Cell Biol. *186*, 805–816.

Wang, H., Song, P., Du, L., Tian, W., Yue, W., Liu, M., Li, D., Wang, B., Zhu, Y., Cao, C., et al.

(2011). Parkin ubiquitinates Drp1 for proteasome-dependent degradation: Implication of dysregulated mitochondrial dynamics in Parkinson disease. J. Biol. Chem. *286*, 11649–11658.

Wang, L., Wansleeben, C., Zhao, S., Miao, P., Paschen, W., and Yang, W. (2014). SUMO2 is essential while SUMO3 is dispensable for mouse embryonic development. EMBO Rep. *15*, 878–885.

Wappler, E.A., Institoris, A., Dutta, S., Katakam, P.V.G., and Busija, D.W. (2013). Mitochondrial dynamics associated with oxygen-glucose deprivation in rat primary neuronal cultures. PLoS One *8*, e63206.

Wasiak, S., Zunino, R., and McBride, H.M. (2007). Bax/Bak promote sumoylation of DRP1 and its stable association with mitochondria during apoptotic cell death. J. Cell Biol. *177*, 439–450.

Waterham, H.R., Koster, J., van Roermund, C.W.T., Mooyer, P.A.W., Wanders, R.J.A., Leonard, J. V, Roermund, C.W.T. Van, Mooyer, P.A.W., Wanders, R.J.A., and Leonard, J. V (2015). A Lethal Defect of Mitochondrial and Peroxisomal Fission. N. Engl. J. Med. *356*, 1736–1741.

Watts, F.Z. (2004). SUMO modification of proteins other than transcription factors. Semin. Cell Dev. Biol. *15*, 211–220.

Watts, Z., Skilton, A., Boyd, K., Trickey, M., Gardner, L., Ogi, X., and Outwin, A. (2007). Regulation of Protein Function by SUMO Modification Regulation of Protein Function by SUMO Modification.

Wei, W., Yang, P., Pang, J., Zhang, S., Wang, Y., Wang, M.-H., Dong, Z., She, J.-X., and Wang, C.-Y. (2008). A stress-dependent SUMO4 sumoylation of its substrate proteins. Biochem. Biophys. Res. Commun. *375*, 454–459.

Wilkinson, K.A., and Henley, J.M. (2010). Mechanisms, regulation and consequences of protein SUMOylation. Biochem. J. *428*, 133–145.

Woods, A., Johnstone, S.R., Dickerson, K., Leiper, F.C., Fryer, L.G.D., Neumann, D., Schlattner, U., Wallimann, T., Carlson, M., and Carling, D. (2003). LKB1 Is the Upstream Kinase in the AMP-Activated Protein Kinase Cascade. Curr. Biol. *13*, 2004–2008.

Woods, A., Dickerson, K., Heath, R., Hong, S.P., Momcilovic, M., Johnstone, S.R., Carlson, M., and Carling, D. (2005). Ca2+/calmodulin-dependent protein kinase kinase-β acts upstream of AMP-activated protein kinase in mammalian cells. Cell Metab. *2*, 21–33.

Wu, H., Carvalho, P., and Voeltz, G.K. (2018). Here, there, and everywhere: The importance of ER membrane contact sites. Science *361*, 1–11.

Wu, W., Tian, W., Hu, Z., Chen, G., Huang, L., Li, W., Zhang, X., Xue, P., Zhou, C., Liu, L., et al. (2014). ULK1 translocates to mitochondria and phosphorylates FUNDC1 to regulate mitophagy. EMBO Rep. *15*, 566–575.

Xiao, B., Sanders, M.J., Underwood, E., Heath, R., Mayer, F. V., Carmena, D., Jing, C., Walker, P.A., Eccleston, J.F., Haire, L.F., et al. (2011). Structure of mammalian AMPK and its regulation by ADP. Nature *472*, 230–233.

Xu, S., Wang, P., Zhang, H., Gong, G., Gutierrez Cortes, N., Zhu, W., Yoon, Y., Tian, R., and Wang, W. (2016a). CaMKII induces permeability transition through Drp1 phosphorylation during chronic β-AR stimulation. Nat. Commun. *7*, 1–13.

Xu, S., Cherok, E., Das, S., Li, S., Roelofs, B.A., Ge, S.X., Polster, B.M., Boyman, L., Lederer, W.J., Wang, C., et al. (2016b). Mitochondrial E3 ubiquitin ligase MARCH5 controls mitochondrial fission and cell sensitivity to stress-induced apoptosis through regulation of MiD49 protein. Mol. Biol. Cell *27*, 349–359.

Yang, S.-H., Jaffray, E., Hay, R.T., and Sharrocks, A.D. (2003). Dynamic interplay of the SUMO and ERK pathways in regulating Elk-1 transcriptional activity. Mol. Cell *12*, 63–74.

Yang, W., Sheng, H., Warner, D.S., and Paschen, W. (2008). Transient Focal Cerebral Ischemia Induces a Dramatic Activation of Small Ubiquitin-Like Modifier Conjugation. J. Cereb. Blood Flow Metab. *28*, 892–896.

Yau, R., and Rape, M. (2016). The increasing complexity of the ubiquitin code. Nat. Cell Biol. *18*, 579–586.

Yin, Y., Seifert, A., Chua, J.S., Maure, J.-F., Golebiowski, F., and Hay, R.T. (2012). SUMO-targeted ubiquitin E3 ligase RNF4 is required for the response of human cells to DNA damage. Genes Dev. *26*, 1196–1208.

Yonashiro, R., Ishido, S., Kyo, S., Fukuda, T., Goto, E., Matsuki, Y., Ohmura-Hoshino, M., Sada, K., Hotta, H., Yamamura, H., et al. (2006). A novel mitochondrial ubiquitin ligase plays a critical role in mitochondrial dynamics. EMBO J. *25*, 3618–3626.

Youle, R.J., and Van Der Bliek, A.M. (2012). Mitochondrial fission, fusion, and stress. Science. *337*, 1062–1065.

Yu, R., Liu, T., Jin, S.-B., Ning, C., Lendahl, U., Nistér, M., and Zhao, J. (2017). MIEF1/2 function as adaptors to recruit Drp1 to mitochondria and regulate the association of Drp1 with Mff. Sci.

Rep. *7*, 880.

Yu, R., Jin, S., Lendahl, U., Nistér, M., and Zhao, J. (2019). Human Fis1 regulates mitochondrial dynamics through inhibition of the fusion machinery. EMBO J. *38*, 1–21.

Yu, T., Sheu, S.-S., Robotham, J.L., and Yoon, Y. (2008). Mitochondrial fission mediates high glucose-induced cell death through elevated production of reactive oxygen species. Cardiovasc. Res. *79*, 341–351.

Zachari, M., and Ganley, I.G. (2017). The mammalian ULK1 complex and autophagy initiation. Essays Biochem. *61*, 585–596.

Zahedi, A., On, V., Phandthong, R., Chaili, A., Remark, G., Bhanu, B., and Talbot, P. (2018). Deep Analysis of Mitochondria and Cell Health Using Machine Learning. Sci. Rep. *8*, 16354.

Zhang, F.-P., Mikkonen, L., Toppari, J., Palvimo, J.J., Thesleff, I., and Janne, O.A. (2008a). Sumo-1 Function Is Dispensable in Normal Mouse Development. Mol. Cell. Biol. *28*, 5381–5390.

Zhang, X.-D., Goeres, J., Zhang, H., Yen, T.J., Porter, A.C.G., and Matunis, M.J. (2008b). SUMO-2/3 modification and binding regulate the association of CENP-E with kinetochores and progression through mitosis. Mol. Cell *29*, 729–741.

Zhao, J., Liu, T., Jin, S., Wang, X., Qu, M., Uhlén, P., Tomilin, N., Shupliakov, O., Lendahl, U., and Nistér, M. (2011). Human MIEF1 recruits Drp1 to mitochondrial outer membranes and promotes mitochondrial fusion rather than fission. EMBO J. *30*, 2762–2778.

Zhong, S., Müller, S., Ronchetti, S., Freemont, P.S., Dejean, A., and Pandolfi, P.P. (2000). Role of SUMO-1-modified PML in nuclear body formation. Blood *95*, 2748–2752.

Zinovkina, L.A. (2018). Mechanisms of Mitochondrial DNA Repair in Mammals. Biochem. *83*, 233–249.

Zong, H., Ren, J.M., Young, L.H., Pypaert, M., Mu, J., Birnbaum, M.J., and Shulman, G.I. (2002). AMP kinase is required for mitochondrial biogenesis in skeletal muscle in response to chronic energy deprivation. Proc. Natl. Acad. Sci. U. S. A. *99*, 15983–15987.

Zunino, R., Schauss, A., Rippstein, P., Andrade-Navarro, M., and McBride, H.M. (2007). The SUMO protease SENP5 is required to maintain mitochondrial morphology and function. J. Cell Sci. *120*, 1178–1188.

Zunino, R., Braschi, E., Xu, L., and McBride, H.M. (2009). Translocation of SenP5 from the

nucleoli to the mitochondria modulates DRP1-dependent fission during mitosis. J. Biol. Chem. *284*, 17783–17795.

Chapter 8 Appendix

Here I have included supplementary data that, either due to time constraints, lack of repeats or not central to the main narrative was not included in the main results sections, but nonetheless are of interest and may lead to new avenues of investigation. Included at the back is published work , reporting parkin-mediate ubiquitination of MFF in its constitutive turnover (Lee *et al*., 2019).

Bacterial MFF SUMOylation

It is unlikely that bacteria can maintain a SUMO chain, so the SUMO-MFF band in bacteria expressing SUMO and MFF (Figure 8.1) is likely a mono SUMO-MFF species, and due to steric effects, resolves higher than expected.

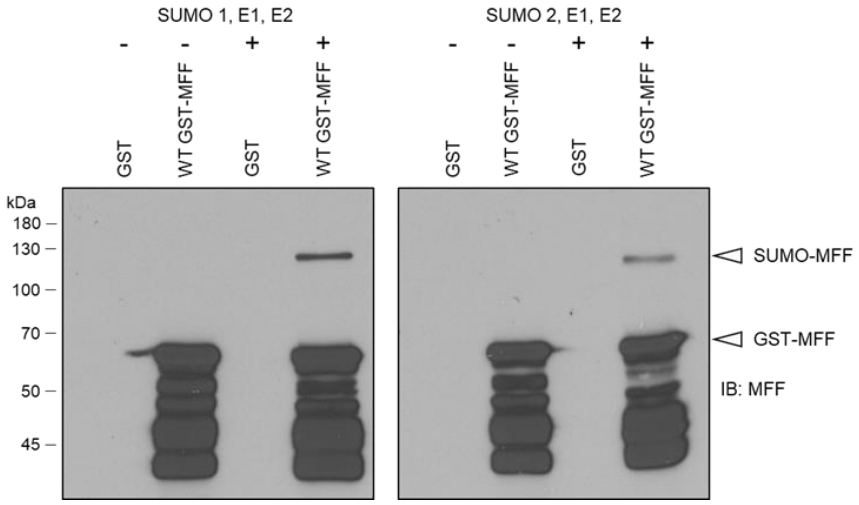

Figure 8.1 Bacterial MFF SUMOylation assay

GST and GST-MFF expressing contructs were transformed into bacteria in presence or absence of a construct expressing SUMO-1, E1 and E2. GST-MFF expression was activated by 0.5mM IPTG and incubated at room temperature for 6hrs. Cells were lysed in 1x sample buffer, sonicated and boiled. Lysate resolved and probed for MFF expression, method described in Uchimura *et al*., 2004.

MFF SUMOylation in AMPK α-null cells

To more directly test the importance of AMPK-mediated phosphorylation of MFF on SUMOylation, I used HEK cells null for both AMPK-α subunits, a kind gift from Professor Jeremy Tavaré (Thomas *et al*., 2018). I tested modification of wildtype-MFF with SUMO-1 and observed SUMOylated MFF is almost completely abolished by ablation of AMPK.

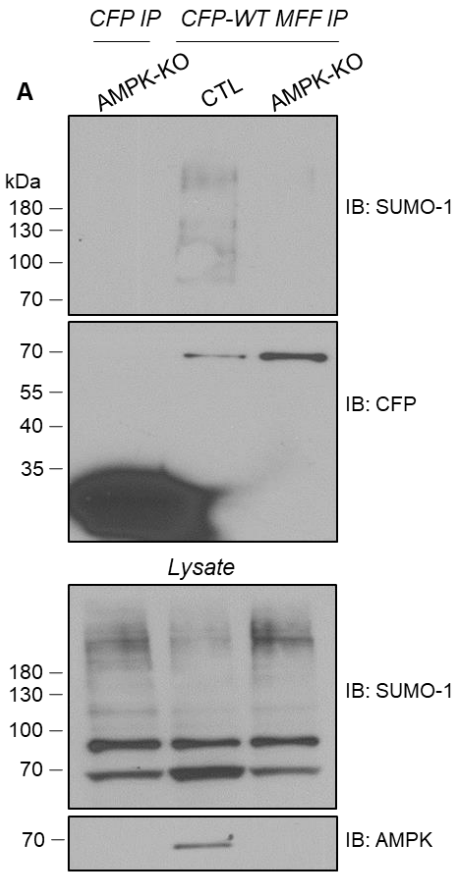

Figure 8.2 MFF SUMOylation in AMPK-α null cells

AMPK-α subunit-null or control HEK cells were trasiently tranfected with wildtype CFP-MFF for 2 days. GFP immunoprecipitation carried out on lysate and resolved by SDS-PAGE and probed for endogenous SUMO-1. Lysate was probed for SUMO-1 and AMPK-α, n=1.

Effect of MFF 2SA and 2SD on neuronal mitochondria

To confirm previous observations that MFF double phospho-mimetic (2SD) acts as a gain of function (Toyama *et al*., 2016), I transiently transfected 2SA and 2SD CFP-tagged MFF constructs into primary hippocampal neurons. I observe smaller mitochondria with 2SD, and larger mitochondria in 2SA expressing cells, confirming previous findings.

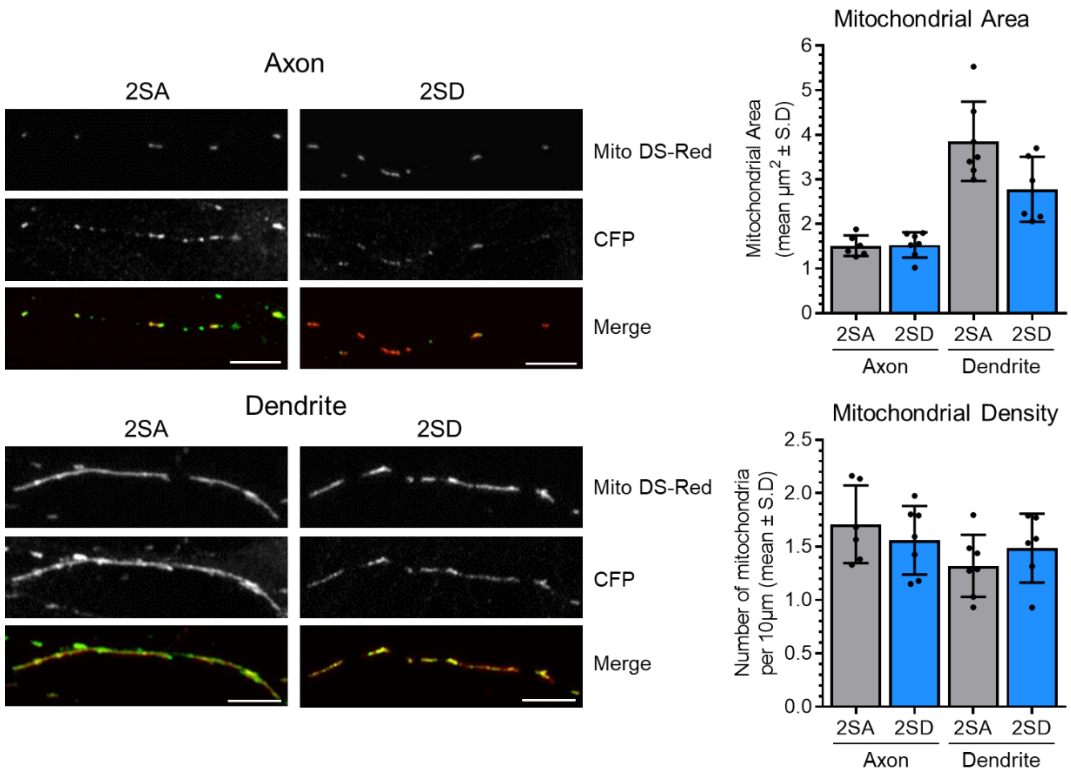

Figure 8.3 MFF phosphorylation-induced mitochondrial changes in neurons

DIV 14 hippocampal neurons were co-transfected for two days with 1µg Mito DS-Red and either CFP-MFF 2SA or 2SD. Following fixation, neurons were stained for ankyrin-G and GFP to enahnce CFP signal. Scale bar 20µm. Mitochondrial area and mitochondrial density analysed for axons and dendrites. Data gathered from one culture, 7 cells analysed per condition.

Non-covalent interaction between SUMO-1 and MiD49

I repeated the blot in Figure 4.4 with just MiD49, and confirm the observation made that MiD49 non-covalently interacts with SUMO-1.

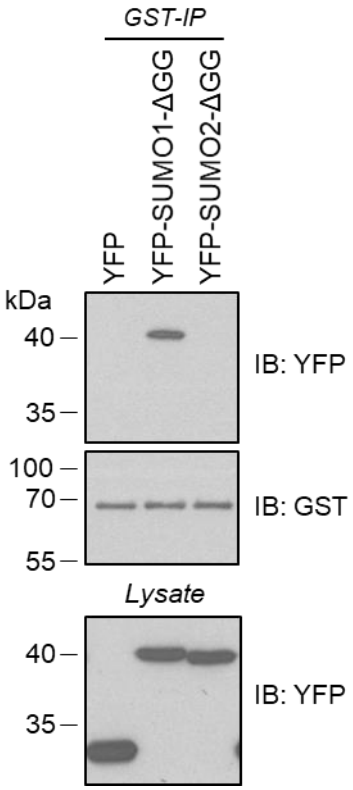

Figure 8.4 MiD49 contains a SIM for SUMO-1

HEK293T cells were transiently co-transfected with GST-MiD49 (mouse) and either YFP, YFP-SUMO1-ΔGG or YFP-SUMO2-ΔGG for 48hrs. GST pulldown carried out on supernatant and samples were blotted for YFP and GST. 4% lysate blotted for YFP.

Putative SUMO Interacting motifs (SIM) of DRP1 and MiD49

DRP1 putative SIM

Results for putatifs SIM [PSmax=38.183 | Cut-off=2.032]					
Position site	Sequence	Type	a/S stretch	PS	DB Hit
AA 28-31	ADIIQLPQIVVVGTQSSGKS	SIM Type a	[N][SIM][Y]	3.012	
AA 144-147	SPNVVNLTLVDLPGMTKVPV	SIM Type 1	[N][SIM][N]	2.379	

MiD49 putative SIM

Results for putatifs SIM [PSmax=38.183 | Cut-off=0.269]					
Position site	Sequence	Type	a/S stretch	PS	DB Hit
AA 199-202	ADHVRLLVPLVLEPGLWSLV	SIM Type 4	[N][SIM][N]	0.352	
AA 301-304	QHERLELTVAVLVAVPGVDA	SIM Type 2	[N][SIM][N]	1.583	1

Figure 8.5 Putative SIM motifs in human DRP1 and MiD49

The DRP1 and MiD49 sequences (Uniprot entries: O00429 and Q96C03, respectively) were input into the Joined Advanced SUMOylation Site and Sim Analyser (JASSA, www.jassa.fr) which identifies possible regions of SUMOylation and SIMs. Both DRP1 and MiD49 contain sites of possible SIM motifs, and so should be investigated further as having potential roles in the regulation of SUMO-mediated mitochondrial dynamics.

PLOS ONE

RESEARCH ARTICLE

Parkin-mediated ubiquitination contributes to the constitutive turnover of mitochondrial fission factor (Mff)

Laura Lee, Richard Seager, Yasuko Nakamura, Kevin A. Wilkinson, Jeremy M. Henley*

School of Biochemistry, Centre for Synaptic Plasticity, Biomedical Sciences Building, University of Bristol, Bristol, United Kingdom

* j.m.henley@bristol.ac.uk

Citation: Lee L, Seager R, Nakamura Y, Wilkinson KA, Henley JM (2019) Parkin-mediated ubiquitination contributes to the constitutive turnover of mitochondrial fission factor (Mff). PLoS ONE 14(5): e0213116. https://doi.org/10.1371/journal.pone.0213116

Editor: David Chau, University College London, UNITED KINGDOM

Received: February 14, 2019

Accepted: May 6, 2019

Published: May 21, 2019

Data Availability Statement: All relevant data are within the manuscript and its Supporting Information files.

Funding: We are grateful to the British Heart Foundation (PG/14/60/31014; JMH), Wellcome Trust (105384/Z/14/A, studentship to RS), MRC (MR/L003791; KAW, JMH) and BBSRC (BB/R00787X; KAW, JMH) for financial support. The funders had no role in study design, data collection and analysis, decision to publish, or preparation of the manuscript.

Abstract

The mitochondrial outer membrane protein Mitochondrial Fission Factor (Mff) plays a key role in both physiological and pathological fission. It is well established that at stressed or functionally impaired mitochondria, PINK1 recruits the ubiquitin ligase Parkin which ubiquitinates Mff and other mitochondrial outer membrane proteins to facilitate the removal of defective mitochondria and maintain the integrity of the mitochondrial network. Here we show that, in addition to this clearance pathway, Parkin also ubiquitinates Mff in a PINK1-dependent manner under non-stressed conditions to regulate constitutive Mff turnover. We further show that removing Parkin via shRNA-mediated knockdown does not completely prevent Mff ubiquitination under these conditions, indicating that at least one other ubiquitin ligase contributes to Mff proteostasis. These data suggest that that Parkin plays a role in physiological maintenance of mitochondrial membrane protein composition in unstressed cells through constitutive low-level activation.

Introduction

Mitochondria are double membrane-bound organelles that generate 90% of cellular ATP [1]. In most cells, mitochondria form extensive and dynamic networks, undergoing continuous cycles of fission and fusion. This creates a highly adaptable and efficient energy transfer system to rapidly deliver ATP to where it is most needed [2]. In addition, fission plays a central role in the sequestration and selective degradation of defective mitochondria by mitophagy [3, 4]. Mitochondrial fission and fusion are both tightly regulated processes that are largely orchestrated by GTPases. Dynamin and dynamin-related protein (Drp) mediate fission [5, 6] whereas fusion of the mitochondrial outer and inner membranes is driven by the GTPases mitofusins (Mfn) 1 and 2 and Opa1, respectively [7].

Dynamin-related protein 1 (Drp1) is a predominantly cytosolic protein with only ~3% bound to mitochondria under basal conditions [8]. Nonetheless, in cells lacking functional Drp1 the equilibrium between fission and fusion is perturbed, leading to highly elongated and interconnected mitochondria, largely localised in perinuclear clusters [9]. During cell stress,

Competing interests: The authors have declared that no competing interests exist.

rates of fission and fragmentation increase, causing the release of pro-apoptotic cytochrome *c* from mitochondria, a process that can be delayed by mutation or deletion of Drp1 [10].

Because Drp1 lacks the membrane targeting PH-domain present in conventional dynamins, it requires membrane-bound adaptor/receptor proteins to recruit it to the mitochondrial outer membrane (MOM) [11]. Four mitochondrial Drp1 receptors have been identified; Fis1, MiD49, MiD51 and Mff [12]. Of these, Fis1 is dispensable for mammalian mitochondrial fission [13]. The MiD proteins are specific to higher eukaryotes and although they can each recruit Drp1 to mitochondrial fission sites [14, 15] it remains unclear if MiD proteins facilitate fusion or inhibit fission [16]. Mff facilitates the majority of Drp1 recruitment and is the best characterised Drp1 receptor. It is a ~35kDa protein with a single C-terminal transmembrane domain and interacts with Drp1 via its N-terminus [17]. Like Drp1-null cells, Mff-knockout cells have grossly elongated mitochondria under basal conditions, and attenuated fragmentation and apoptosis following stress [18].

Parkin is a ubiquitin ligase that is inactive in the cytosol but is recruited to damaged/depolarised mitochondria where it is activated by the MOM protein PTEN-induced protein kinase 1 (PINK1). PINK1 is basally maintained at very low levels by rapid proteolytic degradation soon after mitochondrial import [19, 20]. However, loss of membrane potential in damaged or defective mitochondria inhibits PINK1-proteolysis, resulting in its accumulation on the outer membrane, where it phosphorylates mitochondrial ubiquitin at Serine 65 and triggers mitophagy via a multi-step process [21, 22].

Briefly, PINK1-phosphorylated ubiquitin (pUb) binds to and alters the conformation of Parkin. This makes Serine 65 within the Ubiquitin-like domain (UbL) of Parkin accessible for PINK1-mediated phosphorylation, which initiates a cascade of subsequent conformational changes exposing the catalytic site of Parkin [22–24]. In a positive-feedback loop, Parkin ubiquitinates mitochondrial proteins, providing further substrates for PINK1-mediated phosphorylation, which then recruit more Parkin [25, 26]. For example, mitophagy induced by the mitochondrial proton gradient uncoupler carbonyl cyanide m-chlorophenyl hydrazine (CCCP) is largely dependent on Parkin-mediated, non-selective ubiquitination of mitochondrial proteins with K48- and K63-linked ubiquitin chains [27, 28]. Mitochondrial depolarisation leads to PINK1 accumulation on the surface of mitochondria that recruits Parkin to indiscriminately tag MOM proteins with K48- linked ubiquitin chains, marking them for excision and proteasomal degradation [27, 29]. The remaining portion of the mitochondrion is then tagged with K63-linked ubiquitin that recruits phagosomal adaptors including p62 [30] resulting in the engulfment of the organelle into an autophagosome prior to lysosomal fusion and degradation [31, 32]. Thus, this elegant quality control mechanism identifies damaged mitochondria and targets proteins for degradation.

Moreover, in cells lacking functional PINK1 and/or Parkin, mitochondria undergo fragmentation due to excessive Drp1-mediated fission [33–35]. However, the roles of Parkin in non-stressed mitochondria have not been extensively investigated. Here we show that, independent of stress-induced mitophagy, Mff is ubiquitinated by Parkin and at least one other E3 ligase under basal conditions. Our data indicate that Parkin-mediated ubiquitination triggers lysosomal degradation of Mff, suggesting a role for Parkin in homeostatic maintenance of Mff levels and mitochondrial integrity.

Materials and methods

Molecular biology

21bp short hairpin (shRNA) constructs used in Figs 1–4: targeting human shParkin: `5′-ACCAGCATCTTCCAGCTCAAG-3′`

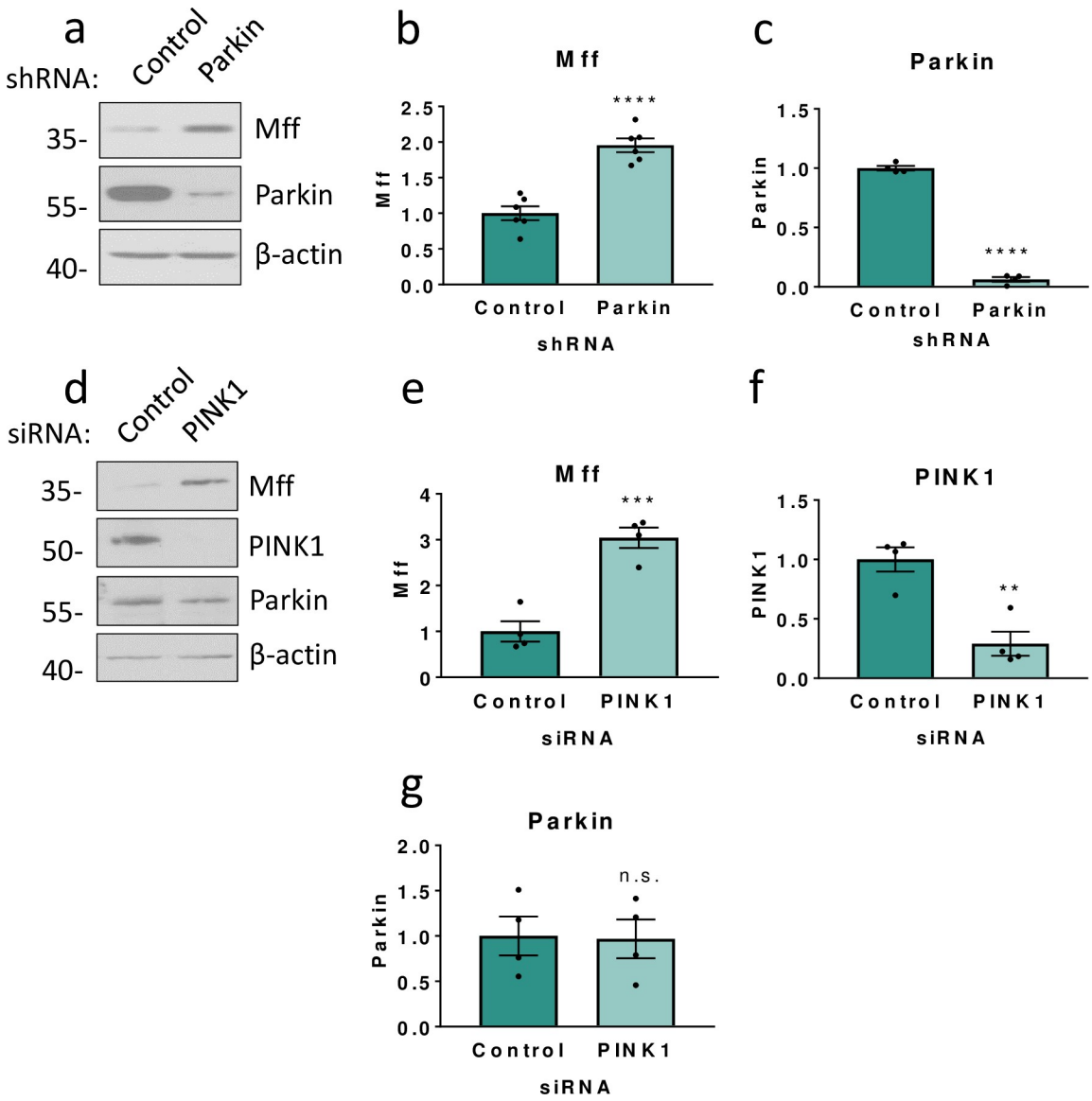

Fig 1. The PINK1/Parkin pathway is involved in Mff stability. a) HEK293T cells were transfected with either shRNA targeting human Parkin or a scrambled control shRNA. Western blots for Mff, Parkin and β-actin. N = 4–7. b,c) Quantitative analysis of Mff and Parkin levels using Student's unpaired t-test. d) HEK293T cells were transfected with either siRNA targeting human PINK1 or a control siRNA (firefly luciferase). Western blots for Mff, PINK1, Parkin and β-actin. N = 4. e,f,g) Quantitative analysis of Mff, PINK1 and Parkin levels. Data presented as mean ± SEM. ** $p < 0.01$, *** $p < 0.001$, **** $p < 0.0001$.

https://doi.org/10.1371/journal.pone.0213116.g001

non-specific shControl: 5′- AACGTACGCGGAATACTTCGA-3′

were cloned under a H1 promoter into a modified pSUPER vector co-expressing mCherry driven by a PGK promoter. Alternative Parkin shRNAs (S1 Fig) were cloned in the same way, with target sequences:

5′- GCTTAGACTGTTTCCACTTAT-3′ (Parkin (Berger))

5′-AACTCCAGCCATGGTTTCCCA-3′ (Parkin (other)).

Parkin (Berger) target sequence was previously published [36]. Other Parkin shRNA target sequences were designed as part of this study. PINK1 knockdown was performed using MISSION esiRNA human PINK1 (EHU057101, Sigma Aldrich). Mff knockdown (S2 Fig) was

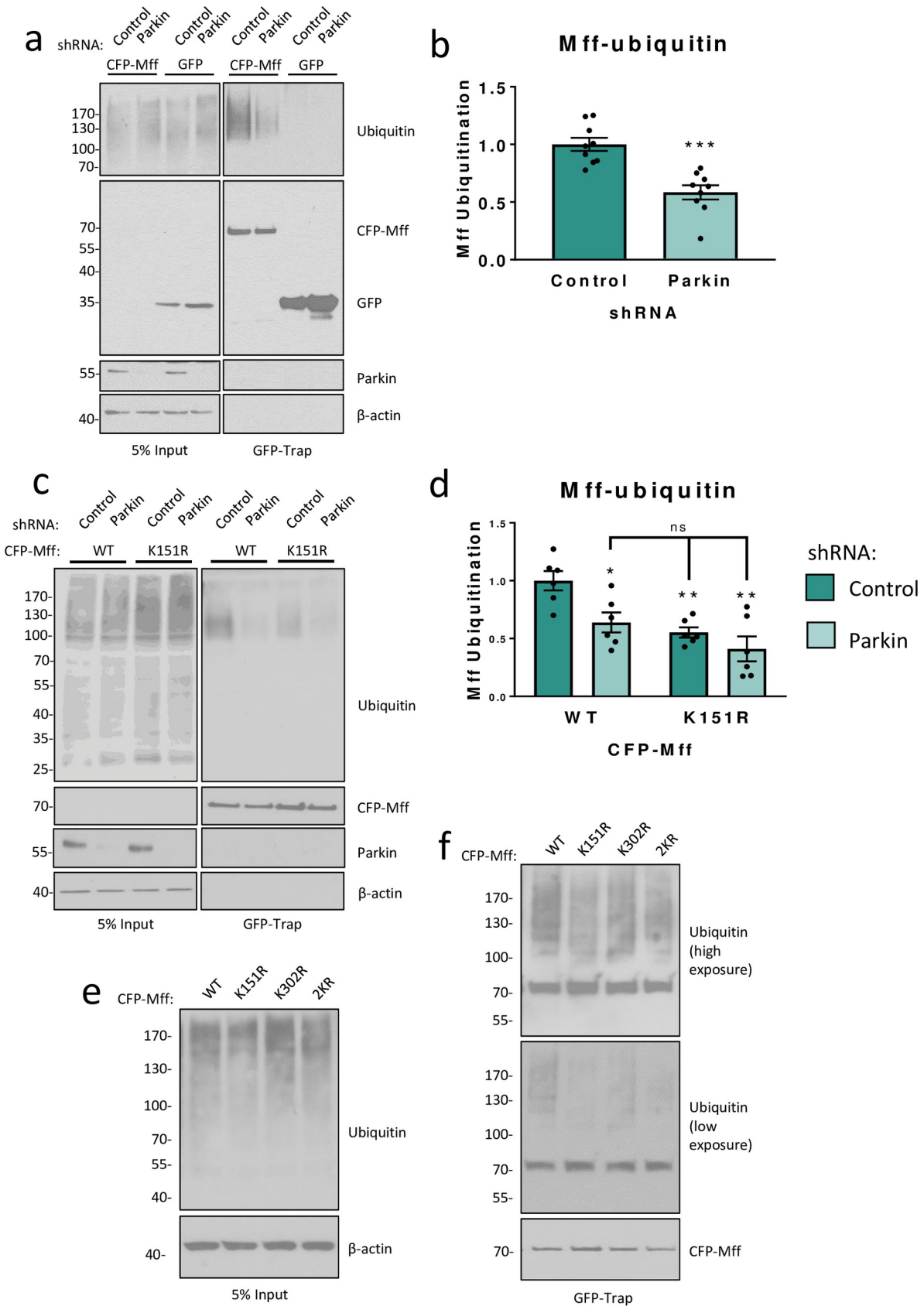
a
shRNA:
Control
Parkin
CFP-Mff
GFP
170-
130-
100-
70-
Ubiquitin
70-
55-
40-
35-
CFP-Mff
GFP
55-
Parkin
40-
β-actin
5% Input
GFP-Trap
b
Mff-ubiquitin
Mff Ubiquitination
1.5
1.0
0.5
0.0
***
Control
Parkin
shRNA
c
shRNA:
CFP-Mff:
WT
K151R
170-
130-
100-
70-
55-
40-
35-
25-
Ubiquitin
70-
CFP-Mff
55-
Parkin
40-
β-actin
5% Input
GFP-Trap
d
Mff-ubiquitin
Mff Ubiquitination
ns
*
**
**
WT
K151R
CFP-Mff
shRNA:
Control
Parkin
e
CFP-Mff:
WT
K151R
K302R
2KR
170-
130-
100-
70-
55-
40-
Ubiquitin
40-
β-actin
5% Input
f
CFP-Mff:
WT
K151R
K302R
2KR
170-
130-
100-
70-
55-
Ubiquitin
(high
exposure)
Ubiquitin
(low
exposure)
70-
CFP-Mff
GFP-Trap

Fig 2. Parkin ubiquitinates Mff at K151 under basal conditions. a) HEK293T cells were co-transfected with CFP-Mff or GFP and shRNA (scrambled control or Parkin-targeting). Western blots of GFP-immunoprecipitation. CFP-tagged Mff immunoprecipitates with endogenous, covalently attached ubiquitin. b) Knockdown of Parkin significantly reduces Mff ubiquitination. N = 9. Analysed using unpaired two-tailed Students' t-test. Data presented as mean ± SEM. $p < 0.001$. c) GFP-immunoprecipitations of exogenously expressed CFP-Mff WT or K151R in HEK293T cells reveal that the K151R mutant has significantly reduced endogenous ubiquitination compared to the WT. d) Quantitative analysis showing that knockdown of Parkin significantly reduces ubiquitination of WT CFP-Mff, but not CFP-Mff K151R. N = 6. Analysed using ordinary two-way ANOVA with Tukey's correction for multiple comparisons with a pooled variance. * $p < 0.05$, ** $p \leq 0.01$. e,f) Input and GFP-immunoprecipitations from HEK293T cells transfected with CFP-Mff WT or mutants showing that K151 and K302 are not the only sites of Mff ubiquitination. Replacement of lysine 151 or 302 with arginine reduces, but does not abolish, ubiquitination. Double replacement of K151 and K302 (2KR) also does not abolish ubiquitination, indicative of at least 1 other site.

https://doi.org/10.1371/journal.pone.0213116.g002

performed using siRNA with the target sequence 5′- CCAUUGAAGGAACGUCAGA-3′ (Eurofins genomics). Firefly Luciferase siRNA was used as a negative control (MISSION esiRNA Firefly Luciferase, EHUFLUC, Sigma Aldrich).

The open reading frame of human Mff (isoform I, accession number: Q9GZY8) was cloned into pECFP between 5' KpnI and 3' BamHI restriction sites. CFP-Mff expression was driven by a CMV promoter. The open reading frame of human Parkin (full length, accession number: O60260) was cloned into pcDNA3.1(+) between 5' HindIII and 3' BamHI restriction sites. Parkin expression was driven by a CMV promoter. CFP-Mff K151R, K302R and 2KR, Parkin S65A and S65D were generated by site-directed mutagenesis.

HEK293T cell culture and transfection

Human Embryonic Kidney (HEK293T) cells were obtained from The European Collection of Cell Cultures (ECACC). Cultures were maintained at 37˚C in a humidified cell culture incubator, supplied with 5% CO2, in Dulbecco's Modified Eagle's Medium (Lonza) supplemented with 10% (v/v) Foetal Bovine Serum (Sigma) and 2mM L-Glutamine (Gibco). For transfection, cells were plated on dishes pre-coated with 0.1mg/mL poly-L-lysine to promote adhesion. Lipofectamine 2000 transfection reagent (Invitrogen) was used according to manufacturer's protocol. Cells were lysed 48 hours (protein over-expression) or 72 hours (protein knock-down) post-transfection.

Protein biochemistry

For immunoblotting, cells were lysed in sample buffer (1x concentrate) containing 2% SDS (w/v), 5% glycerol (v/v), 62.5mM Tris-HCl pH6.8 and 5% (v/v) 2-β-mercaptoethanol. Lysates were heated to 95˚C for 10 minutes prior to gel electrophoresis. For immunoprecipitation, cells were lysed in lysis buffer containing 20mM Tris pH7.4, 137mM NaCl, 2mM sodium pyrophosphate, 2mM EDTA, 1% (v/v) Triton X-100, 0.1% (w/v) SDS, 25mM β-glycerophosphate, 10% glycerol (v/v), 1x cOmplete protease inhibitor cocktail (Roche) and 20mM N-Ethylmaleimide (NEM, Sigma). Lysates were incubated with GFP-Trap agarose beads (ChromoTek) at 4˚C for 90 minutes with gentle agitation. Beads were pelleted, washed 3 times with wash buffer (lysis buffer without protease inhibitor cocktail or NEM) and unbound material aspirated. 2x concentrate sample buffer was used to elute immunoprecipitated proteins from the beads. Samples were heated to 95˚C for 10 minutes prior to gel electrophoresis.

Denaturing SDS-PAGE was performed on 10–15% (v/v) poly-acrylamide gels. Western blotted PDVF membranes were blocked in 5% (w/v) non-fat milk powder or 4% (w/v) Bovine Serum Albumin (BSA, Sigma) in PBS-T. Primary antibodies used were: Parkin (mouse monoclonal, 1:1000, Santa Cruz sc-32282), Mff (mouse monoclonal, 1:1000, Santa Cruz sc-398731), PINK1 (rabbit monoclonal, 1:1000, Cell Signaling D83G 6946), ubiquitin (mouse monoclonal, 1:1000, P4D1 3936S), Mfn2 (rabbit monoclonal, 1:1000, Cell Signaling, D2D10 9482S), Mid49 (rabbit polyclonal, 1:1000, ProteinTech, I64I3-I-AP), VDAC (rabbit polyclonal, 1:1000, Santa

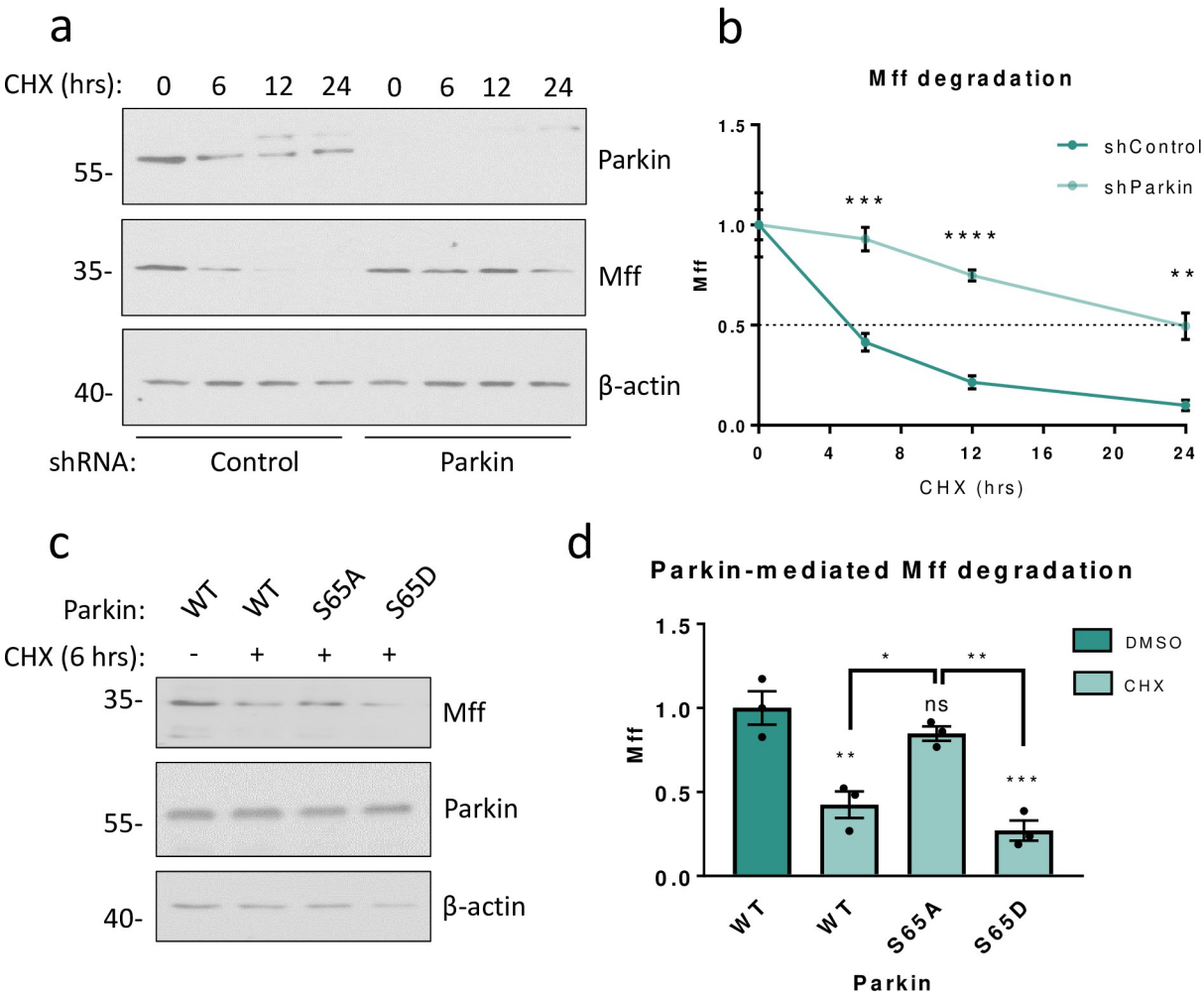

Fig 3. Parkin mediates PINK1-dependent degradation of Mff. a) HEK293T cells were transfected with either scrambled shRNA (control) or shRNA targeting human Parkin. Prior to lysis 72 hours post-transfection, cells were treated with 25μg/mL cycloheximide (CHX) for 0, 6, 12 or 24 hours (0-hour CHX received 24-hour DMSO treatment). Lysates were then Western blotted for Parkin, Mff and β-actin. b) Quantitative analysis of (a), data presented as mean ± SEM. Analysed using unpaired two-tailed Student's t-tests. N = 4. ** $p < 0.01$, *** $p < 0.001$, **** $p < 0.0001$. c) HEK293T cells were transfected with WT or mutant Parkin. Prior to lysis 48 hours post- transfection, cells were treated with 25μg/mL cycloheximide (CHX) for 6 hours (control treated with DMSO for 6 hours). Lysates were then Western blotted for Mff, Parkin and β-actin. d) Quantitative analysis of (c), data presented as mean ± SEM. Analysed using one-way ANOVA with Tukey's correction for multiple comparisons with a pooled variance. N = 3. * $p < 0.05$, ** $p < 0.01$, *** $p < 0.001$.

https://doi.org/10.1371/journal.pone.0213116.g003

Cruz, FL-283 sc-98708), Fis1 (rabbit monoclonal, 1:1500, ProteinTech, 10956-1-AP), LC3 (rabbit polyclonal, 1:1000, Cell Signaling, 2775S), GFP (rat monoclonal, 1:10,000, Chromotek 3H9), β-actin (mouse monoclonal, 1:10,000, Sigma-Aldrich A5441). For protein detection, membranes were incubated with HRP-conjugated secondary antibodies (1:10,000; Sigma-Aldrich) and visualised by enhanced chemiluminescence. Protein bands were quantified by densitometry using ImageJ (NIH). Mff- and Parkin-antibody specificity was validated by endogenous protein knockdown (S1 and S2 Figs).

Results

Knockdown of PINK1 or Parkin increase levels of Mff

We first investigated the effects of Parkin knockdown on Mff by transfecting HEK293T cells with plasmids encoding an shRNA sequence targeted to the human Parkin transcript

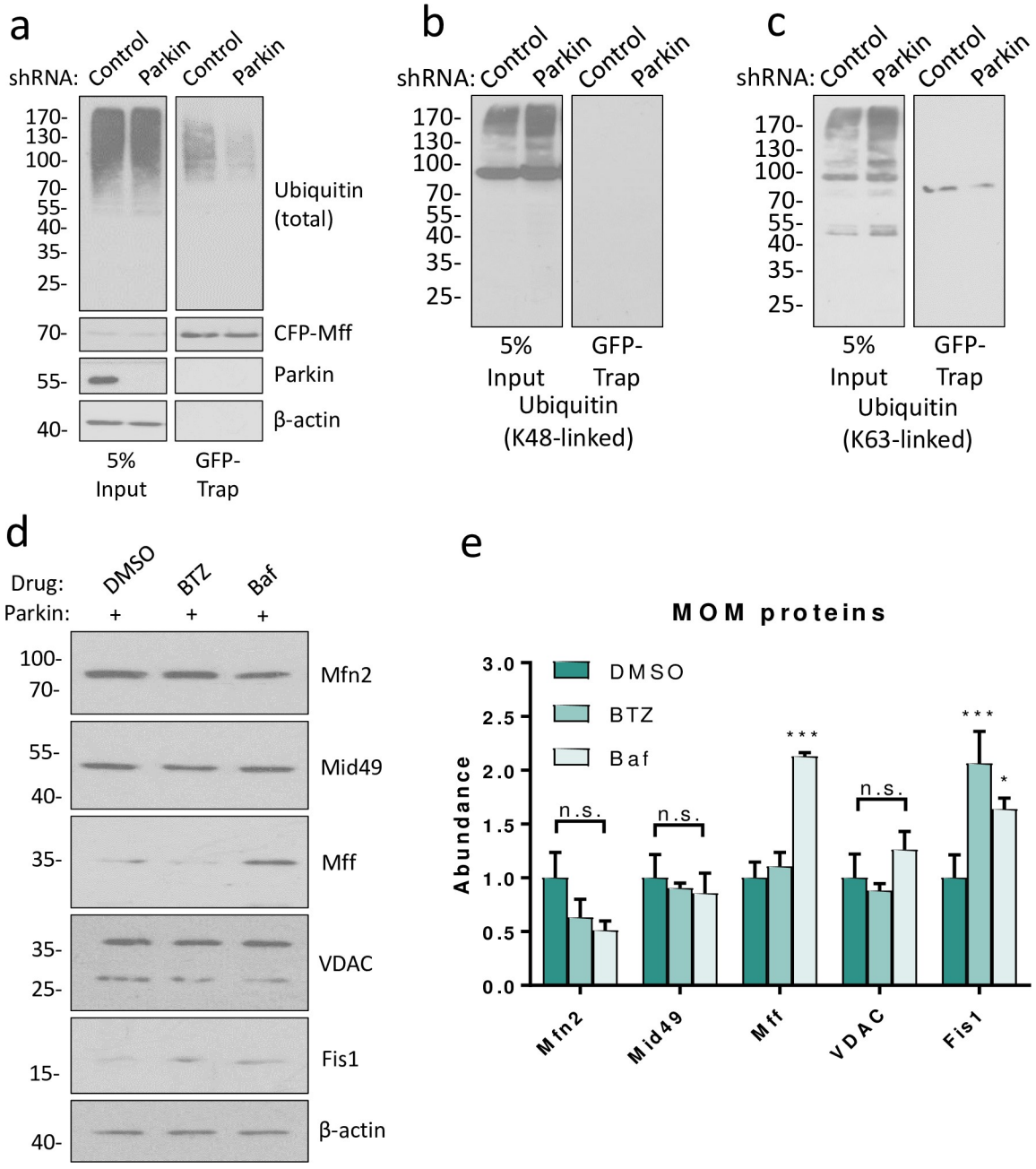

Fig 4. Parkin mediated degradation of Mff is lysosome-dependent. a) HEK293T cells were co-transfected with CFP-Mff or GFP and shRNA (scrambled control or Parkin-targeting). Western blots of GFP-immunoprecipitation. As in Fig 2, knockdown of Parkin reduces total Mff ubiquitination. b) Samples from (a), showing no co-immunoprecipitation of K48-linked ubiquitin with CFP-Mff. c) Samples from (a), showing co-immunoprecipitation of a single K63-linked ubiquitinated CFP-Mff species. d) HEK293T cells were transfected with untagged Parkin. Prior to lysis 48 hours post- transfection, cells were treated with DMSO (control), bortezomib (BTZ, proteasomal inhibitor, 1μM) or bafilomycin (Baf, lysosomal inhibitor, 100nM) for 6 hours. Lysates were then Western blotted for Mff and other mitochondrial membrane proteins. e) Quantitative analysis of (d), data presented as mean ± SEM. Analysed using ordinary two-way ANOVA with Dunnett's correction for multiple comparisons. N = 3. * $p < 0.05$, *** $p < 0.001$.

https://doi.org/10.1371/journal.pone.0213116.g004

(shParkin) or a control shRNA sequence. shParkin reduced Parkin levels to 6% of control levels 72 hours after transfection (Fig 1A and 1C). Consistent with Parkin-mediated degradation of Mff there was a corresponding increase in levels of Mff (Fig 1A and 1B). To exclude the

possibility of the Mff increase being due off-target effects of the Parkin shRNA, two further Parkin shRNAs were generated and tested in HEK293T cells, with the same effect on Mff levels (S1 Fig).

To determine if the effect of Parkin on Mff levels was PINK1-dependent we next knocked down PINK1 in HEK293T cells [1–3]. 72 hours post-transfection, PINK1 was significantly knocked down to 30% of control values (Fig 1D and 1F). As expected, loss of PINK1 also significantly increased total levels of Mff (Fig 1E). Moreover, total levels of Parkin were unaffected by knockdown of PINK1, indicating that it is Parkin activity, rather than expression, that causes the increase in Mff (Fig 1G).

Knockdown of Parkin reduces steady-state ubiquitination of Mff

Parkin has been reported to ubiquitinate Mff at K251 in HEK293 cells over-expressing HA-tagged Parkin and treated with CCCP to induce mitochondrial depolarisation [30]. Our data suggest that the PINK1/Parkin pathway may also control Mff levels in the absence of global or applied cell stress. To determine if endogenous Parkin regulates Mff expression under basal, non-stressed conditions, HEK293T cells were co-transfected with CFP-tagged Mff and shRNA targeting Parkin or a scrambled control. 72 hours after transfection, cells were lysed and CFP-Mff retained on GFP-Trap agarose beads. Steady-state levels of Mff ubiquitination were significantly decreased by Parkin knockdown (Figs 2A and 1B). These data demonstrate a role for Parkin in Mff ubiquitination that is not dependent on global mitochondrial stress.

Parkin ubiquitinates Mff at K151

A recent study has reported that Mff is phosphorylated by AMPK at conserved sites S155 and S172 (highlighted in S2 Fig) [37]. We hypothesised that, given its conservation and density of modifiable residues, this region could be a 'hotspot' for Mff post-translational modifications. We therefore selected K151 as an alternative possible target for ubiquitination. To specifically test if Parkin ubiquitinates Mff at K151 under basal conditions, HEK293T cells were co-transfected with CFP-Mff WT or a mutant in which lysine 151 had been replaced with a non-ubiquitinatable arginine (K151R), and either Parkin-targeting or control shRNA. 72 hours post-transfection, cells were lysed and GFP-Trap agarose beads used to precipitate CFP-Mff. Once again, knockdown of Parkin reduced levels of WT Mff ubiquitination (Fig 2C and 2D). However, Parkin knockdown had no significant effect on ubiquitination of CFP-Mff K151R, indicating that under these conditions Parkin preferentially ubiquitinates Mff at K151 (Fig 2C and 2D). Interestingly, while, CFP-Mff K151R had significantly reduced ubiquitination compared to WT, some ubiquitin modification was still present.

The Mff isoform used in the study by Gao et al [30] was isoform II (291 amino acids) which is a truncated protein, lacking a large portion of the N-terminus as well as a central region. Here we used Mff isoform I, which is the full-length protein comprising 342 amino acids. Accounting for these differences in the length of the isoforms, K251 in Isoform II corresponds to K302 in Isoform I (S2 Fig). We therefore generated a CFP-Mff mutant in which lysine 302 was replaced with arginine (K302R). HEK293T cells were co-transfected with CFP-Mff WT or K302R. 48 hours post-transfection, cells were lysed and GFP-Trap agarose beads used to precipitate CFP-Mff. Mutation of Mff K302 to arginine (K302R) reduced, but did not abolish, ubiquitination of Mff isoform I (Fig 2E and 2F). Furthermore, replacing both K151 and K302 with arginines (K151R and K302R; 2KR) also fails to abolish Mff ubiquitination (Fig 2E and 2F). These results indicate that Mff isoform I has several sites of ubiquitination under non-stressed conditions which include K151 and K302, as well as at least one other lysine.

Parkin mediates PINK1-dependent turnover of Mff

Our results show that Parkin knockdown significantly decreases Mff ubiquitination and increases Mff levels. We next directly tested the role of Parkin in Mff degradation. HEK293T cells were transfected with Parkin-targeting shRNA or a scrambled shRNA control. Prior to lysis 72 hours post-transfection, cells were treated with the protein translation inhibitor cycloheximide (CHX) for up to 24 hours. In cells expressing control shRNA ~90% of Mff was degraded within 24 hours, with a half-life of ~5 hours. In the Parkin knockdown cells, however, the rate of degradation was dramatically slower, increasing the half-life of Mff to ~24 hours (Fig 3A and 3B). Taken together, these data indicate that Parkin-mediated ubiquitination plays a role in physiological Mff degradation under non-stressed conditions.

Parkin ligase activity requires phosphorylation at S65 by PINK1 [22]. To further investigate the roles of Parkin and PINK1 in Mff turnover, we generated phospho-null (S65A) and phospho- mimetic (S65D) untagged Parkin S65 mutants. We reasoned that Parkin S65A would be unable to efficiently translocate to mitochondria or catalyse ubiquitin-transfer due to its PINK1-insensitivity, whereas Parkin S65D would be constitutively active.

HEK293T cells were transfected with WT, S65A or S65D Parkin. Prior to lysis 48 hours post-transfection, cells were treated with CHX or DMSO (vehicle control) for 6 hours. Samples were then Western blotted for Mff (Fig 3C and 3D). Levels of over-expressed Parkin WT, S65A and S65D relative to endogenous Parkin under the same conditions are shown in S3 Fig. Consistent with a PINK1-dependent role for Parkin in Mff turnover, expression of Parkin WT or S65D resulted in significant loss of Mff during 6 hours of inhibited protein translation, whereas Parkin S65A had no effect on Mff levels compared to control. These data demonstrate that PINK1-mediated activation via phosphorylation of Parkin at S65 is required for its activity in Mff turnover.

Parkin mediates specific lysosomal degradation of Mff

To establish whether constitutive Parkin-mediated degradation of Mff is mediated via the lysosome or the proteasome, we used GFP-Trap immunoprecipitation to pull down CFP-Mff from cells expressing control or Parkin-targeting shRNA. These samples were then probed for total ubiquitin, K48-linked ubiquitin and K63-linked ubiquitin (Fig 4A, 4B and 4C respectively). Indicative of Mff not being a proteasome substrate, no K48-linked ubiquitin was detected on CFP-Mff (Fig 4B). However, a single K63-linked ubiquitin-reactive species was present (Fig 4C), which was reduced in the absence of Parkin, suggesting a role for the lysosome in Parkin-mediated degradation of Mff.

We next investigated the mechanism of Parkin-mediated degradation of Mff by transfecting HEK293T cells with untagged WT Parkin and treating with the proteasomal inhibitor bortezomib [38] or bafilomycin, which inhibits fusion of the autophagosome and lysosome [39] for 6 hours. Over-expression of Parkin WT compared to non-transfected samples is shown in S3B Fig. The efficacy of proteasomal inhibition by 1μM bortezomib was demonstrated by the accumulation of high molecular weight ubiquitin conjugates and a reduction of free ubiquitin compared to DMSO or bafilomycin treatment (S3 Fig). The efficacy of autophagic inhibition by 100nM bafilomycin was confirmed by an increase in LC3-ii/i ratio (S3 Fig). Consistent with Parkin mediating lysosomal degradation of Mff, bafilomycin significantly increased Mff levels, whereas bortezomib treatment had no effect (Fig 4D and 4E). Interestingly, other MOM proteins tested (Mfn2, Mid49, VDAC) were not affected by bafilomycin, while Fis1 was increased by both proteasomal and lysosomal inhibition (Fig 4D and 4E). VDAC and Mfn2 have both been reported to be ubiquitinated by Parkin during induced mitophagy, yet neither were increased by inhibition of mitophagy under the basal conditions of this experiment [32, 40]. These data therefore suggest that under conditions of basal mitophagy, the Parkin-mediated

turnover of Mff far exceeds that of other MOM proteins, which could be indicative of an additional selective Parkin-mediated degradative pathway.

Discussion

Our data show that under basal conditions endogenous Parkin ubiquitinates Mff at K151. For this ubiquitination and subsequent Mff degradation Parkin needs to be activated by PINK1-dependent phosphorylation at S65. This Parkin-mediated ubiquitination of Mff coincides with Parkin-mediated Mff degradation, suggesting that Mff turnover is regulated by a Parkin-dependent, ubiquitin-mediated pathway. Mff is not a substrate of K48-linked ubiquitination but is a substrate of K63-linked ubiquitination. Furthermore, inhibition of the lysosome, but not the proteasome, rescues Mff from Parkin-mediated degradation. These data support a model in which Parkin-mediated degradation of Mff occurs via K63-linked ubiquitination and the lysosome. Interestingly, this activity appears to be in addition to mitophagy, in which depolarised mitochondria recruit Parkin to indiscriminately ubiquitinate MOM proteins prior to their degradation. Of the five MOM proteins assayed in Parkin-overexpressing cells, only Mff and, to a lesser extent, Fis1 were significantly rescued from degradation by inhibition of the lysosome (Fis1 was also rescued by proteasomal inhibition). Mfn2, Mid49 and VDAC were not significantly changed, despite Mfn2 and VDAC being known targets of CCCP-induced, Parkin-mediated mitophagy [32, 40, 41]. These data may indicate that mitophagy is not solely responsible for the changes we observe. Thus, we propose that Parkin may have a selective effect on the turnover of Mff, in addition to its role in mitophagy-dependent Mff degradation. The degradation of Mff by Parkin under basal conditions, together with its inactivity toward other known substrates under the same conditions, suggest that Parkin-mediated degradation of Mff is a regulatory mechanism independent of stress-dependent mechanisms. Moreover, since PINK1 is maintained at low levels in the MOM of healthy mitochondria, we propose that this mechanism plays a critical background role in maintaining mitochondrial integrity in the absence of induced stress.

Intriguingly, our data demonstrate that K302 is not the sole site of ubiquitination of Mff isoform I, and we identified an additional ubiquitination site at K151. However, even in mutants in which both K151 and K302 were ablated, residual Mff ubiquitination remained, indicating the presence of at least one other ubiquitination site. Moreover, our observation that ubiquitination of CFP-Mff K151R is unaffected by Parkin knockdown strongly suggests that the sole, or at least predominant, site of Parkin-mediated ubiquitination under non-stressed conditions is K151.

Our data, combined with previous reports of Mff ubiquitination and phosphorylation [30, 37] indicate Mff is subject to multiple post-translational modifications and suggest that the region around K151 could be an important regulatory 'hotspot'. Given its role as the primary receptor for Drp1 in mitochondrial fission, further work will be needed to elucidate how these modifications, and the interplay between them, regulate Mff abundance and activity in health and disease.

Supporting information

S1 Fig. Validation of Parkin antibody and knockdown constructs. a) Parkin antibody and shRNA are specific. HEK293T cells were transfected with control (scrambled sequence) shRNA or shRNA targeting human Parkin. Cells were lysed 72 hours post-transfection and lysates used for Western blotting with anti-Parkin antibody (Santa Cruz sc-32282). A single band of around 55kDa was detected (predicted MW: 52kDa), which was abolished by Parkin shRNA.

b) Effect of Parkin knockdown on Mff is specific. HEK293T cells were transfected with control (scrambled sequence) shRNA or one of 3 shRNAs targeting human Parkin. Cells were lysed 72

hours post-transfection and lysates used for Western blotting with anti-Parkin antibody (Santa Cruz sc-32282) and anti-Mff antibody (Santa Cruz sc-398731). shRNA construct target sequences: Parkin (blue) 5′-ACCAGCATCTTCCAGCTCAAG-3′, Parkin-Berger (purple) 5′-GCTTAGACTGTTTCCACTTAT-3′, Parkin-other (red) 5′-AACTCCAGCCATGGTTTCCCA-3′. Parkin (Berger) shRNA target sequence taken from [4].
c) Partial sequence alignments of human Parkin (Uniprot: O60260) and shRNAs, coloured as in a) and b).
(TIF)

S2 Fig. Mff isoform alignment. a) Mff antibody is specific. HEK293T cells were transfected with control (Firefly luciferase) siRNA or human Mff siRNA (5′-CCAUUGAAGGAACGUCAGATT-3′, Eurofins genomics). Cells were lysed 72 hours post-transfection and lysates used for Western blotting with anti-Mff antibody (Santa Cruz sc-398731). No bands were detected in Mff knockdown cells.
b) Alignment of all five isoforms of human Mff. Isoform I (green, 342 amino acids) is the longest and was used to generate CFP-Mff constructs. Isoform II (orange, 291 amino acids) was used in the study by Gao et al. Residue numbers are given according to their position in Isoform I. S155 and S172 are present in all isoforms of Mff (red). K151 (blue) and K302 (purple) are also present in all isoforms. Alignment produced using ClustalOmega. Uniprot identifiers are as shown (Q9GZY8).
(TIF)

S3 Fig. Parkin over-expression and further controls for Figs 3 and 4. a) Samples from Fig 3C (over-expressing Parkin WT, S65A or S65D, in the presence of CHX) alongside non-transfected HEK293T cells in the presence of CHX. Lysates probed for Parkin, Mff and β-actin.
b) Samples from Fig 4D (over-expressing Parkin WT, in the presence of DMSO, BTZ or Baf) alongside non-transfected HEK293T cells in the presence of DMSO. Lysates probed for Parkin, ubiquitin, LC3 and β-actin.
c) Quantitative analysis of (c), data presented as mean ± SEM. Analysed using ordinary one-way ANOVA with Tukey's correction for multiple comparisons with a pooled variance. N = 3. * $p < 0.05$.
(TIF)

Author Contributions

Conceptualization: Laura Lee, Kevin A. Wilkinson, Jeremy M. Henley.

Data curation: Laura Lee.

Formal analysis: Laura Lee, Kevin A. Wilkinson.

Funding acquisition: Jeremy M. Henley.

Investigation: Laura Lee, Richard Seager.

Methodology: Richard Seager, Yasuko Nakamura, Kevin A. Wilkinson.

Project administration: Yasuko Nakamura.

Resources: Richard Seager, Yasuko Nakamura, Kevin A. Wilkinson.

Supervision: Jeremy M. Henley.

Writing – original draft: Laura Lee, Jeremy M. Henley.

Writing – review & editing: Kevin A. Wilkinson, Jeremy M. Henley.

References

1. Pessayre D, Mansouri A, Fromenty B. Nonalcoholic steatosis and steatohepatitis. V. Mitochondrial dysfunction in steatohepatitis. Am J Physiol Gastrointest Liver Physiol. 2002; 282(2):G193–9. https://doi.org/10.1152/ajpgi.00426.2001 PMID: 11804839
2. Piquereau J, Godin R, Deschenes S, Bessi VL, Mofarrahi M, Hussain SN, et al. Protective role of PARK2/Parkin in sepsis-induced cardiac contractile and mitochondrial dysfunction. Autophagy. 2013; 9 (11):1837–51. https://doi.org/10.4161/auto.26502 PMID: 24121678
3. Skulachev VP. Mitochondrial filaments and clusters as intracellular power-transmitting cables. Trends Biochem Sci. 2001; 26(1):23–9. PMID: 11165513
4. Song M, Mihara K, Chen Y, Scorrano L, Dorn GW, 2nd. Mitochondrial fission and fusion factors reciprocally orchestrate mitophagic culling in mouse hearts and cultured fibroblasts. Cell Metab. 2015; 21 (2):273–86. https://doi.org/10.1016/j.cmet.2014.12.011 PMID: 25600785
5. van der Bliek AM, Shen Q, Kawajiri S. Mechanisms of mitochondrial fission and fusion. Cold Spring Harb Perspect Biol. 2013; 5(6).
6. Zamponi N, Zamponi E, Cannas SA, Billoni OV, Helguera PR, Chialvo DR. Mitochondrial network complexity emerges from fission/fusion dynamics. Sci Rep. 2018; 8(1):363. https://doi.org/10.1038/s41598-017-18351-5 PMID: 29321534
7. Hoppins S, Lackner L, Nunnari J. The machines that divide and fuse mitochondria. Annu Rev Biochem. 2007; 76:751–80. https://doi.org/10.1146/annurev.biochem.76.071905.090048 PMID: 17362197
8. Smirnova E, Griparic L, Shurland DL, van der Bliek AM. Dynamin-related protein Drp1 is required for mitochondrial division in mammalian cells. Mol Biol Cell. 2001; 12(8):2245–56. https://doi.org/10.1091/mbc.12.8.2245 PMID: 11514614
9. Frank S, Gaume B, Bergmann-Leitner ES, Leitner WW, Robert EG, Catez F, et al. The role of dynamin-related protein 1, a mediator of mitochondrial fission, in apoptosis. Dev Cell. 2001; 1(4):515–25. PMID: 11703942
10. Munoz-Pinedo C, Guio-Carrion A, Goldstein JC, Fitzgerald P, Newmeyer DD, Green DR. Different mitochondrial intermembrane space proteins are released during apoptosis in a manner that is coordinately initiated but can vary in duration. Proc Natl Acad Sci U S A. 2006; 103(31):11573–8. https://doi.org/10.1073/pnas.0603007103 PMID: 16864784
11. Yoshida Y, Mogi Y. How do plastids and mitochondria divide? Microscopy (Oxf). 2018.
12. Osellame LD, Singh AP, Stroud DA, Palmer CS, Stojanovski D, Ramachandran R, et al. Cooperative and independent roles of Drp1 adaptors Mff and MiD49/51 in mitochondrial fission. J Cell Sci. 2016.
13. Osellame LD, Singh AP, Stroud DA, Palmer CS, Stojanovski D, Ramachandran R, et al. Cooperative and independent roles of the Drp1 adaptors Mff, MiD49 and MiD51 in mitochondrial fission. J Cell Sci. 2016; 129(11):2170–81. https://doi.org/10.1242/jcs.185165 PMID: 27076521
14. Loson OC, Song Z, Chen H, Chan DC. Fis1, Mff, MiD49, and MiD51 mediate Drp1 recruitment in mitochondrial fission. Mol Biol Cell. 2013; 24(5):659–67. https://doi.org/10.1091/mbc.E12-10-0721 PMID: 23283981
15. Otera H, Miyata N, Kuge O, Mihara K. Drp1-dependent mitochondrial fission via MiD49/51 is essential for apoptotic cristae remodeling. J Cell Biol. 2016; 212(5):531–44. https://doi.org/10.1083/jcb.201508099 PMID: 26903540
16. Palmer CS, Osellame LD, Laine D, Koutsopoulos OS, Frazier AE, Ryan MT. MiD49 and MiD51, new components of the mitochondrial fission machinery. EMBO Rep. 2011; 12(6):565–73. https://doi.org/10.1038/embor.2011.54 PMID: 21508961
17. Otera H, Wang C, Cleland MM, Setoguchi K, Yokota S, Youle RJ, et al. Mff is an essential factor for mitochondrial recruitment of Drp1 during mitochondrial fission in mammalian cells. J Cell Biol. 2010; 191(6):1141–58. https://doi.org/10.1083/jcb.201007152 PMID: 21149567
18. Gandre-Babbe S, van der Bliek AM. The novel tail-anchored membrane protein Mff controls mitochondrial and peroxisomal fission in mammalian cells. Mol Biol Cell. 2008; 19(6):2402–12. https://doi.org/10.1091/mbc.E07-12-1287 PMID: 18353969
19. Jin SM, Lazarou M, Wang C, Kane LA, Narendra DP, Youle RJ. Mitochondrial membrane potential regulates PINK1 import and proteolytic destabilization by PARL. J Cell Biol. 2010; 191(5):933–42. https://doi.org/10.1083/jcb.201008084 PMID: 21115803
20. Yamano K, Youle RJ. PINK1 is degraded through the N-end rule pathway. Autophagy. 2013; 9 (11):1758–69. https://doi.org/10.4161/auto.24633 PMID: 24121706
21. Chen Y, Dorn GW 2nd. PINK1-phosphorylated mitofusin 2 is a Parkin receptor for culling damaged mitochondria. Science. 2013; 340(6131):471–5. https://doi.org/10.1126/science.1231031 PMID: 23620051

22. Wauer T, Swatek KN, Wagstaff JL, Gladkova C, Pruneda JN, Michel MA, et al. Ubiquitin Ser65 phosphorylation affects ubiquitin structure, chain assembly and hydrolysis. EMBO J. 2015; 34(3):307–25. https://doi.org/10.15252/embj.201489847 PMID: 25527291

23. Caulfield TR, Fiesel FC, Springer W. Activation of the E3 ubiquitin ligase Parkin. Biochem Soc Trans. 2015; 43(2):269–74. https://doi.org/10.1042/BST20140321 PMID: 25849928

24. Gladkova C, Maslen SL, Skehel JM, Komander D. Mechanism of parkin activation by PINK1. Nature. 2018; 559(7714):410–4. https://doi.org/10.1038/s41586-018-0224-x PMID: 29995846

25. Caulfield TR, Fiesel FC, Moussaud-Lamodiere EL, Dourado DF, Flores SC, Springer W. Phosphorylation by PINK1 releases the UBL domain and initializes the conformational opening of the E3 ubiquitin ligase Parkin. PLoS Comput Biol. 2014; 10(11):e1003935. https://doi.org/10.1371/journal.pcbi.1003935 PMID: 25375667

26. Wauer T, Simicek M, Schubert A, Komander D. Mechanism of phospho-ubiquitin- induced PARKIN activation. Nature. 2015; 524(7565):370–4. https://doi.org/10.1038/nature14879 PMID: 26161729

27. Yoshii SR, Kishi C, Ishihara N, Mizushima N. Parkin mediates proteasome-dependent protein degradation and rupture of the outer mitochondrial membrane. J Biol Chem. 2011; 286(22):19630–40. https://doi.org/10.1074/jbc.M110.209338 PMID: 21454557

28. Chan NC, Salazar AM, Pham AH, Sweredoski MJ, Kolawa NJ, Graham RL, et al. Broad activation of the ubiquitin-proteasome system by Parkin is critical for mitophagy. Hum Mol Genet. 2011; 20(9):1726–37. https://doi.org/10.1093/hmg/ddr048 PMID: 21296869

29. Tanaka A. Parkin-mediated selective mitochondrial autophagy, mitophagy: Parkin purges damaged organelles from the vital mitochondrial network. FEBS Lett. 2010; 584(7):1386–92. https://doi.org/10.1016/j.febslet.2010.02.060 PMID: 20188730

30. Gao J, Qin S, Jiang C. Parkin-induced ubiquitination of Mff promotes its association with p62/SQSTM1 during mitochondrial depolarization. Acta Biochim Biophys Sin (Shanghai). 2015; 47(7):522–9.

31. Kabeya Y, Mizushima N, Ueno T, Yamamoto A, Kirisako T, Noda T, et al. LC3, a mammalian homologue of yeast Apg8p, is localized in autophagosome membranes after processing. EMBO J. 2000; 19 (21):5720–8. https://doi.org/10.1093/emboj/19.21.5720 PMID: 11060023

32. Geisler S, Holmstrom KM, Skujat D, Fiesel FC, Rothfuss OC, Kahle PJ, et al. PINK1/Parkin-mediated mitophagy is dependent on VDAC1 and p62/SQSTM1. Nat Cell Biol. 2010; 12(2):119–31. https://doi.org/10.1038/ncb2012 PMID: 20098416

33. Yu W, Sun Y, Guo S, Lu B. The PINK1/Parkin pathway regulates mitochondrial dynamics and function in mammalian hippocampal and dopaminergic neurons. Hum Mol Genet. 2011; 20(16):3227–40. https://doi.org/10.1093/hmg/ddr235 PMID: 21613270

34. Lutz AK, Exner N, Fett ME, Schlehe JS, Kloos K, Lammermann K, et al. Loss of parkin or PINK1 function increases Drp1-dependent mitochondrial fragmentation. J Biol Chem. 2009; 284(34):22938–51. https://doi.org/10.1074/jbc.M109.035774 PMID: 19546216

35. Mortiboys H, Thomas KJ, Koopman WJ, Klaffke S, Abou-Sleiman P, Olpin S, et al. Mitochondrial function and morphology are impaired in parkin-mutant fibroblasts. Ann Neurol. 2008; 64(5):555–65. https://doi.org/10.1002/ana.21492 PMID: 19067348

36. Berger AK, Cortese GP, Amodeo KD, Weihofen A, Letai A, LaVoie MJ. Parkin selectively alters the intrinsic threshold for mitochondrial cytochrome c release. Hum Mol Genet. 2009; 18(22):4317–28. https://doi.org/10.1093/hmg/ddp384 PMID: 19679562

37. Toyama EQ, Herzig S, Courchet J, Lewis TL Jr., Loson OC, Hellberg K et al. Metabolism. AMP-activated protein kinase mediates mitochondrial fission in response to energy stress. Science. 2016; 351 (6270):275–81. https://doi.org/10.1126/science.aab4138 PMID: 26816379

38. Hjerpe R, Thomas Y, Chen J, Zemla A, Curran S, Shpiro N, et al. Changes in the ratio of free NEDD8 to ubiquitin triggers NEDDylation by ubiquitin enzymes. Biochem J. 2012; 441(3):927–36. https://doi.org/10.1042/BJ20111671 PMID: 22004789

39. Mauvezin C, Neufeld TP. Bafilomycin A1 disrupts autophagic flux by inhibiting both V- ATPase-dependent acidification and Ca-P60A/SERCA-dependent autophagosome- lysosome fusion. Autophagy. 2015; 11(8):1437–8. https://doi.org/10.1080/15548627.2015.1066957 PMID: 26156798

40. Basso V, Marchesan E, Peggion C, Chakraborty J, von Stockum S, Giacomello M, et al. Regulation of ER-mitochondria contacts by Parkin via Mfn2. Pharmacol Res. 2018; 138:43–56. https://doi.org/10.1016/j.phrs.2018.09.006 PMID: 30219582

41. Tanaka A, Cleland MM, Xu S, Narendra DP, Suen DF, Karbowski M, et al. Proteasome and p97 mediate mitophagy and degradation of mitofusins induced by Parkin. J Cell Biol. 2010; 191(7):1367–80. https://doi.org/10.1083/jcb.201007013 PMID: 21173115